INSTITUTO
UNIVERSITÁRIO
DE LISBOA

Risk-neutral distributions implied from stochastic volatility jump-diffusion models

José Miguel Serejo Neves

Master in Financial Mathematics

Supervisors:
PhD João Pedro Vidal Nunes, Full Professor,
ISCTE-IUL

PhD João Pedro Bento Ruas, Assistant Professor,
ISCTE-IUL

October, 2025

Finance Department

Mathematics Department

Risk-neutral distributions implied from stochastic volatility jump-diffusion models

José Miguel Serejo Neves

Master in Financial Mathematics

Supervisors:
PhD João Pedro Vidal Nunes, Full Professor,
ISCTE-IUL

PhD João Pedro Bento Ruas, Assistant Professor,
ISCTE-IUL

October, 2025

Acknowledgments

I would like to thank my supervisor, Professor João Pedro Nunes, for patient guidance, careful reading, and steady support throughout this dissertation.

I am also grateful to Professor João Pedro Ruas for co-supervision and for providing the dataset used in this study.

I thank my classmates Afonso, Cláudio, and Sérgio for their support and encouragement during the programme.

I would also like to thank José Cruz for generous advice and valuable input, which greatly improved this work.

Resumo

Esta dissertação investiga a extração e análise de densidades neutras ao risco (RNDs) a partir de opções mensais sobre o S&P 500, no âmbito de uma estrutura de valorização baseada em transformadas de Fourier. O estudo centra-se em três modelos afins com difusão e saltos, nomeadamente os modelos de Merton (1976), Kou (2002) e Bakshi, Cao and Chen (1997), com o objetivo de avaliar a sua capacidade de reproduzir as distribuições implícitas nas opções e captar a dinâmica das expectativas de mercado. Para cada modelo, é derivada a função característica sob a medida *T-forward*, que é posteriormente integrada numericamente na fórmula de valorização unificada de Lee (2004). As densidades neutras ao risco extraídas são analisadas para avaliar a capacidade de cada modelo representar as expectativas de mercado, relativamente à evolução futura dos preços e ao risco de cauda. Investiga-se também se a suavização da superfície de volatilidade implícita antes da calibração, utilizando as interpolações cúbica e de Hermite, melhora o desempenho do modelo de Bakshi e a estabilidade dos parâmetros estimados.

A análise empírica é realizada com opções mensais sobre o S&P 500 no período de janeiro a maio de 2022. O desempenho dos modelos é avaliado através de um conjunto abrangente de métricas de erro de valorização e de uma análise detalhada da forma e distribuição das RNDs, incluindo momentos, caudas, quantis e medidas de divergência.

Os resultados indicam uma hierarquia clara, com o modelo de Bakshi a apresentar o melhor ajustamento global e erros de valorização 7 a 13 vezes menores do que os de Kou e Merton. Ao mesmo tempo, as densidades extraídas pelo modelo de Bakshi exibem assimetrias próximas de zero e baixa curtose, apontando para calibrações dominadas pela difusão que subestimam o risco de cauda em períodos de tensão de mercado. Este comportamento está associado ao processo de calibração baseado na minimização dos erros de valorização, que atribui maior peso a opções com preços mais elevados, e ao filtro de dados, que tende a excluir opções muito *out-of-the-money*.

A suavização da volatilidade reduz o RMSE em cerca de 5% e a variabilidade dos parâmetros em aproximadamente 80%, sendo a interpolação de Hermite a que proporciona o melhor equilíbrio entre precisão e robustez.

Palavras-chave: Valorização de opções; Transformada de Fourier; Densidades neutras ao risco; Modelos afim com difusão por saltos; Suavização da volatilidade implícita; Opções S&P 500; Risco de cauda; Modelo de Merton; Modelo de Kou; Modelo de Bakshi Cao e Chen.

Abstract

This dissertation investigates the extraction and analysis of risk-neutral densities from S&P 500 monthly options within a Fourier-based valuation framework. The study focuses on three affine jump-diffusion models, namely Merton (1976), Kou (2002), and Bakshi and Chen (1997) models, to assess their ability to capture the dynamics of option-implied distributions. For each model, we derive the characteristic function under the forward T-measure and integrate it into Lee (2004) unified pricing formula. The extracted risk-neutral densities are analysed to assess each model's ability to represent market expectations regarding future price movements and tail risk.
We also investigate whether smoothing the implied volatility surface prior to calibration, using cubic and Hermite spline interpolations, improves model performance and parameter stability for the Bakshi model.

An extensive empirical analysis is conducted using S&P 500 monthly options from January to May 2022. Model performance is evaluated using a comprehensive set of pricing error metrics and a detailed examination of the RNDs shape and distribution, including their moments, tails, quantiles and divergence measures.

Results indicate a clear hierarchy, with Bakshi delivering the best overall fit and achieving pricing errors 7 to 13 times lower than those of Kou and Merton. At the same time, Bakshi's extracted densities display near-zero skewness and low kurtosis, which points to diffusion-dominated calibrations that understate downside risk in stressed markets. This pattern appears linked to calibrating by minimising pricing errors, which implicitly places more weight on higher-priced options, and to option filtering that disproportionately removes deep out-of-the-money puts.

Volatility smoothing reduces RMSE by about 5% and cuts parameter variability by roughly 80%, with Hermite providing the best balance between accuracy and robustness.

Keywords: Option Pricing; Fourier transform; Risk-neutral densities; Affine stochastic volatility jump models; Implied volatility smoothing; S&P 500 options; Tail risk; Merton model; Kou model; Bakshi Cao e Chen model.

Contents

Acknowledgments i

Resumo iii

Abstract v

Chapter 1. Introduction 1

Chapter 2. Risk-neutral densities 3
2.1. Implied risk-neutral densities: an overview 3
2.2. A brief literature review on risk-neutral valuation 4
2.3. Extracting the risk-neutral density from option prices 8

Chapter 3. Affine stochastic volatility jump-diffusion models 11
3.1. Background 11
3.2. Affine jump-diffusion framework 12
3.2.1. Definition and characterisation of affine processes 12
3.2.2. The affine jump-diffusion process 13
3.2.3. Pricing solution for plain-vanilla European style options 15

Chapter 4. Option valuation using Fourier transform methods 17
4.1. Background 17
4.2. Lee (2004) framework 18
4.2.1. Numeraires and Martingale measures 18
4.2.2. The discounted characteristic function 19
4.2.3. The option pricing formula 21

Chapter 5. Stochastic volatility jump-diffusion models 27
5.1. Background 27
5.2. The generic stochastic volatility jump-diffusion model 28
5.2.1. Stochastic volatility dynamics 28
5.2.2. Jump-diffusion process 29
5.2.3. Jump-diffusion models 31
5.2.4. Stochastic volatility jump-diffusion models 31
5.3. Merton Jump-diffusion model 32
5.3.1. Merton's model as a special case of Duffie, Pan, and Singleton (2000) 34
5.4. Kou jump-diffusion model 36
5.4.1. Kou's model as a special case of Duffie, Pan, and Singleton (2000) 38

5.5. Bakshi, Cao and Chen (1997) model 39
5.5.1. Bakshi's as a particular case of Duffie, Pan, and Singleton (2000) 40

Chapter 6. Empirical analysis 47
6.1. Introduction 47
6.2. Data and pre-processing 47
6.3. Model calibration 48
6.4. Empirical results 49
6.4.1. Model fit and comparative performance 49
6.4.2. Risk-neutral densities 52
6.4.3. Explaining Bakshi's RND characteristics 60
6.5. Implied-volatility smoothing and calibration design 61
6.5.1. Spline interpolation methods 62
6.5.2. Sample period and implementation issues 63
6.5.3. Comparative results and main findings 63
6.5.4. Smoothing impact on calibration time 66

Chapter 7. Conclusions 67
7.1. Main findings 67
7.2. Limitations and future work 68

References 69

Appendix A. General Definitions i

Appendix B. Lévy processes iii
B.1. Definition of Lévy processes iii
B.2. Poisson process and main definitions iii
B.3. Lévy measure vi
B.3.1. Lévy-Khintchine representation vi
B.4. Itô's lemma for Lévy processes vii
B.5. Propositions and definitions viii
B.6. Additional results and proofs ix

Appendix C. Affine jump-diffusion framework xiii
C.1. Propositions and definitions xiii
C.1.1. *Duffie, Pan, and Singleton (2000) framework-one dimensional case* xiii

Appendix D. Lee (2004) framework xix
D.1. Equivalent Martingale measures and change of numeraires xix
D.2. Theorems and propositions from Lee (2004) xx
D.3. Option pricing under the *Lee (2004) framework* xxviii
D.3.1. Singularities and residues for the *complex Fourier transform of the unmodified option price* xxix

D.3.2. Pricing formulas for different $\boldsymbol{\alpha}$ cases xxx

Appendix E. Jump-diffusion models xlvii
E.1. Theorems, definitions and propositions xlvii
E.2. Additional results and proofs xlvii
E.3. Chapter 5 jump-diffusion models proofs xlviii
E.3.1. Merton (1973) jump-diffusion model xlviii
E.3.2. Kou's model xlix
E.3.3. Bakshi, Cao and Chen (1997) model l

Appendix F. Results lxvii
F.1. Fourier inversion of the risk-neutral density lxvii
F.2. Data and pre-processing information lxix
F.2.1. Data filtering effect lxix
F.2.2. Final sample statistics lxxi
F.3. Additional market data lxxi
F.4. Pricing Error Metrics lxxii
F.4.1. Sum of Squared Errors (SSE) lxxiii
F.4.2. Root Mean Squared Error (RMSE) lxxiii
F.4.3. Mean Absolute Error (MAE) lxxiii
F.4.4. Mean Absolute Percentage Error (MAPE) lxxiii
F.4.5. Symmetric Mean Absolute Percentage Error (sMAPE) lxxiii
F.4.6. Coefficient of Determination (R^2) lxxiii
F.4.7. Unexplained Variance (in basis points) lxxiii
F.5. Cubic Spline and Hermite Spline Smoothing lxxiii
F.5.1. Cubic Spline Interpolation lxxiii
F.5.2. Hermite (Piecewise Cubic Hermite) Spline lxxiv
F.6. Calibration initial parameters and bounds lxxiv
F.7. Final parameters statistics for the three models calibrated lxxv
F.7.1. Calibrated parameter statistics for Merton (1976) JD model lxxv
F.7.2. Calibrated parameter statistics for Kou (2002) model lxxv
F.7.3. Calibrated parameter statistics for Bakshi and Chen (1997) model lxxvi
F.8. Detailed calibration performance metrics and robustness tests lxxvi
F.8.1. Robustness checks lxxvii
F.9. Statistical moments and quantiles of RND using mean instead of median lxxx
F.10. Other relevant error metrics and 3D RND figures lxxxiii
F.11. Additional risk measures: statistical distances, Value-at-Risk and Expected Shortfall measure tables lxxxv
F.11.1. Statistical Distances by Maturity lxxxv
F.12. Bakshi smoothing error metrics by maturity lxxxvii

CHAPTER 1

Introduction

Option pricing theory is a well-established framework in quantitative finance for valuing financial options. Under this setting, the risk-neutral density plays a fundamental role as it contains a large amount of information about risk preferences and market's expectation of the future prices of financial assets. These densities are built under the assumption that all market participants are risk-neutral, where all investors are indifferent to risk and, therefore, do not require any compensation for assuming additional risk.

The objective of this thesis is to study the conditions under which risk-neutral densities can be obtained from option prices and to examine how affine jump-diffusion models perform within a Fourier-based valuation framework. Concretely, we derive forward-measure characteristic functions for the Merton (1976), Kou (2002) e Bakshi, Cao and Chen (1997) models, price options using Lee (2004) unified formulation, and extract the corresponding risk-neutral densities. We then conduct a comparative analysis using six pricing-error metrics and a detailed examination of the implied distributions, complemented by a volatility-smoothing study for the Bakshi, Cao and Chen (1997) model.

The remainder of this dissertation is organised as follows. Chapter 2 provides a detailed overview of risk-neutral densities, discussing their theoretical foundations and importance, with particular emphasis on the extraction method originally proposed by Breeden and Litzenberger (1978), and later extended by Figlewski (2018). Chapter 3 introduces the affine stochastic volatility jump-diffusion framework of Duffie, Pan, and Singleton (2000) and sets up a transform-based approach using affine characteristic functions for option valuation and the forward-measure formulation. In Chapter 4, we develop option valuation via Fourier transform methods, adopting Lee (2004) unified framework as a central computational tool. The approach recasts prices as damped contour integrals, providing stable inversion schemes and a direct link to model characteristic functions. We use this representation for option pricing and for risk-neutral density extraction. Chapter 5 combines the affine stochastic volatility framework of Duffie, Pan, and Singleton (2000) with Lee (2004) Fourier-based valuation method. The characteristic functions derived from the affine setup are implemented in Lee's unified pricing formula to obtain option prices and risk-neutral densities for the Merton (1976), Kou (2002), and Bakshi, Cao and Chen (1997) models. The resulting functions provide the basis for option valuation and for the extraction of risk-neutral densities. The empirical results and comparative analysis are presented in Chapter 6. Model performance is evaluated using a comprehensive set of six pricing-error metrics, followed by an analysis of the extracted risk-neutral densities (3D

and model-specific) focusing on moments, tails, quantiles, and divergence measures. A volatility-smoothing study for the Bakshi model using Cubic and Hermite schemes relative to a baseline is also conducted, with diagnostics on errors, coefficient-of-variation statistics, convergence, outliers, and runtime. Finally, Chapter 7 presents the main conclusions of the dissertation, summarising the key findings, discussing the study's limitations, and outlining directions for future research. The appendices provide supporting definitions and propositions and gather the proofs of the main results.

CHAPTER 2

Risk-neutral densities

2.1. Implied risk-neutral densities: an overview

Option pricing theory is a well-known and widely accepted framework in finance used to determine the value of financial options. Under this structure, the risk-neutral density (RND) plays a fundamental role as it contains a large amount of information about investors' price expectations and risk preferences.

Risk-neutral densities are probability density functions (PDF) that reflect the market's expectation of the future prices of financial assets. These densities are constructed under the assumption that all market participants are risk-neutral, where all investors are indifferent to risk and, therefore, do not require any compensation for assuming additional risk.

In this context, RNDs are derived from the option prices and reflect the probabilities assigned to different future price levels of the underlying asset at a specific point in time.

According to this approach, in the risk-neutral world, the expected return on all assets is equal to the risk-free rate. Using this assumption, it is possible to construct a risk-neutral probability measure, often denoted as $\mathbb{Q}$, under which the discounted expected payoff of a derivative is equal to its current market price. In other words, by incorporating risk-neutral densities into option pricing models, one can calculate the fair value of derivative instruments, such as options, without explicitly considering the expected returns and risk preferences of market participants. Instead, the derivative fair value can be obtained by discounting the expected future payoffs at the risk-free rate under a risk-neutral probability measure.

The RND is often derived by using the option prices observed in the market. By reversing the option pricing process and solving for the expected future price densities that would lead to the observed option prices, one can derive the implied risk-neutral densities function, which in turn is implied by the market's collective view on the potential future price movements of the underlying asset. The information incorporated in option implied RND can be used for determining future market beliefs, pricing of illiquid derivatives, hedging purposes, and monetary policies.

For this reason, risk-neutral densities have become a fundamental tool in option pricing theory. By allowing the extracting of information on market expectations on future price outcomes, they allow for consistent and coherent pricing models that align with the financial market dynamics, enabling investors to make informed decisions regarding option valuation, risk management, and hedging strategies.

2.2. A brief literature review on risk-neutral valuation

The estimation of risk-neutral densities is a relatively recent research topic in the risk-neutral valuation and asset pricing theories.

The Black and Scholes (1973) pivotal work laid the foundation for option pricing theory, with their novel, closed-form solution for pricing European-style options, assuming constant volatility, a risk-free interest rate, and a log-normal distribution of stock returns. While this paper did not explicitly refer to risk-neutral pricing, it established the groundwork for subsequent research. It also served to introduce the idea that relevant pricing information, especially the future volatility of the underlying stock, could be extracted from option market prices by inverting the valuation formula. In the same year, Merton (1973) extended the Black-Scholes model by incorporating the notion of continuous-time stochastic processes, namely the process that is currently known as geometric Brownian motion, and by allowing for more realistic assumptions, such as the consideration of dividend payments and the inclusion of transaction costs. In an influential paper, Merton (1976) addressed a key limitation of the Black-Scholes model by acknowledging that stock prices do not follow a continuous path but instead can exhibit jumps or discontinuities. By incorporating jump-diffusion processes into the continuous-time model to capture the possibility of sudden changes in the underlying asset's value, Merton (1976) provided a more realistic representation of asset price dynamics, particularly in situations where significant events or news announcements can cause abrupt movements in stock prices.

Option risk-neutral valuation was first introduced by Cox and Ross (1976), and further developed by Cox, Ross, and Rubinstein (1979). In the latter, Cox, Ross, and Rubinstein presented the binomial option-pricing model, a discrete-time framework that utilises a binomial tree to model the possible price movements of the underlying asset. One of the notable advancements was the introduction of risk-neutral pricing, a concept that played a fundamental role in option valuation. By deriving risk-neutral probabilities from the risk-free rate, the model enabled the calculation of option values without explicitly considering the risk preferences of individuals, reaching the conclusion that the shape of investors´ utility functions do not affect the option prices as long as the agents prefer more wealth to less (the so-called non-satiation condition). This fact allows the pricing of options by calculating their expected values in the risk-neutral world, using the risk-free discount rate to determine the option's fair value.

Rubinstein (1976) and Brennan (1979) investigated the joint conditions on the returns process of the underlying asset and the utility function of a representative agent such that risk-neutral pricing in discrete-time models is valid in the absence of arbitrage opportunities. Rubinstein (1976) and Brennan (1979) established that log-normal returns, which follow a logarithmic normal distribution, and a utility function with constant relative risk aversion are both necessary and sufficient conditions for option values to satisfy the Black-Scholes equation. Stapleton and Subrahmanyam (1984) later expanded the proofs to include the multivariate setup.

Until the early 1970s, the Black-Scholes model was the main reference in finance for valuing financial options. As such, when extracting information from listed option prices to perform their studies, most researchers ended up focusing only on the implied volatility estimation, as it was the only parameter of the Black-Sholes formula that was not directly observable in the market. However, as the financial market evolved and the number of listed contracts increased over time, academics soon began to explore alternative approaches to extract, understand, and make use of the potentially valuable information obtained from option market prices, such as the investor expectations and risk preferences contained in the risk-neutral densities.

The first paper to address this topic was Ross (1976). In his paper, Ross showed how to retrieve the full risk-neutral probability distribution from a set of European options prices, in a complete market, where every contingent claim can be replicated. Notwithstanding, Breeden and Litzenberger (1978) seminal paper remains one of the most cited studies to date on this matter. Continuing Ross's work, the authors illustrated how the RND can be obtained from option prices with a continuum of strike prices, by calculating the second partial derivative of the call option price with respect to the strike price.

Since Breeden and Litzenberger (1978) findings, numerous methods of estimating the option implied risk-neutral densities have been proposed. While some scholars, such as Cont (1997) and, to some extent, Bahra (1997), advocate a different classification, the majority divides the approaches for extracting RNDs from listed option prices into two main categories: parametric and non-parametric methods, each with its respective advantages and drawbacks. That said, and although the purpose of this dissertation is not to describe the main methods to infer RNDs from option prices, it is important to describe, in general terms, what distinguishes each of the main approaches. To this end, the classification proposed by Jackwerth (1999) was followed. The parametric methods refer to the approaches that assume a specific functional form or model for risk-neutral density. These methods involve selecting a parametric distribution, such as the Normal or Log-normal distribution, and estimating the parameters that best fit the observed option prices or implied volatilities. By fitting the chosen distribution to the market data, the method provides a parametric representation of the risk-neutral density, allowing for further analysis and pricing of derivative instruments. Parametric methods can be divided into three distinct groups: i) expansion methods; ii) generalised distribution methods, and iii) mixture methods. The first group comprises the expansion methods, which are usually related to the expansion of a function in a Taylor series around a point. Expansion methods usually start with a simpler distribution, typically Normal or Log-normal, and then correction terms are added in order to obtain a risk-neutral distribution with a more adaptable shape, which is then fitted to the observed option prices.

One of the earliest studies on expansion methods is Abadir and Rockinger (1997). In this paper, the researchers calculated an option price function across strikes in a closed form, incorporating a risk-neutral density derived using confluent hypergeometric (or

Kummer's) functions. Abken, Madan, and Ramamurtie (1996a, 1996b) presented the four-parameter Hermite polynomials, relating them to the consecutive derivatives of the normal density function, and providing four correction terms for the normal distribution. Rockinger (1998) and Corrado and Su (1997) developed the work on four-parameter Hermite polynomials, by introducing restrictions on some of the coefficients and focusing on Gram-Charlier expansions. Brenner and Eom (1997) employed Laguerre polynomials as corrections to a gamma distribution, enabling them to approximate the risk-neutral distribution with the advantageous outcome of achieving unbiased moments. Edgeworth expansions were explored by Jarrow and Rudd (1982), Corrado and Su (1996), Longstaff (1995), and Rubinstein (1998). Finally, Potters, Cont, and Bouchaud (1998) presented a research on the use of cumulant expansions, adding a single correction term to a normal distribution, which adjusts for the kurtosis of the risk-neutral distribution.

The second group includes the generalised distribution methods. This class of statistical techniques offers increased flexibility compared to traditional parametric distributions by introducing additional parameters to the distribution beyond the two parameters of the normal or log-normal distributions. The use of generalised distribution methods in finance can be attributed to Bookstaber and McDonald (1987). The application of these four-parameter distributions typically involves the usage of the log-normal, gamma, exponential and Burr type distributions. Aparicio and Hodges (1998) expanded the previous work by employing generalised beta functions of the second kind, while Posner and Milevsky (1998) chose to utilise Johnson densities. Johnson (1949) showed how to introduce two more parameters while transmuting normal distributions using logarithmic and hyperbolic sine transformations. Lastly, different Burr distributions applications can be seen in Sherrick, Garcia, and Tirupattur (1995), and Sherrick, Irwin, and Forster (1992, 1996) studies.

The third set of parametric approaches is the mixture methods. As the name implies, it refers to statistical technics in which new distributions are created from mixtures of simple distributions, each with a distinct parametrisation. These methods leverage the strengths of different models to capture the complexity and uncertainty inherent in financial data, resulting in more robust and reliable results. A problem with mixtures is that the number of parameters increases very fast. Research on mixture approaches includes Melick and Thomas (1997), and Ritchey (1990). Regarding the second category, the non-parametric methods, are also divided into three different groups according to Jackwerth (1999) classification: i) kernel methods; ii) maximum-entropy methods, and iii) curve fitting methods. The kernel methods are the first group of non-parametric methods. These approaches can be understood as having a conceptual relationship with regressions, as they aim to fit a function to available data. However, the key distinction lies in the fact that kernel regression does not require specifying the parametric form of the function in advance. Instead, allows for more flexibility by utilising kernel functions to estimate the relationship between variables. Kernel methods have been widely used in finance to

estimate risk-neutral densities. Aït-Sahalia and Lo (1998a) introduced a non-parametric approach using kernel density estimation to infer state-price densities. Pritsker (1997) focused on computing implied volatility using kernel methods. Fan and Yao (2003) developed efficient techniques for estimating conditional covariance matrices in stochastic regression models, improving inference on risk-neutral densities. Aït-Sahalia and Duarte (2003) extended kernel methods to non-parametric option pricing under shape restrictions. Chiu, Li, and Todorov (2014) employed kernel methods to estimate risk-neutral densities implied by bond yields, proposing a flexible quadratic term structure model. Chen, Davis, and Landwehr (2019) utilised kernel methods within a Bayesian framework for robust density forecasting in finance.

The second group of non-parametric approaches relates to the maximum-entropy methods. In finance, entropy refers to a concept derived from information theory that measures the degree of uncertainty or randomness present in the financial system by assessing the disorder and lack of clear patterns in data or information, with higher entropy indicating increased disorder, uncertainty, and risk. It is important to note that while maximum entropy methods can provide more accurate option prices in certain situations, they may also require more data and computational resources compared to simpler models. Several influential papers have focused on the application of entropy methods in estimating risk-neutral densities. Buchen and Kelly (1996) proposed a maximum entropy approach to estimate risk-neutral densities from option prices using the uniform and log-normal distributions. Stutzer (1996) extended this work by incorporating moment constraints, allowing for more precise modelling of risk-neutral densities. Barndorff-Nielsen and Shephard (2001) introduced non-Gaussian Ornstein-Uhlenbeck models. Additionally, Christoffersen and Pelletier (2004) used entropy methods in backtesting value-at-risk models, employing duration-based tests to evaluate risk measures based on estimated risk-neutral densities. Finally, regarding the third and last class of non-parametric approaches, the curve fitting methods, are technics that try to fit the implied volatilities or the risk-neutral probabilities, typically by adjusting the parameters of a chosen curve or function to minimize the difference between the predicted values and the actual data points. Common curve-fitting methods include polynomial fitting and splines, minimising the sum of squared differences (least squares) and minimising the integral of squared second derivatives. When it comes to fitting the volatility smile, various methods have been developed to capture the implied volatility dynamics. Shimko (1993) introduced one of the first curve-fitting methods by utilising a quadratic polynomial to fit implied volatilities, which then translates into option prices to derive the risk-neutral distribution by employing the second derivatives of option prices with respect to strike prices, as outlined in Breeden and Litzenberger (1978). Malz (1997) proposed a variation of Shimko's method by fitting a quadratic polynomial to implied volatilities across call option deltas instead of strike prices. Brown and Toft (1999) extended Shimko's approach by utilising seventh-order splines for curve fitting. Campa, Chang, and Reider (1998) employed cubic splines, while

Andersen and Bollerslev (1998) used cubic B-splines from a particular polynomial family. Rosenberg and Engle (1997) employed a polynomial fitted to the logarithm of the smile to prevent negative implied volatilities, with Rosenberg (1996) extending this to the bivariate case. Jackwerth (1999) focused on maximizing smile smoothness to control the trade-off between option price fit and smoothness. Carr and Madan (1999) introduced the Fast Fourier Transform (FFT) method for efficient option pricing and estimation of the implied volatility surface.

In terms of fitting risk-neutral densities directly, various methods have been proposed. Rubinstein (1994) minimised the distance between discretised probabilities and a log-normal prior distribution while ensuring the correct pricing of observed options and the underlying asset. Jackwerth and Rubinstein (1996) showed that different distance measures have minimal impact on the resulting risk-neutral distribution as long as a sufficient number of option prices are observed. Mayhew (1995) focused on maximising distribution smoothness and used cubic splines to approximate the density. Hartvig, Jensen, and Pedersen (1999) constructed the density by combining density functions using an Hermite polynomial expansion. Carr and Wu (2004) introduced a non-parametric method to estimate risk-neutral densities directly from option prices without assuming a specific parametric form. Andersen and Bollerslev (1998) suggested using continuous-time models, such as stochastic volatility models, to estimate risk-neutral densities and capture dynamic asset price behaviour. Finally, Bollerslev and Zhou (2006) conducted empirical tests comparing various parametric and non-parametric methods for estimating implied volatility functions and risk-neutral densities.

2.3. Extracting the risk-neutral density from option prices

The introduction of the Black–Scholes option pricing model in 1973 led, among other contributions, to the recognition that relevant information could be extracted from option market prices by inverting the valuation formula. While at first researchers focused mainly on the estimation of the underlying asset implied volatility, as it was the only parameter of the Black-Scholes formula that was not directly observable in the market, it soon became clear that not only volatility, but the entire probability distribution for the future asset price could be inferred from the options market prices.

As a result, the risk-neutral density quickly became an instrument of the utmost importance, as it contains valuable information for economic agents, investors, and academics, such as investors' beliefs about the true returns process, the market's aggregation of their preferences over future states of the world, the expectations on the future asset prices, and the trading constraints and limits to arbitrage.

Since the risk-neutral pricing framework was initially addressed by Cox and Ross (1976), several academics have focused on extracting, understanding, and making use of the valuable information contained in the risk-neutral densities. However, one of the most relevant and influential articles on this topic is Breeden and Litzenberger (1978), who demonstrated how to obtain the full RND from options prices, with a continuum of

strikes. The authors were the first to identify a relationship between the option price and the underlying price distribution, showing that the risk-neutral density could be extracted by deriving the option price twice with respect to the strike. Figlewski (2018) later expanded Breeden and Litzenberger's work, by developing a methodology that adapted their theoretical result to allow the use of market-observed option prices.

Taking these results into account, and using the representation theorem put forth by Harrison and Kreps (1979), which establishes that, under certain non-arbitrage conditions, any pricing kernel can be expressed as the exponential of a linear combination of a riskless asset and a set of risky assets, it is possible to evaluate contingent claims by expressing their prices as expectations of their payoffs with respect to the pricing kernel.

Nevertheless, to ensure the consistency of prices and the absence of arbitrage opportunities required by the *Law of One Price*, which states that, in a liquid and efficient market, identical assets and instruments should have the same price, these expectations must be calculated using, not the probability density function of the underlying asset, commonly known as p, but rather using the risk-neutral density q.

Moreover, according to Harrison and Kreps (1979), in a market where asset prices are described by stochastic processes that satisfy certain regularity conditions, namely the absence of arbitrage opportunities, there is a probability measure $\mathbb{Q}$, equivalent[1] to the physical probability measure $\mathbb{P}$ - the *equivalent martingale measure* - such that all (discounted) asset prices are $\mathbb{Q}$-martingales.

That said, the present value of an asset V, whose payoff at the maturity is some function $h(S_T)$ of the stock price at the time T, is given by the following expected value under the risk-neutral measure $\mathbb{Q}$:

$$V_0 = \mathbb{E}_{\mathbb{Q}}[e^{-rT}h(S_T)] = \int_{\Omega} e^{-rT}h(S_T)dQ = e^{-rT}\int_0^{+\infty} h(S_T)q(S_T)dS_T, \tag{2.1}$$

where $q(S_T)$ is the risk-neutral density of the stock price at time T that can be obtained from options prices (i.e., the $\mathbb{Q}$-density), and the exponential is the discounting factor assuming a constant interest rate r.

The $\mathbb{P}$ and $\mathbb{Q}$ distributions are related to each other through the pricing kernel. Also known as the stochastic discount factor, it represents the investor's risk preferences and the underlying dynamics of the markets, and can be defined as follows:

$$k(S_T) = e^{-rT}\frac{d\mathbb{Q}}{d\mathbb{P}}(S_T). \tag{2.2}$$

Through the pricing kernel, it is possible to write an equivalent expression for equation (2.1), using the probability density function $\mathbb{P}$ (see Figlewski (2018), p. 331):

$$V_0 = e^{-rT}\int_0^{+\infty} h(S_T)q(S_T)dS_T = \int_0^{+\infty} h(S_T)k(S_T)p(S_T)dS_T, \tag{2.3}$$

[1]Two probability measures $\mathbb{Q}$ and $\mathbb{P}$ are said to be equivalent if they define the same set of impossible events, i.e., if for any event A, $\mathbb{P}(A) = 0$ iff $\mathbb{Q}(A) = 0$.

where $p(S_T)$ is the historical or empirical density function of the same random variable S_T (i.e., the $\mathbb{P}$-density), and, again, $k(S_T)$ represents the pricing kernel.

Additionally, based on the equivalence established by equation (2.3), the following relationship between the $\mathbb{P}$ and $\mathbb{Q}$ densities can also be deducted:

$$e^{-rT}q(S_T) = k(S_T)p(S_T), \textit{ for all states of the world in the p(.) and q(.) domain.} \quad (2.4)$$

Considering now V as a European-style option, with strike price X and a payoff at maturity T equal to that of a typical call, i.e., $C(S_T) = \max(0, S_T - X)$, the price of such instrument is, according to the martingale property exhibited in equation (2.1), given by:

$$c_0 = \mathbb{E}_{\mathbb{Q}}[e^{-rT}(S_T - X)^+] = e^{-rT}\int_X^{+\infty}(S_T - X)q(S_T)dS_T, \quad (2.5)$$

in which the integral is over the risk-neutral density $q(S_T)$ when the call has a positive payoff (i.e., $S_T > X$). S_T is the underlying stock price at the maturity T, and r is the continuously compounded constant risk-free rate. Differentiating the call price with respect to the exercise price X, we get the following result:

$$\frac{\partial c}{\partial X} = -e^{-rT}\int_X^{+\infty} q(S_T)dS_T. \quad (2.6)$$

After multiplying both sides by e^{rT}, we get:

$$e^{rT}\frac{\partial c}{\partial X} = -\int_X^{+\infty} q(S_T)dS_T. \quad (2.7)$$

Since the cumulative risk-neutral distribution function of the stock price at time T, denoted by $Q(S_T)$, is given by $Q(S_T) = 1 - \int_{S_T}^{+\infty} q(S_T)dS_T$. we can rewrite (2.7) and obtain

$$1 + e^{rT}\frac{\partial c}{\partial X}\bigg|_{S_T=X} = Q(S_T). \quad (2.8)$$

Taking, once again, the partial derivative with respect to X, we obtain the risk-neutral density function as the future value of the second partial derivative of the call price with respect to the exercise price:

$$e^{rT}\frac{\partial^2 c}{\partial X^2}\bigg|_{X=S_T} = q(S_T). \quad (2.9)$$

This approach thus provides a direct link between option prices and the risk-neutral distribution. However, its practical implementation relies on the availability of option prices across a sufficiently dense grid of strikes, which is often a limitation in real markets. To address this limitation, alternative methods have been developed, with Fourier inversion techniques playing a central role.

CHAPTER 3

Affine stochastic volatility jump-diffusion models

3.1. Background

Affine stochastic volatility jump-diffusion (ASVJD) models have emerged as a prominent class of models in quantitative finance, constituting a flexible framework for capturing the complex dynamics of financial markets and allowing a more accurate representation of market behaviour. These models combine the advantages of stochastic volatility models, affine models, and jump-diffusion models, providing a more realistic representation of both asset price and volatility dynamics. On the one hand, by incorporating the features of both continuous diffusion and discrete jump components, ASVJD models are capable of capturing extreme events and fat-tailed distributions and account for significant price movements and market shocks commonly observed in real-world financial markets, which are not adequately represented by traditional diffusion models. On the other hand, by also integrating stochastic volatility, in contrast to prior models that assumed constant volatility, ASVJD models are able to incorporate time-varying and mean-reverting volatility, accounting for the changing nature of volatility over time and acknowledging its tendency to revert to a long-term average. Finally, ASVJD models exhibit the analytical tractability inherent in affine models. The linear relationship between state variables and asset prices or returns provides these models with the flexibility to effectively capture complex market dynamics such as volatility clustering, the volatility smile, and interest rate term structures. Additionally, the affine structure yields closed-form solutions that are easy to implement and evaluate, allowing derivatives to be priced without relying on numerical approximation methods.

Throughout history, numerous models and frameworks have played pivotal roles in the development and evolution of affine stochastic volatility jump-diffusion models, each focusing on different aspects of financial modelling. Despite belonging to a different class of models and serving a different purpose, affine models, such as the Vasiček (1977), the square-root Cox-Ingersoll-Ross (1985), the Hull and White (1990), and the Chen and Scott (1995) models, have established the groundwork for modelling the term structure of interest rates with mean-reversion dynamics, offering closed-form solutions and analytical tractability to the ASVJD models. In the context of jump-diffusion models, the Merton (1976) model marked an important milestone, as it was the first to introduce the concept of jumps in asset prices, capturing sudden and discontinuous movements observed in financial markets. The inception of stochastic volatility models took place with the pivotal model for currency and equity prices proposed by Heston (1993), which played a fundamental role in advancing our understanding of volatility dynamics in quantitative finance

by incorporating a mean-reverting square root process for volatility. Although the original model did not incorporate jumps, it served as the basis for more advanced models and subsequent extensions. Bates (1996) extended the Heston (1993) model by introducing jumps in asset prices. Other notable models, including the Variance Gamma model proposed by Madan and Seneta (1990), the Ball and Torous (1995) model, Bates (1996), and Bakshi, Cao and Chen (1997), have contributed to the advancement of stochastic volatility modelling. These were all influential models. However, it was the ground-breaking framework presented by Duffie, Pan, and Singleton (2000) that solidified the understanding and application of affine stochastic volatility jump-diffusion models. This framework introduced affine jump-diffusion processes, emphasising the use of transform analysis, integrating both stochastic volatility dynamics and jumps into the modelling process and leveraging mathematical tools such as the Laplace transform to derive closed-form solutions for pricing various financial assets. By incorporating these elements, the Duffie, Pan, and Singleton (2000) framework offered a more sophisticated approach to modelling and pricing complex financial assets, providing a solid foundation for subsequent research.

3.2. Affine jump-diffusion framework

The framework proposed by Duffie, Pan, and Singleton (2000), introduced a powerful and widely accepted approach for modelling financial asset prices and their underlying dynamics. This approach, known as the general *affine jump-diffusion (AJD) framework*, marked a departure from earlier models by introducing the concept of affine jump-diffusion processes and incorporating stochastic volatility directly within the affine framework.

To effectively present this framework, it is crucial to first establish a precise definition of an affine process.

3.2.1. Definition and characterisation of affine processes

In simple terms, the affine process can be described as a Markov process, whose conditional log-characteristic function is an affine function of its initial state vector.

Recall that a Markov process, also known as a Markov chain, is a stochastic process that satisfies the so-called Markov property, which implies that the probability distribution of the next state depends solely on the current state and, therefore, is independent of the past states. This property makes Markov processes memoryless and allows them to be characterised by transition probabilities. As such, a Markov process can be defined in the following manner:

Definition 3.1 (*Markov process*). *Let $(\Omega, \mathcal{F}, \mathbb{P})$ be a probability space with a filtration $(\mathcal{F}_t)_{\geq 0}$ and let $(X_t)_{t\geq 0}$ be a stochastic process adapted to $(\mathcal{F}_t)_{\geq 0}$.*
We say that $(X_t)_{t\geq 0}$ is a Markov process if it satisfies the following Markov property, for every bounded and Borel-measurable function $f : \mathbb{R} \to \mathbb{R}$ and for $0 \leq s \leq t < +\infty$:

$$\mathbb{E}[(f(X_t)|\mathcal{F}_s)] = \mathbb{E}[(f(X_t)|X_s)]. \tag{3.1}$$

With the definition of the Markov process clarified, we can now define an affine process as:

Definition 3.2 (*Affine process).* *Consider the state space $\mathcal{D} = \mathbb{R}^m_{\geq 0} \times \mathbb{R}^n$. An affine process is a stochastically continuous, time-homogeneous Markov process $(X_t, \mathbb{P}^x)_{t\geq 0,\, x\in D}$ with state space $\mathcal{D}$, whose conditional characteristic function is an exponentially affine function of the state vector. That is, there exist $\mathbb{C}-$ and $\mathbb{C}^d$-valued functions $\phi(t,u)$ and $\psi(t,u)$, respectively, with jointly continuous t-derivatives satisfying*

$$\mathbb{E}\left[e^{u^\top X_T}|\mathcal{F}_t\right] = e^{\phi(T-t,u)+\psi(T-t,u)^\top X_t}, \tag{3.2}$$

for all $x \in \mathcal{D}$, and for all $(t,u) \in \mathbb{R}_{\geq 0} \times \mathbb{C}^d$ such that the expectation exists.

3.2.2. The affine jump-diffusion process

With a clear understanding of the affine process, we can now explore the *AJD framework*, starting with the description of affine jump-diffusion processes.
Let us consider a probability space $(\Omega, \mathcal{F}, \mathbb{Q})$ with a filtration $(\mathcal{F}_t)_{\geq 0}$, where $\mathbb{Q}$ represents the risk-neutral measure when the money market account is used as numeraire.
Additionally, assume X is a Markov process with n state variables, defined in the admissible state space $D \subset \mathbb{R}^n$, and solving the following stochastic differential equation (*SDE*), under the equivalent martingale measure $\mathbb{Q}$:

$$dX_t = \mu(X_t,t)dt + \sigma(X_t,t)dW_t^{\mathbb{Q}} + dZ_t^{\mathbb{Q}}, \tag{3.3}$$

where both $\mu(X_t,t) \in \mathbb{R}^n$ and $\sigma(X_t,t) \in \mathbb{R}^{n\times n}$ satisfy the typical growth and *Lipschitz* conditions[1]; $\{W_t^{\mathbb{Q}}\}_{t\geq 0}$ is a $\mathcal{F}_t$-standard Brownian motion and $\{Z_t^{\mathbb{Q}}\}_{t\geq 0}$ is a pure-jump process, both defined in $\mathbb{R}^n$ under the risk-neutral measure $\mathbb{Q}$. The jump process $\{Z_t^{\mathbb{Q}}\}_{t\geq 0}$ exhibit jumps with an arrival intensity $\lambda(X_t,t) \in [0,+\infty[$ and its associated jump-size state-independent distribution ν_t can be characterised by the following jump transform, provided the transform integral is well-behaved and satisfies certain well-defined conditions:

$$\theta(c,t) := \int_{\mathbb{R}^n} exp(c^\top.z)d\nu_t(z), \tag{3.4}$$

where z is a vector in $\mathbb{R}^n$ representing the variable of integration, c is a constant vector in $\mathbb{C}^n$ and $c^\top \in \mathbb{C}^n$ is the transpose of the complex vector c.

Following the framework proposed by Duffie, Pan, and Singleton (2000), we will now impose an affine structure on the jump-diffusion model.
Let us then assume the initial state vector X follows an affine jump-diffusion process, which means the drift vector $\mu(X_t,t)$, the 'instantaneous' covariance matrix, the jump intensities $\lambda(X_t,t)$ and the short-term interest rate $r(X_t,t)$, all have affine dependence on vector X. This dependence is determined by the coefficients (K,H,l,ρ) and can be represented as follows:

$$\mu(X_t,t) = K_0(t) + K_x(t)X_t, \tag{3.5}$$

[1]Growth conditions: $|\mu| \leq C(1+|x|)$ and $|\sigma| \leq C(1+|x|)$, for $\mu \in \mathbb{R}^n$ and $\sigma \in \mathbb{R}^n$.
Lipschitz conditions: $|\mu(x)-\mu(y)| \leq C|x-y|$ and $|\sigma(x)-\sigma(x)| \leq C|x-y|$, for $\mu \in \mathbb{R}^n$ and $\sigma \in \mathbb{R}^n$.

for $K_0(t) \in \mathbb{R}^n$ and $K_x(t) \in \mathbb{R}^{n\times n}$,

$$\sigma(X_t,t)\sigma(X_t,t)^\top = H_0(t) + \sum_{k=1}^{n} H_x^k(t)(X_t)_k, \tag{3.6}$$

where $H_0(t) \in \mathbb{R}^{n\times n}$ and $H_x^k(t) \in \mathbb{R}^{n\times n}$ are symmetric matrices (for $k = 1, ..., n$),

$$\lambda(X_t,t) = l_0(t) + l_x(t)^\top X_t, \tag{3.7}$$

where $l_0(t) \in \mathbb{R}$, and $l_x(t) \in \mathbb{R}^n$, and

$$r(X_t,t) = \rho_0(t) + \rho_x(t)^\top X_t, \tag{3.8}$$

where $\rho_0(t) \in \mathbb{R}$, and $\rho_x(t) \in \mathbb{R}^n$.
Note that with the coefficients (K, H, l, ρ) and a given initial condition X_0, it is possible to fully determine the distribution of X. Moreover, the parameter vector $\mathcal{X}_{\mathbb{Q}}$=($K^{\mathbb{Q}}$,$H^{\mathbb{Q}}$,$l^{\mathbb{Q}}$,$\theta^{\mathbb{Q}}$,ρ) allows us to characterise both the 'risk-neutral' distribution and the effects associated with any discounts, and to determine the following complex-valued transform, under the equivalent martingale measure $\mathbb{Q}$:

$$\psi^{\mathcal{X}_{\mathbb{Q}}}(u,t,T,X_t) := \mathbb{E}_{\mathbb{Q}}\left[exp\left[-\int_t^T r(X_s,s)ds\right] exp\left(u^\top X_T\right)\Big|\mathcal{F}_t\right], \tag{3.9}$$

where $u \in \mathbb{C}^n$ and $t \leq T$. Through the $\psi^{\mathcal{X}_{\mathbb{Q}}}$ transform, we can accurately and efficiently price a diverse and extensive set of European-style options. In particular, setting $u = 0$ in equation (3.9), we get the following risk-neutral price for a zero coupon bond

$$\psi^{\mathcal{X}_{\mathbb{Q}}}(0,t,T,X_t) := \mathbb{E}_{\mathbb{Q}}\left[exp\left[-\int_t^T r(X_s,s)ds\right]\Big|\mathcal{F}_t\right], \tag{3.10}$$

which is usually denoted by $P(t,T)$.

In this context, under the technical regularity conditions specified in Duffie, Pan, and Singleton (2000) Proposition 1, an exponential-affine solution can be derived for the transform $\psi^{\mathcal{X}_{\mathbb{Q}}}$ in equation (3.9), leading to the following expression (for a detailed proof of the one-dimensional case see Proposition C.1) :

$$\psi^{\mathcal{X}_{\mathbb{Q}}}(u,t,T,X_t) = exp\left[\alpha(t,T,u) + \beta(t,T,u)^\top X_T\right], \tag{3.11}$$

where $\beta \in \mathbb{C}^n$ and $\alpha \in \mathbb{C}$ satisfy the following complex-valued ordinary differential equations (ODEs)[2]:

$$\dot{\beta}(t,T,u) = \rho_x(t) - K_x(t)^\top\beta(t,T,u) - \frac{1}{2}\left[\beta(t,T,u)H_x(t)\beta(t,T,u)\right] - \left[\theta(\beta(t,T,u),t) - 1\right] l_x(t), \tag{3.12}$$

[2]The term $\beta(t,T,u)H_x(t)\beta(t,T,u)$ represents a vector in $\mathbb{C}^n$, whose k-th element is given by $\sum_{i,j=1}^n(\beta(t,T,u))_i(\beta(t,T,u))_j\left(H_x^{(k)}(t)\right)_{i,j}$, where $(\beta)_i$ is the i^{th} component of the vector β, and $\left(H_x^{(k)}(t)\right)_{i,j}$ is the element in the i^{th} row and j^{th} column of the matrix $H_x^{(k)}(t)$.

and

$$\dot{\alpha}(t,T,u) = \rho_0(t) - \beta(t,T,u)^\top K_0(t) - \frac{1}{2}\beta(t,T,u)^\top H_0(t)\beta(t,T,u) - [\theta(\beta(t,T,u),t) - 1]\, l_0(t), \tag{3.13}$$

constrained by the boundary conditions $\beta(T,T,u) = u$ and $\alpha(T,T,u) = 0$. Note that, for simplicity of notation, we henceforth omit the superscript and denote the transform simply by ψ.

Now, to ensure that the transform ψ defined in equation (3.9) takes the exponential–affine form in equation (3.11), the parameter vector $(K^{\mathbb{Q}}, H^{\mathbb{Q}}, l^{\mathbb{Q}}, \theta^{\mathbb{Q}}, \rho)$ must be well-behaved at (u,T), as established in Duffie, Pan, and Singleton (2000) Proposition 1. To fulfil this requirement, two prerequisites must be met. First, the ODEs (3.12) and (3.13) must admit unique solutions which we denote by β and α. Second, the technical regularity conditions *(i) to (iii)* outlined in the subsequent definition need to be satisfied.

Definition 3.3. *The parameter vector* $(K^{\mathbb{Q}}, H^{\mathbb{Q}}, l^{\mathbb{Q}}, \theta^{\mathbb{Q}}, \rho)$ *is well-behaved at* $(u,T) \in \mathbb{C}^n \times [0, +\infty[$ *if equations (3.12) and (3.13) are solved uniquely by* β *and* α*, and if*

(i) $\mathbb{E}\left[\int_0^T \left|\gamma_t\right| dt\right] < +\infty$*, where* $\gamma_t = \Psi_t(\theta(\beta(t)) - 1)\lambda(X_t)$*,*

(ii) $\mathbb{E}\left[\left(\int_0^T \eta_t^\top \eta_t dt\right)^{\frac{1}{2}}\right] < +\infty$*, where* $\eta_t = \Psi_t \beta(t)^\top \sigma(X_t)$*, and*

(iii) $\mathbb{E}\left[\left|\Psi_T\right|\right] < +\infty$*, where* $\Psi_t = exp\left(-\int_0^t r(X_s,s)ds\right) e^{\alpha(t)+\beta(t)^\top X(t)}$.

The ODEs (3.12) and (3.13) can be easily inferred by applying Ito's formula to equation (3.11).

3.2.3. Pricing solution for plain-vanilla European style options

The Duffie, Pan, and Singleton (2000) framework proposes a single (and one-dimensional) integral pricing solution for plain-vanilla European-style options. In particular, under the risk-neutral measure $\mathbb{Q}$, the price of a European-style call option with maturity T and strike K can be expressed in terms of the transform ψ through the auxiliary function $G_{a,b}(\cdot)$. The call price at time 0 is given by:

$$C_0 = G_{\varepsilon(i),-\varepsilon(i)}(-\ln(K); X_0, T, \chi_{\mathbb{Q}}) - K\, G_{0,-\varepsilon(i)}(-\ln(K); X_0, T, \chi_{\mathbb{Q}}), \tag{3.14}$$

where $\varepsilon(i)$ denotes the ith canonical basis vector in $\mathbb{R}^d$ (i.e., the unit vector with 1 in the ith coordinate and 0 elsewhere), and $\chi_{\mathbb{Q}} = (K^{\mathbb{Q}}, H^{\mathbb{Q}}, l^{\mathbb{Q}}, \theta^{\mathbb{Q}}, \rho)$ is the parameter vector under the risk-neutral measure $\mathbb{Q}$.

The auxiliary function $G_{a,b}$ appearing in equation (3.14) is defined by:

$$G_{a,b}(y; X_0, T, \chi) = \frac{\psi^\chi(a, X_0, 0, T)}{2} - \frac{1}{\pi}\int_0^\infty \mathrm{Im}\left[\frac{\psi^\chi(a + i\nu b, X_0, 0, T)e^{-i\nu y}}{\nu}\right] d\nu, \tag{3.15}$$

with $\mathrm{Im}(\cdot)$ denoting the imaginary part of a complex number and ψ^χ is given by equation (3.11).

CHAPTER 4

Option valuation using Fourier transform methods

4.1. Background

Since the Black-Scholes model was first introduced in 1973, numerous researchers have proposed extensions to refine and expand the methodologies underpinning option valuation. This led to novel ideas and approaches aimed at enhancing the precision and applicability of option pricing techniques.

A noteworthy evolution in this trajectory occurred with the integration of Fourier analysis, as a powerful computational tool for ascertaining option prices. Originally developed by Joseph Fourier in the early 19th century, Fourier transforms have found profound applications in finance, especially in option valuation, where intricate pricing models demand efficient and precise calculations.

Influential works by authors such as Bakshi and Chen (1997), Scott (1997), Bates (1996), Heston (1993), and Chen and Chen and Scott (1992) have demonstrated the efficacy of using Fourier analysis in option pricing. They utilise Fourier-analytic solutions to express option prices in terms of Fourier-inversion integrals, which are then evaluated numerically. However, while these papers yielded valuable insights, they did not fully exploit the potential of the fast Fourier transform (FFT), a computational technique pioneered by Walker (1996) that has revolutionised scientific computing. Moreover, the methodology employed in most of these studies involves the decomposition of the option price into probability components, which, although conceptually appealing, is numerically undesirable due to the discontinuity of payoffs.

In response, Carr and Madan (1999) presented an approach, capitalising on the efficiency of the FFT to enhance the precision and speed of option valuation. Unlike earlier methods, which often required numerical approximations, they introduced a method that leveraged the analytical understanding of the characteristic function of the risk-neutral density, refining option pricing further.

Following this, a large and growing family of financial models appeared, which relied on the characteristic function of state variables to accurately determine option prices. Among them, Lee (2004) work stands out as a significant milestone. In his paper, Lee presents a framework that generalises Carr and Madan (1999), combining it with extensions of relevant parts from Duffie, Pan, and Singleton (2000), Lewis (2001), and Bakshi and Madan (2000), and develops error bounds and error minimization strategies.

On one hand, Lee (2004) expanded the use of Carr-Madan's analytic calculation of Fourier transforms to include all derivative structures discussed in Duffie, Pan, and Singleton (2000), allowing for payoffs dependent on multidimensional state variables.

On the other hand, assuming Bakshi and Madan (2000) discounted characteristic function, the Carr-Madan model was extended to handle stochastic interest rates.

Finally, building upon Lewis (2001) observation that option price representations as transforms can be interpreted as contour integrals in the complex plane, Lee (2004) developed alternative pricing formulas by adjusting these contours, involving integrals over (a translate of) the real line, and resulting in a unified pricing formula.

In this chapter, we will present and study the Lee (2004) framework, using Lee's unified pricing formula to price a European-style call option.

4.2. Lee (2004) framework

In this section, we begin by setting forth the option pricing problem and outlining the main assumptions. Following Lee's work, we do not assume specific characteristic functions for the underlying state variables, nor do we assume a particular probability distribution with a specified density. The state variables may be one-dimensional or multidimensional, and time and the state space may be continuous or discrete. Additionally, we consider that interest rates and dividends may be deterministic or stochastic. Therefore, as long as the discounted characteristic function for such dynamics is known, option prices are computable.

In our analysis, we will focus solely on a single type of payoff. The objective is to numerically calculate the time-t price C_t of a European call option, which yields a random payment C_T at time T. To this end, let us assume a filtered probability space $(\Omega, \mathbb{Q}, \mathcal{F}_t)$. In this space, Ω represents the set of all possible outcomes, $\mathcal{F}_t$ denotes the σ-algebra of events at a time-t, and $\mathbb{Q}$ is the risk-neutral measure, where the numeraire is the money market account. Let $M_t := e^{\int_0^t r_s ds}$ represent the time-t value of the numeraire under this measure, and let r_t be the interest rate process, which can be stochastic. Finally, assume $B_t := \mathbb{E}[M_T^{-1} M_t | \mathcal{F}_t] = P(t,T)$ is the time-t value of a discount bond maturing at T.

Having established the context, we now introduce the numeraire and the martingale measures within Lee's framework.

4.2.1. Numeraires and Martingale measures

The risk-neutral probability measure $\mathbb{Q}$ is widely used in finance for valuing financial instruments. Under this measure, any asset price discounted by the money market account is a $\mathbb{Q}$-martingale. With this understanding, we can express the option value at time-t as:

$$C_t = \mathbb{E}_{\mathbb{Q}}\left[M_T^{-1} M_t C_T | \mathcal{F}_t\right] = \mathbb{E}_{\mathbb{Q}}\left[e^{-\int_t^T r_s ds} C_T | \mathcal{F}_t\right]. \tag{4.1}$$

Similarly, the value of the bond at time-0 can be represented by:

$$B_t = \mathbb{E}_{\mathbb{Q}}\left[M_T^{-1} M_t | \mathcal{F}_t\right] = \mathbb{E}_{\mathbb{Q}}\left[e^{-\int_t^T r_s ds} | \mathcal{F}_t\right] = P(t,T). \tag{4.2}$$

However, for instruments with more complex and exotic payoffs, the risk-neutral measure may not always be the most suitable approach. In such cases, an equivalent martingale measure is preferable. Within his framework, Lee proposes a transition from the risk-neutral measure $\mathbb{Q}$ to the forward measure $\mathbb{Q}^T$. In line with Lee's proposition, we will

adjust the numeraire accordingly, using the *Radon-Nikodým* derivative of $\mathbb{Q}^T$ with respect to $\mathbb{Q}$:

$$\left.\frac{d\mathbb{Q}^T}{d\mathbb{Q}}\right|_{\mathcal{F}_t} := \frac{N_T/N_t}{M_T/M_t} = \frac{B_T}{B_t}\frac{e^{\int_0^t r_s ds}}{e^{\int_0^T r_s ds}} = \frac{1}{B_t}e^{-\int_t^T r_s ds}, \tag{4.3}$$

where N denotes the new numeraire B_t (i.e., the price of a T-maturity discount bond), and M represents the old numeraire M_t (i.e., the money-market account as in Appendix D.2). Note that under this new T-forward measure, the discounted price of any asset is a $\mathbb{Q}^T$-martingale. With this new insight, we can establish the following relationship between expectations under the two measures:

$$\mathbb{E}_{\mathbb{Q}^T}\left[C_T\right] = \mathbb{E}_{\mathbb{Q}}\left[\frac{d\mathbb{Q}^T}{d\mathbb{Q}}C_T|\mathcal{F}_t\right] = \mathbb{E}_{\mathbb{Q}}\left[\frac{1}{B_t}e^{-\int_t^T r_s ds}C_T|\mathcal{F}_t\right]. \tag{4.4}$$

Based on this, we can now reformulate the option price using the new forward measure. As a result, equation (4.1) becomes:

$$C_t = B_t\mathbb{E}_{\mathbb{Q}^T}\left[C_T|\mathcal{F}_t\right]. \tag{4.5}$$

It is worth noting that when deterministic interest rates are applied, the forward measure is equal to the risk-neutral measure $\mathbb{Q}$. In our case, however, interest rates can be stochastic, and the measures are not necessarily identical. Nonetheless, the forward measure has the significant advantage of discounting outside the expectation.

4.2.2. The discounted characteristic function

In the Lee (2004) framework, the cornerstone of option valuation lies in the *discounted characteristic function* of the state variable. Unlike other characteristic functions in probability theory, its definition contains a discount factor within the expectation, which is required for pricing under stochastic interest rates. Let us then start by defining these functions.

Definition 4.1 (Discounted characteristic function). *Assume X is an $\mathbb{R}^n$-valued random variable and let A_X denote the interior of the set $\{\nu \in \mathbb{R}^n : \mathbb{E}e^{\nu\cdot X_T} < \infty\}$. Also, let the complex vectors with negated imaginary parts in A_X form the following "strip" or "tube" in the complex plane:*

$$\Lambda_X := \{\zeta \in \mathbb{C}^n : -Im(\zeta) \in A_X\}. \tag{4.6}$$

Thus, the discounted characteristic function of X, with respect to a discount factor $e^{-\int_t^T r_s ds}$, is defined as the function $f : \Lambda_X \to \mathbb{C}$, where:

$$f_t(\zeta) := \mathbb{E}_{\mathbb{Q}}[e^{-\int_t^T r_s ds}e^{i\zeta\cdot X_T}|\mathcal{F}_t]. \tag{4.7}$$

An important special case occurs when $\zeta = 0$. In this case, equation (4.7) reduces to:

$$f_t(0) = \mathbb{E}_{\mathbb{Q}}\left[e^{-\int_t^T r_s ds}\middle|\mathcal{F}_t\right] = P(t,T), \tag{4.8}$$

which is precisely the time-t price of a T-maturity discount bond. Note that under deterministic interest rates, this simplifies to $f_t(0) = e^{-r(T-t)}$. This identity also provides

a convenient normalization that links the risk-neutral and forward measures. Based on this definition, it is possible to determine the characteristic function, but now in relation to the forward measure $\mathbb{Q}^T$.

Definition 4.2 (Characteristic function under the forward measure). *Assume again that X remains an $\mathbb{R}^n$-valued random variable. Let A_X denote the interior of the set $\{\nu \in \mathbb{R}^n : \mathbb{E}[e^{\nu \cdot X_T}] < \infty\}$. Additionally, let the complex vectors with negated imaginary parts in A_X form the "strip" $\Lambda_X := \{\zeta \in \mathbb{C}^n : -Im(\zeta) \in A_X\}$.*
Moreover, consider the discounted characteristic function of X, $f : \Lambda_X \to \mathbb{C}$ defined in equation (4.7). Using the price of a T-maturity discount bond $B_t = P(t,T)$ from equation (4.8) as the numeraire, we obtain:

$$\frac{f_t(\zeta)}{f_t(0)} := \mathbb{E}_{\mathbb{Q}^T}[e^{i\zeta \cdot X_T} | \mathcal{F}_t], \tag{4.9}$$

which (for ζ restricted to $\mathbb{R}^n$) is the usual characteristic function of X with respect to the forward measure $\mathbb{Q}^T$.

Proof. The proof is a direct application of Abstract Bayes' theorem for change of probability measure in Theorem D of Appendix D.1 (see also Geman et al. (1995, Corollary 2). □

Theorem 4.1. *The discounted characteristic function f is well-defined and analytic in L_X, which is a convex set. As a result, partial derivatives of f may be taken through the expectation.*

Proof. Following Lee (2004, Theorem 4.1), the proof can be found in Zemanian (1966, Theorems 4 and 5). □

Remark 4.1 (Notation bridge and connection to the literature). *In the option-pricing literature it is common to express the marginal characteristic function of the terminal log price of the underlying asset under a martingale measure $\mathbb{Q}_j$ as*

$$f_j(T, \phi; X_t) := \mathbb{E}^{\mathbb{Q}_j}\left[e^{i\phi X_T} \middle| \mathcal{F}_t\right], \tag{4.10}$$

with $j = 1$ denoting the risk-neutral measure, $j = 2$ the T-forward measure, for all $\phi \in \mathbb{C}$ for which the expectation is well defined, where $i = \sqrt{-1}$.

Lee's framework, however, uses a slightly different notation, so we spell out the link. Because his approach is formulated under the T-forward measure $\mathbb{Q}^T$, we focus only on the marginal characteristic function f_2. For convenience, we can write:

$$f_2(T, \phi; X_t) = \frac{f_t(\phi)}{f_t(0)}, \tag{4.11}$$

which is precisely the characteristic function given in Definition 4.2. For simplicity and to be consistent with Chapter 5, from this point forward we denote this characteristic function by $f_2(t, \phi) := f_t(\phi)/f_t(0)$. Additionally, henceforth we use ϕ (instead of ζ) for the complex transform variable.

4.2.3. The option pricing formula

Having defined the *discounted characteristic function*, our focus now turns to deriving the general pricing formula for evaluating a European-style call option. First, we will define the payoff and the call price in terms of the characteristic function of X_t. Next, we will calculate analytically the Fourier transform of the call price function, damped to enforce integrability. Finally, inverting this Fourier transform and then undamping, we will obtain the option price as a function of the strike price.

4.2.3.1 Payoff definition

Let the state variable X be a $\mathcal{F}_T$-measurable random variable with values in $\mathbb{R}^n$. Assuming a payoff function $G : \mathbb{R}^n \times \mathbb{R} \to \mathbb{R}$, the time-$t$ price of an option paying $G(X, k)$ at the maturity T can be defined as:

$$C_G(k) := B_t \mathbb{E}_{\mathbb{Q}^T}[G(X, k)|\mathcal{F}_t], \tag{4.12}$$

where k is the trigger of the contract.
Since our analysis solely focuses on the European-style call option, we can express the payoff as:

$$G(X, k) = (e^X - e^k)^+, \text{ with } X \in \mathbb{R}, \tag{4.13}$$

where k denotes the logarithm of the strike price K. Note that if we choose X to be a bond yield, the logarithm of a stock price, or even an FX rate, we will obtain a call on a stock, bond, or currency, respectively.

4.2.3.2 Option valuation using Fourier transforms

In Lee (2004) framework, Fourier analysis plays a fundamental role in option valuation. In this paper, characteristic functions are represented as Fourier transforms of probability density functions and typically have an analytic extension (a generalised Fourier transform) $u \to z \in \mathbb{C}$, regular in some strip Λ_X parallel to the real z-axis (see Lewis (2001)). Another central idea in Lee's approach is the recognition that option payoff functions also have simple generalised Fourier transforms. This aspect will prove to be of utmost importance because, as we will see, the usual Fourier transform does not exist. To better understand this issue, let us consider the Fourier transform (see definition A.3) of the initial option price $C_G(k)$:

$$\hat{C}_G(u) = \int_{-\infty}^{+\infty} e^{iuk} C_G(k) dk = \int_{-\infty}^{X} e^{iuk} B_t \mathbb{E}_{\mathbb{Q}^T} \left[\left(e^X - e^k \right) |\mathcal{F}_t \right] dk. \tag{4.14}$$

Solving the previous expression leads to the following result, as detailed in Proposition D.1 of Appendix D:

$$\hat{C}_G(u) = \mathbb{E}_{\mathbb{Q}^T} \left[B_t \left(e^{(iu+1)X} \left(\frac{1}{iu} - \frac{1}{iu+1} \right) - \lim_{t \to -\infty} \left(\frac{e^{iut+X}}{iu} + \frac{e^{(iu+1)t}}{iu+1} \right) \right) |\mathcal{F}_t \right]. \tag{4.15}$$

It is easy to note that the transform $\hat{C}_G(u)$ does not exist since the call price $C_G(k)$ does not decay as k approaches $-\infty$, indicating that the call pricing function is not square-integrable. To address this problem, we should adopt an approach originally proposed by Carr and Madan (1999), which involves using a modified call price. Thus, following Lee's terminology and assuming a *damping constant* $\alpha > 0$, we define the *damped option price* function $c_{\alpha,G} : \mathbb{R} \to \mathbb{R}$ as follows:

$$c_{\alpha,G}(k) := e^{\alpha k} C_G(k). \tag{4.16}$$

This definition ensures that the *damped option price* $c_{\alpha,G}$ is integrable in k over the entire real line, guaranteeing that its Fourier transform exists and is well-defined (see Remark 4.1), provided that α is chosen appropriately. As a result, the Fourier transform of the *damped option price* can be represented as $\hat{c}_{\alpha,G} \colon \mathbb{R} \to \mathbb{C}$ and obtained using the following definition:

$$\hat{c}_{a,G}(u) := \int_{-\infty}^{\infty} e^{iuk} c_{\alpha,G}(k) dk. \tag{4.17}$$

Now, substituting in the *damped option price* function, given by equation (4.16), and replacing $C_G(k)$ by the corresponding valuation formula (4.12), adjusted by the payoff function (4.13), yields:

$$\hat{c}_{\alpha,G}(u) = \int_{-\infty}^{+\infty} e^{iuk} e^{\alpha k} C_G(k) dk = \int_{-\infty}^{X} e^{iuk} e^{\alpha k} B_t \mathbb{E}_{\mathbb{Q}^T} \left[\left(e^X - e^k \right) | \mathcal{F}_t \right] dk. \tag{4.18}$$

Applying *Fubini's Theorem* to adjust the order of integration and solving the integral, we arrive at the following outcome:

$$\begin{aligned} \hat{c}_{\alpha,G}(u) =& B_t \mathbb{E}_{\mathbb{Q}^T} \left[\left[\frac{e^{(iu+\alpha)k+X}}{iu+\alpha} - \frac{e^{(iu+\alpha+1)k}}{iu+\alpha+1} \right]_{-\infty}^{X} | \mathcal{F}_t \right] \\ =& B_t \mathbb{E}_{\mathbb{Q}^T} \left[\left(\frac{e^{(iu+\alpha+1)X}}{iu+\alpha} - \frac{e^{(iu+\alpha+1)X}}{iu+\alpha+1} \right) | \mathcal{F}_t \right]. \end{aligned} \tag{4.19}$$

The introduction of the exponential damping factor $e^{\alpha k}$ produces now a convergent integral inside the expectation. This way we guarantee that:

$$\int_{-\infty}^{+\infty} |\hat{c}_{\alpha,G}(u)| \, dk = \int_{-\infty}^{+\infty} |e^{\alpha k} C_G(k)| \, dk < \infty. \tag{4.20}$$

This condition ensures that $\hat{c}_{\alpha,G}(u)$ is integrable, thereby establishing the existence of the Fourier transform for the damped option price.

Finally, using the discounted characteristic function of X with respect to the forward measure $\mathbb{Q}^T$ presented in Definition 4.2, we obtain the following result for the Fourier transform of the damped option price:

Theorem 4.2. ***(Fourier transform of the damped option price)*** *Assume a damping constant $\alpha > 0$. For any such α, the Fourier transform $\hat{c}_{\alpha,G}(u)$ of the damped option price $c_{\alpha,G}(k)$ exists and can be represented as follows:*

$$\hat{c}_{\alpha,G}(u) = \frac{f_t \left(u - (\alpha + 1) i \right)}{\alpha^2 + \alpha - u^2 + i \left(2\alpha + 1 \right) u}. \tag{4.21}$$

Proof. The complete proof for the Fourier transform of the *damped option price* can be found in Proposition D.2 of Appendix D. □

With the Fourier transform of the damped option price established, option prices can now be obtained using the inverse Fourier transform (see definition A.3).

Theorem 4.3. ***(Inverse Fourier transform for the damped option price)*** *Let $\alpha > 0$ be a damping constant. For any such α, both the damped option price function $c_{\alpha,G}$ and its Fourier transform $\hat{c}_{\alpha,G}$ exist and belong to L^1, ensuring they are absolutely integrable over their entire domain (i.e., $\int_{-\infty}^{+\infty} |c_{\alpha,G}|dk < \infty$ and $\int_{-\infty}^{+\infty} |\hat{c}_{\alpha,G}|du < \infty$).*
Then, the call option price is determined by:

$$C_G(k) = \frac{e^{-\alpha k}}{2\pi} \int_{-\infty}^{+\infty} e^{-iuk} \hat{c}_{\alpha,G}(u) du = \frac{e^{-\alpha k}}{\pi} \int_{0}^{+\infty} Re\left[e^{-iuk} \hat{c}_{\alpha,G}(u)\right] du. \tag{4.22}$$

Proof. The proof of the inverse Fourier transform used to obtain the damped option price can be found in Theorem D.2 in Appendix D. □

4.2.3.3 Transforms of option prices as contour integrals in the complex plane

The transform representations of option prices may be interpreted as contour integrals in the complex plane. By shifting the contours and applying Residual Calculus it is possible to generate alternative pricing formulae.

Proposition 4.1. ***(Complex Fourier transform of the unmodified option price)*** *Let Γ be the set $\Gamma_{X,G} := \{z \in \mathbb{C} : -Im(z)b_0 + b_1 \in A_X\}$. For a positive α, the complex Fourier transform of the unmodified option price $C_G(k)$, can be specified as $\hat{\mathscr{C}_G} \colon \Gamma_{X,G} \to \mathbb{C}$, and its definition is given by the following equation:*

$$\hat{\mathscr{C}_G}(z) := \frac{f_t(z-i)}{iz - z^2}. \tag{4.23}$$

Corollary 4.1. ***(Insights from the complex Fourier transform proposition)*** *Following Proposition D.3, which sets the link between the Fourier transform of the damped option price specified in equation* (D.12)*, and the complex Fourier transform outlined in equation* (D.20)*, a relationship can be established between the two definitions, knowing, once again, that $z = u - \alpha i$.*
Therefore, for a positive α and $\alpha b_0 + b_1 \in A_X$ (with $b_0 := 1, b_1 := 1$), we have:

$$\hat{c}_{\alpha,G}(u) = \hat{\mathscr{C}_G}(u - \alpha i), \tag{4.24}$$

and hence, for $z \in \Gamma$, such that $-Im(z) > 0$, we can also derive the following representation for the complex Fourier transform of the unmodified option price $C_G(k)$:

$$\hat{\mathscr{C}_G}(z) = \int_{-\infty}^{+\infty} e^{izk} C_G(k) dk. \tag{4.25}$$

Proof. The proof for the corollary is detailed in Theorem D.1 of Appendix D. □

Theorem 4.4. ***(Complex inverse Fourier transform for the unmodified option price)*** *Let us consider the set* $\Gamma_{X,G} := \{z \in \mathbb{C} : -Im(z)b_0 + b_1 \in A_X\}$ *and define the complex Fourier transform of the unmodified option price* $C_G(k)$ *as* $\hat{\mathscr{C}_G} := \Gamma_{X,G} \to \mathbb{C}$. *Then, the unmodified call option price can be obtained by integrating the complex inverse Fourier transform* $\hat{\mathscr{C}_G}(z)$ *along the contour* $Im(z) = -\alpha$ *in the complex plane, as follows:*

$$C_G(k) = \frac{1}{2\pi}\int_{-\infty-\alpha i}^{+\infty-\alpha i} e^{-ikz}\hat{\mathscr{C}_G}(z)dz = R_{\alpha,G} + \frac{1}{\pi}\int_{0-\alpha i}^{+\infty-\alpha i} Re\left[e^{-ikz}\hat{\mathscr{C}_G}(z)\right]dz, \tag{4.26}$$

where

$$R_{\alpha,G} := \begin{cases} f_t(-i) - e^k f_t(0) & \text{if } \alpha < -1 \\ f_t(-i) - \frac{e^k f_t(0)}{2} & \text{if } \alpha = -1 \\ f_t(-i) & \text{if } -1 < \alpha < 0 \\ \frac{f_t(-i)}{2} & \text{if } \alpha = 0 \\ 0 & \text{if } \alpha > 0 \end{cases} \tag{4.27}$$

Proof. The proof for the Theorem 4.4 is detailed in section D.3.2 of Appendix D. □

4.2.3.4 Pricing formula deduction

Having considered all scenarios with different alpha parametrisations, we find that the optimal fit between theoretical and market prices occurs when $\alpha = -1$. This choice lies on the admissible strip implied by Lee (2004), ensuring that the required exponential moments exist and that the transform is well defined. Fixing $\alpha = -1$ places the parameter at the boundary that still guarantees integrability, provides sufficient tail decay for stable numerical quadrature, yields the simplest boundary correction $R_{\alpha,G}$, and avoids both over and under-damping of the payoff. Taken together, these considerations make $\alpha = -1$ the most appropriate choice for pricing European-style plain-vanilla options.

Henceforth, we use the corresponding option pricing parametrisation as a basis to derive the final pricing formula, crucial for calibrating diverse theoretical models.

Thus, using the $\alpha = -1$ Lee (2004) formula for the *unmodified option price* as a starting point, we have:

$$C_G(k) = \frac{1}{\pi}\int_{0+1i}^{+\infty+1i} \text{Re}\left[e^{-ikz}\hat{\mathscr{C}_G}(z)\right]dz + f(-i) - \frac{e^k f_t(0)}{2}. \tag{4.28}$$

As a first step, we substitute the complex Fourier transform $\hat{\mathscr{C}_G}(z)$ of the unmodified option price by its definition, specified in Proposition 4.1.

Knowing that the *discounted characteristic function* of x under $\mathbb{Q}$ is given by $f(t,\zeta) := f_t(\zeta) = \mathbb{E}^{\mathbb{Q}}\left[e^{-\int_t^T r_s ds}e^{i\zeta X}|\mathcal{F}_t\right]$, we can find the price of a T-maturity discount bond $B_t := f_t(0) = \mathbb{E}^{\mathbb{Q}}\left[e^{-\int_t^T r_s ds}|\mathcal{F}_t\right]$, used as the numeraire under the $T-$ forward measure, and write $f_t(-i)$ as $\mathbb{E}^{\mathbb{Q}}\left[e^{-\int_t^T r_s ds}e^{X}|\mathcal{F}_t\right]$. Finally, representing the discount bond $f_t(0)$ by $P(t,T)$,

denoting the strike e^k by K and e^X by S_T, equation (4.28) can be rewritten as follows:

$$C_G(k) = \frac{1}{\pi}\int_{0+1i}^{+\infty+1i} \text{Re}\left[\frac{e^{-ikz}f(z-i)}{iz-z^2}\right]dz + \mathbb{E}^{\mathbb{Q}}\left[e^{-\int_t^T r_s ds}e^X|\mathcal{F}_t\right] - \frac{e^k P(t,T)}{2}. \quad (4.29)$$

Using, again, the discounted characteristic function of X, this time for $\zeta = z - i$, we have that $f_t(z-i) = \mathbb{E}^{\mathbb{Q}}\left[e^{-\int_t^T r_s ds}e^{i(z-i)X}|\mathcal{F}_t\right]$. Performing a change of variable to the first right-hand side integral, such that $z = \phi + i$, then:

$$C_G(k) = \frac{1}{\pi}\int_0^{+\infty} \text{Re}\left[\frac{e^{-ik(\phi+i)}\mathbb{E}^{\mathbb{Q}}\left[e^{-\int_t^T r_s ds}e^{i\phi X}|\mathcal{F}_t\right]}{i(\phi+i)-(\phi+i)^2}\right]d\phi + \mathbb{E}^{\mathbb{Q}}\left[e^{-\int_t^T r_s ds}e^X|\mathcal{F}_t\right] - \frac{e^k P(t,T)}{2}. \quad (4.30)$$

Recalling that $e^X = S_T$ and $e^k = K$, we have:

$$\begin{aligned} C_G(K) &= \frac{1}{\pi}\int_0^{+\infty} \text{Re}\left[\frac{e^{-i\ln(K)\phi}K\mathbb{E}^{\mathbb{Q}}\left[e^{-\int_t^T r_s ds}e^{i\phi\ln(S_T)}|\mathcal{F}_t\right]}{i\phi - 1 - (\phi^2 + 2\phi i + i^2)}\right]d\phi + \mathbb{E}^{\mathbb{Q}}\left[e^{-\int_t^T r_s ds}S_T|\mathcal{F}_t\right] - \frac{KP(t,T)}{2} \\ &= \frac{K}{\pi}\int_0^{+\infty} \text{Re}\left[\frac{e^{-i\ln(K)\phi}\mathbb{E}^{\mathbb{Q}}\left[e^{-\int_t^T r_s ds}e^{i\phi\ln(S_T)}|\mathcal{F}_t\right]}{-\phi^2 - \phi i}\right]d\phi + \mathbb{E}^{\mathbb{Q}}\left[e^{-\int_t^T r_s ds}S_T|\mathcal{F}_t\right] - \frac{KP(t,T)}{2} \\ &= -\frac{K}{\pi}\int_0^{+\infty} \text{Re}\left[\frac{e^{-i\ln(K)\phi}\mathbb{E}^{\mathbb{Q}}\left[e^{-\int_t^T r_s ds}e^{i\phi\ln(S_T)}|\mathcal{F}_t\right]}{\phi^2 + \phi i}\right]d\phi + S_t e^{-q(T-t)} - \frac{KP(t,T)}{2}, \end{aligned} \quad (4.31)$$

since by risk-neutral valuation the discounted $S_t e^{qt}$ must be a $\mathbb{Q}$-martingale. Additionally, since $f_t(\phi) = \mathbb{E}^{\mathbb{Q}}\left[e^{-\int_t^T r_s ds}e^{i\phi\ln(S_T)}|\mathcal{F}_t\right]$ and by Proposition (4.9), $\frac{f_t(\phi)}{f_t(0)} = \mathbb{E}^{\mathbb{Q}^T}\left[e^{i\phi\ln(S_T)}|\mathcal{F}_t\right]$, we have:

$$\begin{aligned} C_G(K) &= -\frac{Kp(t,T)}{\pi}\int_0^{+\infty} \text{Re}\left[\frac{e^{-iln(K)\phi}}{\phi^2 + \phi i}\frac{\mathbb{E}^{\mathbb{Q}}\left[e^{-\int_t^T r_s ds}e^{i\phi\ln(S_T)}|\mathcal{F}_t\right]}{f_t(0)}\right]d\phi + S_t e^{-q(T-t)} - \frac{KP(t,T)}{2} \\ &= -\frac{Kp(t,T)}{\pi}\int_0^{+\infty} \text{Re}\left[e^{-iln(K)\phi}\frac{\mathbb{E}^{\mathbb{Q}^T}\left[e^{i\phi\ln(S_T)}|\mathcal{F}_t\right]}{\phi^2 + \phi i}\right]d\phi + S_t e^{-q(T-t)} - \frac{KP(t,T)}{2}. \end{aligned} \quad (4.32)$$

Defining the characteristic function of $ln(S_T)$ under the forward T-measure by

$$f_2(t,\phi,S_t,Y_t) := \frac{f_t(\phi)}{f_t(0)} = \mathbb{E}^{\mathbb{Q}^T}\left[e^{i\phi\ln(S_T)}|\mathcal{F}_t\right], \quad (4.33)$$

and

$$\Omega(t,K,T,S_t) = \frac{P(t,T)}{\pi}\int_0^{+\infty} \text{Re}\left[e^{-iln(K)\phi}\frac{f(t,\phi,S_t,Y_t)}{\phi^2 + \phi i}\right]d\phi, \quad (4.34)$$

the price of a call option is

$$C_G(K) = S_t e^{-q(T-t)} - \frac{KP(t,T)}{2} - K\Omega(t,K,T,S_t). \quad (4.35)$$

4.2.3.5 Approximation of the improper Integral

The computation of the improper integral in equation (4.34) can be performed using several numerical integration techniques, such as Gauss–Legendre and Gauss–Laguerre quadratures, or adaptive Gauss–Lobatto quadrature. However, in this analysis we adopted the Gauss–Kronrod quadrature rule. This choice was motivated by the fact that Gauss –Laguerre quadrature encounters numerical instabilities when the integrand exhibits poles or discontinuities near the integration domain, as is the case in our pricing formula.

In contrast, the Gauss–Kronrod method demonstrated superior performance due to its adaptive error estimation and efficient node reuse across iterations, which significantly reduces computational cost while maintaining accuracy. Applying this rule, we estimated the integral in equation (4.34) as follows:

$$\int_0^{+\infty} g(x)\,dx \approx \sum_{j=1}^{N} w_j g(x_j), \tag{4.36}$$

where w_j and x_j are the weights and the nodes of the associated Gauss-Kronrod quadrature rule. Applying Gauss-Kronrod quadrature rule we estimate the integral in equation (4.34) in the following way:

$$\int_0^{+\infty} \mathrm{Re}\left[e^{-iln(K)\phi}\frac{f_2(t,\phi,S_t,Y_t)}{\phi^2+\phi i}\right] d\phi \approx \sum_{j=1}^{N} w_j g(\phi_j),$$

where $g(\phi)$ is given by:

$$g(\phi) = \mathrm{Re}\left[e^{-iln(K)\phi}\frac{f_2(t,\phi,S_t,Y_t)}{\phi^2+\phi i}\right].$$

As a result, the call price given by equation (4.30) becomes:

$$C_G(K) = S_t e^{-q(T-t)} - KP(t,T)\left(\frac{1}{2} + \frac{1}{\pi}\sum_{j=1}^{N} w_j g(\phi_j)\right). \tag{4.37}$$

Having established the general pricing framework based on Lee's approach, we now turn to the specification of three jump-diffusion models and the derivation of their corresponding characteristic functions $f_2(t,\phi)$.

CHAPTER 5

Stochastic volatility jump-diffusion models

5.1. Background

Stochastic volatility jump-diffusion (SVJD) models are a class of financial models designed to capture complex asset price movements, by incorporating time-varying volatility and sudden, discontinuous changes.

Despite the relevance of the BSM model in option pricing, its assumptions of continuous price paths, constant volatility, and normally distributed returns do not usually reflect the observed market behaviour. Empirical data shows that asset returns frequently exhibit fat tails, excess kurtosis, negative skewness and abrupt jumps, especially during periods of market stress. Moreover, these discontinuities are frequently associated with shifts in volatility patterns, since volatility is naturally time-varying. It tends to cluster, revert toward a long-term mean, and respond asymmetrically to price movements. This behaviour is reflected in the volatility smile usually observed in option markets. Such features are not captured by pure diffusion models, leading to systematic mispricing of derivatives and to an underestimation of extreme-event risk.

To address some of these limitations, stochastic volatility (SV) models were developed. By modelling volatility as a stochastic process, these models address some of the issues identified in the BSM framework, most notably the implied volatility smile. A well-known example is the Heston (1993) model, which specifies volatility as a mean-reverting square-root diffusion and yields a closed-form solution for option prices.

In parallel, jump-diffusion (JD) models were introduced to account for discontinuities in price movements as well as for the heavy tails observed in return distributions. Merton (1976) JD model specified normally distributed jumps, and Kou (2002) later extended this framework using a double-exponential distribution that allows for asymmetry and heavier tails. Although these models improve the empirical fit of asset returns, they do not capture volatility clustering or mean reversion.

These complementary approaches ultimately gave rise to stochastic volatility jump-diffusion (SVJD) models, which extend the traditional diffusion framework by incorporating stochastic volatility and discontinuous price jumps. In these models, volatility typically follows a mean-reverting process, while jumps are represented by a compound Poisson component. This dual structure allows the model to capture both the evolving nature of volatility and sudden, sizeable price movements, offering a better representation of financial markets, namely during periods of stress or in response to unexpected events such as macroeconomic announcements, earnings surprises, geopolitical shocks, or systemic crises.

This chapter presents an overview of the most influential extensions of the jump-diffusion framework, beginning with Merton (1976) JD model, continuing with Kou (2002) double-exponential model that introduces jump asymmetry and heavier tails, and culminating in the more general specification proposed by Bakshi, Cao and Chen (1997), which incorporates stochastic volatility, stochastic interest rates, and jumps. Each model is presented with its theoretical formulation, practical relevance, advantages, and limitations.

5.2. The generic stochastic volatility jump-diffusion model

5.2.1. Stochastic volatility dynamics

Empirical evidence indicates that financial market volatility is neither constant nor deterministic. Instead, it evolves stochastically over time, often displaying features such as mean reversion, where volatility tends to return to a long-term average, and volatility clustering, a form of temporal dependence in which large price fluctuations are typically followed by further periods of high variance. To capture these features, stochastic volatility models introduce an additional stochastic process driving the variance dynamics, yielding a more realistic and flexible description of asset price behaviour.
Formally, under a stochastic volatility framework, the dynamics of the asset price S are given by:

$$dS_t = (\mu - q)S_t\,dt + \sqrt{V_t}S_t\,dW_t^S, \tag{5.1}$$

where μ denotes the drift under the physical measure $\mathbb{P}$, q is the continuous dividend yield, V_t represents the instantaneous variance of the asset at time t, and $\{W_t^S\}_{t\geq 0}$ is a standard Brownian motion capturing the source of randomness in the asset price.
In addition, the variance process V_t is generally assumed to follow a mean-reverting diffusion process of the form:

$$dV_t = \kappa(t)(\theta(t) - V_t)\,dt + \xi(t, V_t)\,dW_t^v, \tag{5.2}$$

where $\kappa(t)$ denotes the speed of mean reversion, determining how quickly the variance returns to the long-run level $\theta(t)$, and $\xi(t, V_t)$ is the diffusion coefficient of the variance process (commonly referred to as the volatility of volatility), which controls the magnitude of stochastic fluctuations and may depend on both time and the current variance level.
The functions $\kappa(t)$, $\theta(t)$, and $\xi(t, V_t)$ are specified such that the variance process V_t is well-defined and remains non-negative. Finally, $\{W_t^v\}_{t\geq 0}$ is a standard Brownian motion introducing randomness into the variance dynamics.
In most formulations, W_t^v is assumed to be correlated with the Brownian motion W_t^S that drives the asset price, where the instantaneous correlation ρ is defined as:

$$\mathbb{E}[dW_t^S dW_t^v] = \rho\,dt, \quad \rho \in [-1, 1]. \tag{5.3}$$

While stochastic volatility significantly improves the model's ability to capture key dynamics of financial markets, it remains insufficient to account for the discontinuous price movements frequently observed in asset returns. To address this, a jump-diffusion component is incorporated into the model.

5.2.2. Jump-diffusion process

Jump-diffusion models extend the continuous diffusion and stochastic volatility processes by capturing sudden, discontinuous movements in asset prices that these models cannot fully explain. Starting from a standard diffusion model, such as the Black-Scholes framework, a jump component is incorporated to account for significant and abrupt price changes. These jumps are typically modelled using a compound Poisson process, which captures both the frequency and magnitude of each jump. The following sections present the formal specification of these two components in detail.

Jump arrival process

The arrival of jumps is governed by a Poisson process with intensity λ, which determines both the expected frequency and the random timing of jumps within a given time interval. The number of jumps occurring over a fixed period follows a Poisson distribution. However, for sufficiently small time increments, this distribution can be approximated by a Bernoulli variable. In this case, the probability distribution of observing jumps within an infinitesimal interval dt is given by:

$$\begin{aligned} P(N_{t+dt} - N_t = 0) &\approx 1 - \lambda\, dt. \\ P(N_{t+dt} - N_t = 1) &\approx \lambda dt \\ P(N_{t+dt} - N_t \geq 2) &\approx 0. \end{aligned} \tag{5.4}$$

Here, λdt represents the probability of exactly one jump occurring in the time-instant dt, while $1 - \lambda dt$ is the probability of no jumps taking place. The probability of observing more than one jump is negligible for small dt.

Jump size and distribution

The jump factor U_t is an independent and identically distributed (i.i.d.) random variable that follows a specific probability distribution, such as the normal or log-normal distribution. It acts as a multiplicative factor that determines the change in the asset price when a jump occurs. Formally, the asset price immediately after a jump satisfies $S_t = U_t S_{t-}$, where S_{t-} denotes the asset price just before the jump. Then, the relative jump size can be expressed as follows:

$$\frac{dS_t}{S_{t-}} = \frac{U_t S_{t-} - S_{t-}}{S_{t-}} = U_t - 1. \tag{5.5}$$

Although the formulation in terms of U_t is valid, it is often preferable to express the jump as the percentage change in the asset price $J_t = U_t - 1$.

Together, the jump timing and size distributions form the foundation of the jump component within asset price models. These models can be viewed as particular cases of a broader class of stochastic processes, known as Lévy processes. A Lévy process is a stochastic process that starts at zero, with stationary and independent increments, meaning that changes over non-overlapping time intervals are independent of each other, so the process depends only on its current state, and that the distribution of the changes over any time interval of a given length remains the same, regardless of when it occurs. In addition, Lévy processes are stochastically continuous, indicating that as the time interval

becomes very small, the probability of a significant change in the process approaches zero. This class of processes can be completely characterised by their characteristic functions, expressed in terms of the Lévy–Khintchine triplet (γ, σ^2, ν). In particular, the triplet allows the decomposition of a Lévy process into three independent components: a deterministic linear drift, a Brownian motion, and a pure-jump Lévy process.

The jump behaviour of a Lévy process X_t is fully determined by the Lévy measure ν, which specifies the expected number of jumps per unit time with magnitudes falling within a given set, and governs both the frequency and size distribution of jumps. The Lévy measure is expressed as $\nu = \lambda f$, where f is the density of the jumps of the stochastic process X_t and λ is the intensity of jumps arrivals.

Another important class in asset pricing is the exponential Lévy model. In this framework, the asset price is modelled as the exponential of a Lévy process X_t, ensuring that log-returns are positive, independent, and stationary:

$$S_t = S_0 e^{X_t}. \tag{5.6}$$

Since in the context of exponential Lévy models the asset price is defined as $S_t = S_0 e^{X_t}$ (for further details, see Appendix B.7), it is important to characterise how the relative jump size is determined within this framework. This leads to the following expression:

$$\frac{dS_t}{S_{t-}} = \frac{S_t - S_{t-}}{S_{t-}} = \frac{e^{X_t} - e^{X_{t-}}}{e^{X_{t-}}} = e^{\Delta X_t} - 1, \tag{5.7}$$

where $\Delta X_t = X_t - X_{t-}$ represents the jump in the Lévy process X_t, and $e^{\Delta X_t} - 1$ reflects the percentage change in the asset price. Note that throughout this section, x will also denote a generic realisation of the jump size ΔX_t. Moreover, the formulation in equation (5.7) is consistent with the general description in equation (5.5), from which it follows that $U_t = e^{\Delta X_t}$, thereby establishing the link between the exponential Lévy representation and the standard jump framework.

It is also convenient to express the compound Poisson process associated with the asset's jump size distribution V_i, $\sum_{i=1}^{N_t} V_i$ in integral form (for further details see Proposition B.2):

$$\sum_{i=1}^{N_t} V_i = \int_0^t \int_{\mathbb{R}} S_{u-}(e^x - 1) N_X(du, dx), \tag{5.8}$$

where N_X is the Poisson random measure. This measure is defined by $N_X([0,t] \cap A) = \#\{s \in [0,t] : \Delta X_s \in A\}$, which gives the number of jumps per unit of time, whose amplitude belongs to A. Observe that, for each Borel set A, $\{N_X(t, A), t \geq 0\}$ is a Poisson process with postulate given by (5.4), and mean number of jumps per unit time given by $\nu(A) = \mathbb{E}[N(1, A)] = \lambda f_X(A)$ where f is the density of the jumps of the stochastic process X_t and λ is the intensity of the jumps arrival. Finally, W_t and N_X are independent sources of randomness. Among the various types of Lévy models, jump-diffusion models are particularly relevant in finance and will be introduced next.

5.2.3. Jump-diffusion models

The jump-diffusion model combines a standard Brownian motion with drift and a compound Poisson process, capturing both continuous fluctuations and abrupt price jumps in asset dynamics such as market crashes or major corporate events.
The process is typically expressed as follows:

$$X_t = \mu t + \sigma W_t + \sum_{i=1}^{N_t} Y_i, \tag{5.9}$$

where μt represents the drift term, σW_t the Brownian motion, and the jump component $\sum_{i=1}^{N_t} Y_i$ is a compound Poisson process. Here, N_t is a Poisson process with intensity λ that counts the number of jumps up to time t, and Y_i, $i = 1, 2, 3, \ldots$, are i.i.d. random variables with distribution f. For completeness, formal definitions of the Poisson and compound Poisson processes are given in Definition B.2 of Appendix B.
As a classical example, in Merton (1976) model, the process X_t follows a jump-diffusion model, as defined in equation (5.9).

Applying Itô's Lemma to the exponential function defined in equation (5.6), and using the dynamics of the jump-diffusion process X_t specified in equation (5.9), taking into account the existence of dividends, i.e with drift $\mu - q$, we obtain the stochastic differential equation (SDE) for the asset price S, under the physical measure $\mathbb{P}$:

$$dS_t = (\mu - q)S_{t-}dt + \sigma S_{t-}dW_t^{\mathbb{P}} + \int_{\mathbb{R}} S_{t-}(e^x - 1)N_X(dt, dx). \tag{5.10}$$

Here, S_t denotes the asset price at time t, and S_{t-} represents its left-limit, accounting for possible jumps. The parameter μ is the drift under the physical measure $\mathbb{P}$, q is the continuous dividend yield, and σ is the volatility coefficient associated with the standard Brownian motion. $N_X(dt, dx)$ is a Poisson random measure counting the number of jumps of size $dx \in \mathbb{R}$ occurring in the interval $[t, t + dt)$. Finally, note that $W_t^{\mathbb{P}}$ and N_X are independent sources of randomness.

This equation reflects both the continuous fluctuations and the discontinuous jumps in the asset price. A full derivation of SDE (5.10), including all intermediate steps from the application of Itô's Lemma to the exponential function, is provided in Appendix A.

Having established the jump component, we can now integrate it into the dynamics of the classical diffusion model, leading to the class of stochastic volatility models with jumps.

5.2.4. Stochastic volatility jump-diffusion models

Stochastic volatility and jump-diffusion models each address important shortcomings of the standard diffusion framework, but neither alone fully captures the empirical behaviour of asset prices. To account for both time-varying volatility and discontinuous price changes, these components can be integrated into a unified stochastic volatility jump-diffusion model, formalised by the following system of stochastic differential equations, under the physical measure $\mathbb{P}$:

$$dS_t = (\mu - q)\, S_{t-} dt + \sqrt{V_t} S_{t-} dW_t^S + \int_{\mathbb{R}} S_{t-}(e^x - 1) N_X(dt, dx), \tag{5.11a}$$

$$dV_t = \kappa(t)(\theta(t) - V_t)dt + \xi(t, V_t) dW_t^v. \tag{5.11b}$$

In this model, equation (5.11a) extends the stochastic volatility dynamics specified in equation (5.1) by incorporating the jump component from equation (5.10), while the variance process in equation (5.11b) remains unchanged from equation (5.2). The processes $\{W_t^S\}_{t\geq 0}$ and $\{W_t^v\}_{t\geq 0}$ are standard Brownian motions, driving the asset price and the variance dynamics, respectively, and are correlated with instantaneous correlation coefficient $\rho \in [-1, 1]$, such that $\mathbb{E}[dW_t^S dW_t^v] = \rho\, dt$.
The jump component is modelled via a compound Poisson process, represented by:

$$\int_0^t \int_{\mathbb{R}} S_{u-}(e^x - 1) N_X(du, dx).$$

Furthermore, W_t^S and W_t^v are assumed to be independent of the Poisson random measure N_X governing the random arrival times of jumps, ensuring that continuous and discontinuous sources of randomness remain uncorrelated. This formulation allows for both continuous and discontinuous changes in asset prices and provides a rich framework for capturing several empirical phenomena, such as volatility clustering, asymmetric return distributions, heavy tails, and sudden price movements.

5.3. Merton Jump-diffusion model

The Merton (1976) jump-diffusion model, introduced by Robert C. Merton in 1976, was the first to incorporate jumps into asset-pricing models. It represents a significant advancement over the Black-Scholes-Merton framework by addressing one of its core limitations. While the BSM model assumes that asset prices follow a continuous path driven solely by geometric Brownian motion, the JD model incorporates the possibility of sudden, discontinuous changes in asset prices. As discussed in the previous sections, this feature allows the model to more accurately reflect the empirical behaviour of financial markets, where abrupt shifts in asset prices occur alongside continuous fluctuations.

In Merton (1976) specification, the dynamics of S_t are described by the following stochastic differential equation (SDE), combining a continuous Brownian motion with constant volatility and a jump component driven by a Poisson process:

$$dS_t = (\mu - q)\, S_{t-} dt + \sigma S_{t-} dW_t^{\mathbb{P}} + \int_{\mathbb{R}} S_{t-}(e^x - 1) N_X(dt, dx). \tag{5.12}$$

Here, μ denotes the drift rate of the asset under the physical measure $\mathbb{P}$, q corresponds to the continuous dividend yield, σ represents the constant volatility of the diffusion component, and W_t is a standard Brownian motion. As in the general specification, $W_t^{\mathbb{P}}$ and the Poisson process N_X are assumed to be independent, ensuring that the continuous and jump components constitute distinct sources of randomness.

Since in this framework the asset price is modelled in exponential form as presented in equation (5.6), it is natural to describe the asset price dynamics in terms of the logarithmic

process X_t. In Merton (1976) model, this process follows the jump-diffusion process in equation (5.9), where the jump size variables Y_i are i.i.d. and normally distributed with mean m and variance δ. Accordingly, the random percentage jump size can be written as $J_t = e^{\Delta X_t} - 1$, which implies that:

$$ln(1 + J_t) \sim N(m, \delta). \tag{5.13}$$

Therefore, the corresponding Lévy measure can be characterised by the following density:

$$\nu(dx) = \lambda \frac{1}{\sqrt{2\pi\delta}} e^{-\frac{(x-m)^2}{2\delta}} dx, \tag{5.14}$$

where $m \in \mathbb{R}$ and $\lambda, \delta > 0$ are given parameters.

Having specified the Lévy measure, we now proceed to the risk-neutral formulation. For option pricing, asset dynamics need to be expressed under $\mathbb{Q}$ rather than the physical measure $\mathbb{P}$. To perform this change, we apply Girsanov's theorem, which provides the following relation between the Brownian motions under the two measures:

$$dW_t^{\mathbb{P}} = \varphi_t dt + dW_t^{\mathbb{Q}}, \tag{5.15}$$

with φ_t denoting the Girsanov kernel, defined as:

$$\varphi_t = \frac{r - \mu - \int_{\mathbb{R}} (e^x - 1)\, \nu(dx)}{\sigma}. \tag{5.16}$$

Then, substituting equation (5.15) into equation (5.12), yields:

$$dS_t = (r - q - \int_{\mathbb{R}} e^x - 1\, \nu(dx)) S_{t-} dt + \sigma S_{t-} dW_t^{S,\mathbb{Q}} + \int_{\mathbb{R}} S_{t-}(e^x - 1) N_X(dt, dx). \tag{5.17}$$

In this expression, r denotes the deterministic instantaneous spot interest rate, and $\{W_t^{S,\mathbb{Q}}\}_{t \geq 0}$ is a standard Brownian motion under the risk-neutral measure $\mathbb{Q}$.

Noting that, in the Merton (1976) jump-diffusion model, the Lévy measure (5.14) can be written as $\nu(dx) = \lambda f(dx)$, where $f(dx)$ is the density of a Normal distribution representing the jump size Y_i of the compound Poisson Process $\sum_{i=1}^{N_t} Y_i$, the integral term in Girsanov's kernel simplifies to:

$$\int_{\mathbb{R}} (e^x - 1)\, \nu(dx) = \lambda \int_{\mathbb{R}} (e^x - 1)\ f(dx) = \lambda \mu_J. \tag{5.18}$$

with $\mu_J = \mathbb{E}[e^{\Delta X_t} - 1]$ representing the average percentage jump size.

Substituting this result into equation (5.17), we obtain:

$$dS_t = (r - q - \lambda \mu_J) S_{t-} dt + \sigma S_{t-} dW_t^{S,\mathbb{Q}} + \int_{\mathbb{R}} S_{t-}(e^x - 1) N_X(dt, dx), \tag{5.19}$$

where, in this case, μ_J is given by (see Corollary E.1):

$$\mu_J = \mathbb{E}[e^{\Delta X_t} - 1] = e^{m + \frac{1}{2}\delta} - 1. \tag{5.20}$$

5.3.1. Merton's model as a special case of Duffie, Pan, and Singleton (2000)

The Merton (1976) jump-diffusion model can be seen as a particular case of the Duffie, Pan, and Singleton (2000) framework introduced in Chapter 3. Embedding the model in this setting allows us to identify the corresponding affine coefficients and derive the exponential–affine transform. This provides a convenient way to obtain the marginal characteristic function of the terminal log–price, the key input for option pricing.
In this formulation, X_t is a 1-dimensional vector, defined as:

$$X_t = ln(S_t), \tag{5.21}$$

where the natural logarithm of the asset price is the only element of the state vector. That said, applying the generalised Itô's Lemma presented in Definition B.6 to X_t, we get:

$$\begin{aligned} dln(S_t) = &\frac{dS}{S} - \frac{1}{2}\frac{d(S^c, S^c)_t}{S^2} \\ &+ \int_{\mathbb{R}} \left[ln(S_{t^-} + S_{t^-}(e^x - 1)) - ln(S_{t^-}) - \frac{1}{S_{t^-}} S_{t^-}(e^x - 1) \right] N_X(dt, dx). \end{aligned} \tag{5.22}$$

Plugging in the dynamics of S_t specified in equation (5.19) and simplifying the integral term yields:

$$\begin{aligned} dln(S_t) = &(r - q - \lambda\mu_J)dt + \sigma dW_t^{S,\mathbb{Q}} + \int_{\mathbb{R}} (e^x - 1) N_X(dt, dx) - \frac{1}{2}\frac{\sigma^2 S_t^2}{S_t^2} dt \\ &+ \int_{\mathbb{R}} \left[x - (e^x - 1) \right] N_X(dt, dx). \end{aligned} \tag{5.23}$$

As the Lévy measure in Merton (1976) model has finite activity and finite variation, the two integral terms can be combined. Thus, cancelling the integral $\int_{\mathbb{R}} (e^x - 1) N_X(dt, dx)$ and rearranging the dt terms, we arrive at:

$$dln(S_t) = (r - q - \lambda\mu_J - \frac{1}{2}\sigma^2)dt + \sigma dW_t^{S,\mathbb{Q}} + \int_{\mathbb{R}} x N_X(dt, dx). \tag{5.24}$$

Comparing the dynamics in (5.24) with Duffie's affine structure given in equation (3.3), we identify the drift $\mu(t, X_t)$ and the volatility term $\sigma(t, X_t)$ as:

$$\mu(t, X_t) = r - q - \lambda\mu_J - \tfrac{1}{2}\sigma^2 \tag{5.25a}$$

$$\sigma(t, X_t) = \sigma. \tag{5.25b}$$

Noting that Duffie's framework imposes an affine form on both the drift $\mu(t, X_t)$ and the symmetric matrix $\sigma(t, X_t)\sigma(t, X_t)^\top$, as specified in equations (3.5) and (3.6), respectively, we obtain:

$$K_0(t) = r - q - \lambda\mu_J - \frac{1}{2}\sigma^2, \;\; K_x(t) = 0. \tag{5.26}$$

Regarding the diffusion component, the affine structure of $\sigma(t, X_t)\sigma(t, X_t)^\top$ takes the form:

$$\sigma(t, X_t)\sigma(t, X_t)^\top = \sigma^2, \tag{5.27}$$

from which it follows that:

$$H_0(t) = \sigma^2,\ H_x^{(1)}(t) = 0. \tag{5.28}$$

The short-term interest rate, R_t is also specified by an affine structure, as in equation (3.8). In this case, as $R_t = r$ is a deterministic constant, the coefficients are:

$$\rho_0(t) = r,\ \rho_x(t) = 0. \tag{5.29}$$

Finally, the dynamics of the one dimensional pure jump process Z_t described in equation (3.3) corresponds to the integral term specified in (5.24):

$$dZ_t^{\mathbb{Q}} = \int_{\mathbb{R}} x\, N_X(dt, dx). \tag{5.30}$$

Thus, the jump process $Z_t^{\mathbb{Q}} = \int_0^t \int_{\mathbb{R}} x N_X(ds, dx)$ is consistent with the compound Poisson process introduced in equation (5.9), whose jumps have an arrival intensity $\lambda(X_t, t) = \lambda \in [0, +\infty[$. This implies that the jump intensity is constant and, under Duffie's framework, follows the affine structure given in equation (3.7), where:

$$l_0(t) = \lambda,\ l_x(t) = 0. \tag{5.31}$$

In turn, the associated jump-size probability distribution ν_t can be characterised through the following jump transform θ defined in equation (3.4):

$$\begin{aligned} \theta(c,t) &= \int_{\mathbb{R}} e^{cz} d(\nu_t(z)) \\ &= \int_{\mathbb{R}} e^{cz} \frac{1}{\sqrt{2\pi\delta}} e^{-\frac{1}{2}\frac{(z-m)^2}{\delta}} dz \\ &= e^{cm + \frac{1}{2}c^2\delta}, \end{aligned} \tag{5.32}$$

where we used the result given in equation (B.2). Note that $\nu_t(dz)$ presented in equation (3.4) refers only to the jump-size distribution, denoted by $f(dz)$ in the Merton (1976) model, and should not be confused with the Lévy measure introduced earlier. Moreover, μ_J can be directly recovered from the jump transform θ, where $\mu_J = \theta(1,t) - 1$. The derivation of this relation follows from straightforward algebra and is provided in Proposition E.3 and Remark E.1 in the Appendix.

With these elements in place, we now turn to the system of ODEs that characterises the exponential–affine transform. Recall that the ODE for β used in the transform (3.11) is given by equation (3.12), i.e.,

$$\beta'(t,T,u) = \rho_x(t) - K_x(t)^\top \beta(t,T,u) - \tfrac{1}{2}\big[\beta(t,T,u) H_x(t) \beta(t,T,u)\big] - \big[\theta(\beta(t,T,u),t) - 1\big]\, l_x(t).$$

Substituting the relevant terms from equations (5.26), (5.28), (5.29), (5.31) and (5.32) into this ODE, and using the boundary condition $\beta(T,T,u) = u$, we obtain $\beta'(t,T,u) = 0$, which results in:

$$\beta(t,T,u) = u. \tag{5.33}$$

Applying the same substitutions to the ODE for α given in equation (3.13), we have:

$$\begin{aligned}\alpha'(t,T,u) &= \rho_0(t) - \beta(t,T,u)^\top K_0(t) - \frac{1}{2}\beta(t,T,u)^\top H_0(t)\beta(t,T,u) - [\theta(\beta(t,T,u),t) - 1]\, l_0(t) \\ &= r - u(r - q - \lambda\mu_J - \frac{1}{2}\sigma^2) - \frac{u^2\sigma^2}{2} - \left[e^{u\cdot m + \frac{1}{2}\delta u^2} - 1\right]\lambda.\end{aligned}$$

Using the boundary condition $\alpha(T,T,u) = 0$ yields the following solution to this ODE:

$$\alpha(t,T,u) = -r\tau + u(r - q - \lambda\mu_J - \frac{1}{2}\sigma^2)\tau + \frac{u^2\sigma^2}{2}\tau + \left[e^{u\cdot m + \frac{1}{2}\delta u^2} - 1\right]\lambda\tau, \tag{5.34}$$

where $\tau = T - t$.

This way, in the case of Merton (1976) model, the exponential-affine solution for the transform (3.9) is given by:

$$\psi(u,t,T;X_t) = \exp\left[\alpha(t,T,u) + \beta(t,T,u)\ln(S_t)\right], \tag{5.35}$$

with $u \in \mathbb{C}$ and $t \leq T$, and where α and β are given by equations (5.34) and (5.33), respectively.

Since in Merton (1976) model the interest rate is constant, the price of a zero-coupon bond is the usual discount factor:

$$P(t,T) = e^{-r\tau}, \tag{5.36}$$

where r is the short-term interest rate and $\tau = T - t$.

Following the notation introduced in Chapter 4, more precisely the one presented in Remark 4.1, we can express the marginal characteristic function f_2 under the forward T-measure in the following manner:

$$f_2(T,\phi;S_t) = \frac{\mathbb{E}^{\mathbb{Q}}\left[\exp\left(-\int_t^T r(X_s,s)\,ds\right)e^{i\phi\ln(S_T)}\middle|\mathcal{F}_t\right]}{P(t,T)}. \tag{5.37}$$

Given that the numerator in equation (5.37) is a special case of the general exponential–affine transform in equation (3.9), we can further write:

$$f_2(T,\phi;S_t) = \frac{\psi(i\phi,t,T;\ln(S_t))}{e^{-r\tau}}.$$

Thus, in Merton (1976) model, the marginal characteristic function under the forward T-measure is given by:

$$f_2(T,\phi;S_t) = \exp\left[i\phi(r - q - \lambda\mu_J - \frac{1}{2}\sigma^2)\tau - \frac{\phi^2\sigma^2}{2}\tau + \left[e^{i\phi\cdot m - \frac{1}{2}\delta\phi^2} - 1\right]\lambda\tau + i\phi\ln(S_t)\right].$$

5.4. Kou jump-diffusion model

Another widely used specification is the double exponential jump-diffusion model introduced by Kou (2002). This formulation refines Merton (1976) framework by replacing the normally distributed jump sizes with an asymmetric double exponential distribution. In this way, it addresses the limitations of earlier approaches by capturing key features of

asset returns, such as heavy tails, negative skewness, and implied volatility smiles, which the Merton model fails to capture adequately.

As in the previous case, Kou's jump-diffusion combines a diffusion term with a compound Poisson jump component, following the same process as in equation (5.9), differing only in the distribution of the jump sizes. Formally, in Kou (2002) model, the distribution of the jump size Y is characterised as follows:

$$Y \overset{d}{=} \begin{cases} \xi^+ & \text{with probability } p_1 \\ -\xi^- & \text{with probability } p_2 \end{cases},$$

where ξ^+ and ξ^- are exponential random variables with means $\frac{1}{\eta_1}$ and $\frac{1}{\eta_2}$, respectively. The parameters η_1 and η_2 correspond to the level of decay of the distribution and determine the rate of the positive and negative jumps, respectively, while p_1 and p_2 represent the probabilities of the jumps occurring in the positive or negative direction. In this model, the Poisson process N_t, the Brownian motion W_t, and the jump sizes Y_i are assumed to be independent.

The jump size distribution can equivalently be expressed in terms of the Lévy measure, which is given by $\nu(dx) = \lambda f(dx)$, where $f(dx)$ is defined as:

$$f(dx) = p_1\eta_1 e^{-\eta_1 .x}\mathbb{1}_{\{x\geq 0\}} + p_2\eta_2 e^{\eta_2 x}\mathbb{1}_{\{x<0\}}dx, \tag{5.38}$$

with $\eta_1 > 1$, $\eta_2 > 0$, $p_1 > 0$, $p_2 > 0$ and $p_1 + p_2 = 1$. The restriction $\eta_1 > 1$ not only ensures that S_t has finite expected value but also prevents the mean upward jump from exceeding 100%, which is both mathematically consistent and economically reasonable.

This modelling specification has several important implications. First, it captures asymmetric leptokurtosis, as return distributions exhibit a sharper peak, heavier tails, and skewness relative to the normal distribution. Second, it explains the volatility smile observed in option markets, as implied volatilities under this model vary with strike prices. Third, it provides an economic interpretation, where heavy tails correspond to market overreaction to news and the sharp peak reflects underreaction (see Kou (2002)). In addition, this model retains much of the analytical tractability of the Black–Scholes framework. Closed-form or semi-analytical pricing formulas exist for a wide class of derivatives, including European- and American-style options, barrier options, and lookback options. Finally, the exponential distribution underlying the jump sizes has the memoryless property, meaning that the probability of a future jump does not depend on past jumps.

Having outlined its main implications, we now turn to the dynamics of the asset price under Kou (2002) model. Recalling that the dynamics of the asset price is again given by equation (5.19), we can apply generalised the Ito's Lemma (see Definition B.6), as done in steps (5.22) and (5.23) to $X_t = ln(S_t)$, and obtain:

$$dln(S_t) = (r - q - \lambda\mu_J - \frac{1}{2}\sigma^2)dt + \sigma dW_t^{S,\mathbb{Q}} + \int_{\mathbb{R}} xN_X(dt, dx), \tag{5.39}$$

where μ_J in Kou (2002) model is given by (see Corollary E.2):

$$\mu_J = \mathbb{E}[e^{\Delta X_t} - 1] = \frac{p_2\eta_2}{1+\eta_2} - \frac{p_1\eta_1}{1-\eta_1} - 1. \tag{5.40}$$

5.4.1. Kou's model as a special case of Duffie, Pan, and Singleton (2000)

Kou (2002) model can also be viewed as a special case of Duffie, Pan, and Singleton (2000). Since it shares the same dynamics as Merton (1976) model, the process $X_t = \ln(S_t)$ has the same drift $\mu(t, X_t)$ and volatility term $\sigma(t, X_t)$ as specified in equation (5.25). Thus, $K_0(t)$ and $K_x(t)$ are also obtained from equation (5.26). Similarly, the positive definite matrix $\sigma(t, X_t)\sigma(t, X_t)^\top$ is given by equation (5.27) and $H_0(t)$ and $H_x(t)$ are likewise given by equation (5.28). As $R_t = r$ is a deterministic constant, we have (5.29). Finally, the arrival intensity $\lambda(X_t, t) = \lambda$ is also a deterministic constant and given by equation (5.31). As a result, the corresponding coefficients take the following form:

$$\begin{aligned} &K_0(t) = r - q - \lambda\mu_J - \frac{1}{2}\sigma^2,\ K_x(t) = 0,\ H_0(t) = \sigma^2,\ H_x^{(1)}(t) = 0, \\ &\rho_0(t) = r,\ \rho_x(t) = 0,\ l_0(t) = \lambda,\ l_x(t) = 0. \end{aligned} \tag{5.41}$$

In addition, the jump transform θ, in the case of Kou (2002) model, is given by:

$$\begin{aligned} \theta(c,t) &= \int_{\mathbb{R}} e^{cz} d(\nu_t(z)) \\ &= \int_{\mathbb{R}} e^{cz}(p_1\eta_1 e^{-\eta_1 z}\mathbb{1}_{\{z\geq 0\}} + p_2\eta_2 e^{\eta_2 z}\mathbb{1}_{\{z<0\}})\, dz \\ &= p_2\eta_2 \int_{-\infty}^{0} e^{(c+\eta_2)z} dz + p_1\eta_1 \int_0^{+\infty} e^{(c-\eta_1)z} dz \\ &= p_2\eta_2 \left[\frac{e^{(c+\eta_2)z}}{c+\eta_2}\right]_{-\infty}^{0} + p_1.\eta_1 \left[\frac{e^{(c-\eta_1)z}}{c-\eta_1}\right]_0^{+\infty}, \\ &= \frac{p_2\eta_2}{c+\eta_2} - \frac{p_1\eta_1}{c-\eta_1}. \end{aligned} \tag{5.42}$$

Again, μ_J can be obtained from the jump transform as $\mu_J = \theta(1, t) - 1$ (for more details see Proposition E.3 and Remark E.2 in the Appendix).

Following the same steps as in Merton (1976) model, we get the same solution $\beta(t, T, u) = u$ as in equation (5.33). With regard to α, the corresponding ODE takes the form:

$$\begin{aligned} \alpha'(t,T,u) &= \rho_0(t) - \beta(t,T,u)^\top K_0(t) - \frac{1}{2}\beta(t,T,u)^\top H_0(t)\beta(t,T,u) - [\theta(\beta(t,T,u),t) - 1]\, l_0(t) \\ &= r - u(r - q - \lambda\mu_J - \frac{1}{2}\sigma^2) - \frac{u^2\sigma^2}{2} - \left[\frac{p_2\eta_2}{u+\eta_2} - \frac{p_1\eta_1}{u-\eta_1} - 1\right]\lambda. \end{aligned}$$

Applying the boundary condition $\alpha(t, T, u) = 0$, we obtain the following solution:

$$\alpha(t,T,u) = -r\tau + u(r - q - \lambda\mu_J - \frac{1}{2}\sigma^2)\tau + \frac{u^2\sigma^2}{2}\tau + \left[\frac{p_2\eta_2}{u+\eta_2} - \frac{p_1\eta_1}{u-\eta_1} - 1\right]\lambda\tau, \tag{5.43}$$

where $\tau = T - t$.

In the Kou (2002) model the exponential-affine solution for the transform (9) is given by

equation (5.35), where α and β are specified in equations (5.43) and (5.33), respectively. As in the previous case, the interest rate is deterministic, which means that the price of a zero coupon bond is given by equation (5.36). Performing similar steps as in Merton (1976) model, we obtain the following marginal characteristic function under the T-forward measure:

$$f_2(T,\phi;S_t) = \exp\Big[\mathrm{i}\phi\big(r-q-\lambda\mu_J-\tfrac{1}{2}\sigma^2\big)\tau-\tfrac{\phi^2\sigma^2}{2}\,\tau+\Big(\tfrac{p_2\eta_2}{\mathrm{i}\phi+\eta_2}-\tfrac{p_1\eta_1}{\mathrm{i}\phi-\eta_1}-1\Big)\lambda\tau+\mathrm{i}\phi\ln S_t\Big].$$

It is worth noting that the main difference between Merton's and Kou's marginal characteristic function lies in the characteristic function of the jump size distribution Y_i. In the former, it is given by $e^{i\phi m-\frac{1}{2}\delta\phi^2}-1$, whereas in the latter it takes the form $\frac{p_2\eta_2}{i\phi+\eta_2}-\frac{p_1\eta_1}{i\phi-\eta_1}-1$. Correspondingly, the expected percentage jump size μ_J also differs, as defined in equation (5.20) for Merton (1976) model and in equation (5.40) for Kou's model.

5.5. Bakshi, Cao and Chen (1997) model

The Bakshi, Cao and Chen (1997) SVSI-J model is a geometric jump-diffusion process that incorporates stochastic volatility, stochastic interest rates, and jumps in asset prices. Under the risk-neutral measure $\mathbb{Q}$, the dynamics of the underlying asset price S_t are described by the following geometric jump-diffusion process:

$$dS_t = (R_t - q - \lambda\mu_J)S_{t-}dt + \sqrt{V_t}S_{t-}dW_t^{S,\mathbb{Q}} + \int_{\mathbb{R}} S_{t-}(e^x-1)N_X(dt,dx), \tag{5.44}$$

where R_t is the time-t instantaneous short rate, q denotes the continuous dividend yield, and V_t is the diffusion component of the return variance. The stochastic process $\{W_t^{S,\mathbb{Q}}, t\geq 0\}$ is a standard Brownian motion under the risk-neutral measure $\mathbb{Q}$, related to the dynamics of the asset price, with S_{t-} representing the asset price immediately before the jump. As in the previous models, N_X denotes the Poisson random measure associated with the jumps and is assumed independent of the Brownian motion $W_t^{S,\mathbb{Q}}$.

In the Bakshi, Cao and Chen (1997) model, the random percentage jump size is defined as $J_t = e^{\Delta x}-1$, with mean μ_J, and is independent of N_X. Hence, $1+J_t$ is lognormally distributed, with:

$$ln(1+J_t) \sim N(ln(1+\mu_J) - \frac{1}{2}\sigma_J^2, \sigma_J^2). \tag{5.45}$$

The dynamics of the instantaneous variance of asset returns, conditional on no jumps occurring, follows the mean-reverting square root process:

$$dV_t = (\theta_v - \kappa_v V_t)dt + \sigma_v\sqrt{V_t}\,dW_t^{v,\mathbb{Q}}, \tag{5.46}$$

where κ_v denotes the speed of mean reversion, θ_v the long-run mean level of variance, and σ_v the volatility of variance (vol-of-vol), all assumed to be non–negative.

The process $\{W_t^{v,\mathbb{Q}}\}_{t\geq 0}$ is a standard Brownian motion under the risk-neutral measure $\mathbb{Q}$, which is assumed to be correlated with $W_t^{S,\mathbb{Q}}$, such that:

$$d\langle W_t^{S,\mathbb{Q}}, W_t^{v,\mathbb{Q}}\rangle = \rho\,dt, \tag{5.47}$$

with $-1 < \rho < 1$.
Finally, the short-term interest rate is modelled by the Cox-Ingersoll-Ross (1985) process:

$$dR_t = (\theta_r - \kappa_r R_t)dt + \sigma_r \sqrt{R_t}\, dW_t^{r,\mathbb{Q}}, \tag{5.48}$$

where κ_r, θ_r, and σ_r denote the speed of mean reversion, the long-run mean level, and the volatility of the short rate, respectively, with all parameters assumed to be non–negative. Here, the standard Brownian motion $W_t^{r,\mathbb{Q}}$ is uncorrelated with both $W_t^{S,\mathbb{Q}}$ and $W_t^{v,\mathbb{Q}}$.
It is important to note that the Bakshi, Cao and Chen (1997) SVSI-J model provides a general framework that encompasses almost all the known closed-form option formulas as special cases. For instance, when only the interest rate follows a stochastic process while volatility is constant and no jumps occur, one recovers the SI models, such as Vasiček (1977) or Cox-Ingersoll-Ross (1985). When jumps are excluded and the interest rate is deterministic, the specification reduces to Heston (1993) SV model. If jumps are included while the interest rate is deterministic and volatility is constant, it results in the classical JD models of Merton (1976) and Kou (2002). When both the variance and the short rate are stochastic, but jumps are ruled out, the model corresponds to the SVSI specification. Finally, when stochastic volatility is combined with jumps, one obtains the SVJ model of Bates (1991). In the absence of both jumps and stochastic components, the framework becomes the classical Black and Scholes (1973) model.

5.5.1. Bakshi's as a particular case of Duffie, Pan, and Singleton (2000)

The Bakshi, Cao and Chen (1997) can also be regarded as a particular case of the affine framework of Duffie, Pan, and Singleton (2000) presented in 3. As in the previous models, this representation is used to identify the affine coefficients and derive the characteristic function of $\ln(S_T)$. However, unlike Merton's and Kou's specifications, where the affine state vector reduces to the log-price, the SVSI-J model incorporates both stochastic volatility and a stochastic short rate, leading to a three-dimensional affine representation.

Following the same steps as in the Merton case, we apply the generalised Ito's Lemma presented in Definition B.6 to $ln(S_t)$, plug in the dynamics of S_t specified in equation (5.44) and simplify the integral term and obtain:

$$dln(S_t) = (R_t - q - \lambda\mu_J - \frac{1}{2}V_t)dt + \sqrt{V_t}dW_t^{S,\mathbb{Q}} + \int_{\mathbb{R}} xN_X(dt, dx). \tag{5.49}$$

In this affine structure, the vector X_t is a 3-dimensional vector defined as:

$$X_t = [ln(S_t), V_t, R_t], \tag{5.50}$$

where the natural logarithm of the asset price is the first element of the state vector, and $Y_t = [V_t, R_t]$ represents the vector of additional state variables for some admissible state space $D_y \subset \mathbb{R}^2$. With this setting, we can write Bakshi, Cao and Chen (1997) model in

matrix form, as follows:

$$\begin{bmatrix} dln(S_t) \\ dV_t \\ dR_t \end{bmatrix} = \begin{bmatrix} R_t - q - \lambda\mu_J - \frac{1}{2}V_t \\ \theta_v - \kappa_v V_t \\ \theta_r - \kappa_r R_t \end{bmatrix} dt + \begin{bmatrix} \sqrt{V_t}\sqrt{1-\rho^2} & \rho\sqrt{V_t} & 0 \\ 0 & \sigma_v\sqrt{V_t} & 0 \\ 0 & 0 & \sigma_r\sqrt{R_t} \end{bmatrix} \begin{bmatrix} d\overline{W}_t^{S,\mathbb{Q}} \\ d\overline{W}_t^{v,\mathbb{Q}} \\ d\overline{W}_t^{r,\mathbb{Q}} \end{bmatrix} + \begin{bmatrix} dZ_1 \\ 0 \\ 0 \end{bmatrix}. \tag{5.51}$$

where $\overline{W}_t^{S,\mathbb{Q}}, \overline{W}_t^{v,\mathbb{Q}}$ and $\overline{W}_t^{r,\mathbb{Q}}$ are uncorrelated Brownian Motions and $dZ_1 = \int_{\mathbb{R}} xN_X(dt,dx)$. Recall that Duffie's model imposes an affine structure for both the drift $\mu(t,X_t) = K_0 + K_1X_t$ and the definite positive matrix $\sigma(t,X_t)\sigma(t,X_t)^\top = H_0(t) + \sum_{k=1}^n H_x^k(t)(X_t)_k$ (see equations (3.5) and (3.6)). Then, we can conclude that:

$$K_0(t) = \begin{bmatrix} -q - \lambda\mu_J \\ \theta_v \\ \theta_r \end{bmatrix}, \; K_x(t) = \begin{bmatrix} 0 & -\frac{1}{2} & 1 \\ 0 & -\kappa_v & 0 \\ 0 & 0 & -\kappa_r \end{bmatrix}. \tag{5.52}$$

Since the definite positive matrix $\sigma(t,X_t)\sigma(t,X_t)^\top$ is given by:

$$\sigma(t,X_t)\sigma(t,X_t)^\top = \begin{bmatrix} V_t & \sigma_v\rho V_t & 0 \\ \sigma_v\rho V_t & \sigma_v^2 V_t & 0 \\ 0 & 0 & \sigma_r^2 R_t \end{bmatrix}, \tag{5.53}$$

we get:

$$(H_0(t))_{i,j} = \left(H_x^{(1)}(t)\right)_{i,j} = 0, \text{for } i,j = 1,2,3 \tag{5.54}$$

$$H_x^{(2)} = \begin{bmatrix} 1 & \sigma_v\rho & 0 \\ \sigma_v\rho & \sigma_v^2 & 0 \\ 0 & 0 & 0 \end{bmatrix}, \tag{5.55}$$

$$\left(H_x^{(3)}(t)\right)_{i,j} = \sigma_r^2 \mathbb{1}\{i=j=3\}. \tag{5.56}$$

Since R_t is assumed to be affine, i.e $R_t = \rho_0(t) + \rho_x(t)^\top X_t$ we obtain:

$$\rho_0(t) = 0, \; \rho_x(t) = \begin{bmatrix} 0 & 0 & 1 \end{bmatrix}^\top. \tag{5.57}$$

Since the process $Z_{t,1}^{\mathbb{Q}} = \int_0^t \int_{\mathbb{R}} xN_X(dt,dx)$ has jumps with an arrival intensity $\lambda(X_t,t) = \lambda$, and by the affine structure imposed by Duffie $\lambda(X_t,t) = l_0(t) + l_x(t)^\top X_t$ implies:

$$l_0(t) = \lambda, l_x(t) = \begin{bmatrix} 0 & 0 & 0 \end{bmatrix}^\top. \tag{5.58}$$

The associated probability distribution ν_t, can be defined through the following jump transform θ:

$$\begin{aligned} \theta(c,t) &= \int_{\mathbb{R}^3} e^{c'z} d(\nu_t(z)) \\ &= \int_{\mathbb{R}} e^{c_1 z_1} \frac{1}{\sqrt{2\pi\sigma_J^2}} e^{-\frac{1}{2}\frac{(z_1 - ln(1+\mu_J) + \frac{1}{2}\sigma_J^2)^2}{\sigma_J^2}} dz_1 \\ &= e^{c_1(ln(1+\mu_J) - \frac{1}{2}\sigma_J^2) + \frac{1}{2}c_1^2\sigma_J^2}. \end{aligned} \tag{5.59}$$

Again, μ_J can be directly recovered from the jump transform θ, where $\mu_J = \theta(1,t) - 1$. The derivation of this relation can be found in the Appendix in Proposition E.3.

We next consider the system of ODEs that characterises the exponential–affine transform. Thus, recall that the ODE for β used in the transform (3.11) is given by equation (3.12), i.e.,

$$\beta'(t,T,u) = \rho_x(t) - K_x(t)^\top \beta(t,T,u) - \tfrac{1}{2}\left[\beta(t,T,u)H_x(t)\beta(t,T,u)\right] - \left[\theta(\beta(t,T,u),t) - 1\right] l_x(t), \tag{5.60}$$

where in this case $\beta(t,T,u)H_x(t)\beta(t,T,u)$ is a 3-dimensional vector.
With regard to α, it is defined in equation (3.13), as follows:

$$\alpha'(t,T,u) = \rho_0(t) - \beta(t,T,u)^\top K_0(t) - \tfrac{1}{2}\,\beta(t,T,u)^\top H_0(t)\,\beta(t,T,u) - \left[\theta(\beta(t,T,u),t) - 1\right] l_0(t). \tag{5.61}$$

Now, replacing the relevant terms from equations (5.52), (5.54), (5.56), (5.57), (5.58) and (5.59) into the ODE (5.60), knowing that $\beta_1'(t,T,u) = 0$, and using the terminal condition $\beta(T,T,u) = u$, we obtain the solution to the first ODE:

$$\beta_1(t,T,u) = u_1. \tag{5.62}$$

In turn, substituting this result into equation (5.60), we arrive at the particular solution for β_2:

$$\beta_2(t,T,u) = \frac{2u_2\xi_v(u_1) + \left[u_2(u_1\rho\sigma_v - \kappa_v - \xi_v(u_1)) + u_1(u_1-1)\right]\left[1 - e^{-\xi_v(u_1)\tau}\right]}{2\xi_v(u_1) - \gamma_v^+(u_1,u_2)[1 - e^{-\xi_v(u_1)\tau}]}, \tag{5.63}$$

where $\tau = T - t$, and:

$$\begin{aligned} \gamma_v^+(u_1,u_2) &= u_2\sigma_v^2 - \kappa_v + u_1\rho\sigma_v + \xi_v(u_1), \\ \xi_v(u_1) &= \sqrt{(\kappa_v - u_1\rho\sigma_v)^2 - u_1(u_1-1)\sigma_v^2}. \end{aligned} \tag{5.64}$$

A complete derivation of β_2, covering both the general and particular solutions, is provided in Appendix E.3.3.2.
Regarding the third component of β we proceed in the same way by substituting β_1 in equation (5.60), resulting as in the previous case in a Riccati equation with solution given by:

$$\beta_3 = \frac{2u_3\xi_r(u_1) + [2(u_1-1) - u_3(\xi_r(u_1) + k_r)][1 - e^{-\xi_r(u_1)\tau}]}{2\xi_r(u_1) - \gamma_r^+(u_1,u_3)[1 - e^{-\xi_r(u_1)\tau}]}, \tag{5.65}$$

where $\tau = T - t$, and:

$$\begin{aligned} \gamma_r^+(u_1,u_3) &= u_3\sigma_r^2 - \kappa_r + \xi_r(u_1), \\ \xi_r(u_1) &= \sqrt{\kappa_r^2 - 2\sigma_r^2(u_1-1)}. \end{aligned} \tag{5.66}$$

Once again, a detailed derivation of the solution for β_3 can be found in Appendix E.3.3.3.
Having derived the different values of $\beta(t,T,u)$, we now proceed to determine $\alpha(t,T,u)$ using ODE (5.61). Following a procedure analogous to that used for the β ODE, we apply the same substitutions to the ODE for α in equation (5.61), and replace the solutions obtained for β_1, β_2 and β_3. Finally, imposing the boundary condition $\alpha(T,T,u) = 0$, and recalling that $\beta_1(t,T,u) = u_1$ (derived in equation (5.62)), we obtain the following

solution for α:

$$\begin{aligned}
\alpha(t,T,u) &= -\theta_v \frac{u_2\left(\xi_v(u_1)-\kappa_v+u_1\rho\sigma_v\right)+u_1(u_1-1)}{\gamma_v^-(u_1,u_2)}\tau \\
&- \theta_v\left(\frac{2u_1(u_1-1)+2u_2(u_2\sigma_v^2-2\kappa_v+2u_1\rho\sigma_v)}{\gamma_v^-(u_1,u_2)\gamma_v^+(u_1,u_2)}\right)\times\ln\left(1-\frac{\gamma_v^+(u_1,u_2)\left(1-e^{-\xi_v(u_1)\tau}\right)}{2\xi_v(u_1)}\right) \\
&- \theta_r \frac{u_3\left(\xi_r(u_1)-\kappa_r\right)+2(u_1-1)}{\gamma_r^-(u_1,u_3)}\tau \\
&- \theta_r\left(\frac{4(u_1-1)+2u_3(u_3\sigma_r^2-2k_r)}{\gamma_r^-(u_1,u_3)\gamma_r^+(u_1,u_3)}\right)\times\ln\left(1-\frac{\gamma_r^+(u_1,u_3)(1-e^{-\xi_r(u_1)\tau})}{2\xi_r(u_1)}\right) \\
&+ \lambda\tau\left[(1+\mu_J)^{u_1}e^{u_1(u_1-1)\frac{\sigma_J^2}{2}}-1\right]-\lambda u_1\mu_J\tau-qu_1\tau,
\end{aligned} \tag{5.67}$$

where $\tau = T-t$, and $\gamma_v^{\pm}(u_1,u_2)$, $\xi_v(u_1)$, $\gamma_r^{\pm}(u_1,u_3)$ and $\xi_r(u_1)$ are given by:

$$\begin{aligned}
\gamma_v^{\pm}(u_1,u_2) &= u_2\sigma_v^2-\kappa_v+u_1\rho\sigma_v\pm\xi_v(u_1), \\
\xi_v(u_1) &= \sqrt{\left(\kappa_v-u_1\rho\sigma_v\right)^2-u_1(u_1-1)\sigma_v^2}, \\
\gamma_r^{\pm}(u_1,u_3) &= u_3\sigma_r^2-\kappa_r\pm\xi_r(u_1), \\
\xi_r(u_1) &= \sqrt{\kappa_r^2-2\sigma_r^2(u_1-1)}.
\end{aligned} \tag{5.68}$$

For completeness, a detailed derivation of $\alpha(t,T,u)$ is provided in Appendix E.3.3.4.
With all coefficients determined, the exponential-affine solution for the transform (3.9) takes the form:

$$\psi(u,t,T;X_t) = \exp\left[\alpha(t,T,u)+\beta_1(t,T,u)\ln(S_t)+\beta_2(t,T,u)V_t+\beta_3(t,T,u)R_t\right], \tag{5.69}$$

with $u\in\mathbb{C}^3$ and $t\le T$, and where α, β_1, β_2 and β_3 are given by equations (5.67),(5.62),(5.63) and (5.65), respectively.
As done in previous models, we need to compute the time-t price of a risk-free pure discount bond which can also be expressed in terms of the same transform:

$$\begin{aligned}
P(t,T) &= \mathbb{E}^{\mathbb{Q}}\left[\exp\left(-\int_t^T r(X_s,s)\,ds\right)\Big|\mathcal{F}_t\right] \\
&= \psi((0,\underline{0}),t,T,X_t) \\
&= \exp\left[\alpha(t,T,(0,\underline{0}))+\beta(t,T,(0,\underline{0}))'\cdot X_t\right],
\end{aligned} \tag{5.70}$$

where $\underline{0}$ is a null vector in $\mathbb{R}^2$ and X_t is the 3-dimensional vector defined in equation (5.50).
Note that setting $u_1=0$ and $u_2=0$ in equations (5.62) and (5.63), we conclude that both β_1 and β_2 are zero. Applying the same procedure to equation (5.65), we arrive at the following expression for β_3:

$$\beta_3(t,T,0) = \frac{2(e^{-\xi_r(0)\tau}-1)}{2\xi_r(0)+(\xi_r(0)-\kappa_r)(e^{-\xi_r(0)\tau}-1)}, \tag{5.71}$$

where $\tau = T - t$, and $\xi_r(0) = \sqrt{\kappa_r^2 + 2\sigma_r^2}$.
With this result, we can now proceed to determine α. Building on the fact that $\gamma_r^+(0,0) = \sqrt{\kappa_r^2 + 2\sigma_r^2} - \kappa_r$ and $\gamma_r^-(0,0) = -\sqrt{\kappa_r^2 + 2\sigma_r^2} - \kappa_r$, and setting $u_1 = u_2 = u_3 = 0$, we arrive at following expression for α:

$$\alpha(t,T,0) = -\theta_r \left[\frac{2\tau}{\sqrt{\kappa_r^2 + 2\sigma_r^2} + \kappa_r} + \frac{2}{\sigma_r^2} \ln\left(1 - \frac{(\sqrt{\kappa_r^2 + 2\sigma_r^2} - \kappa_r)(1 - e^{-\tau\sqrt{\kappa_r^2 + 2\sigma_r^2}})}{2\sqrt{\kappa_r^2 + 2\sigma_r^2}} \right) \right]. \tag{5.72}$$

Having determined the β_1, β_2, β_3 and α, the price of the risk-free pure discount bond defined in equation (5.70) can be expressed as:

$$P(t,T) = \exp\left[\alpha(t,T,0) + \beta_3(t,T,0) R_t\right], \tag{5.73}$$

where $\alpha(t,T,0)$ is defined as specified in equation (5.72), and $\beta_3(t,T,0)$ as in equation (5.71).
Finally, within Lee's framework, the call option price can be expressed in terms of the marginal characteristic function of the terminal log-price under the forward-T measure. As explained when presenting the general definition in equation (4.10), in this setting the function corresponds to f_2. Therefore, in Bakshi, Cao and Chen (1997) model the marginal characteristic function under $\mathbb{Q}^T$ takes the form:

$$f_2(T,\phi;S_t,Y_t) = \frac{\mathbb{E}^{\mathbb{Q}}\left[\exp\left(-\int_t^T r(X_s,s)\,ds\right) e^{i\phi\ln(S_T)} \middle| \mathcal{F}_t\right]}{P(t,T)}. \tag{5.74}$$

Since the numerator in equation (5.74) is a special case of the general exponential–affine transform in equation (3.9), we can write Bakshi's marginal characteristic function under the forward T-measure, as follows:

$$f_2(T,\phi;S_t,Y_t) = \frac{\psi(i\phi,\underline{0},t,T;(\ln(S_t),Y_t))}{P(t,T)}, \tag{5.75}$$

with ψ being defined as:

$$\begin{aligned} \psi(i\phi,\underline{0},t,T;(\ln(S_t),Y_t)) = \exp[&\alpha(t,T,i\phi,\underline{0}) + \beta_1(t,T,i\phi,\underline{0})\ln(S_t) \\ &+ \beta_2(t,T,i\phi,\underline{0})V_t + \beta_3(t,T,i\phi,\underline{0})R_t], \end{aligned} \tag{5.76}$$

where $\tau = T - t$, and:

$$\begin{aligned}
\alpha(t,T,i\phi,\underline{0}) &= -\theta_v \frac{i\phi(i\phi-1)}{\gamma_v^-(i\phi,0)}\tau \\
&\quad - \theta_v \left(\frac{2i\phi(i\phi-1)}{\gamma_v^-(i\phi,0)\gamma_v^+(i\phi,0)}\right) \times \ln\left(1 - \frac{\gamma_v^+(i\phi,0)\left(1-e^{-\xi_v(i\phi)\tau}\right)}{2\xi_v(i\phi)}\right) \\
&\quad - \theta_r \frac{2(i\phi-1)}{\gamma_r^-(i\phi,0)}\tau \\
&\quad - \theta_r \left(\frac{4(i\phi-1)}{\gamma_r^-(i\phi,0)\gamma_r^+(i\phi,0)}\right) \times \ln\left(1 - \frac{\gamma_r^+(i\phi,0)(1-e^{-\xi_r(u_1)\tau})}{2\xi_r(i\phi)}\right) \\
&\quad + \lambda\tau\left[(1+\mu_J)^{i\phi} e^{i\phi(i\phi-1)\frac{\sigma_J^2}{2}} - 1\right] - \lambda i\phi\mu_J\tau - qi\phi\tau\,,
\end{aligned} \tag{5.77}$$

$$\beta_1(t,T,i\phi,\underline{0}) = i\phi,$$

$$\beta_2(t,T,i\phi,\underline{0}) = \frac{[i\phi(i\phi-1)]\left[1-e^{-\xi_v(i\phi)\tau}\right]}{2\xi_v(i\phi) - \gamma_v^+(i\phi,0)[1-e^{-\xi_v(i\phi)\tau}]}, \text{ and}$$

$$\beta_3(t,T,i\phi,\underline{0}) = \frac{[2(i\phi-1)]}{2\xi_r(i\phi) - \gamma_r^+(i\phi,0)\left[1-e^{-\xi_r(i\phi)\tau}\right]}.$$

The marginal characteristic functions f_2 for the Merton, Kou, and Bakshi models, obtained in this chapter, serve as key inputs to Lee's option pricing formulas derived in Chapter 4. In the next chapter, we implement these models by incorporating their respective characteristic functions into this framework to compute call option prices under the three specifications.

CHAPTER 6

Empirical analysis

6.1. Introduction

This chapter presents the main results obtained from the calibration of the three option pricing models introduced earlier. The aim is to assess how well each model fits market data, both globally and across maturities, using several error metrics to evaluate their performance. The analysis also examines the corresponding risk-neutral distributions, studding their shape and tail behaviour. Each dataset was calibrated separately to allow an adequate comparison between models, highlighting their consistency with the previously established theoretical framework.

6.2. Data and pre-processing

The empirical analysis is based on European-style S&P 500 index monthly options obtained from the Chicago Board Options Exchange (CBOE) for the period between 1 January and 31 May 2022, comprising 103 trading days.

This period was characterised by three major macroeconomic events. First, inflation in the United States reached its highest level since 1982 (8.6% in May 2022), driven by the effects of the COVID-19 pandemic and expansionary fiscal policy. Second, Russia's invasion of Ukraine on 24 February 2022 triggered a geopolitical crisis, which led to higher energy prices and increased global uncertainty. Third, the Federal Reserve initiated one of its most aggressive monetary tightening cycles since 2000, raising the federal funds rate from an initial target range of 0.00–0.25% to 0.75–1.00% over the sample period (25 bps on 16 March, and 50 bps on 4 May). As a result, the S&P 500 declined 21% between its January peak (USD 4,796) and its bottom in May (USD 3,810). The CBOE volatility index (VIX) averaged 27 points, approximately 42% above its long-term mean. Such volatility levels and monetary policy conditions represent a good stress testing scenario for both stochastic volatility and jump-diffusion models. Additional market data are presented in Appendix F.3.

To ensure an homogeneous and liquid sample, only options from the SPX cycle (monthly expiration on the third Friday of each month) were retained.

For each trading day, the dataset includes the option mid-price, strike K, time to maturity τ, the continuously compounded risk-free rate r, the dividend yield q, the underlying mid-quote S_t, and the implied volatility (IV), which serve as inputs for model calibration. The risk-free rate was obtained from U.S. Treasury constant-maturity yields, and the dividend yield was implied from S&P 500 option prices via put–call parity.

Several filters were applied to ensure data quality and consistency with the option pricing models. Contracts with fewer than seven calendar days to maturity were excluded, and option mid-prices were required to exceed three-eighths of a dollar (≈ 0.375). Both strike and underlying mid-quotes had to be strictly positive, and observations with missing or non-positive implied volatilities were removed.

For each strike, a single out-of-the-money (OTM) leg was retained to avoid put–call duplication and to limit microstructure noise around the at-the-money region. The price filter was applied before the strike-level selection to guarantee that all retained options meet the minimum quality threshold, consistent with standard practice (see Bakshi, Cao and Chen (1997) and Bates (2000)).

Note that the filtering sequence affects both the final sample size and the composition of strikes. When the filters are applied in reverse order, with the OTM filter preceding the price filter, the strike distribution becomes markedly more asymmetric, increasing the share of put options from 56.2% to 69.5% (see Appendix F.2.1.1). This occurs because applying the OTM filter first retains a larger set of deep OTM puts in the lower tail. When these puts are converted to synthetic in-the-money calls via put–call parity, the resulting calls exhibit higher prices and are not subject to elimination by the price threshold. Consequently, the proportion of puts increases to 69.5% while information about the left tail of the risk-neutral distribution is preserved. The implications for estimated RND moments are discussed in Appendix F.2.1.

The final calibration sample consists of 329,106 option observations comprising 23 distinct maturities, with time-to-maturity ranging from 7 to 1,810 days (with a mean of 437 days). This corresponds to an average of 3,195 observations per trading day and 14,309 per maturity. Additional descriptive statistics are presented in Appendix F.2.2.

6.3. Model calibration

Calibration was performed separately by trading day and by maturity (t, T). For each cross-section, the model parameter vector $\underline{\boldsymbol{\theta}} \in \mathbb{R}^p$ was estimated using non-linear least squares, minimising the sum of squared pricing errors (SSE) between model-implied and observed option mid-market prices. Following the filtering described in Section 6.2, all retained options are expressed as calls for calibration. If $K < F_{t,T}$, the put was converted to a synthetic call via put–call parity, as follows:

$$C \;=\; P \;+\; e^{-r\tau}\big(F_{t,T} - K\big), \tag{6.1}$$

where C is the price of a European-style call with strike K and maturity T, P is the price of corresponding European-style put. $F_{t,T}$ is the forward price of the underlying observed at time t for delivery at T, r is the risk-free rate, and τ is the time-to-maturity in years.

Otherwise, the call was used. The forward $F_{t,T}$ was taken directly from the dataset, and it also computed using put–call parity. This approach reflects the liquidity asymmetry in equity index option markets, where puts are more actively traded than calls for strikes

below the forward price (see Bates (2000)), producing a uniform panel of call prices for each (t, T) that stabilises calibration and density recovery.

Option prices for each specification are obtained by integrating the model's characteristic function derived in Chapter 5, using adaptive Gauss–Kronrod quadrature with the semi-infinite integration domain mapped onto a finite interval and an absolute error tolerance of 10^{-6}. Alternative numerical approaches such as Laguerre-based quadrature, Gauss–Lobatto and Clenshaw–Curtis rules were tested but proved less stable at low values (including near the $\phi = 0$ singularity). By contrast, Gauss–Kronrod was the most reliable and consistent across maturities.

Optimisation used MATLAB's fmincon (interior-point) solver with simple box constraints, tight convergence tolerances, and warm starts from the previous maturity to improve numerical stability. Solver settings, initial values, and parameter bounds are presented in Appendix F.6, while the three models' calibrated parameters are listed in Appendix F.7.

Risk-neutral densities were recovered for all models by Fourier inversion of the fitted characteristic function on a common terminal-price grid for each trading day, evaluated numerically with Gauss–Kronrod quadrature. Each density was normalised to integrate to one within a small numerical area tolerance and checked for non-negativity and smoothness. The inversion formula and its derivation are provided in the Appendix F.1.

All models were treated identically in terms of dataset, numerical settings and inputs to ensure strict comparability.

6.4. Empirical results

6.4.1. Model fit and comparative performance

This section reports the calibration results and comparative performance of the Merton, Kou, and Bakshi option pricing models, using a common dataset and identical calibration settings. The performance is assessed using standard error metrics (RMSE, MAE, MAPE (%), and SSE) and the goodness-of-fit measure R^2, computed on the full dataset and, separately, by maturity date (see Appendix F.4 for more details). The analysis is presented at two levels of aggregation, first assessing the global fit across all maturities and then within maturity buckets, to capture potential term-structure effects.

At the global level, aggregate error metrics were obtained by assigning equal weight to all contract observations, regardless of maturity or trading day. An alternative aggregation method that first averaged errors within each trading day and then across trading days was also implemented. The resulting rankings are qualitatively similar, and full details are reported in Appendix F.8.1.1 for robustness.

For the maturity bucket analysis, each contract was assigned to one of six buckets based on time to expiration. Within each bucket, errors were first averaged by trading day and then across days. This two-stage aggregation smooths daily variability and preserves term-structure patterns. As with the global fit, a direct bucket-level aggregation yields qualitatively similar results and is also presented in Appendix F.8.1.1 for

robustness. In our analysis, the maturity buckets follow a market tenor approach, with contracts grouped into six categories as reported in Table 6.1. This classification is in line with standard market practice and facilitates comparison with existing literature. Alternative aggregation methods based on short-term maturity splits (Table F.8.1.2), market liquidity (Table F.8.1.3), and sample quantiles (Table F.8.1.4) were also examined and yield qualitatively consistent results.

The following table summarises the calibration results for each model, both globally and at the bucket level.

Table 6.1. Pricing errors by maturity bucket

Maturity	N_{obs}	Model	RMSE	MAE	MAPE (%)	SSE	R^2	$1-R^2$ (bps)
0–30d	85	Merton	1.613	1.135	22.70	3 461.21	0.999973	0.273071
		Kou	2.444	1.761	34.12	4 632.16	0.999956	0.438585
		Bakshi	0.006	0.004	0.21	0.09	0.999999	0.000005
31–90d	204	Merton	2.299	1.801	12.10	1 934.15	0.999985	0.149846
		Kou	2.074	1.717	24.92	1 648.03	0.999986	0.143659
		Bakshi	0.012	0.009	0.13	0.06	0.999999	0.000004
91–180d	304	Merton	3.827	2.969	3.82	3 749.56	0.999972	0.278204
		Kou	2.346	1.754	3.83	1 419.05	0.999989	0.106722
		Bakshi	0.032	0.026	0.19	0.29	0.999999	0.000022
181–270d	301	Merton	5.318	4.347	5.50	4 017.28	0.999968	0.324361
		Kou	3.209	2.564	5.63	1 486.32	0.999988	0.119892
		Bakshi	0.066	0.056	0.54	0.65	0.999999	0.000054
271–365d	318	Merton	5.722	4.543	4.54	4 511.74	0.999963	0.368434
		Kou	3.325	2.607	5.50	1 535.10	0.999987	0.127731
		Bakshi	0.106	0.090	0.70	1.69	0.999999	0.000148
>365d	673	Merton	10.888	8.247	6.83	12 137.55	0.999862	1.377478
		Kou	5.380	3.735	3.60	4 242.39	0.999950	0.495490
		Bakshi	1.304	0.847	0.95	464.58	0.999994	0.057415
All maturities	1 885	Merton	6.607	5.107	7.10	6 656.56	0.999933	0.671079
		Kou	3.703	2.729	8.12	2 622.10	0.999973	0.268558
		Bakshi	0.502	0.333	0.60	166.40	0.999998	0.020465

Note: N_{obs} = number of option contracts per bucket. RMSE = root mean squared error; MAE = mean absolute error; MAPE = mean absolute percentage error; SSE = sum of squared errors; R^2 = coefficient of determination; $1-R^2$ (bps) = $(1 - R^2) \times 10{,}000$.

Table 6.1 shows a clear hierarchy in model performance. Across all 1,885 contracts, Bakshi, Cao and Chen (1997) model substantially outperforms both alternatives, achieving a RMSE of 0.502 compared with 3.703 for Kou and 6.607 for Merton. This corresponds to pricing errors approximately seven times smaller than Kou and thirteen times smaller than Merton. The pattern holds consistently across all error measures. MAE declines from 5.107 for Merton and 2.729 for Kou to 0.333 for Bakshi, MAPE drops from 7.10% and 8.12% to 0.60%, and SSE decreases from 6,656.56 and 2,622.10 to 166.40.

Regarding the coefficient of determination, all three models report R^2 values above 0.9999. However, clear differences remain in the unexplained variance. In terms of basis points, $(1 - R^2)$ equals 0.671 for Merton, 0.269 for Kou, and 0.020 for Bakshi, which means Bakshi explains about 0.25 basis points more variance than Kou and about 0.65 basis points more than Merton (for a visual representation of pricing errors with dispersion measures across maturity buckets, see Appendix F.10).

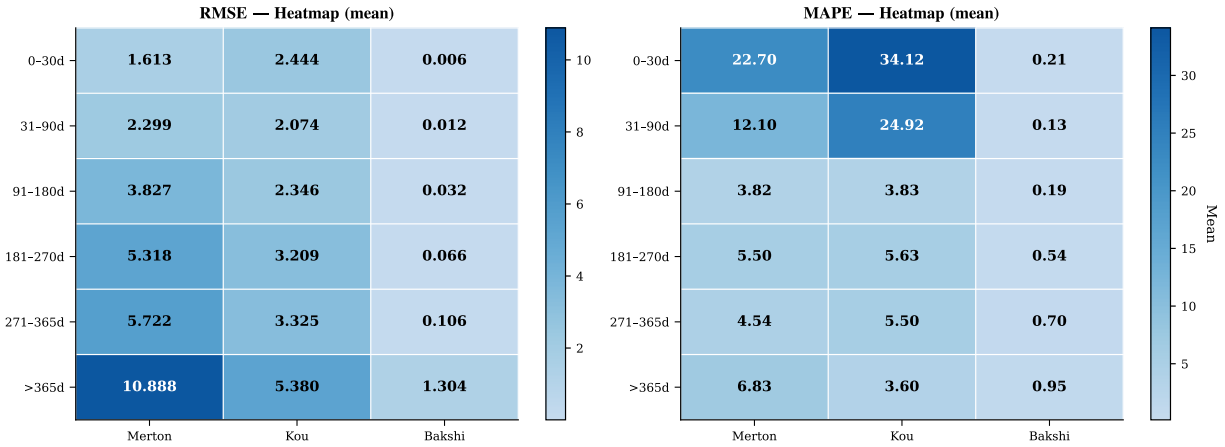
Examining the performance across maturity buckets three patterns arise. First, pricing errors increase consistently with time to maturity for all three models. The Bakshi, Cao and Chen (1997) model keeps RMSE at or below 0.106 for maturities up to one year and rises to 1.304 for contracts exceeding 365 days, whereas Kou and Merton rise to 5.380 and 10.888 in the longest bucket, respectively. This behaviour reflects the uncertainty over extended horizons, where small modelling errors compound into material pricing differences.

Second, Bakshi dominates uniformly across the curve. Even in the shortest bucket (0–30 days), Bakshi records an RMSE of 0.006 compared with 2.444 for Kou and 1.613 for Merton. The advantage persists through intermediate and long maturities and is most pronounced at the long end, where Bakshi's RMSE is about four times lower than Kou's and about eight times lower than Merton's.

Finally, the relative performance of Kou and Merton depends on maturity. At the very short term 0–30 days, Merton reports marginally lower RMSE than Kou. Between 31 and 90 days, Kou gains Merton on level errors, and from 91 days onward Kou remains superior, widening the gap as maturity increases. In the longest bucket, Kou's RMSE is 5.380 versus 10.888 for Merton. Bakshi's dominance reflects the importance of stochastic volatility, while Kou's asymmetric jumps become more valuable at longer horizons, where skewness and tail asymmetry matter more.

While all models maintain R^2 above 0.9998 across all buckets, the unexplained variance shows a clear differentiation. In the shortest bucket (0–30 days), $1-R^2$ reach almost 0.000 basis points for Bakshi, 0.273 for Merton, and 0.439 for Kou. Across intermediate maturities (31–365 days), Kou consistently outperforms Merton with unexplained variance between 0.107 and 0.144 versus 0.150 to 0.368 for Merton. In the longest bucket (>365 days), $1 - R^2$ equals 0.057 for Bakshi, 0.495 for Kou, and 1.377 for Merton. This pattern indicates that volatility dynamics become progressively more important for pricing accuracy over longer horizons.

To visualise the differences across maturities and models, the next figure presents heatmaps of RMSE and MAPE by maturity bucket and model. Darker tones indicate larger errors and weaker fit.



(A) RMSE by maturity bucket

(B) MAPE by maturity bucket

Figure 6.1. Heatmaps of RMSE and MAPE across maturity buckets. Panel (A) reports RMSE and panel (B) reports MAPE. Darker tones indicate larger errors.

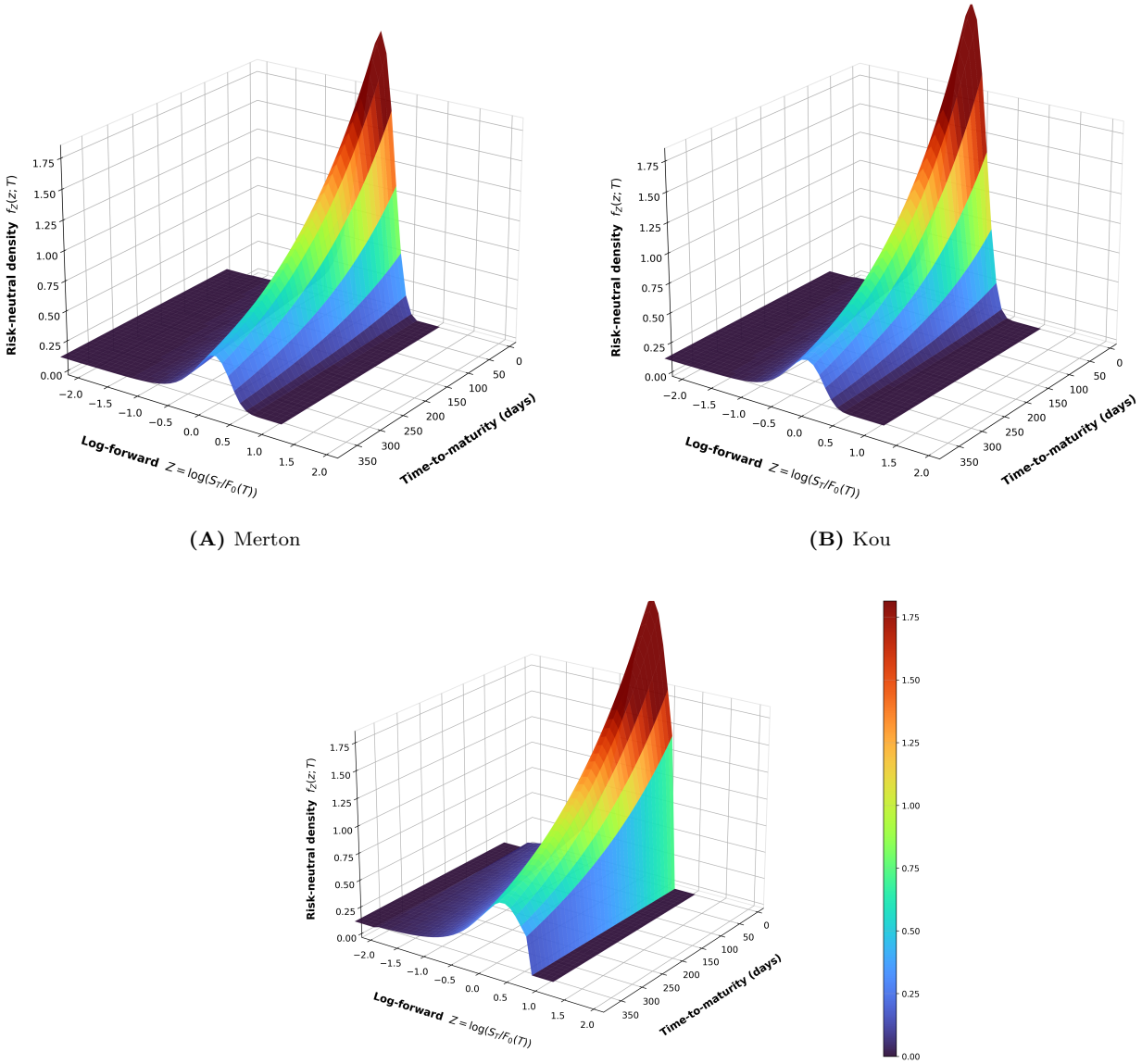
Figure 6.1 complements the previous analysis by providing a visual summary across maturity buckets and models. Errors rise with maturity for all models, and Bakshi maintains low RMSE and MAPE across the grid, while Merton and Kou darken at longer horizons. The crossover between the two jump diffusion benchmarks is evident, with Merton marginally better in the 0–30 day bucket and Kou ahead from 31 days onward. Both panels display the same ordering across maturity, confirming that Bakshi's dominance holds almost uniformly over the option surface.

These findings align with theoretical expectations. Bakshi's stochastic volatility with a jump component provides the flexibility needed to match the implied volatility surface, particularly under the volatile market conditions of early 2022. Kou's asymmetric jumps improve upon Merton's symmetric specification, yet remain substantially less accurate than Bakshi, confirming the importance of stochastic volatility for option pricing under volatile market conditions.

Having established the relative calibration fit, we now focus on the risk-neutral densities implied by each model.

6.4.2. Risk-neutral densities

While the preceding analysis focused on pricing accuracy, the ultimate objective is to extract reliable risk-neutral densities that reflect market expectations for future prices. We begin by visualising the RNDs in three dimensions. Figure 6.2 presents three-dimensional surfaces of the RNDs as functions of log-returns Z_T and time-to-maturity τ, using a common colour scale to permit a direct comparison of the density shape, tail behaviour, and mass concentration across models. For each maturity level τ, the surface displays the average RND computed by averaging across all trading days in the sample period on which that maturity was observed. This aggregation smooths out day-to-day fluctuations and highlights the systematic evolution of density shape and tail behaviour as maturity increases.



(A) Merton

(B) Kou

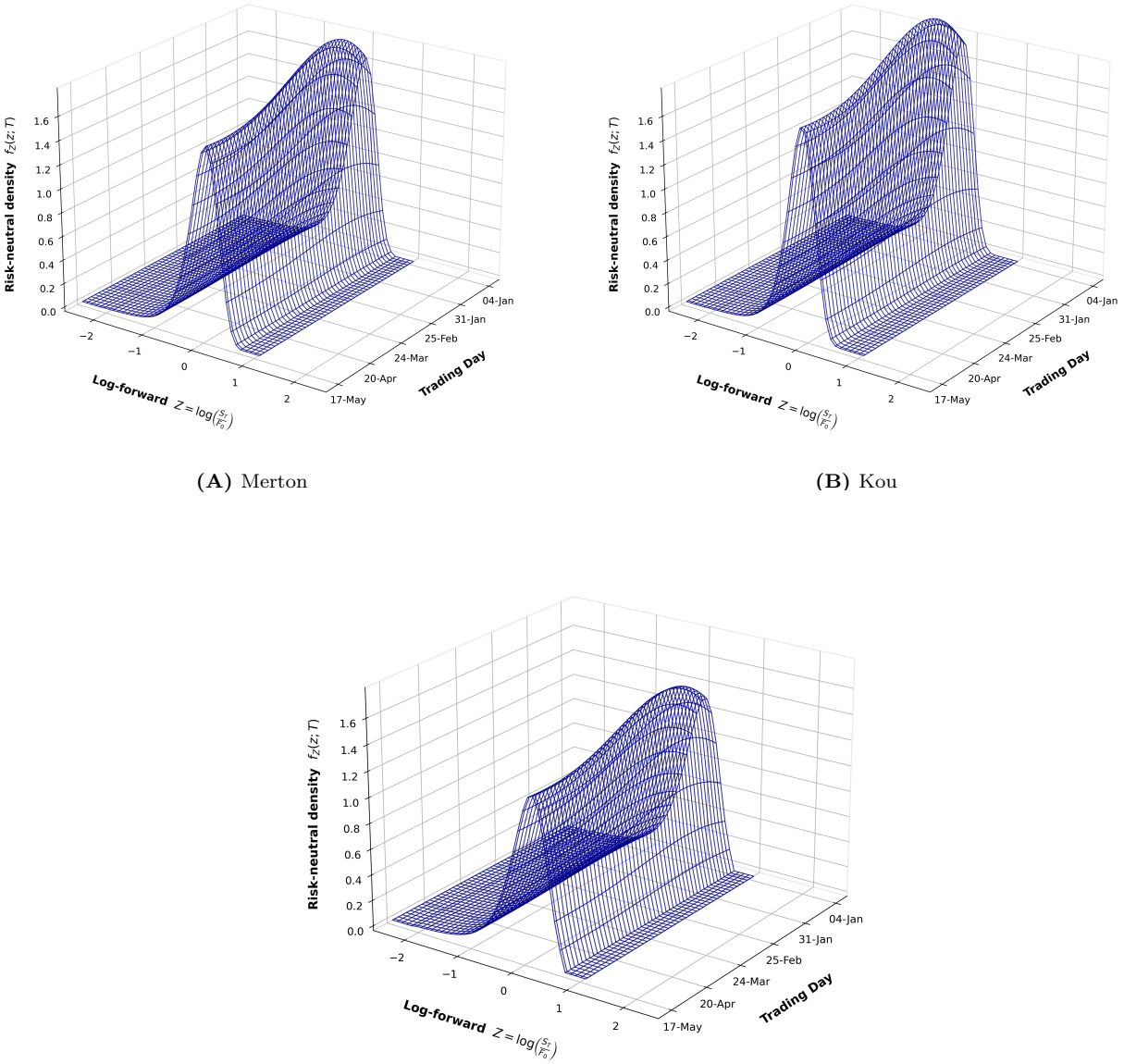
(C) Bakshi

Figure 6.2. Risk-neutral density (RND) *surfaces* as a function of log-returns Z_T and time-to-maturity τ for the three models. All panels share the same color scale and viewing angle for direct comparison of mass and tail height.

Figure 6.2 shows clear differences in the risk-neutral density surfaces across models (for details on 3D RND contours see Appendix F.10). Merton presents relatively narrow densities with a near-lognormal core and thin tails. The left tail thickens only slightly as maturity increases and the shape remains overly symmetric around the mode, consistent with symmetric Gaussian jumps and constant volatility. This structural limitation is consistent with the larger errors observed for OTM options. In contrast, Kou shifts mass to the downside and yields visibly asymmetric densities. Dispersion and left-tail weight increase with maturity, representing a clear improvement over Merton from 31 days onward, although the evolution of skew remains relatively rigid across maturities, limiting the model's ability to capture time varying asymmetry in the observed volatility surface.

Among the three models, Bakshi presents the most economically plausible surfaces. Dispersion and kurtosis rise smoothly with maturity, the left tail is materially thicker, the mode shifts in line with observed skews, and the temporal evolution is smooth, indicating a good cross-section fit without overfitting.

Turning to the time dimension, Figure 6.3 displays daily wireframes for the 31 to 90 day bucket, a liquid and well populated segment that is representative of the sample.



(A) Merton

(B) Kou

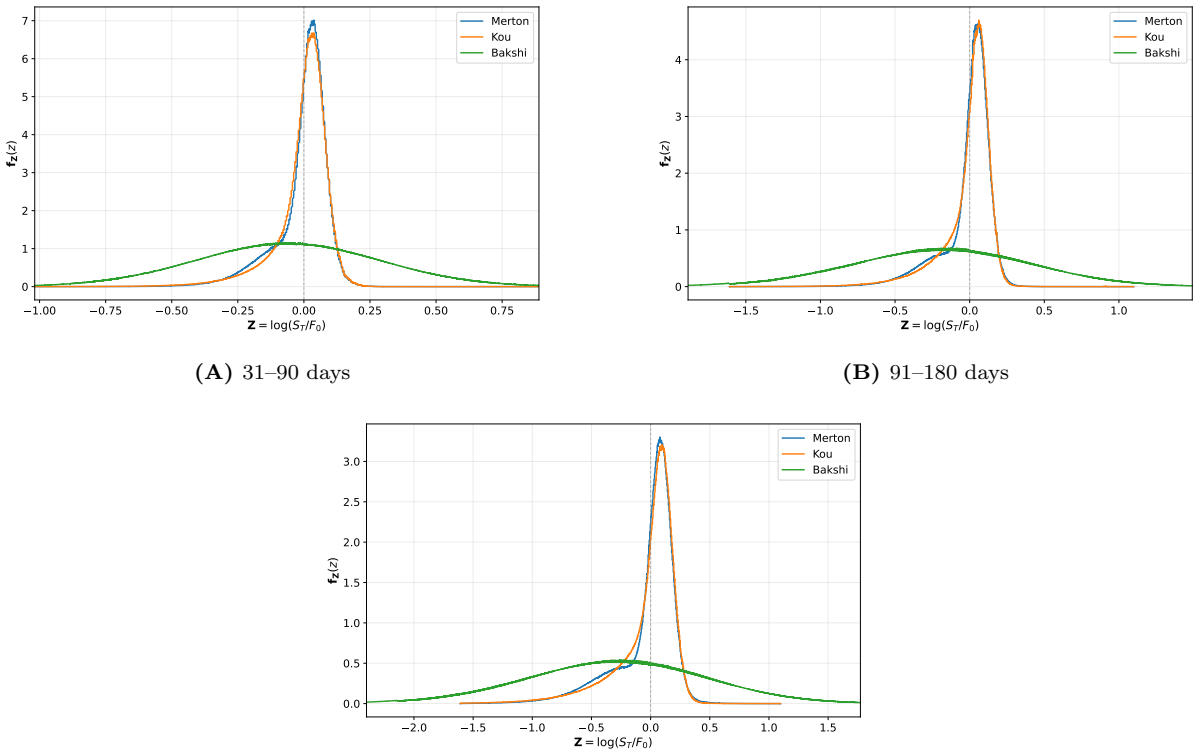
(C) Bakshi

Figure 6.3. RND wireframes over trading days for the 31–90 day maturity bucket. All three panels use the same vertical limit (z) and viewing angle for comparability.

The wireframes mirror the surface patterns shown in Figure 6.2. Merton is rigid through time. The mode drifts from day to day but the shape remains narrow and nearly symmetric with thin tails, which is consistent with constant volatility and symmetric jumps

and helps explain difficulty with downside risk. Kou introduces a persistent downside skew and improves on Merton beyond one month, however, the degree of skew changes only modestly across days, and both left tail thickening and time variation are limited. Bakshi shows the most plausible evolution. Dispersion and left tail weight respond well to the evolution of market conditions and the wires widen gradually smoothly, indicating an adaptive and stable fit. In sum, the wireframes show that the qualitative features seen in the surfaces persist through time within this reference bucket.

We now examine the distributional shape and tail behaviour of risk-neutral densities for different maturity buckets and assess whether they are consistent with theoretical expectations.



(A) 31–90 days

(B) 91–180 days

(C) 270–365 days

Figure 6.4. Risk–neutral densities f_{Z_T} with **Merton, Kou, and Bakshi** overlaid in three representative maturity buckets. The x-axis range is identical across panels, and the same y-axis limit is used for strict comparability.

Figure 6.4 displays the risk-neutral densities for three representative maturity buckets, representing the short, medium and long terms. In the short-term bucket (31–90 days), Merton produces a relatively narrow and almost symmetric distribution with limited tail weight. Kou introduces visible negative skewness through its asymmetric double-exponential jumps, shifting mass to the downside. Bakshi exhibits the most pronounced left tail and the smoothest transition from core to tail, consistent with stochastic volatility and correlated jumps. As maturity increases, for the 91–180 days and 271–365 days buckets, dispersion rises for all models, but the relative patterns persist. Merton remains

overly symmetric, Kou maintains moderate downside skew, and Bakshi continues to show the thickest left tail and most gradual decay.

These visual patterns motivate the quantitative analysis of moments, tail quantiles, and distributional distances presented in the following subsections. To characterise the statistical properties of the risk-neutral densities, we computed moments (mean, standard deviation, skewness, kurtosis), quantiles for each individual daily RND extracted from the calibrated models (tail risk measures, such as Value-at-Risk and Expected Shortfall measure can be found in F.14). The daily statistics were then aggregated across maturity by taking the median value, following the approach used in studies of option implied moments (e.g., Bali, Hu, and Scott (2017) and Stilger, Kostakis, and Poon (2017)). This methodology preserves the temporal variability of the distributions and provides robust measures, particularly in the presence of extreme market events, as the median is less sensitive to outlier observations than the mean. As a robustness check, we verified that computing statistics from pooled densities across time, yields qualitatively consistent results, with a median difference of 1.37% across all measures, confirming the stability of our findings (see Appendix F.12).

6.4.2.1 Moments

To characterise the statistical properties of the risk-neutral densities, we computed the moments (mean, standard deviation, skewness, kurtosis), quantiles, and tail risk measures for each individual daily RND extracted from the calibrated models. As previously mentioned, these daily statistics were subsequently aggregated across time by taking the median value for each model-maturity combination. This methodology preserves the temporal variability of the distributions and provides robust measures, particularly in the presence of extreme market events, as the median is less sensitive to outlier observations than the mean. The table 6.2 presents the aggregated moments.

Table 6.2. Statistical moments and quantiles of risk-neutral densities

Maturity	Model	Mean	Std Dev	Skewness	Kurtosis	Q10	Q50	Q90
0–30d	Merton	−0.002	0.070	−0.6824	4.2429	−0.089	0.004	0.082
	Kou	−0.002	0.073	−1.3054	11.5802	−0.083	0.003	0.083
	Bakshi	−0.014	0.168	0.0006	3.0141	−0.229	−0.014	0.201
31–90d	Merton	−0.005	0.109	−1.3874	6.1232	−0.149	0.015	0.107
	Kou	−0.005	0.114	−1.8298	10.0373	−0.136	0.013	0.108
	Bakshi	−0.066	0.364	−0.0037	2.9948	−0.534	−0.066	0.400
91–180d	Merton	−0.012	0.168	−1.6904	7.2001	−0.244	0.027	0.145
	Kou	−0.012	0.173	−1.9721	9.4597	−0.228	0.028	0.145
	Bakshi	−0.156	0.554	0.0326	2.7731	−0.879	−0.158	0.566
181–270d	Merton	−0.021	0.223	−1.7630	7.1182	−0.337	0.037	0.179
	Kou	−0.021	0.227	−2.0016	8.7312	−0.311	0.039	0.179
	Bakshi	−0.224	0.671	0.0265	2.8316	−1.093	−0.225	0.640
271–365d	Merton	−0.028	0.260	−1.6814	6.5235	−0.403	0.045	0.204
	Kou	−0.028	0.265	−1.9037	7.7379	−0.376	0.046	0.205
	Bakshi	−0.308	0.781	−0.0066	2.8169	−1.322	−0.304	0.698
> 365d	Merton	−0.051	0.358	−1.2907	4.8437	−0.575	0.053	0.275
	Kou	−0.047	0.358	−1.5644	5.8572	−0.549	0.049	0.284
	Bakshi	−0.459	0.968	−0.0327	2.7875	−1.730	−0.440	0.781
All maturities	Merton	−0.026	0.248	−1.5441	6.1424	−0.383	0.040	0.197
	Kou	−0.026	0.253	−1.8006	7.7345	−0.355	0.041	0.198
	Bakshi	−0.272	0.739	0.0031	2.8155	−1.239	−0.274	0.688

Note: Statistical moments and quantiles of RNDs extracted from S&P 500 options for the period Jan–May 2022, across six maturity buckets and aggregated across all maturities. All metrics are computed in normalised return space ($Z = \ln(S_T/F)$). Mean and standard deviation measure central tendency and dispersion; skewness captures asymmetry; kurtosis measures tail thickness. Q10, Q50, Q90 represent the 10th percentile, median, and 90th percentile of the risk-neutral distribution. Values represent medians across daily observations.

Table 6.2 reports the statistical moments and quantiles of the RNDs extracted from S&P 500 monthly options for the period from January to May 2022. All calculations were made in a normalised log-return space, $Z_t = \ln(S_T/F)$, where S_T is the terminal stock price and F is the forward price (for boxplots showing the distribution of RND moments by maturity bucket, see Appendix F.10).

The results show clear differences in how each model characterises the risk-neutral distribution. Merton and Kou models present a similar aggregate mean of -0.026. The mean becomes more negative with increasing maturity for all three models. For Merton, it ranges from -0.002, for the 0–30d bucket, to -0.051 beyond one year (> 365d). Kou exhibits a similar pattern, ranging from -0.002 to -0.047 over the same period. Bakshi shows substantially more negative means throughout, reaching -0.459 at the longest maturity.

In all three models, the standard deviation increases with maturity. At the aggregate level, Merton has a standard deviation of 0.248 and Kou 0.253, while Bakshi is substantially higher at 0.739. This pattern holds across maturities. At 0–30d, standard deviation is 0.070 for Merton, 0.073 for Kou, and 0.168 for Bakshi. In the $>$ 365-day bucket, it reaches 0.358 for both Merton and Kou, and 0.968 for Bakshi. Bakshi is consistently two to three times more dispersed than the jump-diffusion models across all maturities.

The main difference between Merton and Kou appears in the higher-order moments. Aggregate skewness is -1.80 for Kou versus -1.54 for Merton. Aggregate kurtosis is 7.73 for Kou versus 6.14 for Merton. This holds across all maturity buckets. Bakshi behaves differently, with aggregate skewness of 0.0031 and kurtosis of 2.82, indicating an approximately symmetric distribution with near-normal tails.

The quantile analysis provides a clear representation of these differences. For Merton and Kou, the left tail extends almost twice as far as the right (e.g., Merton aggregate: Q10 is -0.383 vs. Q90 is 0.197), consistent with their negative skewness. Conversely, Bakshi's quantiles are symmetric (Q10 is -1.239 vs. Q90 is 0.688), confirming the near-zero skewness and wider dispersion.

This symmetric pattern in the Bakshi, Cao and Chen (1997), with near-zero median skewness (0.0031) and kurtosis close to normality (2.82), contrasts with the typical behaviour of S&P 500 options, which generally exhibit negative skewness. This suggests that the jump component contributes little to asymmetry, resulting in a distribution closer to normality than expected for equity index options during stress periods. As a result, the model achieves superior fit for mid-priced options but produces RNDs with weaker left-tail asymmetry and heavier right tails than expected for equity markets during market stress. This is most evident in skewness, where mean aggregation produces -0.007905 while the median yields 0.003074. Despite this difference, the underlying RND dynamics remain consistent across both aggregation methods, as shown in Appendix Tables F.9 and F.12. A detailed analysis of these results is provided in Section 6.4.3.

6.4.2.2 Tail behaviour

Table 6.3 presents the tail probabilities at extreme thresholds at aggregate level and maturity.

Table 6.3. Tail probabilities at extreme thresholds by maturity

Maturity	Model	Left Tail (%)			Right Tail (%)		
		$Z<-0.36$ (≈-30%)	$Z<-0.22$ (≈-20%)	$Z<-0.11$ (≈-10%)	$Z>0.10$ (≈+10%)	$Z>0.18$ (≈+20%)	$Z>0.26$ (≈+30%)
0–30d	Merton	0.04	0.75	7.17	5.79	0.02	0.00
	Kou	0.26	1.16	6.08	6.18	0.07	0.00
	Bakshi	2.02	10.59	29.19	25.46	11.99	4.88
31–90d	Merton	1.05	4.96	14.21	13.10	0.63	0.03
	Kou	1.60	4.84	13.13	13.27	0.70	0.02
	Bakshi	21.17	33.28	45.63	32.78	24.72	18.26
91–180d	Merton	5.00	11.16	19.13	23.59	4.21	0.43
	Kou	4.90	10.21	19.27	24.03	3.91	0.34
	Bakshi	36.21	45.41	53.67	32.64	27.32	22.80
181–270d	Merton	9.13	14.98	21.83	30.90	9.37	1.75
	Kou	8.25	14.14	22.57	31.83	9.39	1.42
	Bakshi	42.23	50.07	56.95	31.80	27.34	23.56
271–365d	Merton	11.68	17.73	24.25	35.28	13.67	3.63
	Kou	10.60	16.65	24.83	36.13	14.13	3.32
	Bakshi	47.29	54.07	59.90	30.57	26.81	23.55
> 365d	Merton	17.90	23.95	30.44	42.15	23.87	11.15
	Kou	15.94	22.13	29.98	42.12	25.29	12.34
	Bakshi	53.38	58.68	63.24	29.35	26.35	23.52
All maturities	Merton	10.92	16.75	23.67	33.85	12.41	3.07
	Kou	9.85	15.83	24.22	34.82	12.72	2.77
	Bakshi	45.66	52.65	58.67	30.90	26.80	23.43

Note: Tail probabilities of RNDs extracted from S&P 500 options for the period Jan–May 2022, across six maturity buckets and aggregated across all maturities. All metrics are computed in a normalised return space ($Z = \ln(S_T/F)$). Left tail probabilities represent the likelihood of losses exceeding the specified threshold; right tail probabilities represent the likelihood of gains exceeding the specified threshold. Values shown as percentages and represent medians across daily observations.

Table 6.3 summarises risk-neutral tail probabilities at fixed thresholds in the normalised log-return space $Z = \ln(S_T/F)$. For all models, tail mass increases with maturity on both sides, reflecting the increase in standard deviation across maturities reported in Table 6.2. Comparing the jump–diffusion models, Kou assigns slightly more probability to large negative outcomes than Merton at most horizons, while right-tail probabilities are very similar. This is consistent with Kou's more negative skewness and higher kurtosis. In contrast, the Bakshi, Cao and Chen (1997) model places substantially more mass in both tails, and the increase with maturity is more pronounced. Aggregated across maturities, the probability of $Z < -0.22$ is about 16–17% for Merton and Kou, against roughly 53% for Bakshi. On the right side, $P(Z > 0.18)$ is about 12–13% for Merton and Kou and around 27% for Bakshi. Once more, these results suggest a trade off, where achieving a better fit to option prices comes at the cost of a more symmetric and less negatively skewed risk neutral density.

6.4.2.3 Divergence and distance measures

The next table presents the statistical distances between models for all maturities.

Table 6.4. Statistical distances between models – All Maturities

Comparison	Jensen-Shannon	Hellinger	Wasserstein-1
Merton vs Kou	0.002	0.049	0.009
Bakshi vs Kou	0.240	0.529	0.475
Bakshi vs Merton	0.239	0.529	0.475

Note: Statistical distances between RNDs for the period Jan–May 2022, aggregated across all maturities. Jensen-Shannon divergence measures information-theoretic distance (range: [0, $\ln(2) \approx 0.693$], lower = more similar); Hellinger distance measures geometric similarity (range: [0, 1], lower = more similar); Wasserstein-1 (Earth Mover's Distance) measures the minimum "cost" to transform one distribution into another in $Z = \ln(S_T/F)$ space. Values represent medians of daily distances across the sample period. Small distances between Merton and Kou (< 0.01 for JS and W1) indicate these models produce very similar risk-neutral densities, while large distances between Bakshi and the other models (> 0.2 for JS, > 0.5 for Hellinger, > 0.4 for W1) indicate fundamentally different distributional characteristics.

Table 6.4 summarises three standard, symmetric distances between pairs of model implied RNDs, aggregated across all maturities. Jensen–Shannon divergence captures information-theoretic differences, Hellinger distance measures geometric overlap between distributions, and Wasserstein-1 quantifies the mass transportation required to map one density into another. Lower values indicate greater similarity.

Merton–Kou shows uniformly small values, with JS = 0.002, Hellinger = 0.049, and W1 = 0.009, which indicates very similar shapes across maturities. By contrast, distances between Bakshi and either jump–diffusion model are much larger, with JS ≈ 0.240, Hellinger ≈ 0.529, and W1 ≈ 0.475, which implies a substantial departure. The near equality of the Bakshi–Kou and Bakshi–Merton values indicates that Bakshi is roughly equidistant from the two, while Merton and Kou lie close together. Merton and Kou are relatively concentrated and left-skewed, whereas Bakshi is closer to symmetric and more dispersed.

6.4.3. Explaining Bakshi's RND characteristics

As shown in Section 6.4.2.1, Bakshi exhibits a distinctive pattern, with near-zero skewness and kurtosis close to normality despite achieving superior pricing fit. This outcome warrants further investigation to understand why the model produces RNDs that diverge from typical equity market characteristics during stress periods.

Analysing the calibrated parameters, we observe a diffusion-heavy calibration pattern. As detailed in Appendix F.6, the calibrated mean jump intensity ($\lambda_J = 0.138$) is substantially lower than typical equity calibrations (0.5 to 1.5 jumps per year), with 66.3% of calibrations at the lower bound, indicating that the jump component is largely inactive. In contrast, mean reversion speed ($\kappa_v = 0.23$) operates at the lower bound in 74.5% of calibrations, indicating slow mean reversion and persistent stochastic volatility that dominates the pricing dynamics. Consistent with this diffusion-heavy calibration, the leverage

effect is weak ($\rho \approx -0.24$), and long-run variance (θ_v) operates near the lower bound in 97.9% of calibrations. Together, these patterns explain the near zero skewness. Without active jumps, the diffusion component alone cannot generate the pronounced left tail asymmetry typical of equity markets during stress.

Additionally, several factors may have contributed to this outcome. First, the objective function minimises squared pricing errors with equal weighting across all options, which implicitly assigns greater weight to higher-priced options (those closer to ATM) and less weight to lower-priced deep OTM options, where jumps matter. Second, because the USD 3/8 price filter was applied before the OTM filter, deep out-of-the-money puts, which are typically low-priced, were disproportionately eliminated before the OTM filter could retain them (61.4% of puts retained in the reduced sample, as shown in Appendix F.2.1). As a result, the left tail of the risk-neutral distribution was truncated and information about downside risk was reduced. Furthermore, the sample period exhibits elevated but non-extreme volatility (VIX ranged between 25 and 27, with peaks of 36 points) rather than discrete jumps. Finally, this pattern is also influenced by the aggregation choice, as the use of median rather than mean downweights extreme days and can shift moments upwards when negative outliers are present.

One may ask why these factors affect only Bakshi's results. The answer lies in the model's flexibility, as Bakshi's adaptive structure allows the calibration to exploit the data characteristics, whereas Merton and Kou impose structural asymmetry through their jump specifications, making them more rigid and better at preserving left-tail mass despite the same filtering bias. Additionally, insufficient information from available strikes to identify both volatility and jump components separately may lead the model to allocate more weight to stochastic volatility, further enhancing its adaptation to market prices. These results suggest a trade-off in which achieving a better fit to option prices, as measured by pricing-error metrics, comes at the cost of a more symmetric, less negatively skewed risk-neutral density.

This was the main reason why we decided to use the log-return space $Z = \ln(S_T/F_0)$ for risk analysis, as this metric removes scale effects and maintains the expected negative skewness across all models, correcting Bakshi's near-zero or positive skewness when using the S_T space.

6.5. Implied-volatility smoothing and calibration design

In this section we investigate whether smoothing the implied volatility surface prior to calibration improves model performance compared to the baseline approach using raw market data. To this end, we will use the Bakshi, Cao and Chen (1997) SVSI-J model, as it is the only model among those reviewed that incorporates stochastic volatility.

The motivation for smoothing implied volatility surfaces stems from three main reasons. First, market-observed implied volatilities usually contain microstructure noise. As such, they can be decomposed in two components as $\sigma_{\text{observed}} = \sigma_{\text{true}} + \varepsilon$, where σ_{true} represents the "real" volatility structure and ε denotes microstructure noise arising from

bid-ask spreads, discrete trading, and market impact. Smoothing techniques effectively filter out the high-frequency noise component ε, while preserving the lower-frequency structural dynamics captured by σ_{true}. This is particularly critical for optimisation algorithms, which may overfit to noise rather than signal, leading to unstable parameter estimates. Then, raw market data often violate no-arbitrage conditions, which require that call prices increase with maturity (calendar spread arbitrage) and exhibit convexity in strike (butterfly spread arbitrage). Spline interpolation enforces continuity, reducing arbitrage violations between observed strikes and producing economically coherent and arbitrage-free volatility surfaces. Finally, smoothing results in optimisation efficiency. As model calibration involves minimising an objective function over a high dimensional parameter space, when market prices are noisy, the objective function becomes rugged with many local minima that trap gradient optimisation algorithms. Smoothing regularises this space, facilitating convergence to the global optimum and reducing computational time as we will later see.

Before proceeding, it is important to mention that two calibration approaches were considered regarding the calibration target. One where the model would be calibrated against smoothed option prices, isolating model performance from surface noise, and another where the model would be calibrated directly against raw market prices, testing the joint smoothing and pricing performance. Following the literature, the first was chosen, as it gives a clearer assessment of the model's structural fit.

6.5.1. Spline interpolation methods

Two spline methodologies were employed to smooth the implied-volatility surface, each with distinct continuity properties. We used cubic splines with C^2 continuity, producing smooth first and second derivatives across the entire surfaces, and the cubic Hermite method, which enforces C^1 continuity, by allowing second derivatives to be discontinuous.

Cubic splines are piecewise cubic polynomials that minimise the integrated squared second derivative while satisfying natural boundary conditions at the endpoints. In this case, the method was implemented using MATLAB's `spline` function (see Appendix F.5). For each maturity segment, the implied volatility surface was interpolated in log-returns space rather than strike space for numerical stability. However, this global optimisation approach makes cubic splines sensitive to outliers, where a single extreme point can distort the entire curve. They may also show oscillations near the boundaries of the interpolation range, a numerical effect known as Runge's phenomenon, in which the interpolated curve develops artificial fluctuations that are not present in the underlying smooth data.

In contrast, Hermite splines are segmented cubic polynomials with different continuity requirements. Unlike cubic splines, which determine derivatives through global minimisation of the integrated squared second derivative, Hermite splines estimate slopes locally from the data, allowing more localised control. We implemented Hermite splines using MATLAB's piecewise cubic Hermite interpolating polynomial function (see Appendix F.5 for more details). This algorithm automatically estimates derivatives using

a shape-preserving algorithm that guarantees monotonicity preservation, meaning that if input data is monotonic, the interpolant remains monotonic without introducing unwanted oscillations. It also prevents overshooting, ensuring the interpolant stays within the data range, which makes Hermite splines robust to outliers because changes to one data point affect only neighbouring intervals rather than propagating across the entire curve. However, the Hermite method has reduced smoothness (C^1 rather than C^2), which can result in discontinuous second derivatives. For calibration, this is often offset by greater robustness to data anomalies.

6.5.2. Sample period and implementation issues

Our final sample comprises 300 independent calibrations from 30 trading days with 10 maturities per day. To assess calibration quality, both smoothing methods were run under identical calibration settings.

During preliminary testing, two implementation challenges emerged. First, cubic splines showed increased sensitivity to outliers. This issue motivated the adoption of the Hermite method in our analysis. Then, percentage-based metrics became unstable when option prices were close to zero. To prevent overflow and division by zero, we add a small epsilon to denominators equal to MATLAB's double-precision machine epsilon ($\approx 2.22 \times 10^{-16}$). This value is negligible relative to typical prices, including deep OTM options, and it prevents non-finite or undefined values that would otherwise disrupt the optimisation process.

For this reason, and in addition to the six standard metrics, we introduce the symmetric mean absolute percentage error (sMAPE). The sMAPE treats over- and under-prediction symmetrically, is bounded between 0% and 100%, and remains well defined near zero because the denominator includes both market and model prices. The formal definition of the sMAPE metric is reported in Appendix F.4.5.

6.5.3. Comparative results and main findings

6.5.3.1 Model fit and convergence stability

As in section 6.4.1, the errors were summarised using two aggregates, a global measure that gives equal weight to all contracts across maturities and trading days, and a maturity-bucket measure that groups contracts into six time-to-expiry buckets and averages errors by day within each bucket and then across days. However, in this case, the bucket levels are different because the sample is smaller and contains fewer observations for maturities above one year. The thresholds were adjusted to maintain the same number of buckets and ensure the analysis remains comparable. The following table presents these results by bucket and for all maturities.

Table 6.5. Pricing errors by maturity

Maturity	N_{obs}	Method	RMSE	MAPE (%)	sMAPE (%)	Conv (%)	CV (%)
0–30d	26	Baseline	0.0106	0.23	0.24	96.15	91.53
0–30d	26	Cubic	0.0036	0.16*	7.71	100.00	34.39
0–30d	26	Hermite	0.0036	0.16	0.14	100.00	34.18
30–60d	34	Baseline	0.0076	0.15	0.24	100.00	29.16
30–60d	34	Cubic	0.0075	0.11	3.46	100.00	29.07
30–60d	34	Hermite	0.0075	0.11	0.13	100.00	29.59
60–90d	28	Baseline	0.0116	0.09	0.10	100.00	25.98
60–90d	28	Cubic	0.0114	0.09	2.68	100.00	40.19
60–90d	28	Hermite	0.0114	0.09	0.13	100.00	40.87
90–180d	90	Baseline	0.0237	0.12	0.13	100.00	23.21
90–180d	90	Cubic	0.0229	0.12	3.40	100.00	34.85
90–180d	90	Hermite	0.0229	0.12	0.15	100.00	34.15
180–270d	85	Baseline	0.0563	0.49	0.51	100.00	15.64
180–270d	85	Cubic	0.0543	0.48	18.70	100.00	22.69
180–270d	85	Hermite	0.0543	0.51	0.57	100.00	23.19
270–365d	37	Baseline	0.0822	0.71	0.76	100.00	12.14
270–365d	37	Cubic	0.0789	0.70	28.06	100.00	15.34
270–365d	37	Hermite	0.0789	0.75	0.84	100.00	15.97
All maturities	300	Baseline	0.0362	0.31	0.33	99.67	51.81
All maturities	300	Cubic	0.0344	0.30	11.20	100.00	41.39
All maturities	300	Hermite	0.0344	0.31	0.36	100.00	41.39

Note: RMSE = Root Mean Squared Error; MAPE = Mean Absolute Percentage Error; sMAPE = Symmetric Mean Absolute Percentage Error; Conv (%) = percentage of calibrations that converged; CV (%) = Coefficient of Variation. For *Cubic* in bucket **0–30d** on 05-Jan-2022 there was an extreme outlier: MAPE $\approx 4.95\times10^{11}$%. Entries marked with * (0–30d, Cubic) indicate this outlier is excluded from the reported statistics.

Table 6.5 presents the error metrics for the three calibration methods: Cubic spline, Hermite spline and the original baseline approach[1]. The results show that smoothing significantly enhances calibration quality across several dimensions, in line with what is reported in the literature (see, for instance, Fengler (2005), or Andreasen and Huge (2011)). The Hermite spline methodology achieves the best overall performance, with an average RMSE of 0.034439, representing a 4.95% reduction compared to the original baseline (RMSE = 0.036232). The cubic spline methodology performs nearly identically, with an RMSE of 0.034445, indicating a 4.93% improvement over the baseline.

Regarding MAPE, the original baseline model exhibits a global MAPE of 0.31%, which is marginally reduced by the Cubic model to 0.30%, representing an overall improvement of approximately 3.2%. The Hermite model shows no improvement at the global level, with a MAPE of 0.31%. This enhancement is not uniform across all maturities. A granular analysis shows that the most substantial gains occur in the short-term buckets. The Cubic

[1]The pricing errors presented here are significantly lower than those reported in Section 6.1, reflecting a smaller sample composed primarily of short- and very short-term maturities, where errors tend to be lower.

and Hermite models reduce the MAPE by approximately 30% in the 0–30d bucket (from 0.23% to 0.16%) and by over 26% in the 30-60d bucket (from 0.15% to 0.11%). As the time-to-maturity increases, the relative accuracy of all three models converges. For the 60-90d and 90-180d buckets, the smoothing techniques offer no improvement in MAPE. In the long-term buckets (e.g., 180–365 days), the improvements are only marginal, with the Cubic model offering a reduction of just 2% in the 180-270d bucket and 1.4% in the 270-365d bucket. This confirms that the main benefit of the Cubic and Hermite models lies in mitigating the pricing instability in the short-term, where the market noise is higher.

The sMAPE gives a scale-independent assessment of pricing accuracy. Hermite splines achieve an sMAPE of 0.36%, while Cubic splines achieve 11.20%, both compared with the baseline (sMAPE = 0.33%). This pattern varies across maturities. This pattern varies across maturities. In the short-term buckets (0–60d), the Hermite model achieves values of 0.14% and 0.13%, improving over the original sMAPE of 0.24%, while the Cubic model exhibits elevated values of 7.71% and 3.46% due to outlier sensitivity. For mid-term maturities (60–180d), the Hermite model maintains stable performance (0.13–0.15%), comparable to the original (0.10–0.13%), while the Cubic model shows values of 2.68–3.40%. In long-term buckets (180–365d), the Hermite model shows values of 0.57–0.84%, marginally higher than the baseline 0.51–0.76%, while the Cubic model escalates to 18.70–28.06%. These results demonstrate that the Hermite spline maintains stable sMAPE across all maturities, while the Cubic spline shows increasing error for longer-term options.

Regarding the coefficient of variation (CV), it is used to assess the temporal stability of the pricing error, with a lower CV indicating more reliable performance. The baseline model exhibits a global CV of 51.81%, which is reduced to 41.39% by both spline methods, representing an improvement of approximately 20%. This improvement is concentrated in the short-term bucket (0–30d), where the splines reduce the CV from 91.53% to approximately 34%. For mid-term maturities (60–180d), the pattern reverses as the original model registers CV values of 25.98% and 23.21%, while the splines increase these to 34–40%. For long-term buckets (180–365d), the Original model maintains lower CV values (12–16%) compared to the splines (15–23%). In conclusion, the spline methods offer superior global stability but mainly in the short-term bucket. However, for mid-term and long-term maturities, the original model shows better temporal consistency.

Finally, we tested robustness to numerical outliers. On 5 January 2022, the cubic spline produced an extreme MAPE due to near-zero option prices with short time to expiry, where the near-zero denominator inflated the percentage error. For the same calibration, the Hermite method returned a normal MAPE. Across the full sample of 300 calibrations, the Hermite method produced zero such outliers (defined as MAPE $> 1000\%$), whereas the cubic spline produced one, which represents 0.3% of the sample. The outlier magnitude was approximately $4.95 \times 10^{11}\%$. Overall, the Hermite method matches or exceeds the cubic spline in pricing accuracy while providing stronger convergence, parameter stability, and better robustness to numerical issues.

6.5.3.2 Parameter robustness

We further assessed parameter stability by computing the coefficient of variation (CV) of the calibrated for all Bakshi parameters.

Table 6.6. Summary Statistics of Calibrated Parameters

	Baseline			Cubic Spline			Hermite Spline		
Param.	**Mean**	**SD**	**CV (%)**	**Mean**	**SD**	**CV (%)**	**Mean**	**SD**	**CV (%)**
θ_v	0.0057	0.0054	95.15	0.0053	0.0007	12.81	0.0053	0.0007	12.87
σ_v	0.0821	0.0118	14.42	0.0790	0.0106	13.46	0.0791	0.0105	13.28
κ_v	0.2962	0.4515	152.43	0.2422	0.0685	28.30	0.2424	0.0686	28.31
ρ	-0.1868	0.0728	38.95	-0.1930	0.0601	31.14	-0.1923	0.0585	30.41
θ_r	0.0065	0.0036	55.48	0.0061	0.0019	30.54	0.0059	0.0015	25.06
σ_r	0.0256	0.0208	81.43	0.0376	0.0205	54.48	0.0390	0.0216	55.29
κ_r	1.8055	0.5414	29.99	1.7973	0.5528	30.76	1.7533	0.5687	32.44
λ_j	0.1047	0.0216	20.60	0.1357	0.1149	84.68	0.1339	0.1146	85.55
μ_j	-0.0634	0.0371	58.59	-0.0471	0.0426	90.40	-0.0477	0.0431	90.39
σ_j	0.0592	0.0265	44.71	0.0567	0.0259	45.75	0.0565	0.0251	44.46

Notes. SD = standard deviation; CV = coefficient of variation. Means/SDs in level units; CV in percent.

Table 6.6 reports CVs for the ten Bakshi parameters. The coefficient of variation (CV) measures parameter stability across the sample for the three smoothing methods. Given the large number of parameters in the model, we focus on the key findings. The spline methods significantly improve the stability of volatility-related parameters, with the coefficient of variation for both θ_v and κ_v reduced by approximately 80% compared to the original baseline method. In contrast, the spline methods introduce greater variability in the jump parameters (λ_j and μ_j), suggesting that while they stabilise the volatility structure, they may capture jump events less consistently.

6.5.4. Smoothing impact on calibration time

Table 6.7 compares the average computational times required to calibrate the model under the Original, Cubic, and Hermite spline interpolation schemes.

Table 6.7. Calibration time comparison (seconds)

Method	Mean	Median	Std Dev	Min	Max
Baseline	253.5	150.3	356.1	1.1	1980.0
Cubic	2407.5	895.8	6623.4	139.6	37103.1
Hermite	2572.0	1126.1	7641.6	163.2	42791.0

Table 6.7 presents the calibration time statistics for the three methods. The results show that the spline methods require substantially longer computational time, with both Cubic and Hermite methods taking approximately 9 times longer than the baseline method. This significant computational cost represents the main limitation of the spline based approaches, despite their improvements in pricing accuracy and parameter stability.

CHAPTER 7

Conclusions

7.1. Main findings

This chapter presents the main conclusions from the calibration and comparison of the Merton (1973), Kou (2002), and Bakshi, Cao and Chen (1997) option pricing models on S&P 500 monthly options from January to May 2022.

All models converged successfully and exhibited robust estimation and excellent fit, yielding economically interpretable parameters. We assessed performance using a comprehensive set of pricing error metrics and analysed the structure and shape of the risk-neutral densities, including its moments, distances, tails, and quantiles. Finally, we evaluated parameter stability under cubic-spline and Hermite smoothing.

Global results reveal a clear hierarchy aligned with theoretical expectations. Bakshi model substantially outperforms alternatives, achieving pricing errors approximately 7 times smaller than Kou and 13 times smaller than Merton. This hierarchy is evident in the unexplained variance, with Bakshi showing significantly superior precision across all maturity buckets.

Performance varies across maturities. For very short-term options (0–30 days), Merton's symmetric jumps prove more adequate, outperforming Kou. However, from 31 days onward, Kou dominates Merton due to its double-exponential structure better capturing asymmetry and tail thickness, consistently achieving RMSE values 30 to 40% lower. Bakshi delivers the best fit across all maturity buckets, though this superior performance comes at the cost of higher model complexity.

Analysis of the recovered RNDs confirms the pricing hierarchy and reveals distinct tail behaviors. While Merton and Kou capture negative skewness and elevated kurtosis consistent with equity market expectations, Bakshi's RNDs exhibit near-zero skewness and kurtosis close to normality, despite delivering superior pricing fit. This outcome is inconsistent with market expectations, especially in equity markets, during periods of market stress such as the Russia-Ukraine conflict and change in interest rate policies, where strong negative skewness is expected.

This finding reflects a diffusion-heavy calibration where the jump component is largely inactive, while stochastic volatility dominates pricing dynamics. Three main factors may have contributed to this pattern. First, the objective function implicitly weights toward ATM options, reducing the influence of deep OTM options where jumps matter. Second, applying the 3/8 USD price filter first disproportionately removes deep out-of-the-money puts, truncating the left tail of the risk-neutral distribution. Finally, the sample period exhibits persistent volatility rather than discrete jumps. As a result, the model achieves

superior fit for mid-priced options but produces RNDs with weaker left-tail asymmetry than expected for equity markets during stress.

Bakshi was the only model to exhibit this effect, as its adaptive structure allows the calibration to exploit the data characteristics, whereas Merton and Kou impose structural asymmetry through their jump specifications, making them more rigid and better at preserving left-tail mass despite the same filtering bias.

Regarding the smoothing of calibrated parameters, the results show that it significantly enhances calibration quality across several dimensions, in line with the literature. The Hermite spline methodology achieves the best overall performance, with RMSE reductions of approximately 5% compared to the baseline. Granular analysis shows that the most substantial gains occur in the short-term bucket (0–30 days), where MAPE is reduced by approximately 30%.

With respect to parameter stability, the spline methods reduce the global coefficient of variation by approximately 20%, with volatility-related parameters (θ_v and κ_v) showing reductions of approximately 80%, compared to the baseline method. the spline methods introduce greater variability in the jump parameters (λ_J and μ_j), suggesting that, while they stabilise the volatility structure, they may capture jump events less consistently. Overall, the Hermite method is preferred due to its superior robustness to numerical outliers and shape-preserving properties. The main limitation is the computational cost, as spline-based approaches require approximately nine times longer calibration time than the baseline method, representing a significant computational burden despite their improvements in pricing accuracy and parameter stability.

7.2. Limitations and future work

In this study, Bakshi demonstrated maximum flexibility and superior fit across all maturities. However, there are indications of possible overfitting, as the optimisation process relied solely on minimising squared pricing errors, which may have limited the preservation of tail characteristics in the recovered risk-neutral densities. This raises the question of whether alternative objective functions, such as minimising implied volatility errors or using vega-weighted pricing errors, would better preserve tail representation.

Morevover, in our work, the filtering procedure proved to be critical, particularly the OTM filter combined with the 3/8 USD price threshold. It would be interesting to study Bakshi's performance in other market contexts, such as periods with lower volatility, non-stress conditions, or even rising markets.

Finally, we used Fourier inversion to extract risk-neutral densities. A comparative analysis with alternative methods, such as the Breeden and Litzenberger (1978) approach, could assess whether the extraction method introduces bias or whether the results are robust across different techniques.

Much remains to be explored in this field, and it is hoped that this work may contribute to further research.

References

[1] Abadir, Karim M and Rockinger, Michael (1997). On the density of the ratio of two independent Student t random variables. *Discussion Paper*.

[2] Abken, Peter A and Madan, Dilip B and Ramamurtie, Sailesh (1996). Estimation of risk-neutral and statistical densities by Hermite polynomial approximation: With an application to Eurodollar futures options. *Federal Reserve Bank of Atlanta Working Paper*(96-5).

[3] Andersen, Torben G and Bollerslev, Tim (1998). Answering the skeptics: Yes, standard volatility models do provide accurate forecasts. *International Economic Review*:885–905.

[4] Andreasen, J. and Huge, B. (2011). Volatility interpolation. *Risk Magazine*, September, 76–79.

[5] Aparicio, Stephen D and Hodges, Stewart (1998). Implied risk-neutral distribution: A comparison of estimation methods. *Journal of Derivatives*.

[6] Applebaum, David (2004). *Lévy Processes and Stochastic Calculus*. Cambridge Studies in Advanced Mathematics, Vol. 93. Cambridge University Press, Cambridge.

[7] Aït-Sahalia, Yacine and Lo, Andrew W (1998a). Nonparametric estimation of state-price densities implicit in financial asset prices. *The Journal of Finance*, 53(2):499–547.

[8] Aït-Sahalia, Yacine and Duarte, Jefferson (2003). Nonparametric risk management and implied risk aversion. *Journal of Econometrics*, 94(1-2):9–51.

[9] Bahra, Bhupinder (1997). Implied risk-neutral probability density functions from option prices: theory and application. *Bank of England Working Paper*(66).

[10] Bakshi, Gurdip and Cao, Charles and Chen, Zhiwu (1997). Empirical performance of alternative option pricing models. *The Journal of Finance*, 52(5):2003–2049.

[11] Bakshi, Gurdip and Chen, Zhiwu (1997). Spanning and derivative-security valuation. *Journal of Financial Economics*, 55(2):205–238.

[12] Bakshi, Gurdip and Madan, Dilip (2000). Spanning and derivative-security valuation. *Journal of Financial Economics*, 55(2):205–238.

[13] Bali, Turan G., Hu, Jianfeng, and Scott, Jeffrey H. (2017). A new approach to measuring risk-neutral skewness. *Journal of Financial and Quantitative Analysis*, 52(5):2199–2229.

[14] Ball, Ray and Torous, Walter N (1995). An investigation of the informational role of event-study abnormal returns. *Journal of Empirical Finance*, 2(4):321–352.

[15] Barndorff-Nielsen, Ole E and Shephard, Neil (2001). Non-Gaussian Ornstein–Uhlenbeck-based models and some of their uses in financial economics. *Journal of the Royal Statistical Society: Series B (Statistical Methodology)*, 63(2):167–241.

[16] Bates, David S. (1991). The crash of '87: Was it expected? The evidence from options markets. *Journal of Finance*, 46(3):1009–1044.

[17] Bates, David S (1996, 1997). Jumps and stochastic volatility: Exchange rate processes implicit in Deutsche mark options. *The Review of Financial Studies*, 9(1):69–107.

[18] Bates, David S (2000). Post-'87 crash fears in the S&P 500 futures option market. *Journal of Econometrics*, 94(1-2):181–238.

[19] Black, Fischer and Scholes, Myron (1973). The pricing of options and corporate liabilities. *Journal of Political Economy*, 81(3):637–654.

[20] Bollerslev, Tim and Zhou, Hao (2006). Expected stock returns and variance risk premia. *The Review of Financial Studies*, 19(4):1009–1044.

[21] Bookstaber, Richard M and McDonald, James B (1987). A general distribution for describing security price returns. *Journal of Business*:401–424.

[22] Breeden, Douglas T and Litzenberger, Robert H (1978). Prices of state-contingent claims implicit in option prices. *Journal of Business*:621–651.

[23] Brennan, Michael J (1979). The pricing of contingent claims in discrete time models. *The Journal of Finance*, 34(1):53–68.

[24] Brenner, Menachem and Eom, Young Ho (1997). Alternative methods for estimating implied volatility. *Financial Analysts Journal*, 53(5):71–81.

[25] Brown, Gregory and Toft, Klaus Bjerre (1999). Implied volatility functions: Empirical tests. *The Journal of Finance*, 54(6):2059–2095.

[26] Buchen, Peter W and Kelly, Michael (1996). The maximum entropy distribution of an asset inferred from option prices. *Journal of Financial and Quantitative Analysis*, 31(1):143–159.

[27] Campa, Jose Manuel and Chang, P H Kevin and Reider, Robert L (1998). Implied exchange rate distributions: Evidence from OTC option markets. *Journal of International Money and Finance*, 17(1):117–160.

[28] Carr, Peter and Madan, Dilip B (1999). Option valuation using the fast Fourier transform. *Journal of Computational Finance*, 2(4):61–73.

[29] Carr, Peter and Wu, Liuren (2004). Time-changed Lévy processes and option pricing. *Journal of Financial Economics*, 71(1):113–141.

[30] Chen, Ren-Raw and Scott, Louis (1992). Pricing interest rate options in a two-factor Cox–Ingersoll–Ross model of the term structure. *The Review of Financial Studies*, 5(4):613–636.

[31] Chen, Ren-Raw and Scott, Louis (1995). Multi-factor Cox-Ingersoll-Ross models of the term structure: Estimates and tests from a Kalman filter model. *Journal of Real Estate Finance and Economics*, 10(2):143–172.

[32] Chen, Ren-Raw and Davis, Mark and Landwehr, John (2019). Risk-neutral densities: Estimation, comparison, and interpretation. *Journal of Derivatives*, 26(3):9–27.

[33] Christoffersen, Peter and Pelletier, Denis (2004). Backtesting value-at-risk: A duration-based approach. *Journal of Financial Econometrics*, 2(1):84–108.

[34] Chiu, Ching-Wai and Li, Junye and Todorov, Viktor (2014). Option-implied objective measures of market risk. *Working Paper*.

[35] Christoffersen, Peter and Jacobs, Kris and Mimouni, Karim (2004). Option valuation with conditional skewness. *Journal of Econometrics*, 131(1-2):253–284.

[36] Cont, Rama (1997). Retrieving Lévy processes from option prices: regularization of an ill-posed inverse problem. *SIAM Journal on Control and Optimization*, 45(1):1–25.

[37] Cont, Rama and Peter Tankov (2004). *Financial Modelling with Jump Processes*. Chapman & Hall/CRC, Boca Raton, FL.

[38] Corrado, Charles J and Su, Tie (1996). Recovering probability distributions from option prices. *Journal of Derivatives*, 3(4):55–63.

[39] Corrado, Charles J and Su, Tie (1997). The forecast quality of CBOE implied volatility indexes. *Journal of Futures Markets*, 17(9):1087–1107.

[40] Cox, John C (1975). Notes on option pricing I: Constant elasticity of variance diffusions. *Unpublished note, Stanford University, Graduate School of Business*

[41] Cox, John C and Ross, Stephen A (1976). The valuation of options for alternative stochastic processes. *Journal of Financial Economics*, 3(1-2):145–166.

[42] Cox, John C and Ross, Stephen A and Rubinstein, Mark (1979). Option pricing: A simplified approach. *Journal of Financial Economics*, 7(3):229–263.

[43] Cox, John C and Ingersoll Jr, Jonathan E and Ross, Stephen A (1985). A theory of the term structure of interest rates. *Econometrica*:385–407.

[44] Cox, John C (1975). Notes on option pricing I: Constant elasticity of variance diffusions. *Journal of Portfolio Management*.

[45] Duffie, Darrell and Pan, Jun and Singleton, Kenneth (2000). Transform analysis and asset pricing for affine jump-diffusions. *Econometrica*, 68(6):1343–1376.

[46] Eraker, B., M. Johannes, and N. Polson (2004). The volatility premium. *Review of Financial Studies 17*(2), 493–541.

[47] Eraker, B., Johannes, M., and Polson, N. (2003). The impact of jumps in volatility and returns. *Journal of Finance*, 58(3), 1269–1300.

[51] Fan, Jianqing and Yao, Qiwei (2003). Nonlinear time series: nonparametric and parametric methods. *Springer Series in Statistics*.

[49] Figlewski, Stephen (2010). Estimating the implied risk-neutral density for the US market portfolio. *Volatility and Time Series Econometrics: Essays in Honor of Robert F. Engle*, 323–353.

[50] Figlewski, Stephen (2018). Risk–neutral densities: A review. *Annual Review of Financial Economics*, 10(1):329–359.

[51] Fan, Jianqing and Yao, Qiwei (2003). Nonlinear time series: Nonparametric and parametric methods. extitSpringer.

[52] Fengler, M. R. (2005). *Semiparametric Modeling of Implied Volatility*. Lecture Notes in Economics and Mathematical Systems, Vol. 579. Springer, Berlin Heidelberg.

[53] Fourier, Jean Baptiste Joseph (1822). Théorie analytique de la chaleur. Firmin Didot.

[54] Gakhov, F. D. (1990). *Boundary Value Problems*. Dover Publications, New York.

[55] Harrison, J Michael and Kreps, David M (1979). Martingales and arbitrage in multiperiod securities markets. *Journal of Economic Theory*, 20(3):381–408.

[56] Hartvig, Niels Viggo and Jensen, Bjarne Astrup and Pedersen, Jesper (1999). Risk-neutral densities and option prices. *Working Paper, University of Aarhus*.

[57] Heston, Steven L (1993). A closed-form solution for options with stochastic volatility with applications to bond and currency options. *The Review of Financial Studies*, 6(2):327–343.

[58] Hull, John and White, Alan (1990). Pricing interest-rate-derivative securities. *The Review of Financial Studies*, 3(4):573–592.

[59] Jackwerth, Jens Carsten and Rubinstein, Mark (1996). Recovering probability distributions from option prices. *The Journal of Finance*, 51(5):1611–1631.

[60] Jackwerth, Jens Carsten (1999). Option-implied risk-neutral distributions and implied binomial trees: A literature review. *Journal of Derivatives*, 7(2):66–82.

[61] Jarrow, Robert and Rudd, Andrew (1982). Approximate option valuation for arbitrary stochastic processes. *Journal of Financial Economics*, 10(3):347–369.

[62] Johnson, Norman L (1949). Systems of frequency curves generated by methods of translation. *Biometrika*, 36(1/2):149–176.

[63] Kou, Steven G (2002). A jump-diffusion model for option pricing. *Management Science*, 48(8):1086–1101.

[64] Kendall, Maurice G. and Stuart, Alan (1977). *The Advanced Theory of Statistics: Distribution Theory*. 4th edition. Macmillan, London/New York.

[65] Lee, Roger W (2004). Option pricing by transform methods: Extensions, unification, and error control. *Journal of Computational Finance*, 7(3):51–86.

[66] Lewis, Alan L (2001). A simple option formula for general jump-diffusion and other exponential Lévy processes. *Envision Financial Systems and OptionCity. net*.

[67] Longstaff, Francis A (1995). Option pricing and the martingale restriction. *The Review of Financial Studies*, 8(4):1091–1124.

[68] Madan, Dilip B and Seneta, Eugene (1990). The variance gamma process and option pricing. *European Finance Review*, 2(1):79–105.

[69] Malz, Allan M (1997). Estimating the probability distribution of the future exchange rate from option prices. *The Journal of Derivatives*, 5(2):18–36.

[70] Mayhew, Stewart (1995). Implied volatility. *Financial Analysts Journal*, 51(4):8–20.

[71] Melick, William R and Thomas, Charles P (1997). Recovering an asset's implied PDF from option prices: An application to crude oil during the Gulf crisis. *Journal of Financial and Quantitative Analysis*, 32(1):91–115.

[72] Merton, Robert C (1973). Theory of rational option pricing. *The Bell Journal of Economics and Management Science*:141–183.

[73] Merton, Robert C (1976). Option pricing when underlying stock returns are discontinuous. *Journal of Financial Economics*, 3(1-2):125–144.

[74] Muskhelishvili, N. I. (2008). *Singular Integral Equations: Boundary Problems of Function Theory and Their Application to Mathematical Physics*. Dover Publications, Mineola, NY.

[75] Nunes, João Pedro Vidal and Alcaria, Tiago Ramalho Viegas (2015). *Valuation of forward start options under affine jump–diffusion models. Quantitative Finance*, 16(5), 727–747. doi:10.1080/14697688.2015.1108018.

[76] Pan, J. (2002). The jump-risk premia implicit in options: Evidence from an integrated time-series study. *Journal of Financial Economics 63*(1), 3–50.

[77] Posner, Steven E and Milevsky, Moshe A (1998). Valuing exotic options by approximating the SPD with higher moments. *Journal of Financial Engineering*, 7(2):109–125.

[78] Potters, Marc and Cont, Rama and Bouchaud, Jean-Philippe (1998). Hedged Monte-Carlo: low variance derivative pricing with objective probabilities. *Physica A: Statistical Mechanics and its Applications*, 289(3-4):517–525.

[79] Pritsker, Matthew (1997). Nonparametric density estimation and tests of continuous time interest rate models. *The Review of Financial Studies*, 11(3):449–487.

[80] Ritchey, Robert J (1990). Call option valuation for discrete normal mixtures. *Journal of Financial Research*, 13(4):285–296.

[81] Rockinger, Michael (1998). Reading Interest Rate and Bond Futures Options' Smiles Around the 1997 French Snap Election. *CEPR Discussion Paper*, No. 2010.

[82] Rockinger, Michael and Jondeau, Eric (1998). Density forecasting using cross-entropy. *HEC Paris Working Paper*.

[83] Rosenberg, Joshua V (1996). Implied volatility term structures in foreign exchange markets. *International Review of Economics & Finance*, 5(1):55–72.

[84] Rosenberg, Joshua V and Engle, Robert F (1997). Implied volatility functions: A reprise. *Journal of Derivatives*, 5(2):45–52.

[85] Ross, Stephen A (1976). The arbitrage theory of capital asset pricing. *Journal of Economic Theory*, 13(3):341–360.

[86] Rubinstein, Mark (1976). The valuation of uncertain income streams and the pricing of options. *The Bell Journal of Economics*:407–425.

[87] Rubinstein, Mark (1994). Implied binomial trees. *The Journal of Finance*, 49(3):771–818.

[88] Rubinstein, Mark (1998). Edgeworth binomial trees. *Journal of Derivatives*, 5(3):20–27.

[89] Scott, Louis O (1997). Pricing stock options in a jump-diffusion model with stochastic volatility and interest rates: Applications of Fourier inversion methods. *Mathematical Finance*, 7(4):413–426.

[90] Sherrick, Bruce J and Irwin, Scott H and Forster, D Lynn (1992 and 1996). Implied option forecast distributions: An application to live cattle options. *Journal of Futures Markets*, 12(6):659–679.

[91] Sherrick, Bruce J and Garcia, Philip and Tirupattur, Viswanath (1995). Recovering probabilistic information from option markets: Tests of distributional assumptions. *Journal of Futures Markets*, 16(5):545–560.

[92] Shimko, David (1993). Bounds of probability. *Risk*, 6(4):33–37.

[93] Stapleton, Richard C and Subrahmanyam, Marti G (1984). The valuation of options when asset returns are generated by a binomial process. *The Journal of Finance*, 39(5):1525–1539.

[94] Stilger, Przemysław S., Kostakis, Alexandros, and Poon, Ser-Huang (2017). What does risk-neutral skewness tell us about future stock returns? *Management Science*, 63(6):1814–1834.

[95] Stuart, Alan and Ord, J. Keith (1991a). *Kendall's Advanced Theory of Statistics, Volume 2: Classical Inference and Relationship*. 5th edition, Oxford University Press, New York.

[96] Stutzer, Michael (1996). A simple nonparametric approach to derivative security valuation. *The Journal of Finance*, 51(5):1633–1652.

[97] Vasicek, Oldrich (1977). An equilibrium characterization of the term structure. *Journal of Financial Economics*, 5(2):177–188.

[98] Walker, Michael B (1996). Implied distributions from option prices. *Working Paper*.

APPENDIX A

General Definitions

Definition A.1. ***(Moment-generating function of a Normal distribution)*** *Let X be a normally distributed random variable, following a Normal distribution with mean μ and variance σ^2: $X \sim \mathcal{N}(\mu, \sigma^2)$. Then, the moment-generating function of X, represented by $M_X(s)$, is given by:*

$$M_X(s) = \mathbb{E}\left[e^{sX}\right] = \int_{-\infty}^{+\infty} e^{sX} f_X(x) dX = e^{\mu s + \frac{1}{2}\sigma^2 s^2}, \tag{A.1}$$

where, $f_X(x)$ is the probability density function of X and s is a real-valued parameter used to compute the moment-generation function.

Definition A.2. ***(Normal distribution characteristic function)*** *Let X be a normally distributed random variable, following a Normal distribution with mean μ and variance σ^2: $X \sim \mathcal{N}(\mu, \sigma^2)$. Then, the characteristic function of X is given by:*

$$\varphi_X(u) = \mathbb{E}\left[e^{iuX}\right] = \int_{-\infty}^{+\infty} e^{iuX} f_X(x) dX = e^{i\mu u - \frac{1}{2}\sigma^2 s^2}, \tag{A.2}$$

where $\varphi_X(u)$ represents the characteristic function of X evaluated at u, $f_X(x)$ is the p.d.f of X, i is the imaginary unit ($i = \sqrt{-1}$) and u is a real-valued parameter used to compute the moment-generation function.

Definition A.3. ***(Fourier transform)*** *Let $\varphi(x)$ be a function of a real variable x belonging to the set of integrable functions in $\mathbb{R}$.*
Then, the Fourier transform of $\varphi(x) \in L^1(\mathbb{R})$ is defined as:

$$\hat{\varphi}(\xi) = \int_{-\infty}^{+\infty} \varphi(x) e^{i\xi x} dx, \ \xi \in \mathbb{R}, \tag{A.3}$$

where $\hat{\varphi}(\xi)$ is the complex-valued function representing the Fourier transform of $\varphi(x)$, i is the imaginary unit ($i = \sqrt{-1}$) and ξ is the angular frequency variable (a real number),

Definition A.4. ***(Inverse Fourier transform)*** *Let $\psi(\xi)$ be a complex-valued function of a real variable ξ belonging to the set of integrable functions in $\mathbb{R}$.*
Then, the inverse Fourier Transform of $\psi(\xi) \in L^1(\mathbb{R})$ is defined as:

$$\check{\psi}(x) = \frac{1}{2\pi} \int_{-\infty}^{+\infty} \psi(\xi) e^{-i\xi x} d\xi, \ \xi \in \mathbb{R}, \tag{A.4}$$

where $\check{\psi}(x)$ is the function in the time domain obtained from the inverse Fourier transform of $\psi(\xi)$, i is the imaginary unit ($i = \sqrt{-1}$) and ξ is the angular frequency variable (a real number).

APPENDIX B

Lévy processes

This appendix contains several key definitions concerning Lévy processes. We introduce the main concepts, including Lévy processes, Poisson and compound Poisson processes. We also discuss Lévy-Khintchine representation, Itô formula for Lévy processes, among other aspects.

B.1. Definition of Lévy processes

Lévy processes are a class of stochastic processes with discontinuous paths, characterized by three fundamental properties. They possess independent increments, stationary increments and stochastically continuous. Formally, a Lévy process can be defined as follows:

Definition B.1 (*Lévy Process*). *Consider a fixed probability space $(\Omega, \mathcal{F}, \mathbb{Q})$. A stochastic process X_t, such that $X_0 = 0$, is called a Lévy process if:*

i) X_t has independent increments: for every $t_0 < t_1 < ... < t_n$, the random variables $X_{t_0}, X_{t_1} - X_{t_0}, X_{t_2} - X_{t_1}, ..., X_{t_n} - X_{t_{n-1}}$ are independent.

ii) X_t has stationary increments: the law of $X_{t+h} - X_t$ does not depend on t.

iii) X_t is stochastically continuous,i.e., for all $a > 0$ and $s > 0$:

$$\lim_{t \to s} \mathbb{P}[|X_t - X_s| > a] = 0.$$

B.2. Poisson process and main definitions

As an example of a Lévy process, the Poisson process is often regarded as the simplest and most illustrative case. It is a pure-jump process with independent and stationary increments, which starts at zero and has jump sizes always equal to 1, and where the increment over a time interval of length greater than zero follows a Poisson distribution.

Definition B.2. ***(Poisson process)*** *Let $(\tau_i)_i \geq 1$ be a sequence of independent exponential random variables with parameter λ and $T_n = \sum_{i=1}^{n} \tau_i$.*
The counting process $(N_t, t \geq 0)$ defined by:

$$N_t = \sum_{n \geq 1} 1_{t \geq T_n}, \tag{B.1}$$

is called a Poisson process with intensity $\lambda > 0$. This process counts the number of random times (T_n) that occurs between 0 and t, where $T_n - T_{n-1} \geq 1$ is an independent and identically distributed (i.i.d.) sequence of exponential random variables.
For any $t > 0$, N_t follows a Poisson distribution with parameter λt. Therefore, the

expected value and variance of the process N_t are:

$$\mathbb{E}[N_t] = \lambda \text{ and } var[N_t] = \lambda, \tag{B.2}$$

respectively,where λ represents the average intensity of jumps arrival.
Finally, the characteristic function of N_t is given by:

$$\mathbb{E}[e^{iuN_t}] = exp\,[\lambda t(e^{iu} - 1)],\ \forall\, u \in \mathbb{R}. \tag{B.3}$$

Another prominent example of a Lévy process is the compound Poisson process. Unlike the Poisson process, the compound Poisson process introduces additional variability by allowing for random jump sizes. This process can be formally defined as detailed below:

Definition B.3. ***(Compound Poisson process)*** *Let the counting process $(N_t)_{t\geq 0}$ be a Poisson process with intensity $\lambda > 0$, and let jump sizes $(Y_i)_{i>1}$ be a family of i.i.d. random variables with distribution f, and also independent from $(N_t)_{t\geq 0}$.*
A compound Poisson process $\tilde{N}_t$ is a continuous-time (random) stochastic process with jumps that can be represented as:

$$\tilde{N}_t = \sum_{i=1}^{N_t} Y_i,\ t \geq 0, \tag{B.4}$$

where the jumps arrive randomly according to a Poisson process N_t, and the size of the jumps Y_i is also random, with a specified probability distribution.
It is possible to demonstrate that the mean and variance of $\tilde{N}_t$ are, respectively, given by:

$$\mathbb{E}[N_t] = \mu\lambda t \text{ and } var[N_t] = \lambda t(\sigma^2 + \mu^2). \tag{B.5}$$

Definition B.4. ***(Compensated Poisson process)*** *Let the counting process $(N_t, t \geq 0)$ be a Poisson process with intensity $\lambda > 0$.*
A compensated Poisson process is a 'centered' version of the Poisson process $(N_t)_{t>0}$ that can be defined by

$$\tilde{N}_t = N_t - \lambda t, \tag{B.6}$$

where the $(\lambda_t)_{t>0}$ is the compensator of $(N_t)_{t>0}$.
Therefore, the compensated Poisson process $(\tilde{N}_t)_{t\in\mathbb{R}_+}$ is a martingale with respect to $(\mathcal{F}_t)_{t\in\mathbb{R}_+}$ and has an expected value of 0, as follows

$$\mathbb{E}[\tilde{N}_t] = 0. \tag{B.7}$$

Proof. ***(Compensated Poisson martingale)*** Knowing that the compensated Poisson process $(\tilde{N}_t)_{t>0}$ has independents increments, it easy to demonstrate that

$$\mathbb{E}[N_t|N_s, s \leq t] = \mathbb{E}[N_t - N_s + N_s|N_s] = \mathbb{E}[N_t - N_s|N_s] + N_s = \lambda(t-s) + N_s \tag{B.8}$$

thus, the process $(\tilde{N}_t)_{t>0}$ possesses the *martingale property*

$$\forall t > s, \mathbb{E}[\tilde{N}_t|\tilde{N}_s] = \tilde{N}_s. \tag{B.9}$$

□

Finally, the compensated Poisson process has the following characteristic function

$$\phi_{\tilde{N}_t}(z) = exp\left[\lambda t(e^{iz} - 1 - iz)\right]. \tag{B.10}$$

Proposition B.1 (*Characteristic of a compound Poisson process*).
Let N_t be a Poisson process with rate λ, and let Y_i be i.i.d. random variables. The expectation $\mathbb{E}_{\mathbb{Q}_t}\left[\exp\left(iu\sum_{i=1}^{N_t} Y_i\right)\right]$ can then be expressed as:

$$\exp\left(\lambda t(\phi_Y(u) - 1)\right). \tag{B.11}$$

Proof. Applying the *law of iterated expectations* to N_t, we obtain:

$$\mathbb{E}_{\mathbb{Q}_t}\left[\exp\left(iu\sum_{i=1}^{N_t} Y_i\right)\right] = \mathbb{E}_{\mathbb{Q}_t}\left[\mathbb{E}_{\mathbb{Q}_t}\left[\exp\left(iu\sum_{i=1}^{N_t} Y_i\right)\Big|N_t\right]\right]. \tag{B.12}$$

Given $N_t = n$ and since $Y_i \sim i.d.d.$, we have:

$$\begin{aligned}\mathbb{E}_{\mathbb{Q}_t}\left[\mathbb{E}_{\mathbb{Q}_t}\left[\exp\left(iu\sum_{i=1}^{N_t} Y_i\right)|N_t = n\right]\right] &= \mathbb{E}_{\mathbb{Q}_t}\left[\mathbb{E}_{\mathbb{Q}_t}\left[e^{iuY_1}\cdot e^{iuY_2}\cdot\ldots\cdot e^{iuY_{N(t)}}\right]|N(t) = n\right], \\ = \mathbb{E}_{\mathbb{Q}_t}\left[\mathbb{E}_{\mathbb{Q}_t}\left[e^{iuY_1}\right]\mathbb{E}_{\mathbb{Q}_t}\left[e^{iuY_2}\right]\cdot\ldots\cdot\mathbb{E}_{\mathbb{Q}_t}\left[e^{iuY_{N(t)}}\right]\right] &= \mathbb{E}_{\mathbb{Q}_t}\left[\left(\mathbb{E}_{\mathbb{Q}_t}\left[e^{iuY_i}\right]\right)^{N(t)}\right].\end{aligned} \tag{B.13}$$

Here, $\mathbb{E}_{\mathbb{Q}_t}\left[e^{iuY_i}\right]$ is the characteristic function $\phi_Y(u)$ of Y, where Y follows a double exponential (Laplace) distribution:

$$\mathbb{E}_{\mathbb{Q}_t}\left[\left(\mathbb{E}_{\mathbb{Q}_t}\left[e^{iuY_i}\right]\right)^{N(t)}\right] = \mathbb{E}_{\mathbb{Q}_t}\left[\left(\phi_Y(u)\right)^{N(t)}\right]. \tag{B.14}$$

Then equation (B.14) can be rewritten as follows:

$$\mathbb{E}_{\mathbb{Q}_t}\left[\left(\phi_Y(u)\right)^{N(t)}\right] = \mathbb{E}_{\mathbb{Q}_t}\left[e^{log(\phi_Y(u))^{N(t)}}\right] = \mathbb{E}_{\mathbb{Q}_t}\left[e^{N(t)log(\phi_Y(u))}\right]. \tag{B.15}$$

Knowing that the moment generating function of a Poisson random variable $N(t)$ with rate λt is given by the expression $\mathbb{E}_{\mathbb{Q}_t}\left[e^{sN(t)}\right] = \exp\left(\lambda t\left(e^s - 1\right)\right)$, where in this case, $s = \ln\left(\phi_Y\left(u\right)\right)$, the expectation outlined in equation (B.15) can be written as:

$$\mathbb{E}_{\mathbb{Q}_t}\left[\left(\phi_Y(u)\right)^{N_t}\right] = \exp\left(\lambda t(e^{\ln(\phi_Y(u))} - 1)\right). \tag{B.16}$$

Simplifying the exponential term, yields:

$$\mathbb{E}_{\mathbb{Q}_t}\left[\left(\phi_Y(u)\right)^{N_t}\right] = \exp\left(\lambda t(\phi_Y(u) - 1)\right). \tag{B.17}$$

Therefore, we finally reach the following expression for the expectation of the exponential Poisson specified in equation (B.16):

$$\mathbb{E}_{\mathbb{Q}_t}\left[\exp\left(iu\sum_{i=1}^{N_t} Y_i\right)\right] = \exp\left(\lambda t(\phi_Y(u) - 1)\right). \tag{B.18}$$

□

B.3. Lévy measure

The Lévy measure plays a fundamental role in characterising the jump behavior of general Lévy processes. The Lévy measure quantifies the frequency and size of the jumps, providing a detailed description of the distribution of these discontinuities. In precise terms, the Lévy measure is defined as:

Definition B.5 (*Lévy measure*). *Let $(X_t)_{t\geq 0}$ be a Lévy process and assume ν is a Borel measure on $\mathbb{R}$ that satisfies:*

$$\nu(\{0\}) = 0 \text{ and } \int_{\mathbb{R}} (|x|^2 \wedge 1)\, \nu(dx) < \infty. \tag{B.19}$$

Then for every $A \in \mathcal{B}(\mathbb{R})$

$$\nu(A) = \mathbb{E}[\#\{t \in [0,1] : \Delta X_t \neq 0,\, \Delta X_t \in A\}] = \frac{1}{T}\mathbb{E}[\#\{t \in [0,T] : \Delta X_t \neq 0,\, \Delta X_t \in A\}], \tag{B.20}$$

is called the Lévy measure of X. Here, $\nu(A)$ represents the expected number of jumps, per unit of time, whose amplitude belongs to A. If the density of the jump size is represented by $g(x)$ and λ the intensity of jumps then the Lévy measure can be represented in the following way:

$$\nu(dx) = \lambda g(dx). \tag{B.21}$$

Remark B.1. *Note that $\int_{\mathbb{R}}(|x|^2 \wedge 1)\, \nu(dx) < \infty$ is equivalent to the following two conditions:*

$$\int_{-1}^{1} x^2\, \nu(dx) < \infty, \tag{B.22}$$

and

$$\int_{|x|\geq 1} \nu(dx) < \infty, \tag{B.23}$$

meaning that, by definition of Lévy measure, the condition (B.23) *implies that there is only a finite number of big jumps.*

B.3.1. Lévy-Khintchine representation

Next, we introduce a key concept in the theory of Lévy processes known as the Lévy-Khintchine representation. This representation provides a complete characterisation of Lévy processes by specifying their characteristic functions in terms of the Lévy-Khintchine triplet (γ, σ^2, ν). This triplet enables the decomposition of a Lévy process into three independent components: a linear drift, a Brownian motion, and a Lévy jump process. The following theorem provides a detailed explanation:

Theorem B.1 (*Lévy-Khintchine representation*). *Let $X = \{X_t, t \geq 0\}$ be a Lévy process associated with a triplet (γ, σ^2, ν), where $\gamma \in \mathbb{R}$, $\sigma^2 \geq 0$, and ν is a positive measure concentrated on $\mathbb{R} \setminus \{0\}$ that satisfies:*

$$\nu(\{0\}) = 0 \;\; \text{and} \int_{\mathbb{R}} (1 \wedge x^2)\nu(dx) \leq \infty. \tag{B.24}$$

Then, the characteristic function of X_t is given by the following Lévy-Khintchine representation formula:

$$\phi(z) = \mathbb{E}[e^{izX_t}] = e^{t\psi(z)}, \tag{B.25}$$

where the cumulant characteristic function $\psi(z)$, also known as the characteristic exponent, is defined by:

$$\psi(z) = i\gamma z - \frac{\sigma^2 z^2}{2} + \int_{-\infty}^{+\infty} \left(e^{izx} - 1 - izx\mathbf{1}_{|x|\leq 1}\right) \nu(dx), \, \forall \, z \in \mathbb{R}. \tag{B.26}$$

Proof. For a proof, see Cont and Tankov (2004, Sections 8.1–8.3). □

B.4. Itô's lemma for Lévy processes

The following variant of Itô's lemma will be fundamental for our analysis of Lévy processes:

Definition B.6 (*Itô lemma for Lévy type stochastic integrals*). *Let $(X_t)_{t\geq 0}$, be a Lévy stochastic process with Lévy triplet (b, σ^2, ν). Let $f \in C^{1,2}([0,T] \times \mathbb{R})$ and $H, K \in C([0,T] \times \mathbb{R})$, where $H(t,x)$ represents the small jumps and $K(t,x)$ the large jumps. Consider now a Lévy process given by:*

$$dX_t = bdt + \sigma dW_t + \int_{|x|<1} H(t,x)\tilde{J}(dt,dx) + \int_{|x|\geq 1} K(t,x)J(dt,dx), \tag{B.27}$$

where N_X is a Poisson Randon measure and $\tilde{N}_X$ is the compensated Poisson measure, defined by $\tilde{N}_X([0,t] \times A) = N_X([0,t] \times A) - t\nu(A)$. The differential dX_t can be decomposed into two components: a continuous part $dX_t^c = bdt + \sigma dW_t$, which encompasses the drift and volatility terms, and a discontinuous part $dX_t^d = \int_{|x|<1} H(t,x)\tilde{J}(dt,dx) + \int_{|x|\geq 1} K(t,x)J(dt,dx)$, which accounts for both small and large jumps.
Then, the Itô lemma for Lévy type stochastic integrals is given by:

$$\begin{aligned} df(t,X_t) = {} & \frac{\partial f}{\partial t}dt + \frac{\partial f}{\partial x}dX_t^c + \frac{1}{2}\frac{\partial^2 f}{\partial x^2}d[X^c,X^c] \\ & + \int_{|x|<1} \left[f(t,X_t + H(t,x)) - f(t,X_t)\right] \tilde{J}_X(dt,dx) \\ & + \int_{|x|<1} \left[f(t,X_t + H(t,x)) - f(t,X_t) - H(t,x)\frac{\partial f}{\partial x}(t,X_t)\right] \nu(dx)dt \\ & + \int_{|x|\geq 1} \left[f(t,X_t + K(t,x)) - f(t,X_t)\right] J_X(dt,dx). \end{aligned} \tag{B.28}$$

If $H(t,x) = K(t,x)$, then the Itô formula simplifies to:

$$\begin{aligned} df(t,X_t) = {} & \frac{\partial f}{\partial t}dt + \frac{\partial f}{\partial x}dX_t + \frac{1}{2}\frac{\partial^2 f}{\partial x^2}d[X^c,X^c] \\ & + \int_{\mathbb{R}} \left[f(t,X_t + H(t,x)) - f(t,X_t) - H(t,x)\frac{\partial f}{\partial x}(t,X_t)\right] J_X(dt,dx). \end{aligned} \tag{B.29}$$

Proof. For a proof, see Applebaum (2004, Sections 4.3–4.4). □

B.5. Propositions and definitions

Definition B.7. *(**Exponential Lévy model**) Let $(S_t)_{t\geq 0}$ be an stochastic process representing an underlying asset process under a filtered probability space $(\Omega, \mathcal{F}, \{\mathcal{F}_t\}, \mathbb{Q})$, where $\mathbb{Q}$ is a risk–neutral measure under which discounted prices of all traded assets are $\mathbb{Q}$-martingales. The filtration $\{\mathcal{F}_t\}$ represents the price history up to time t. Under $\mathbb{Q}$, S_t follows the exponential Lévy model:*

$$S_t = S_0 e^{X_t}, \tag{B.30}$$

where r is the risk-free rate, q is the (continuous) dividend yield, and X_t is a Lévy process with characteristic triplet (γ, σ^2, ν). In an arbitrage-free market, the dividend-adjusted discounted price $\hat{S}_t := S_t e^{-(r-q)t} = S_0 e^{X_t - (r-q)t}$ is a martingale, which is equivalent to the following conditions imposed on the triplet (γ, σ^2, ν):

$$\int_{|x|>1} e^x \, \nu(dx) < \infty, \quad \gamma = (r-q) - \frac{\sigma^2}{2} - \int_{\mathbb{R}} \left(e^x - 1 - x \, \mathbb{1}_{\{|x|\leq 1\}}\right) \nu(dx). \tag{B.31}$$

The dynamics of S_t under $\mathbb{Q}$ can also be written in integral form:

$$S_t = S_0 + \int_0^t (r-q) \, S_{u-} \, du + \int_0^t S_{u-} \, \sigma \, dW_u + \int_0^t \int_{\mathbb{R}} (e^x - 1) \, S_{u-} \, \tilde{N}_X(du, dx), \tag{B.32}$$

or, equivalently, in differential form:

$$dS_t = (r-q) \, S_{t-} \, dt + \sigma S_{t-} \, dW_t + \int_{\mathbb{R}} (e^x - 1) \, S_{t-} \, \tilde{N}_X(dt, dx), \tag{B.33}$$

where N_X is the jump measure of X and $\tilde{N}_X(dt, dx) := N_X(dt, dx) - \nu(dx)\, dt$ denotes the compensated random measure describing the jumps of X_t.

The next proposition expresses the compensated jump contribution of S_t in terms of the jumps of the Lévy process X_t in integral form.

Proposition B.2 (Integral representation of the compound Poisson component of S_t). *Let the asset price be defined as a exponential Lévy model $S_t = e^{X_t}$, where X_t is a Lévy process. Expressing the absolute jump size of X_t as $\Delta X_t = X_t - X_{t-}$ we can express a compound Poisson Process (as defined in definition B.3) with jump size distributions V_i associated with process S_t, in the following way:*

$$\sum_{i=1}^{N_t} V_i = \int_0^t \int_{\mathbb{R}} S_{u-}(e^x - 1) N_X(du, dx). \tag{B.34}$$

Proof.

$$\begin{aligned}\sum_{i=1}^{N_t} V_i &= \sum_{0\leq u\leq t} \Delta S_u = \sum_{0\leq u\leq t} (S_u - S_{u-}) = \sum_{0\leq u\leq t} (e^{X_u} - S_{u-}) = \sum_{0\leq u\leq t} (e^{X_u - X_{u-} + X_{u-}} - S_{u-}) \\ &= \sum_{0\leq u\leq t} (e^{\Delta X_u} e^{X_{u-}} - S_{u-}) = \sum_{0\leq u\leq t} (e^{\Delta X_u} S_{u-} - S_{u-}) = \sum_{0\leq u\leq t} S_{u-}(e^{\Delta X_u} - 1).\end{aligned}$$

Using the result in Cont and Tankov (2004, Equation. (2.92)), the jump process

$$\sum_{\{n,T_n\in[0,t]\}} f(T_n, Y_n),$$

can be expressed in integral form in the following way:

$$\sum_{\{n,T_n\in[0,t]\}} f(T_n, Y_n) = \int_0^t \int_{\mathbb{R}^d\setminus 0} f(s,y) N_X(ds, dy),$$

where $f(T_n, Y_n)$ is a function representing its jump amplitude, T_n the random variable that represent the time of the jump and where N_X is the Poisson random measure. Given that in our case $f(s,y) = S_{u^-}(e^y - 1)$ with $Y_n = \Delta X_u$ we have:

$$\sum_{0\le u\le t} S_{u-}(e^{\Delta X_u} - 1) = \int_0^t \int_{\mathbb{R}} S_{u-}(e^x - 1) N_X(du, dx),$$

which proves (B.34). □

B.6. Additional results and proofs

Proposition B.3 (Derivation of the jump-diffusion SDE for S_t under the $\mathbb{P}$ measure). *Consider the jump-diffusion process*

$$X_t = (\mu - q)t + \sigma W_t + \int_0^t \int_{\mathbb{R}} x N_X(ds, dx). \tag{B.35}$$

The dynamics for the exponential Lévy model $S_t = S_0 e^{X_t}$ is given by

$$dS_t = (\tilde{\mu} - q) S_t dt + \sigma S_t dW_t + \int_{\mathbb{R}} S_t (e^x - 1) N_X(dt, dx). \tag{B.36}$$

where $\tilde{\mu} = \mu + \frac{1}{2}\sigma^2$, μ is the expected rate of return of the asset, q is the continuous dividend yield, and σ is the volatility associated with the Brownian motion W_t. The term S_{t-} represents the asset price immediately before the jump, N_X is a Poisson random measure. W_t and N_X are independent sources of randomness.

Proof. Applying Ito's Lemma to $f(t, X_t) = S_0 e^{X_t}$ where X_t is given by (B.35), yields:

$$\begin{aligned} dS_t &= \frac{\partial f}{\partial t} dt + \frac{\partial f}{\partial x} dX_t + \frac{1}{2}\frac{\partial^2 f}{\partial x^2} d[X^c, X^c] \\ &\quad + \int_{\mathbb{R}} \left[f(t, X_t + H(t,x)) - f(t, X_t) - H(t,x)\frac{\partial f}{\partial x}(t, X_t) \right] N_X(dt, dx) \\ &= S_t dX_t + \frac{1}{2} S_t d[X^c, X^c] \\ &\quad + \int_{\mathbb{R}} \left[f(t, X_t + H(t,x)) - f(t, X_t) - H(t,x)\frac{\partial f}{\partial x}(t, X_t) \right] N_X(dt, dx). \end{aligned} \tag{B.37}$$

Substituting the dynamics of X_t and the term $d[X^c, X^c] = \sigma^2 dt$ into equation (B.37),

$$\begin{aligned} dS_t &= (\mu - q + \frac{1}{2}\sigma^2) S_t dt + \sigma S_t dW_t + \int_{\mathbb{R}} x S_t N_X(dt, dx) + \\ &\quad + \int_{\mathbb{R}} \left[f(t, X_t + H(t,x)) - f(t, X_t) - H(t,x)\frac{\partial f}{\partial x}(t, X_t) \right] N_X(dt, dx), \end{aligned} \tag{B.38}$$

Knowing that a jump of size $H(t,x) = x$ leads to $f(t, X_t + x) = S_0 e^{X_t + x} = S_t e^x$, we can calculate the jump terms inside the integral as follows:

$$\begin{aligned} f(t, X_t + x) - f(t, X_t) &= S_t(e^x - 1), \\ x\frac{\partial f}{\partial x}(t, X_t) &= xS_t. \end{aligned} \tag{B.39}$$

As a result, the full jump integral term becomes:

$$\int_{\mathbb{R}} \left[f(t, X_t + x) - f(t, X_t) - x\frac{\partial f}{\partial x}(t, X_t) \right] N_X(dt, dx) = \int_{\mathbb{R}} S_t(e^x - 1 - x) N_X(dt, dx). \tag{B.40}$$

Replacing the jump integral in equation (B.38) and simplifying the terms, we obtain the SDE for the jump-diffusion model for the asset price S_t:

$$\begin{aligned} dS_t &= (\mu - q + \frac{1}{2}\sigma^2) S_t dt + \sigma S_t dW_t + \int_{\mathbb{R}} xS_t N_X(dt, dx) + \int_{\mathbb{R}} S_t(e^x - 1 - x) N_X(dt, dx) \\ &= (\mu - q + \frac{1}{2}\sigma^2) S_t dt + \sigma S_t dW_t + \int_{\mathbb{R}} S_t(e^x - 1) N_X(dt, dx). \end{aligned} \tag{B.41}$$

Defining $\tilde{\mu} = \mu + \frac{1}{2}\sigma^2$ we obtain (B.36). □

Having discussed the dynamics of the asset price process under the probability measure $\mathbb{P}$, the next step is to adjust this process to the risk-neutral probability measure used in the Lee (2004) framework. To achieve this, we use Girsanov theorem.

Proposition B.4 (Derivation of the Girsanov kernel $\varphi_t^{\mathbb{Q}}$). *Assume the dynamics of an asset price S_t under the real probability measure $\mathbb{P}$ is described by the following stochastic differential equation (SDE):*

$$dS_t = (\tilde{\mu} - q) S_{t-} dt + \sigma S_{t-} dW_t^{\mathbb{P}} + \int_{\mathbb{R}} S_{t-}(e^x - 1) N_X(dt, dx), \tag{B.42}$$

Then, the Girsanov kernel $\varphi_t^{\mathbb{Q}}$ for transition from the real measure $\mathbb{P}$ to the risk-neutral measure $\mathbb{Q}$ is given by:

$$\varphi_t^{\mathbb{Q}} = \frac{r - \tilde{\mu} - \int_{\mathbb{R}}(e^x - 1)\nu(dx)}{\sigma}. \tag{B.43}$$

Proof. To derive the kernel $\varphi_t^{\mathbb{Q}}$, we begin by applying the Itô's formula for Lévy-type stochastic integral (outlined in Definition B.29 for the case where $H(t,x) = K(t,x)$) to $f(t) = d(S_t e^{-rt+qt})$ yields:

$$\begin{aligned} d(S_t e^{-rt+qt}) &= (q - r) e^{-rt+qt} S_{t-} dt + e^{-rt+qt} dS_t + \frac{1}{2}.0 + \\ &\quad + \int_{\mathbb{R}} \Big((S_{t-} + H) e^{-rt+qt} - S_{t-} e^{-\int_0^t r_s ds + qt} - H e^{-rt+qt} \Big) N_X(dt, dx) \\ &= (q - r) e^{-rt+qt} S_{t-} dt + e^{-rt+qt} dS_t. \end{aligned} \tag{B.44}$$

Now, incorporating the S_t dynamics into the stochastic process, we get:

$$\begin{aligned} d(S_t e^{-rt+qt}) &= e^{-rt+qt}\big[(q-r)S_{t-}dt + (\mu-q)S_{t-}dt + \sigma S_{t-}dW_t^{\mathbb{P}} + \int_{\mathbb{R}} S_{t-}(e^x-1)N_X(dt,dx)\big], \\ &= e^{-rt+qt}\Big[S_{t-}(\mu-r)dt + \sigma S_{t-}dW_t^{\mathbb{P}} + \int_{\mathbb{R}} S_{t-}(e^x-1)N_X(dt,dx)\Big]. \end{aligned} \tag{B.45}$$

Applying the Girsanov transformation $dW_t^{\mathbb{P}} = \varphi_t^{\mathbb{Q}}dt + dW_t^{\mathbb{Q}}$ to the previous equation, and knowing the relationship between the two Poisson measures is given by $\tilde{N}_X(dt,dx) = N_X(dt,dx) - \nu(dx)dt$, we can rewrite equation (B.45) as follows:

$$\begin{aligned} d(S_t e^{-rt+qt}) &= S_{t-}e^{-rt+qt}(\mu-r)dt + \sigma S_{t-}(\varphi_t^{\mathbb{Q}}dt + dW_t^{\mathbb{Q}})e^{-rt+qt} \\ &\quad + e^{-rt+qt}\int_{\mathbb{R}} S_{t-}(e^x-1)(\tilde{N}_X(dt,dx) + \nu(dx)dt) \\ &= S_{t-}e^{-rt+qt}(\mu - r + \sigma\varphi_t^{\mathbb{Q}} + \int_{\mathbb{R}}(e^x-1)\,\nu(dx)dt) \\ &\quad + \sigma S_{t-}e^{-rt+qt}dW_t^{\mathbb{Q}} + e^{-rt+qt}\int_{\mathbb{R}} S_{t-}(e^x-1)\tilde{N}_X(dt,dx). \end{aligned} \tag{B.46}$$

For $S_t e^{-rt+qt}$ to be a martingale, the drift of the stochastic process must be zero, which occurs only when $\mu - r + \sigma\varphi_t^{\mathbb{Q}} + \int_{\mathbb{R}}(e^x-1)\nu(dx) = 0$. Thus, the Girsanov kernel for the transition to the risk-neutral measure $\mathbb{Q}$ is given by:

$$\varphi_t^{\mathbb{Q}} = \frac{r - \mu - \int_{\mathbb{R}}(e^x-1)\,\nu(dx)}{\sigma}. \tag{B.47}$$

□

Proposition B.5. *The asset price dynamics under the risk-neutral measure $\mathbb{Q}$ is given by*

$$dS_t = (r - q - \int_{\mathbb{R}}(e^x-1)\nu(dx))S_{t-}dt + \sigma S_{t-}dW^{\mathbb{Q}} + \int_{\mathbb{R}} S_{t-}(e^x-1)N_X^{\mathbb{Q}}(dt,dx). \tag{B.48}$$

Proof. Since the dynamics of the asset price under $\mathbb{P}$ given by equation (B.36) in Proposition B.36 is as follows

$$dS_t = (\tilde{\mu} - q)S_{t-}dt + \sigma S_{t-}dW_t^{\mathbb{P}} + \int_{\mathbb{R}} S_{t-}(e^x-1)N_X(dt,dx), \tag{B.49}$$

applying the Girsanov transformation $dW_t^{\mathbb{P}} = \varphi_t^{\mathbb{Q}}dt + dW_t^{\mathbb{Q}}$ with the following kernel:

$$\varphi_t^{\mathbb{Q}} = \frac{r - \tilde{\mu} - \int_{\mathbb{R}}(e^x-1)\nu(dx)}{\sigma}. \tag{B.50}$$

we reach SDE (B.48). □

APPENDIX C

Affine jump-diffusion framework

C.1. Propositions and definitions

C.1.1. *Duffie, Pan, and Singleton (2000) framework-one dimensional case*

In this section we prove the one dimensional case, result of Duffie, Pan, and Singleton (2000), and the general case follows with minor adjustments by adopting matrix notation and standard calculus rules.

Proposition C.1 (*Transform Explicit solution one-dimensional case).* *Consider the transform* (3.9) *in the one-dimensional case*

$$\psi^{\mathcal{X}_{\mathcal{Q}}}(u,t,T,X_t) := \mathbb{E}_{\mathbb{Q}}\left[exp\left[-\int_t^T r(X_s,s)ds\right] exp\left(uX_T\right)\Big|\mathcal{F}_t\right], \tag{C.1}$$

where $u \in \mathbb{C}$ *and* $t \leq T$*. An exponential-affine solution can be derived for the transform* $\psi^{\mathcal{X}_{\mathcal{Q}}}$*, under the technical regularity conditions given in Definition 3.3, and is given by the following equation:*

$$\psi^{\mathcal{X}_{\mathcal{Q}}}(u,t,T,X_t) = exp\left[\alpha(t,T,u) + \beta(t,T,u)X_T\right], \tag{C.2}$$

where $\beta \in \mathbb{C}$ *and* $\alpha \in \mathbb{C}$ *satisfy the following complex-valued ordinary differential equations (ODEs):*

$$\dot{\beta}(t,T,u) = \rho_x(t) - K_x(t)\beta(t,T,u) - \frac{1}{2}\left[\beta(t,T,u)H_x(t)\beta(t,T,u)\right] - \left[\theta(\beta(t,T,u),t)-1\right]l_x(t), \tag{C.3}$$

and

$$\dot{\alpha}(t,T,u) = \rho_0(t) - \beta(t,T,u)K_0(t) - \frac{1}{2}\beta(t,T,u)H_0(t)\beta(t,T,u) - \left[\theta(\beta(t,T,u),t)-1\right]l_0(t), \tag{C.4}$$

constrained by the boundary conditions $\beta(T,T,u) = u$ *and* $\alpha(T,T,u) = 0$*.*

Proof. Let $X_t, t \geq 0$, be a stochastic process and dX_t its corresponding dynamics

$$dX_t = \mu(X)dt + \sigma(X)dW_t + dZ_t, \tag{C.5}$$

where dZ_t is a pure-jump process, which can be represented by the following expression

$$dZ_t = \int_{\mathbb{R}} xN_X(dt,dx), \tag{C.6}$$

and where $N_X([0,t] \times A)\#\{\text{s} \in [0,\text{t}]\text{: } \Delta X_s \in \text{A}\}$ is a Poisson process.
As a result, the dynamics of the process X_t, can be defined as follows:

$$dX_t = \mu(X)dt + \sigma(X)dW_t + \int_{\mathbb{R}} xN_X(dt,dx). \tag{C.7}$$

Note that the expression $\int_{\mathbb{R}} xN_x(dt,dx)$, when written in its integral form, is equivalent to the sum of all jumps of all amplitudes (see Cont and Tankov (2004)), and can be written as:

$$\int_0^t \int_{\mathbb{R}} xN_X(dt,dx) = \sum_{0\leq s\leq t} \Delta X_s. \tag{C.8}$$

Equation C.7 can now be divided into two components, one referring to large jumps (i.e., $|x| \geq 1$) and the other relating to small jumps (i.e., $|x| < 1$)

$$dX_t = \mu(X)dt + \sigma(X)dW_t + \int_{|x|\geq 1} xN_X(dt,dx) + \int_{|x|<1} xN_X(dt,dx). \tag{C.9}$$

Knowing that the Poisson process N_X is related with its corresponding compensated process $\tilde{N}_X$ through the Lévy measure $\nu(A)$, i.e., that $N_X = \tilde{N}_X + t\nu(A)$, and aggregating the terms associated with dt, equation (C.9) simplifies to:

$$dX_t = \Big[\mu(X) + \int_{|x|<1} x\nu(dx)\Big]dt + \sigma(X)dW_t + \int_{|x|\geq 1} xN_X(dt,dx) + \int_{|x|<1} x\tilde{N}_X(dt,dx). \tag{C.10}$$

Now, in order to find a solution to the transform $\psi(u,t,T,X_t) = \mathbb{E}[e^{-\int_t^T r(X_s)ds} e^{uX_t}|F_t]$ (as shown in Nunes and Alcaria (2015)), we will perform an *Ansatz*:

$$\psi(u,t,T,X_t) = \mathbb{E}[e^{-\int_t^T r(X_s)ds} e^{uX_T}|\mathcal{F}_t] = f(t,X_t), \tag{C.11}$$

where $f(t,x)$ is the exponential defined by $f(t,x) = e^{a(t)+b(t)x}$.
Then, we apply, as a first step, the generalised Itô's formula (B.29) to the function $f(t,x) = e^{a(t)+b(t)x}$ and, subsequently, substituting, in the dynamics of (C.7) we obtain the following expression:

$$\begin{aligned} df =& \Big[\dot{a}(t) + \dot{b}(t)X_{t-} + b(t)\mu(X_{t-}) + \frac{1}{2}b(t)^2\sigma^2(X_{t-})\Big]f(t,X_{t-})dt + b(t)f(t,X_{t-})\sigma(X)dW_t \\ &+ \int_{\mathbb{R}} \Big[f(t,X_{s^-}+x) - f(t,X_{s^-})\Big]N_X(dt,dx). \end{aligned} \tag{C.12}$$

For the process $\Psi = e^{-\int_0^t r(X_s)ds}\psi$ to be a martingale, we have to ensure that its dynamics have a zero drift, i.e., that there are no elements associated with the term dt. For this purpose we use the compensated Poisson process $\tilde{N}_X(dt,dx) = N_X(dt,dx) - \nu(dx)dt$ which is a martingale (see equation (B.4) and Cont and Tankov (2004, Proposition 2.16)). As a

result, we get:

$$df = \Big[\dot{a}(t) + \dot{b}(t)x + b(t)\mu(X_{t^-}) + \frac{1}{2}b(t)^2\sigma^2(X_{t^-}) + \int_{\mathbb{R}} \big(e^{b(t)x} - 1\big)\nu(dx)\Big] f(t, X_{t^-})dt$$
$$+ b(t)f(t, X_{t^-})\sigma(X_{t^-})dW_t + \int_{\mathbb{R}} \Big[f(t, X_{s^-} + x) - f(t, X_{s^-})\Big]\tilde{N}_X(dt, dx), \tag{C.13}$$

since

$$f(t, X_{s^-} + x) - f(t, X_{s^-}) = e^{a(t)+b(t)(X_s^- + x)} - e^{a(t)+b(t)X_s^-} = f(t, X_{t^-})\big(e^{b(t)x} - 1\big).$$

Using the definition given by equation (B.21) in Definition B.5 that defines the Lévy measure $\nu(dx)$ as $\lambda(X_t)g(dx)$, equation (C.13) turns into:

$$df = \Big[\dot{a}(t) + \dot{b}(t)x + b(t)\mu(X_{t^-}) + \frac{1}{2}b(t)^2\sigma^2(X_{t^-}) + \int_{\mathbb{R}} \big(e^{b(t)x} - 1\big)g(dx)\lambda(X_{t^-})\Big] f(t, X_{t^-})dt$$
$$+ b(t)f(t, X_{t^-})\sigma(X_{t^-})dW_t + \int_{\mathbb{R}} \Big[f(t, X_{s^-} + x) - f(t, X_{s^-})\Big]\tilde{N}_X(dt, dx). \tag{C.14}$$

By the definition of the jump transform $\theta(c)$ given by Definition 3.4, we can write $\theta(b(t)) = \int_{\mathbb{R}} e^{b(t)z}\nu_t(dz)$. Thus, equation (C.14) becomes:

$$df = \Big[\dot{a}(t) + \dot{b}(t)X_{t^-} + b(t)\mu(X_{t^-}) + \frac{1}{2}b(t)^2\sigma^2(X_{t^-}) + \big(\theta(b(t)) - 1\big)\lambda(X_{t^-})\Big] f(t, X_{t^-})dt$$
$$+ b(t)f(t, X_{t^-})\sigma(X_{t^-})dW_t + \int_{\mathbb{R}} \Big[(f(t, X_{s^-} + x) - f(t, X_{s^-})\Big]\tilde{N}_X(dt, dx). \tag{C.15}$$

Now, taking into account the affine structure, given by Duffie, Pan, and Singleton (2000) we have

$$\mu(x) = K_0(t) + K_1(t)x, \sigma^2(x) = H_0(t) + H_1(t)x, \lambda(x) = l_0(t) + l_1(t)x$$

. Substituting the affine structure into (C.15) and rearranging the terms, we reach the following equation:

$$df = \Big[\dot{a}(t) + b(t)K_0(t) + \frac{1}{2}b(t)^2H_0(t) + \big(\theta(b(t)) - 1\big)l_0(t)$$
$$+ X_{t^-}\Big[\dot{b}(t) + b(t)K_1(t) + \frac{1}{2}b(t)^2H_1(t)$$
$$+ \big(\theta(b(t)) - 1\big)l_1(t)\Big]\Big] f(t, X_{t^-})dt + \eta_t dW_t + \int_{\mathbb{R}} \Big[(f(t, X_{s^-} + x) - f(t, X_{s^-})\Big]\tilde{N}_X(dt, dx). \tag{C.16}$$

As such, as a second step, we apply generalised Ito's Lemma to $\Psi = e^{-\int_0^t r(X_s)ds} f(t, X_t)$:

$$d(e^{-\int_0^t r(X_s)ds} f(t, X_t)) = -r(X_s)e^{-\int_0^t r(X_s)ds} f(t, X_t)dt + e^{-\int_0^t r(X_s)ds} df(t, X_t). \tag{C.17}$$

Substituting (C.16) in (C.17) and $f(t,x)e^{-\int_0^t r(X_s)ds}$ by $\Psi(u,t,T,X_t)$ simplifies to:

$$\begin{aligned} d(\Psi(u,t,T,X_t)) = \Psi(u,t,T,X_t)\Big[&\dot{a}(t) + b(t)K_0(t) + \frac{1}{2}b(t)^2H_0(t) + \big(\theta(b(t)) - 1\big)l_0(t) \\ &+ X_t\Big[\dot{b}(t) + b(t)K_1(t) + \frac{1}{2}b(t)^2H_1(t) + \big(\theta(b(t)) - 1\big)l_1(t)\Big] - r(X_s)\Big]dt \\ &+ e^{-\int_0^t r(X_s)ds}\eta_t dW_t + \int_{\mathbb{R}}\Big[(\Psi(s, X_{s^-} + x) - \Psi(s, X_{s^-})\Big]\tilde{N}_X(ds,dx). \end{aligned} \tag{C.18}$$

Finally, plugging in the affine dynamics for $r(X_t)$, where $r(X_t) = \rho_0(t) + \rho_1(t)X_t$, equation (C.18) becomes:

$$\begin{aligned} d(\Psi(u,t,T,X_t)) = \Psi(u,t,T,X_t)\Big[&\dot{a}(t) - \rho_0(t) + b(t)K_0(t) + \frac{1}{2}b(t)^2H_0(t) + \big(\theta(b(t)) - 1\big)l_0(t) \\ &+ X_t\Big[\dot{b}(t) + b(t)K_1(t) + \frac{1}{2}b(t)^2H_1(t) + \big(\theta(b(t)) - 1\big)l_1(t) - \rho_1(t)\Big]\Big]dt \\ &+ e^{-\int_0^t r(X_s)ds}\eta_t dW_t + \int_{\mathbb{R}}\Big[(\Psi(s, X_{s^-} + x) - \Psi(s, X_{s^-})\Big]\tilde{N}_X(ds,dx). \end{aligned} \tag{C.19}$$

Let us now define dM_t by:

$$dM_t = \int_{\mathbb{R}}\Big[(\Psi(s, X_{s^-} + x) - \Psi(s, X_{s^-})\Big]\tilde{N}_X(ds,dx) + e^{-\int_0^t r(X_s)ds}\eta_t dW_t. \tag{C.20}$$

In order for M_t to be a martingale, its two constituent parts must also be considered martingales. Recall that a process X_t is a martingale if it satisfies the following two conditions:

$$\mathbb{E}\big[X_T|\mathcal{F}_t\big] = X_t \ \wedge \ \mathbb{E}\big[|X_t|\big] < +\infty. \tag{C.21}$$

We first verify these conditions for the first term in (C.20). Let us denote this term by Y_t:

$$Y_t = \int_0^t \int_{\mathbb{R}}\Big[\Psi(t, X_{t^-} + x) - \Psi(t, X_{t^-})\Big]\tilde{N}_X(dt,dx).$$

The first condition in (C.21) holds automatically, as it follows directly from the definition of the compensated Poisson random measure $\tilde{N}_X$. To verify the finite moment condition, we apply the triangle inequality together with point (iii) of Definition 3.3, which states that $\mathbb{E}\big[|\Psi_T|\big] \leq C < +\infty$:

$$\begin{aligned} \mathbb{E}\big[|Y_t|\big] &= \mathbb{E}\Big[\Big|\int_0^T \int_{\mathbb{R}}\Big[(\Psi(t, X_{t^-} + x) - \Psi(t, X_{t^-})\Big]\tilde{N}_X(dt,dx)\Big|\Big] \\ &\leq \mathbb{E}\Big[\int_0^T \int_{\mathbb{R}}\Big|(\Psi(t, X_{t^-} + x) - \Psi(t, X_{t^-})\Big|\tilde{N}_X(dt,dx)\Big] \\ &\leq \mathbb{E}\Big[\int_0^T \int_{\mathbb{R}}\Big(\big|C\big| + \big|C\big|\Big)\tilde{N}_X(dt,dx)\Big] \\ &= 2C\mathbb{E}\Big[\int_0^T \int_{\mathbb{R}}\tilde{N}_X(dt,dx)\Big] = 0. \end{aligned} \tag{C.22}$$

Since $e^{-\int_0^t r(X_s)ds}\eta_t dW_t$ is a martingale and well defined process due to point (ii) of Definition 3.3 the process M_t is a martingale which means that $\Psi(u,t,T,X_t)$ is a martingale if and only if the drift of its dynamics is zero (Cont and Tankov (2004, Prop. 8.9; Remark 8.2) provide the result).

$$\begin{aligned}\mu_\Psi = 0 \Leftrightarrow & \dot{a}(t) - \rho_0(t) + b(t)K_0(t) + \frac{1}{2}b(t)^2 H_0(t) + \big(\theta(b(t)) - 1\big)l_0(t) \\ & + X_t\Big[\dot{b}(t) + b(t)K_1(t) + \frac{1}{2}b(t)^2 H_1(t) + \big(\theta(b(t)) - 1\big)l_1(t) - \rho_1(t)\Big] = 0,\end{aligned} \tag{C.23}$$

which, by the *method of undetermined coefficients*, is equivalent to saying that $\Psi(t,T,X_t)$ is a martingale *iff*

$$\Rightarrow \begin{cases} \dot{a}(t) - \rho_0(t) + b(t)K_0(t) + \frac{1}{2}b(t)^2 H_0(t) + \big(\theta(b(t)) - 1\big)l_0(t) = 0 \\ \dot{b}(t) - \rho_1(t) + b(t)K_1(t) + \frac{1}{2}b(t)^2 H_1(t) + \big(\theta(b(t)) - 1\big)l_1(t) = 0\,. \end{cases} \tag{C.24}$$

□

APPENDIX D

Lee (2004) framework

D.1. Equivalent Martingale measures and change of numeraires

Definition D.1. ***(Martingale measure)*** *Let $\mathbb{P}$ denote the physical (or "real world") probability measure, defined on the measurable space $(\Omega, \mathcal{F})$. Additionally, assume X is a random variable on the probability space $(\Omega, \mathcal{F}, \mathbb{P})$.*
A process $(X_t)_{\geq 0}$ is called a martingale under the probability measure $\mathbb{P}$, if:

$$\mathbb{E}_{\mathbb{P}}\left[X_T|\mathcal{F}_t\right] = X_t, \ \forall T \geq t, \tag{D.1}$$

where the conditional expectation $\mathbb{E}_{\mathbb{P}}\left[X_T|\mathcal{F}_t\right]$ is the expected value of the unknown future value that X will assume at time-T $(\geq t)$, based on the information available at the previous time t (i.e., on the $\sigma-$algebra $\mathcal{F}$).

Definition D.2. ***(Money-market or savings account)****: is a deposit that earns interest at the risk-free rate r. Assuming constant interest rates, and continuous compounding, the time-t value of the money-market account is equal to:*

$$M_t = M_0 e^{rt}, \tag{D.2}$$

where M_0 represents the initial value of the money-market account (at time-0).

Definition D.3. ***(Equivalent Martingale measure*** $\mathbb{Q}$***)*** *The martingale probability measure $\mathbb{Q}$ is a probability measure equivalent to the original probability measure $\mathbb{P}$, such that the discounted price of any asset, expressed in units of the numeraire money-market account, is a $\mathbb{Q}$-martingale. Hence, for any financial asset X, we have:*

$$\frac{X_t}{M_t} = E_{\mathbb{Q}}\left[\frac{X_T}{M_T}|\mathcal{F}_t\right], \ \textit{for } T \geq t. \tag{D.3}$$

Now, substituting the money-market account M_t, outlined in the Definition D.2, equation (D.3) becomes:

$$X_t = e^{-r(T-t)} E_{\mathbb{Q}}\left[X_T|\mathcal{F}_t\right], \ \text{for } T \geq t. \tag{D.4}$$

As such, the risk-neutral measure $\mathbb{Q}$ assumes that any financial asset generates a rate of return equal to the risk-free rate.

Theorem D.1. ***(Abstract Bayes' theorem for change of probability measure)*** *Assume that X is a random variable defined on a filtered probability space $(\Omega, \mathcal{F}, (\mathcal{F}_t)_{t\in[0,T]}, \mathbb{P})$, and let $\mathbb{Q}$ be another probability measure on $(\Omega, \mathcal{F}_T)$ with $\mathbb{Q} \ll \mathbb{P}$ on $\mathcal{F}_T$.*

Additionally, let L denote the Radon–Nikodým derivative of $\mathbb{Q}$ with respect to $\mathbb{P}$:

$$L_T \;=\; \frac{d\mathbb{Q}}{d\mathbb{P}}\Big|_{\mathcal{F}_T}. \tag{D.5}$$

Define the density process $L_t := \mathbb{E}_{\mathbb{P}}[\, L_T \mid \mathcal{F}_t\,]$, $t \in [0,T]$. If X_T is $\mathcal{F}_T$-measurable with $\mathbb{E}_{\mathbb{P}}[\,|X_T|\, L_T\,] < \infty$, then for all $t \in [0,T]$ the Abstract Bayes' theorem reads

$$\mathbb{E}_{\mathbb{Q}}[X_T \mid \mathcal{F}_t] \;=\; \frac{\mathbb{E}_{\mathbb{P}}[X_T\, L_T \mid \mathcal{F}_t]}{\mathbb{E}_{\mathbb{P}}[L_T \mid \mathcal{F}_t]} \;=\; \frac{\mathbb{E}_{\mathbb{P}}[X_T\, L_T \mid \mathcal{F}_t]}{L_t} \quad \mathbb{P}\text{-}a.s. \tag{D.6}$$

D.2. Theorems and propositions from Lee (2004)

Proposition D.1. ***(Non-existence of the Fourier transform of the option price.)*** *Let the Fourier transform of initial option price $C_G(k)$ be represented as follows:*

$$\hat{C}_G(u) = \int_{-\infty}^{+\infty} e^{iuk} C_G(k) dk. \tag{D.7}$$

The transform $\hat{C}_G(u)$ does not exist since the call price $C_G(k)$ does not decay as k approaches $-\infty$, indicating that the call pricing function is not square-integrable.

Proof. Let us consider the Fourier transform presented in equation (D.7). Substituting $C_G(k)$ with its definition under the T-forward measure, we obtain the following expression for the transform $\hat{C}_G(u)$:

$$\hat{C}_G(u) = \int_{-\infty}^{+\infty} e^{iuk} B_t \mathbb{E}_{\mathbb{Q}^T}\left[\left(e^X - e^k\right)^+ |\mathcal{F}_t\right] dk = \int_{-\infty}^{X} e^{iuk} B_t \mathbb{E}_{\mathbb{Q}^T}\left[\left(e^X - e^k\right) |\mathcal{F}_t\right] dk. \tag{D.8}$$

Now, applying Fubini's theorem, we can change the order of the integral and the expectation in the previous expression, yielding:

$$\hat{C}_G(u) = \mathbb{E}_{\mathbb{Q}^T}\left[\int_{-\infty}^{X} e^{iuk} B_t \left(e^X - e^k\right)^+ dk |\mathcal{F}_t\right]. \tag{D.9}$$

To address the infinite range of integration, we use an improper integral with a lower limit, resulting in the following expression:

$$\hat{C}_G(u) = \mathbb{E}_{\mathbb{Q}^T}\left[B_t \lim_{t\to-\infty} \int_{t}^{X} e^{iuk} \left(e^X - e^k\right) dk |\mathcal{F}_t\right]. \tag{D.10}$$

Performing the integration and then simplifying, we get:

$$\begin{aligned} \hat{C}_G(u) &= \mathbb{E}_{\mathbb{Q}^T}\left[B_t \lim_{t\to-\infty}\left[\frac{e^{iuk+X}}{iu} - \frac{e^{iuk+k}}{iu+1}\right]_{k=t}^{k=X} |\mathcal{F}_t\right] \\ &= \mathbb{E}_{\mathbb{Q}^T}\left[B_t\left(e^{(iu+1)X}\left(\frac{1}{iu} - \frac{1}{iu+1}\right) - \lim_{t\to-\infty}\left(\frac{e^{iut+X}}{iu} + \frac{e^{(iu+1)t}}{iu+1}\right)\right) |\mathcal{F}_t\right]. \end{aligned} \tag{D.11}$$

It is easy to note that the previous limit does not exist. Using Euler's identity, we can demonstrate that $\lim_{t\to-\infty} e^{iut} = \lim_{t\to-\infty} (\cos(ut) + i\sin(ut)) = \nexists$. This fact prevents existence of the integral, since the option price $C_G(k)$ does not decay as k approaches $-\infty$, making the call pricing function non-square-integrable. Therefore, the Fourier transform of the option price also does not exist, as we intended to prove. □

Proposition D.2. ***(Fourier transform of the damped option price)*** *Assume a damping constant $\alpha > 0$. For any such α, the Fourier transform $\hat{c}_{\alpha,G}(u)$ of the damped option price $c_{\alpha,G}(k)$ exists and can be represented as follows:*

$$\hat{c}_{\alpha,G}(u) = \frac{f_t\left(u - (\alpha+1)\,i\right)}{\alpha^2 + \alpha - u^2 + i\,(2\alpha+1)\,u}. \tag{D.12}$$

Proof. As per Lee (2004) theorem *3.1*, $c_{\alpha,G}(k)$ decays exponentially for $|k| \to \infty$, and, since it is bounded, it follows that $c_{\alpha,G}(k)$ is in L^1 and has a Fourier transform.
Let us recall the definition of the *damped option price* function $c_{\alpha,G} : \mathbb{R} \to \mathbb{R}$, given by the following expression:

$$c_{\alpha,G}(k) = e^{\alpha k} C_G(k), \tag{D.13}$$

where:
$C_G(k) := B_t \mathbb{E}_{\mathbb{Q}^T}[G(X,k)]$ is the time-t option price on state variable X, with $G(X,k) := (e^X - e^k)^+$ representing the *payoff* of a long call at maturity T, and k denoting the contractual strike.
Applying now the Fourier transform to $c_{\alpha,G}(k)$, we obtain:

$$\hat{c}_{\alpha,G}(u) = \int_{-\infty}^{+\infty} e^{iuk} c_{\alpha,G}(k) dk. \tag{D.14}$$

Substituting, first, the *damped option price* by the relation established by equation (D.13), and, then, $C_G(k)$ by the corresponding valuation formula, we get:

$$\begin{aligned} \hat{c}_{\alpha,G}(u) &= \int_{-\infty}^{+\infty} e^{iuk} e^{\alpha k} C_G(k) dk = \int_{-\infty}^{+\infty} e^{iuk} e^{\alpha k} B_t \mathbb{E}_{\mathbb{Q}^T}\left[G\left(X,k\right)|\mathcal{F}_t\right] dk \\ &= \int_{-\infty}^{+\infty} e^{iuk} e^{\alpha k} B_t \mathbb{E}_{\mathbb{Q}^T}\left[\left(e^X - e^k\right)^+ |\mathcal{F}_t\right] dk. \end{aligned} \tag{D.15}$$

Applying *Fubini's Theorem* allows us to adjust the order of integration in the following manner:[1]

$$\begin{aligned} \hat{c}_{\alpha,G}(u) &= B_t \mathbb{E}_{\mathbb{Q}^T}\left[\int_{-\infty}^{+\infty} e^{iuk} e^{\alpha k}\left(e^X - e^k\right)^+ dk|\mathcal{F}_t\right] = B_t \mathbb{E}_{\mathbb{Q}^T}\left[\int_{-\infty}^{X} e^{iuk} e^{\alpha k}\left(e^X - e^k\right) dk|\mathcal{F}_t\right] \\ &= B_t \mathbb{E}_{\mathbb{Q}^T}\left[\int_{-\infty}^{X}\left(e^{(iu+\alpha)k+X} - e^{(iu+\alpha+1)k}\right) dk|\mathcal{F}_t\right]. \end{aligned} \tag{D.16}$$

By solving the integral, we arrive at the following result for $\hat{c}_{\alpha,G}(u)$:[2]

$$\begin{aligned} \hat{c}_{\alpha,G}(u) &= B_t \mathbb{E}_{\mathbb{Q}^T}\left[\left[\frac{e^{(iu+\alpha)k+X}}{iu+\alpha} - \frac{e^{(iu+\alpha+1)k}}{iu+\alpha+1}\right]_{-\infty}^{X} |\mathcal{F}_t\right] \\ &= B_t \mathbb{E}_{\mathbb{Q}^T}\left[\left(\frac{e^{(iu+\alpha+1)X}}{iu+\alpha} - \frac{e^{(iu+\alpha+1)X}}{iu+\alpha+1}\right) - \left(\frac{e^{-(iu+\alpha)\infty+X}}{iu+\alpha} - \frac{e^{-(iu+\alpha+1)\infty}}{iu+\alpha+1}\right)|\mathcal{F}_t\right]. \end{aligned}$$

---

[1] $\int_{-\infty}^{+\infty}\left(e^X - e^k\right)^+ dk = \int_{-\infty}^{X}\left(e^X - e^k\right) dk$, as $\left(e^X - e^k\right)^+ = \begin{cases} \left(e^X - e^k\right), k < X \\ 0 \qquad\quad , k \geq X \end{cases}$.

[2] $\lim_{k\to-\infty} e^{(iu+\alpha)k} = \lim_{k\to-\infty} e^{\alpha k} e^{iuk} = \lim_{k\to-\infty} e^{\alpha k}(cos(uk) + isin(uk)) = 0$, with $\alpha > 0$.

$$= B_t \mathbb{E}_{\mathbb{Q}^T}\left[\left(\frac{e^{(iu+\alpha+1)X}}{iu+\alpha} - \frac{e^{(iu+\alpha+1)X}}{iu+\alpha+1}\right)|\mathcal{F}_t\right] = \left(\frac{1}{iu+\alpha} - \frac{1}{iu+\alpha+1}\right) B_t \mathbb{E}_{\mathbb{Q}^T}\left[e^{(iu+\alpha+1)X}|\mathcal{F}_t\right]$$
$$= \left(\frac{iu+\alpha+1-iu-\alpha}{(iu+\alpha)(iu+\alpha+1)}\right) B_t \mathbb{E}_{\mathbb{Q}^T}\left[e^{(iu+\alpha+1)X}|\mathcal{F}_t\right]$$
$$= \left(\frac{1}{\alpha^2+\alpha-u^2+2\alpha iu+iu}\right) B_t \mathbb{E}_{\mathbb{Q}^T}\left[e^{i(u-\alpha i-i)X}|\mathcal{F}_t\right]. \tag{D.17}$$

Now note that the integral inside the expectation in equation (D.16) exists for positive α. Knowing that the *discounted characteristic function* of X, with respect to the *T-forward measure* $\mathbb{Q}_T$, where a T-maturity discount bond $B_t := \mathbb{E}_{\mathbb{Q}}\left[M_T^{-1} M_t|\mathcal{F}_t\right] = \mathbb{E}_{\mathbb{Q}}\left[e^{-\int_t^T r_s ds}|\mathcal{F}_t\right]$ is used as *numeraire*, is (for ζ restricted to $\mathbb{R}^n$) given by the expression $f_t(\zeta) := f_t(0)\mathbb{E}_{\mathbb{Q}^T}\left[e^{i\zeta X}|\mathcal{F}_t\right]$, equation (D.17) can be rewritten as follows:

$$\hat{c}_{\alpha,G}(u) = \left(\frac{1}{\alpha^2+\alpha-u^2+i(2\alpha+1)u}\right) f_t(0)\mathbb{E}_{\mathbb{Q}^T}\left[e^{i(u-\alpha i-i)X}|\mathcal{F}_t\right], \text{where } f_t(0) \text{ is equal to } B_t. \tag{D.18}$$

Resulting in the expected outcome for the Fourier transform of the *damped option price*, as we set out to prove:

$$\hat{c}_{\alpha,G}(u) = \frac{f_t(u-(\alpha+1)i)}{\alpha^2+\alpha-u^2+i(2\alpha+1)u}, \tag{D.19}$$

assuming, once again, a *positive* α. □

Proposition D.3. ***(Complex Fourier transform of the unmodified option price)*** *Let Γ be the set $\Gamma_{X,G} := \{z \in \mathbb{C} : -Im(z)b_0 + b_1 \in A_X\}$. For a positive α, the complex Fourier transform of the unmodified option price $C_G(k)$, can be specified as $\hat{\mathscr{C}_G}\colon \Gamma_{X,G} \to \mathbb{C}$, and its definition is given by the following equation:*

$$\hat{\mathscr{C}_G}(z) := \frac{f_t(z-i)}{iz-z^2}. \tag{D.20}$$

Proof. Building upon the results of Proposition (D.2), and assuming, once again, a *damping constant* $\alpha > 0$, the Fourier transform of the *damped option price* $c_{\alpha,G}(k)$ can be represented in the following manner:

$$\hat{c}_{\alpha,G}(u) = \frac{f_t\left(u-(\alpha+1)\,i\right)}{\alpha^2+\alpha-u^2+i\left(2\alpha+1\right)u}. \tag{D.21}$$

By rearranging the terms, it is possible to write the previous expression as follows:

$$\hat{c}_{\alpha,G}(u) = \frac{f_t\left(u-\alpha i-i\right)}{i\left(u-\alpha i\right)-\left[\left(\alpha i\right)^2-2\alpha iu+u^2\right]} = \frac{f_t\left(u-\alpha i-i\right)}{i\left(u-\alpha i\right)-\left(u-\alpha i\right)^2}. \tag{D.22}$$

Now, through a substitution, where $z = u - \alpha i \in \mathbb{C}$, we arrive at the definition of *complex Fourier* transform of the unmodified option price $C_G(k)$, as originally intended:

$$\hat{\mathscr{C}_G}(z) = \frac{f_t(z-i)}{iz-z^2}. \tag{D.23}$$

□

Corollary D.1. ***(Insights from the complex Fourier transform proposition)*** *Following Proposition D.3, which sets the link between the Fourier transform of the damped option price specified in equation* (D.12)*, and the complex Fourier transform outlined in equation* (D.20)*, a relationship can be established between the two definitions, knowing, once again, that* $z = u - \alpha i$*.*
Therefore, for a positive α *and* $\alpha b_0 + b_1 \in A_X$ *(with* $b_0 := 1, b_1 := 1$*), we have:*

$$\hat{c}_{\alpha,G}(u) = \hat{\mathscr{C}_G}(u - \alpha i), \tag{D.24}$$

and hence, for $z \in \Gamma$*, such that* $-Im(z) > 0$*, we can also derive the following representation for the complex Fourier transform of the unmodified option price* $C_G(k)$*:*

$$\hat{\mathscr{C}_G}(z) = \int_{-\infty}^{+\infty} e^{izk} C_G(k) dk. \tag{D.25}$$

Proof. Assume the set $\Gamma_{X,G} := \{z \in \mathbb{C} : -Im(z)b_0 + b_1 \in A_X\}$ and consider the following representation for the Fourier transform $\hat{c}_{\alpha,G}(u)$ of the *damped option price* $c_{\alpha,G}(k)$:

$$\hat{c}_{\alpha,G}(u) = \int_{-\infty}^{+\infty} e^{iuk} c_{\alpha,G}(k) dk. \tag{D.26}$$

Applying, both the *damped option price* definition, where $c_{\alpha,G}(k) = e^{\alpha k} C_G(k)$, and the equivalence outlined in equation (D.24), we get:

$$\hat{\mathscr{C}_G}(u - \alpha i) = \int_{-\infty}^{+\infty} e^{iuk} e^{\alpha k} C_G(k) dk. \tag{D.27}$$

Readjusting the terms, we obtain:

$$\hat{\mathscr{C}_G}(u - \alpha i) = \int_{-\infty}^{+\infty} e^{(iu+\alpha)k} C_G(k) dk = \int_{-\infty}^{+\infty} e^{i(u-\alpha i)k} C_G(k) dk. \tag{D.28}$$

By substituting $z = u - \alpha i$ and assuming a positive α, with $z \in \Gamma$ such that $-Im(z) > 0$, we reach the final expression for the *complex Fourier* transform of the unmodified option price $C_G(k)$:

$$\hat{\mathscr{C}_G}(z) = \int_{-\infty}^{+\infty} e^{izk} C_G(k) dk. \tag{D.29}$$

□

Proposition D.4. ***(Conjugate of the Fourier transform of the damped option price)*** *Let* $\hat{c}_{\alpha,G}(u)$ *be the Fourier transform of the damped option price as defined in Proposition* (D.2)*. Then its conjugate corresponds to the transform evaluated at the negative of the variable* u*:*

$$\overline{\hat{c}_{\alpha,G}(u)} = \hat{c}_{\alpha,G}(-u). \tag{D.30}$$

Proof. Being $\hat{c}_{\alpha,G}(u)$ the Fourier transform of the *damped option price*, given by equation (D.12), its conjugate can be express as:

$$\overline{\hat{c}_{\alpha,G}(u)} = \overline{\frac{f_t\left(u - (\alpha+1)\, i\right)}{\alpha^2 + \alpha - u^2 + i\left(2\alpha + 1\right) u}}\,. \tag{D.31}$$

Since the conjugate of a quotient is equal to the quotient of the conjugates $\left(i.e., \overline{\frac{z_1}{z_2}} = \frac{\overline{z_1}}{\overline{z_2}}\right)$, equation (D.31) can be rewritten as:

$$\overline{\hat{c}_{\alpha,G}(u)} = \frac{\overline{f_t\left(u-(\alpha+1)\,i\right)}}{\alpha^2+\alpha-u^2+i\left(2\alpha+1\right)u}\,. \tag{D.32}$$

Knowing that the *discounted characteristic function* of X, with respect to the discount factor $e^{-\int_t^T r_s ds}$, is given by the function $f_t : \Lambda_x \to \mathbb{C}$, such that $f_t(\zeta) := \mathbb{E}_{\mathbb{Q}}\left[e^{-\int_t^T r_s ds} e^{i\zeta X} | \mathcal{F}_t\right]$, we can now perform the following substitution, by setting $\zeta = u-(\alpha+1)\,i$:

$$\overline{\hat{c}_{\alpha,G}(u)} = \frac{\overline{\mathbb{E}_{\mathbb{Q}}\left[e^{-\int_t^T r_s ds} e^{i(u-(\alpha+1)i)X} | \mathcal{F}_t\right]}}{\overline{\alpha^2+\alpha-u^2+i\left(2\alpha+1\right)u}}\,. \tag{D.33}$$

As the conjugate of a product is the product of conjugates ($i.e.$, $\overline{z_1 \cdot z_2} = \overline{z_1} \cdot \overline{z_2}$), we obtain:

$$\begin{aligned}\overline{\hat{c}_{\alpha,G}(u)} &= \frac{\mathbb{E}_{\mathbb{Q}}\left[e^{\int_t^T r_s ds}\overline{e^{i(u-(\alpha+1)i)X}} | \mathcal{F}_t\right]}{\alpha^2+\alpha-u^2-i\left(2\alpha+1\right)u} = \frac{\mathbb{E}_{\mathbb{Q}}\left[e^{\int_t^T r_s ds}\overline{e^{iuX+(\alpha+1)X}} | \mathcal{F}_t\right]}{\alpha^2+\alpha-u^2-i\left(2\alpha+1\right)u} \\ &= \frac{\mathbb{E}_{\mathbb{Q}}\left[e^{\int_t^T r_s ds} e^{-iuX+(\alpha+1)X} | \mathcal{F}_t\right]}{\alpha^2+\alpha-u^2-i\left(2\alpha+1\right)u} = \frac{\mathbb{E}_{\mathbb{Q}}\left[e^{\int_t^T r_s ds} e^{i(-u-(\alpha+1)i)X} | \mathcal{F}_t\right]}{\alpha^2+\alpha-u^2-i\left(2\alpha+1\right)u}\,.\end{aligned}$$

Using, again, the *discounted characteristic function* of X, where $f_t(\zeta) := \mathbb{E}_{\mathbb{Q}}\left[e^{-\int_t^T r_t dt} e^{i\zeta X} | \mathcal{F}_t\right]$, we can execute the inverse substitution, obtaining the corresponding function by setting $\zeta = -u-(\alpha+1)\,i$:

$$\overline{\hat{c}_{\alpha,G}(u)} = \frac{f_t\left(-u-(\alpha+1)\,i\right)}{\alpha^2+\alpha-u^2-i\left(2\alpha+1\right)u}\,. \tag{D.34}$$

Finally, in line with the definition provided in equation (D.2), we can rewrite the previous expression as a function of the Fourier transform of the damped option price, however, in this case, evaluated at $-u$, as we wanted to demonstrate:

$$\overline{\hat{c}_{\alpha,G}(u)} = \hat{c}_{\alpha,G}(-u). \tag{D.35}$$

□

Corollary D.2. ***(Conjugate of the complex Fourier Transform of the damped option price)*** *Let $\hat{\mathscr{C}}_G(u-\alpha i)$ denote the complex Fourier transform of the damped option price defined in Proposition* (D.3)*, where $z = u-\alpha i$. Then its conjugate is given by:*

$$\overline{\hat{\mathscr{C}}_G(u-\alpha i)} = \hat{\mathscr{C}}_G(-u-\alpha i). \tag{D.36}$$

Proof. Let $\hat{c}_{\alpha,G}(u)$ be the Fourier transform of the *damped option price* specified in Proposition (D.2). Additionally, assume that $\hat{\mathscr{C}}_G(u-\alpha i)$ represent the complex Fourier transform of the *damped option price* defined in Proposition (D.3), where $z = u-\alpha i$. Using the results from Corollary D.1, namely the ones given by equation (D.24), we can establish the following relationship between the two Fourier transforms:

$$\hat{c}_{\alpha,G}(u) = \hat{\mathscr{C}}_G(u-\alpha i). \tag{D.37}$$

Applying the conjugate to both sides of equation (D.37), and inverting the terms, we find that:

$$\overline{\hat{\mathscr{C}}_G(u-\alpha i)} = \overline{\hat{c}_{\alpha,G}(u)}. \tag{D.38}$$

Now, building upon Proposition D.4, which sets the equivalence between the Fourier transform of the damped option price and its conjugate, as shown in equation (D.30), we are able to derive a new relationship:

$$\overline{\hat{\mathscr{C}}_G(u-\alpha i)} = \overline{\hat{c}_{\alpha,G}(u)} = \hat{c}_{\alpha,G}(-u). \tag{D.39}$$

Knowing, by definition, that $\hat{c}_{\alpha,G}(-u) = \hat{\mathscr{C}}_G(u-\alpha i)$, we finally conclude:

$$\overline{\hat{\mathscr{C}}_G(u-\alpha i)} = \overline{\hat{c}_{\alpha,G}(u)} = \hat{c}_{\alpha,G}(-u) = \hat{\mathscr{C}}_G(-u-\alpha i). \tag{D.40}$$

□

Theorem D.2. ***(Inverse Fourier transform for damped option price)*** *Let $\alpha > 0$ be a damping constant. For any such α, both the damped option price function $c_{\alpha,G}$ and its Fourier transform $\hat{c}_{\alpha,G}$ exist and belong to L^1, ensuring they are absolutely integrable over their entire domain (i.e., $\int_{-\infty}^{+\infty} |c_{\alpha,G}| < \infty$ and $\int_{-\infty}^{+\infty} |\hat{c}_{\alpha,G}| < \infty$).*
Then, the call option price is determined by:

$$C_G(k) = \frac{e^{-\alpha k}}{2\pi} \int_{-\infty}^{+\infty} e^{-iuk} \hat{c}_{\alpha,G}(u) du = \frac{e^{-\alpha k}}{\pi} \int_{0}^{+\infty} Re\left[e^{-iuk} \hat{c}_{\alpha,G}(u)\right] du. \tag{D.41}$$

Proof. As per Proposition D.2, the *damped option price function* $c_{\alpha,G}(k)$ belongs to L^1 and possesses a Fourier transform, given its exponential decay for $|k| \to \infty$ and its bounded nature. Additionally, in the context of this particular *payoff* structure, and for a *positive* α, it is easy to establish, by the *dominated convergence theorem*, the continuity of $c_{\alpha,G}(k)$. This, combined with the fact that the Fourier transform of the *damped option price* is also in L^1, allows for the recovery of the option price $C_G(k)$ through the inverse Fourier transform using an undamping factor of $e^{-\alpha k}$.
That being said, applying the classical result for the *Fourier inversion theorem* provided by (see, for example, Kendall and Stuart (1977), we can express the recovered *damped option price* $c_{\alpha,G}(k)$ as follows:

$$c_{\alpha,G}(k) = \frac{1}{2\pi} \int_{-\infty}^{+\infty} e^{-iuk} \hat{c}_{\alpha,G}(u) du. \tag{D.42}$$

Using the *damped option price* definition, outlined in equation (D.13), we can substitute the left-hand side of the previous expression with $e^{\alpha k} C_G(k)$:

$$e^{\alpha k} C_G(k) = \frac{1}{2\pi} \int_{-\infty}^{+\infty} e^{-iuk} \hat{c}_{\alpha,G}(u) du. \tag{D.43}$$

Rearranging the terms, we then arrive at the first equality of equation (D.41):

$$C_G(k) = \frac{e^{-\alpha k}}{2\pi} \int_{-\infty}^{+\infty} e^{-iuk} \hat{c}_{\alpha,G}(u) du. \tag{D.44}$$

Decomposing the integral into two components, while preserving the integration limits, we get:

$$C_G(k) = \frac{e^{-\alpha k}}{2\pi}\left(\int_{-\infty}^{0} e^{-iuk}\hat{c}_{\alpha,G}(u)du + \int_{0}^{+\infty} e^{-iuk}\hat{c}_{\alpha,G}(u)du\right). \tag{D.45}$$

Now, performing a change of variable in the first integral by substituting $z = -u$, and subsequently adjusting the corresponding integration limits, we obtain:

$$C_G(k) = \frac{e^{-\alpha k}}{2\pi}\left(\int_{0}^{+\infty} e^{izk}\hat{c}_{\alpha,G}(-z)dz + \int_{0}^{+\infty} e^{-iuk}\hat{c}_{\alpha,G}(u)du\right), \tag{D.46}$$

or equivalently, substituting, again, $z = u$:

$$C_G(k) = \frac{e^{-\alpha k}}{2\pi}\int_{0}^{+\infty}\left[e^{iuk}\hat{c}_{\alpha,G}(-u) + e^{-iuk}\hat{c}_{\alpha,G}(u)\right]du. \tag{D.47}$$

Applying the results of the Proposition D.4 to the first term of the equation, which establishes that $\overline{\hat{c}_{\alpha,G}(u)}$ is equivalent to $\hat{c}_{\alpha,G}(-u)$, as outlined in equation (D.30), we can rewrite the previous expression, resulting in the following outcome:

$$\begin{aligned} C_G(k) &= \frac{e^{-\alpha k}}{2\pi}\int_{0}^{+\infty}\left[e^{iuk}\overline{\hat{c}_{\alpha,G}(u)} + e^{-iuk}\hat{c}_{\alpha,G}(u)\right]du \\ &= \frac{e^{-\alpha k}}{2\pi}\int_{0}^{+\infty}\left[\overline{e^{-iuk}\hat{c}_{\alpha,G}(u)} + e^{-iuk}\hat{c}_{\alpha,G}(u)\right]du. \end{aligned} \tag{D.48}$$

Given that the product of a complex number and its conjugate is equal to twice its real part (*i.e.*, $z + \overline{z} = 2\mathrm{Re}(z)$), we can easily derive an alternative expression for the *unmodified option price*, assuming, once again, a *positive* α:

$$C_G(k) = \frac{e^{-\alpha k}}{\pi}\int_{0}^{+\infty}\mathrm{Re}\left[e^{-iuk}\hat{c}_{\alpha,G}(u)\right]du, \tag{D.49}$$

which corresponds to the second equality of equation (D.41). □

Theorem D.3. ***(Complex inverse Fourier transform for unmodified option price calculation)*** *Let us consider the set* $\Gamma_{X,G} := \{z \in \mathbb{C} : -Im(z)b_0 + b_1 \in A_X\}$ *and define the complex Fourier transform of the unmodified option price* $C_G(k)$ *as* $\hat{\mathscr{C}}_G(z)$ *where* $\hat{\mathscr{C}}_G\colon \Gamma_{X,G} \to \mathbb{C}$ *is defined in* (D.20) *of Proposition D.3.*
Then, the unmodified call option price can be obtained by integrating the complex inverse Fourier transform $\hat{\mathscr{C}}_G(z)$ *along the contour* $Im(z) = -\alpha$ *for a positive* α *and* $\alpha b_0 + b_1 \in A_X$ *(i.e with* $b_0 := 1, b_1 := 1$*) in the complex plane, as follows:*

$$C_G(k) = \frac{1}{2\pi}\int_{-\infty-\alpha i}^{+\infty-\alpha i} e^{-ikz}\hat{\mathscr{C}}_G(z)dz = \frac{1}{\pi}\int_{0-\alpha i}^{+\infty-\alpha i} Re\left[e^{-ikz}\hat{\mathscr{C}}_G(z)\right]dz. \tag{D.50}$$

Proof. Leveraging the results from *Theorem D.2*, namely the first equality of equation (D.41), we can write the call option price as:

$$C_G(k) = \frac{e^{-\alpha k}}{2\pi}\int_{-\infty}^{+\infty} e^{-iuk}\hat{c}_{\alpha,G}(u)du. \tag{D.51}$$

Based on the relationship established in equation (D.24) of Corollary D.1, between the Fourier transform $\hat{c}_{\alpha,G}(u)$ of the damped option price and the representation of the complex Fourier transform $\hat{\mathscr{C}}_G(u-\alpha i)$, we are able to express equation (D.51) as follows:

$$C_G(k) = \frac{e^{-\alpha k}}{2\pi}\int_{-\infty}^{+\infty} e^{-iuk}\hat{\mathscr{C}}_G(u-\alpha i)du = \frac{1}{2\pi}\int_{-\infty}^{+\infty} e^{-i(u-\alpha i)k}\hat{\mathscr{C}}_G(u-\alpha i)du. \tag{D.52}$$

Performing a change of variable, by substituting $z = u - \alpha i \in \mathbb{C}$, and subsequently adjusting the corresponding integration limits, we get:

$$C_G(k) = \frac{1}{2\pi}\int_{\Gamma_{-\alpha}} e^{-ikz}\hat{\mathscr{C}}_G(z)dz, \tag{D.53}$$

where $\Gamma_{-\alpha} = \{z \in \mathbb{C} : Im(z) = -\alpha\,,\, \alpha > 0\}$. Rewriting this expression with explicit integration limits, we obtain: (D.50):

$$C_G(k) = \frac{1}{2\pi}\int_{-\infty-\alpha i}^{+\infty-\alpha i} e^{-ikz}\hat{\mathscr{C}}_G(z)dz, \tag{D.54}$$

which corresponds to the first equality of equation (D.50).
Having established the first equality, we can now proceed to demonstrate the second equality of equation (D.50). Thus, building on the proven relationship between the first terms of equations (D.50) and (D.41), we can set the following link with the second equality of equation (D.41) of Theorem *D.2*:

$$\begin{aligned} C_G(k) &= \frac{1}{2\pi}\int_{-\infty-\alpha i}^{+\infty-\alpha i} e^{-ikz}\hat{\mathscr{C}}_G(z)dz = \frac{e^{-\alpha k}}{2\pi}\int_{-\infty}^{+\infty} e^{-iuk}\hat{c}_{\alpha,G}(u)du \\ &= \frac{e^{-\alpha k}}{\pi}\int_{0}^{+\infty} \mathrm{Re}\left[e^{-iuk}\hat{c}_{\alpha,G}(u)\right]du. \end{aligned} \tag{D.55}$$

Rearranging the terms, yields:

$$C_G(k) = \frac{1}{\pi}\int_{0}^{+\infty} \mathrm{Re}\left[e^{-i(u-\alpha i)k}\hat{c}_{\alpha,G}(u)\right]du. \tag{D.56}$$

Once again, using the relationship between the Fourier transform $\hat{c}_{\alpha,G}(u)$ of the damped option price and the representation of the complex Fourier transform $\hat{\mathscr{C}}_G(u-\alpha i)$, outlined in equation (D.24) of Corollary D.1, leads to:

$$C_G(k) = \frac{1}{\pi}\int_{0}^{+\infty} \mathrm{Re}\left[e^{-i(u-\alpha i)k}\hat{\mathscr{C}}_G(u-\alpha i)\right]du. \tag{D.57}$$

Performing a change of variable by substituting $z = u + \alpha i \in \mathbb{C}$, and subsequently adjusting the corresponding integration limits, we obtain:

$$C_G(k) = \frac{1}{\pi}\int_{\Gamma_{-\alpha}} \mathrm{Re}\left[e^{-ikz}\hat{\mathscr{C}}_G(z)\right]dz. \tag{D.58}$$

Rewriting the previous expression, and assuming a positive α, we finally reach the second equality of equation (D.50), as we intended to prove:

$$C_G(k) = \frac{1}{\pi}\int_{0-\alpha i}^{+\infty-\alpha i} \mathrm{Re}\left[e^{-ikz}\hat{\mathscr{C}}_G(z)\right]dz. \tag{D.59}$$

□

D.3. Option pricing under the *Lee (2004) framework*

To derive the option pricing formula under the Lee (2004) framework, we will build upon the results of *Theorem D.3.* Starting from the second equality of equation (D.50), as an additional step, we will incorporate the value of the residues for each α scenario. Note that, to simplify the notation, we will assume the function f will be always evaluated at time-t, i.e., from now on $f_t = f$.

Defining the residues as $R_{\alpha,G}$, the general pricing formula for the current *payoff* is given by the following expression:

$$C_G(k) = \frac{1}{\pi} \int_{0-\alpha i}^{+\infty-\alpha i} \text{Re}\left[e^{-ikz}\hat{\mathscr{C}}_G(z)\right] dz + R_{\alpha,G}, \tag{D.60}$$

where $C_G(k)$ represents the price of the call, considering the value of the residues.

To determine $R_{\alpha,G}$, we will apply the *Cauchy's residue theorem*, used in complex analysis to evaluate integrals of holomorphic (analytic) functions, by identifying and computing residues at singularities along a specific contour. In our specific scenario, the contour is the vertical line from $0 - \alpha i$ to $+\infty - \alpha i$, and the singularities arise from the integrand in the pricing formula.

This theorem states that for a function $f(z)$ that is holomorphic within (i.e., inside and on) a simple closed contour C in the complex plane, except for a finite set of isolated singularities $z_1, z_2, ..., z_n$ inside C, the contour integral of $f(z)$ is given by:

$$\oint_C f(z)dz = 2\pi i \sum_{k=1}^{n} \text{Res}(f, z_k). \tag{D.61}$$

The term $\text{Res}(f, z_a)$ denotes the residue of f at each singularity z_a and is calculated using the following derivative formula for complex functions, assuming a pole of order n at $z = a$:

$$\text{Res}_f(z = a) = \frac{1}{(n-1)!} \lim_{z \to a} \frac{d^{n-1}}{dz^{n-1}} \left[(z-a)^n f(z)\right]. \tag{D.62}$$

Before proceeding with the contour integral estimates, it is useful to recall a fundamental bound from complex analysis. This inequality, often referred to as the ML inequality, provides an elementary way to control the absolute value of a contour integral in terms of the maximum size of the integrand along the path and the length of the path itself.

Theorem D.4 (ML inequality). *Let C be a rectifiable contour in $\mathbb{C}$ (for instance, a piecewise C^1 curve) and let f be continuous on C. Denote*

$$M \;=\; \max_{z \in C} |f(z)|, \qquad L \;=\; \text{len}(C). \tag{D.63}$$

Then the following bound holds:

$$\left| \int_C f(z)\, dz \right| \;\leq\; M\, L. \tag{D.64}$$

D.3.1. Singularities and residues for the *complex Fourier transform of the unmodified option price*

Having presented the methodology, our focus now shifts to the identification of the singularities and the computation of the corresponding residues associated with the *complex Fourier transform* $\hat{\mathscr{C}_G}(z)$ of the unmodified option price, as outlined in Proposition D.3. We start by defining the following auxiliary function

$$h(z) = \frac{1}{2\pi}\hat{\mathscr{C}_G}(z)e^{-ikz} = \frac{1}{2\pi}\frac{f(z-i)}{iz-z^2}e^{-ikz}, \qquad z \in \mathbb{C}, \tag{D.65}$$

where $\hat{\mathscr{C}_G}(z)$ is given in equation (D.20). The singularities of $h(z)$ arise from the zeros of the denominator. Factoring $iz-z^2 = z(i-z)$, we immediately identify two singular points at $z = 0$ and $z = i$. We then classify each singularity based on its order, by studying the $\lim_{z\to a}[(z-a)^n h(z)]$.

Lemma D.1. *The function $h(z)$ has a simple pole at $z = 0$.*

Proof. We consider

$$(z-0)h(z) = \frac{zf(z-i)e^{-ikz}}{2\pi(iz-z^2)} = \frac{f(z-i)e^{-ikz}}{2\pi(i-z)}. \tag{D.66}$$

Taking the limit as $z \to 0$, we obtain

$$\lim_{z\to 0} zh(z) = \frac{f(-i)}{2\pi i}, \tag{D.67}$$

which is finite and non-zero. Hence, the singularity at $z = 0$ is a pole of order one. □

Lemma D.2. *The function $h(z)$ has a simple pole at $z = i$.*

Proof. We compute

$$(z-i)h(z) = \frac{(z-i)f(z-i)e^{-ikz}}{2\pi(iz-z^2)} = -\frac{f(z-i)e^{-ikz}}{2\pi z}. \tag{D.68}$$

Taking the limit as $z \to i$, we find

$$\lim_{z\to i}(z-i)h(z) = -\frac{f(0)e^{-iki}}{2\pi i}, \tag{D.69}$$

which is finite and non-zero. Therefore, the singularity at $z = i$ is a pole of order one. □

Having identified and classified the singularities as simple poles, let's proceed to calculate the corresponding residues. Since both singularities are simple poles, the residue of $h(z)$ at $z = a$ is given by

$$\text{Res}_h(a) = \lim_{z\to a}(z-a)h(z). \tag{D.70}$$

Lemma D.3. *The residue of $h(z)$ at $z = 0$ is*

$$\text{Res}_h(0) = \frac{-if(-i)}{2\pi}. \tag{D.71}$$

Proof. Applying (D.70) with $a = 0$, we have

$$\mathrm{Res}_h(0) = \lim_{z\to 0} \frac{z f(z-i) e^{-ikz}}{2\pi(iz - z^2)} = \frac{-if(-i)}{2\pi}. \tag{D.72}$$

□

Lemma D.4. *The residue of $h(z)$ at $z = i$ is*

$$\mathrm{Res}_h(i) = \frac{if(0)e^k}{2\pi}. \tag{D.73}$$

Proof. Applying (D.70) with $a = i$, we obtain

$$\mathrm{Res}_h(i) = \lim_{z\to i} \frac{(z-i) f(z-i) e^{-ikz}}{2\pi(iz - z^2)} = \frac{if(0)e^k}{2\pi}, \tag{D.74}$$

where we used $e^{-iki} = e^k$. □

D.3.2. Pricing formulas for different α cases

D.3.2.1 Theorems needed for constructing α cases

Theorem D.5 (Vertical-side vanishing via ML inequality). *Fix real numbers $a < b$ and define the vertical segments*

$$\Gamma_R \;=\; \{\, R + iy \,:\, y \in [a,b] \,\}, \qquad \Gamma_{-R} \;=\; \{\, -R + iy \,:\, y \in [a,b] \,\}. \tag{D.75}$$

Let

$$h(z) \;=\; \frac{1}{2\pi}\, \hat{\mathscr{C}}_G(z)\, e^{-ikz}, \qquad \hat{\mathscr{C}}_G(z) \;=\; \frac{f(z-i)}{iz - z^2}, \tag{D.76}$$

where $f(\zeta) = \mathbb{E}_{\mathbb{Q}}\Big[e^{-\int_t^T r_s\, ds}\, e^{i\zeta X_T} \mid \mathcal{F}_t\Big]$ is the (discounted) characteristic function under $\mathbb{Q}$. Then there is a constant $K > 0$, independent of R, such that

$$\sup_{z\,\in\,\Gamma_{\pm R}} |h(z)| \;\le\; \frac{K}{R^2}, \tag{D.77}$$

and

$$\lim_{R\to\infty} \int_{\Gamma_R} h(z)\, dz \;=\; \lim_{R\to\infty} \int_{\Gamma_{-R}} h(z)\, dz \;=\; 0. \tag{D.78}$$

Proof. Since

$$f(\zeta) = \mathbb{E}_{\mathbb{Q}}\Big[e^{-\int_t^T r_s\, ds}\, e^{i\zeta X_T} \;\Big|\; \mathcal{F}_t\Big], \tag{D.79}$$

for any z with $\mathrm{Im}(z) \in [a,b]$ we obtain

$$\begin{aligned} |f(z-i)| &= \Big|\mathbb{E}_{\mathbb{Q}}\Big[e^{-\int_t^T r_s\, ds}\, e^{i(z-i)X_T} \;\Big|\; \mathcal{F}_t\Big]\Big| \\ &\le \mathbb{E}_{\mathbb{Q}}\Big[e^{-\int_t^T r_s\, ds}\, \big|e^{i(z-i)X_T}\big| \;\Big|\; \mathcal{F}_t\Big] \\ &= \mathbb{E}_{\mathbb{Q}}\Big[e^{-\int_t^T r_s\, ds}\, e^{-(\mathrm{Im}\, z - 1)\, X_T} \;\Big|\; \mathcal{F}_t\Big] \\ &\le M, \end{aligned} \tag{D.80}$$

since we assumed the discounted exponential moments are uniformly finite on that interval, i.e.

$$M \;:=\; \sup_{\beta\in[\,1-b,\,1-a\,]} \mathbb{E}_{\mathbb{Q}}\Big[e^{-\int_t^T r_s\,ds}\,e^{\beta X_T}\;\Big|\;\mathcal{F}_t\Big] \;<\; \infty, \tag{D.81}$$

where $\beta = 1 - \mathrm{Im}(z)$.
For the denominator of $\hat{\mathscr{C}_G}(z)$ we note that, for sufficiently large $|z|$,

$$|iz - z^2| = |z||z - i| \geq |z|(|z| - 1) \geq \tfrac{1}{2}|z|^2, \tag{D.82}$$

so that

$$\frac{1}{|iz - z^2|} \leq \frac{C}{|z|^2}. \tag{D.83}$$

The exponential factor, e^{-ikz}, is uniformly bounded on the strip. Indeed, for $z = x + iy$ with $y \in [a, b]$,

$$|e^{-ikz}| = |e^{-ikx}e^{ky}| = e^{ky} \leq e^{|k|\max\{|a|,|b|\}}. \tag{D.84}$$

Combining these bounds we obtain

$$|h(z)| = |\frac{1}{2\pi}\,\hat{\mathscr{C}_G}(z)\,e^{-ikz}| = \frac{1}{2\pi}\left|\frac{f(z-i)}{iz - z^2}\right| |e^{-ikz}| \leq \frac{K}{|z|^2}, \tag{D.85}$$

for large $|z|$ and for some constant $K > 0$ independent of R. On $\Gamma_{\pm R}$ we have $|z| \geq R$, hence $\sup_{z\,\in\,\Gamma_{\pm R}} |h(z)| \leq K/R^2$. The ML inequality given in Theorem D.4 (length–supremum bound) applied to each vertical segment, whose length is $L = b - a$, yields

$$\Big|\int_{\Gamma_{\pm R}} h(z)\,dz\Big| \;\leq\; L \cdot \sup_{\Gamma_{\pm R}} |h| \;\leq\; (b-a)\,\frac{K}{R^2} \;\xrightarrow[R\to\infty]{}\; 0, \tag{D.86}$$

as claimed. □

Corollary D.3 (Specializations used in Sections *Case 1–5*). *In each of the following settings, Theorem D.5 applies with the indicated strip and vertical segments, so that the two vertical integrals vanish as $R \to \infty$.*

Case 1 ($\alpha > 0$). *Use $a = -\alpha$, $b = 0$:*

$$\Gamma_R = \{\, R + iy :\; y \in [-\alpha, 0]\,\}, \qquad \Gamma_{-R} = \{\, -R + iy :\; y \in [-\alpha, 0]\,\}. \tag{D.87}$$

Case 2 ($-1 < \alpha < 0$). *Use $a = -\alpha$, $b = \alpha$:*

$$\Gamma_R = \{\, R + iy :\; y \in [-\alpha, \alpha]\,\}, \qquad \Gamma_{-R} = \{\, -R + iy :\; y \in [-\alpha, \alpha]\,\}. \tag{D.88}$$

Case 3 ($\alpha = 0$). *For any fixed $0 < \varepsilon < 1$, use $a = -\varepsilon$, $b = 0$:*

$$\Gamma_R = \{\, R + iy :\; y \in [-\varepsilon, 0]\,\}, \qquad \Gamma_{-R} = \{\, -R + iy :\; y \in [-\varepsilon, 0]\,\}. \tag{D.89}$$

Case 4 ($\alpha < -1$). *Use $a = -\alpha$, $b = \alpha$ (a symmetric strip):*

$$\Gamma_R = \{\, R + iy :\; y \in [-\alpha, \alpha]\,\}, \qquad \Gamma_{-R} = \{\, -R + iy :\; y \in [-\alpha, \alpha]\,\}. \tag{D.90}$$

Case 5 ($\alpha = -1$). *For any fixed $\varepsilon > 1$, use $a = 1$, $b = \varepsilon$:*

$$\Gamma_R = \{\, R + iy :\; y \in [1, \varepsilon]\,\}, \qquad \Gamma_{-R} = \{\, -R + iy :\; y \in [1, \varepsilon]\,\}. \tag{D.91}$$

In all cases the length is $L = b - a$, and Theorem D.5 yields

$$\left| \int_{\Gamma_{\pm R}} h(z)\, dz \right| \;\leq\; (b-a)\, \frac{K}{R^2} \;\xrightarrow[R\to\infty]{}\; 0. \tag{D.92}$$

Let us recall the general pricing formula, presented in equation (D.60), before delving into the specific cases and explore their implications:

$$C_G(k) = \frac{1}{\pi} \int_{0-\alpha i}^{+\infty-\alpha i} \mathrm{Re}\left[e^{-ikz} \hat{\mathscr{C}}_G(z) \right] dz + R_{\alpha,G}, \tag{D.93}$$

where $C_G(k)$ represents the call option price, incorporating the residues $R_{\alpha,G}$.

D.3.2.2 Residue theorem for poles on contours

The classical Cauchy residue theorem applies when all poles lie strictly inside or outside the contour of integration. When poles lie exactly on the contour, the following extension is required.

Theorem D.6 (Residue theorem for poles on contours). *Let $h(z)$ be a meromorphic function, and let C be a positively oriented, piecewise smooth closed contour. Denote by $\mathcal{I}$ the set of poles strictly inside C and by $\mathcal{B}$ the set of simple poles on C (crossed transversely by C). Then*

$$\oint_C h(z)\, dz = 2\pi i \sum_{z_k \in \mathcal{I}} Res(h, z_k) + \pi i \sum_{w_j \in \mathcal{B}} Res(h, w_j), \tag{D.94}$$

where the integral is understood in the Cauchy principal value sense when $\mathcal{B} \neq \emptyset$.

Remark D.1. *Poles on the contour ($\mathcal{B}$) contribute half their residue (factor πi instead of $2\pi i$). More generally, if C forms an interior angle $\theta(w_j) \in [0, 2\pi]$ at a pole $w_j \in \mathcal{B}$, replace π by $\theta(w_j)$. This is the standard Sokhotski–Plemelj/indentation result (see both Gakhov (1990, Chapter 1) and Muskhelishvili (2008, Chapter 2)).*

Corollary D.4. *If two contours Γ_1 and Γ_2 (open with the same endpoints, or closed with the same orientation) coincide outside a small neighbourhood of a simple pole a and differ only by a deformation that crosses a once, transversely, without changing the winding numbers around any other singularities, then*

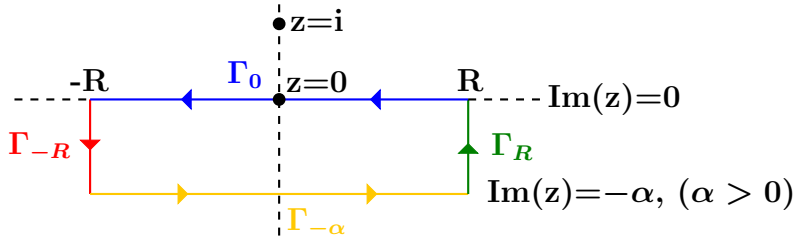
$$\int_{\Gamma_1} h(z)\, dz \;-\; \int_{\Gamma_2} h(z)\, dz \;=\; \pi i\, Res(h, a). \tag{D.95}$$

For multiple crossings or multiple poles, sum the corresponding contributions.

D.3.2.3 Case 1: pricing formula for $\alpha > 0$

For the first scenario, let us consider the case $\alpha > 0$. Then, define C to be a simple closed contour and let $\Gamma = \{z \in \mathbb{C} : \mathrm{Im}(z) = -\alpha,\ \alpha > 0\}$. The function $h(z) = \frac{1}{2\pi} \hat{\mathscr{C}}_G(z) e^{-ikz}$ is analytic inside and on C, since the singularities of order one, $z = 0$ and $z = i$, lie outside the contour.

In this case, the closed contour C can be represented by the following rectangle:



where:

$\Gamma_{-\alpha} = \{z \in \mathbb{C} : Im(z) = -\alpha\,,\ \alpha > 0 \wedge Re(z) \in [-R, R]\}$

$\Gamma_{R} = \{z \in \mathbb{C} : Re(z) = R \wedge Im(z) \in [-\alpha, 0[\}$

$\Gamma_{0} = \{z \in \mathbb{C} : Im(z) = 0 \wedge Re(z) \in [-R, R]\}$

$\Gamma_{-R} = \{z \in \mathbb{C} : Re(z) = -R \wedge Im(z) \in [-\alpha, 0[\}$

$C = \Gamma_{-\alpha} \cup \Gamma_{R} \cup \Gamma_{0} \cup \Gamma_{-R}$

Thus, the line integral of $h(z)$ along the closed contour C can be calculated by summing the integrals representing the four sides of the rectangle:

$$\oint_C h(z)\,dz = \int_{\Gamma_{-\alpha}} h(z)dz + \int_{\Gamma_R} h(z)dz + \int_{\Gamma_0} h(z)dz + \int_{\Gamma_{-R}} h(z)dz \tag{D.96}$$

Given that, in this case, no singularities are enclosed by the contour C, Cauchy's theorem implies that the integral of $h(z)$ over C is equal to zero, yielding:

$$\oint_C h(z)\,dz = 0. \tag{D.97}$$

Then (D.96) becomes:

$$0 = \int_{\Gamma_{-\alpha}} h(z)dz + \int_{\Gamma_R} h(z)dz + \int_{\Gamma_0} h(z)dz + \int_{\Gamma_{-R}} h(z)dz. \tag{D.98}$$

The integrals $\int_{\Gamma_R} h(z)dz$ and $\int_{\Gamma_{-R}} h(z)dz$ vanish as $R \to \infty$ as shown in Case 1 of Corollary D.3, which implies:

$$\int_{\Gamma_{-\alpha}} h(z)dz = -\int_{\Gamma_0} h(z)dz \tag{D.99}$$

The price of the call option is given by the first equality of (D.41):

$$C_G(k) = \int_{-\infty}^{+\infty} \frac{1}{2\pi} \hat{c}_{\alpha,G}(t) e^{-ik(t-\alpha i)} dt. \tag{D.100}$$

Using the relation (D.24) we have:

$$C_G(k) = \int_{-\infty}^{+\infty} \frac{1}{2\pi} \hat{c}_{\alpha,G}(t) e^{-ik(t-\alpha i)} dt = \int_{-\infty}^{+\infty} \frac{1}{2\pi} \hat{\mathscr{C}}_G(t - \alpha i) e^{-ik(t-\alpha i)} dt. \tag{D.101}$$

Performing the change of variables $z = \gamma_{-\alpha}(t) = t - \alpha i$ with $t \in [-R, R]$ when $R \to \infty$, which implies $\gamma'_{-\alpha}(t) = 1$. Using (D.99) we have:

$$C_G(k) = \int_{-\infty}^{+\infty} \frac{1}{2\pi} \hat{\mathscr{C}}_G(z) e^{-ikz} dz = -\int_{\Gamma_0} h(z)dz = \int_{\Gamma_{-\alpha}} h(z)dz. \tag{D.102}$$

The last term can be written in the following way:

$$\begin{aligned}\int_{\Gamma_{-\alpha}} h(z)\,dz &= \int_{-\infty-\alpha i}^{+\infty-\alpha i} \frac{1}{2\pi} e^{-ikz}\hat{\mathscr{C}}_G(z)\,dz \\ &= \int_{-\infty-\alpha i}^{0-\alpha i} \frac{1}{2\pi} e^{-ikz}\hat{\mathscr{C}}_G(z)\,dz + \int_{0-\alpha i}^{+\infty-\alpha i} \frac{1}{2\pi} e^{-ikz}\hat{\mathscr{C}}_G(z)\,dz.\end{aligned} \tag{D.103}$$

Performing the change of variables $z = -u$ in the first term we obtain:

$$\int_{\Gamma_{-\alpha}} h(z)\,dz = \int_{0-\alpha i}^{+\infty-\alpha i} \frac{1}{2\pi} e^{ikz}\hat{\mathscr{C}}_G(-z)\,dz + \int_{0-\alpha i}^{+\infty-\alpha i} \frac{1}{2\pi} e^{-ikz}\hat{\mathscr{C}}_G(z)\,dz. \tag{D.104}$$

Using the fact that $e^{ikz}\hat{\mathscr{C}}_G(-z) = \overline{e^{-ikz}\hat{\mathscr{C}}_G(z)}$ and the property $z + \overline{z} = 2\mathrm{Re}(z)$ we finally obtain:

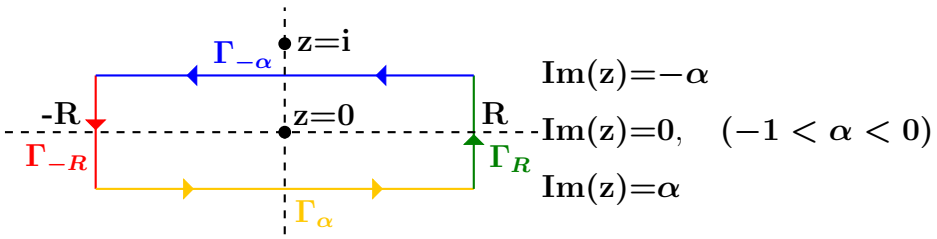
$$\begin{aligned}\int_{\Gamma_{-\alpha}} h(z)\,dz &= \int_{0-\alpha i}^{+\infty-\alpha i} \frac{1}{2\pi} e^{ikz}\hat{\mathscr{C}}_G(-z)\,dz + \int_{0-\alpha i}^{+\infty-\alpha i} \frac{1}{2\pi} e^{-ikz}\hat{\mathscr{C}}_G(z)\,dz \\ &= \int_{0-\alpha i}^{+\infty-\alpha i} \frac{1}{2\pi}\overline{e^{-ikz}\hat{\mathscr{C}}_G(z)} + \frac{1}{2\pi} e^{-ikz}\hat{\mathscr{C}}_G(z)\,dz \\ &= \int_{0-\alpha i}^{+\infty-\alpha i} \frac{1}{\pi}\mathrm{Re}(e^{-ikz}\hat{\mathscr{C}}_G(z))\,dz.\end{aligned} \tag{D.105}$$

Therefore, the pricing formula for the call option when $\alpha > 0$ is given by:

$$C_G(k) = \frac{1}{\pi}\int_{0-\alpha i}^{+\infty-\alpha i} \mathrm{Re}\left[e^{-ikz}\hat{\mathscr{C}}_G(z)\right] dz. \tag{D.106}$$

D.3.2.4 Case 2: Pricing formula for -1 < α < 0

Let us now consider the case where $-1 < \alpha < 0$. Once again, define C as a simple closed contour and assume $h(z) = \frac{1}{2\pi}\hat{\mathscr{C}}_G(z)e^{-ikz}$ is an analytic function in C, except for a finite set of isolated singularities inside C. In this particular scenario, there is only one singularity within the simple closed contour of $h(z)$, at $z = 0$.
As such, C can be represented by the subsequent rectangle:



where:
$\Gamma_\alpha = \{z \in \mathbb{C} : Im(z) = \alpha,\ -1 < \alpha < 0 \wedge Re(z) \in [-R, R]\}$
$\Gamma_R = \{z \in \mathbb{C} : Re(z) = R \wedge Im(z) \in [-\alpha, \alpha]\}$
$\Gamma_{-\alpha} = \{z \in \mathbb{C} : Im(z) = -\alpha,\ 0 < -\alpha < 1 \wedge Re(z) \in [-R, R]\}$
$\Gamma_{-R} = \{z \in \mathbb{C} : Re(z) = -R \wedge Im(z) \in [-\alpha, \alpha]\}$
$C = \Gamma_\alpha \cup \Gamma_R \cup \Gamma_{-\alpha} \cup \Gamma_{-R}$
Thus, the line integral of $h(z)$ along the closed contour C can be calculated by summing

the integrals representing the four sides of the rectangle:

$$\oint_C h(z)\,dz = \int_{\Gamma_{-\alpha}} h(z)dz + \int_{\Gamma_R} h(z)dz + \int_{\Gamma_\alpha} h(z)dz + \int_{\Gamma_{-R}} h(z)dz. \tag{D.107}$$

Following the *Cauchy's residue theorem*, the contour integral is given by the sum of the residues of the poles enclosed by C. Since only $z = 0$ lies inside the contour, the sum will include just the residues given by Lemma D.3, resulting in the following expression:

$$\oint_C h(z)\,dz = 2\pi i \sum_{k=1}^{n} \text{Res}(h, z = 0) = 2\pi i \frac{-i f_t(-i)}{2\pi} = f_t(-i). \tag{D.108}$$

Therefore, substituting the previous results into the equation (D.107), we have that:

$$f_t(-i) = \int_{\Gamma_{-\alpha}} h(z)dz + \int_{\Gamma_R} h(z)dz + \int_{\Gamma_\alpha} h(z)dz + \int_{\Gamma_{-R}} h(z)dz. \tag{D.109}$$

To compute the line integrals, we will need to parametrise the curves and then perform the integration along each curve separately.

Let's start by evaluating the first integral along the curve $\Gamma_{-\alpha}$, denoting its parametrisation by $\gamma_{-\alpha}(t)$. This allows us to express the function $h(z)$ in terms of t, as $h(\gamma_{-\alpha}(t))$. Consequently, the line integral can be expressed as:

$$\int_{\Gamma_{-\alpha}} h(z)dz = \int_{-R}^{R} h\left(\gamma_{-\alpha}(t)\right) \gamma'_{-\alpha}(t)dt, \tag{D.110}$$

where $\gamma_{-\alpha}(t) = -t - \alpha i$ and $t \in [-R, R]$.

Substituting the parametrisation into the equation (D.110) and performing the change of variable $z = -t - \alpha i$, we get:

$$\int_{-R}^{R} h\left(\gamma_{-\alpha}(t)\right) \gamma'_{-\alpha}(t)dt = \int_{-R}^{R} h(-t - \alpha i)(-1)dt = -\int_{-R-\alpha i}^{R-\alpha i} h(z)dz. \tag{D.111}$$

Similarly, evaluating the second integral along Γ_α, and denoting the curve parametrisation by $\gamma_\alpha(t)$, we can define the line integral as:

$$\int_{\Gamma_\alpha} h(z)dz = \int_{-R}^{R} h\left(\gamma_\alpha(t)\right) \gamma'_\alpha(t)dt, \tag{D.112}$$

where $\gamma_\alpha(t) = t + \alpha i$ and $t \in [-R, R]$.

Once again, substituting the parametrisation into the equation (D.112) and performing the change of variable $z = t + \alpha i$, we reach:

$$\int_{-R}^{R} h\left(\gamma_\alpha(t)\right) \gamma'_\alpha(t)dt = \int_{-R}^{R} h(t + \alpha i)(1)dt = \int_{-R+\alpha i}^{R+\alpha i} h(z)dz. \tag{D.113}$$

Regarding the integrals over Γ_R and Γ_{-R}, since they are both zero when $R \to \infty$, as proven in Case 2 of Corollary D.3, they can be excluded from the equation. As a result, (D.109) becomes:

$$f_t(-i) = -\int_{-R-\alpha i}^{R-\alpha i} h(z)dz + \int_{-R+\alpha i}^{R+\alpha i} h(z)dz. \tag{D.114}$$

Replacing $h(z)$ in the previous equation, rearranging the terms and letting $R \to +\infty$, yields:

$$\int_{-\infty+\alpha i}^{+\infty+\alpha i} \frac{1}{2\pi}\hat{\mathscr{C}}_G(z)e^{-ikz}dz = f_t(-i) + \int_{-\infty-\alpha i}^{+\infty-\alpha i} \frac{1}{2\pi}\hat{\mathscr{C}}_G(z)e^{-ikz}dz. \tag{D.115}$$

Knowing that the left-hand side corresponds to the call price as defined by equation (D.54), we are able to rewrite the expression in the following manner:

$$C_G(k) = f_t(-i) + \int_{-\infty-\alpha i}^{+\infty-\alpha i} \frac{1}{2\pi}\hat{\mathscr{C}}_G(z)e^{-ikz}dz. \tag{D.116}$$

Splitting the integral and performing a change of variables, such that $z = -u - \alpha i$ for the first integral, and $z = u - \alpha i$ for the second, we obtain:

$$C_G(k) = f_t(-i) + \frac{1}{2\pi}\left(\int_0^{+\infty} \hat{\mathscr{C}}_G(-u-\alpha i)e^{-ik(-u-\alpha i)}du + \int_0^{+\infty} \hat{\mathscr{C}}_G(u-\alpha i)e^{-ik(u-\alpha i)}du\right). \tag{D.117}$$

Now, applying the results of *Corollary D.2* to the first integral, specified in equation (D.36), which states that $\overline{\hat{\mathscr{C}}_G(u-\alpha i)} = \hat{\mathscr{C}}_G(-u-\alpha i)$, we have:

$$C_G(k) = f_t(-i) + \frac{1}{2\pi}\int_0^{+\infty} \left(\overline{\hat{\mathscr{C}}_G(u-\alpha i)e^{-ik(u-\alpha i)}} + \hat{\mathscr{C}}_G(u-\alpha i)e^{-ik(u-\alpha i)}\right)du. \tag{D.118}$$

Recognising that $z + \overline{z} = 2\mathrm{Re}(z)$, we arrive at:

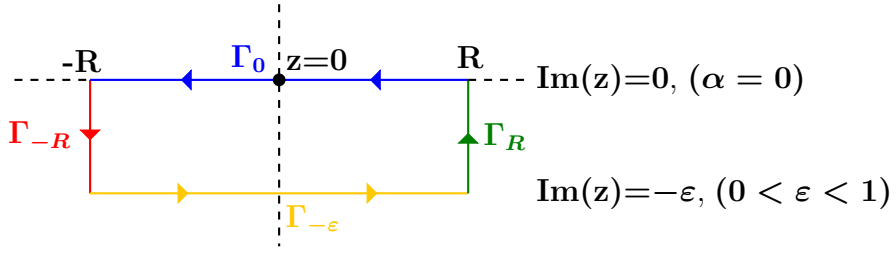
$$C_G(k) = f_t(-i) + \frac{1}{2\pi}\int_0^{+\infty} 2.\mathrm{Re}\left[e^{-ik(u-\alpha i)}\hat{\mathscr{C}}_G(u-\alpha i)\right]du. \tag{D.119}$$

Finally, making one final variable change by setting $z = u - \alpha i$, we reach the final formula for the *unmodified option price* in the case where $-1 < \alpha < 0$:

$$C_G(k) = f_t(-i) + \frac{1}{\pi}\int_{0-\alpha i}^{+\infty-\alpha i} \mathrm{Re}\left[e^{-ikz}\hat{\mathscr{C}}_G(z)\right]dz. \tag{D.120}$$

D.3.2.5 Case 3: pricing formula for $\alpha = 0$

Let us explore the case $\alpha = 0$. For that purpose, assume C remains a simple closed contour and consider a new function $g(z) = \frac{1}{2}\left(\hat{\mathscr{C}}_G(z)e^{-ikz} + \hat{\mathscr{C}}_G(-z)e^{ikz}\right)$, which is analytic in a neighbourhood of C, except for a singularity at $z = 0$ lying on the contour Γ_0. To properly define the contour integral, we introduce a regularised contour C_ε obtained by deforming Γ_0 in a neighbourhood of $z = 0$ with a semicircular indentation of radius $\varepsilon > 0$ in the lower half-plane. The integral along Γ_0 is defined via the regularised contour C_ε, which coincides with the Cauchy principal value.
Hence, the closed contour C can be illustrated by the following rectangle:



where:
$\Gamma_{-\varepsilon}= \{z \in \mathbb{C} : Im(z) = -\varepsilon,\, 0 < \varepsilon < 1 \wedge Re(z) \in [-R, R]\}$
$\Gamma_{R}= \{z \in \mathbb{C} : Re(z) = R \wedge Im(z) \in [-\varepsilon, 0],\, 0 < \varepsilon < 1\}$
$\Gamma_{0}= \{z \in \mathbb{C} : Im(z) = 0 \wedge Re(z) \in [-R, R]\}$, (Cauchy principal value)
$\Gamma_{-R}= \{z \in \mathbb{C} : Re(z) = -R \wedge Im(z) \in [-\varepsilon, 0],\, 0 < \varepsilon < 1\}$
$\mathrm{C} = \Gamma_{-\varepsilon} \cup \Gamma_{R} \cup \Gamma_{0} \cup \Gamma_{-R}$
As established, the line integral of the symmetric auxiliary function $g(z)$ along the closed contour C is given by the sum of its constituent segments:

$$\oint_C g(z)\,dz = \int_{\Gamma_0} g(z)dz + \int_{\Gamma_R} g(z)dz + \int_{\Gamma_{-\varepsilon}} g(z)dz + \int_{\Gamma_{-R}} g(z)dz. \tag{D.121}$$

In the present setting, the path Γ_0 lies on the real axis, where the function $g(z)$ is singular at $z = 0$. To evaluate an integral along a path intersecting such a singularity, we apply the residue theorem for poles on contours to the indented contour C_ε. This construction allows the contour integral to be decomposed into the Cauchy principal value along the real axis and the contribution of the semi-circular indentation Γ_ε around the origin:

$$\oint_{C_\varepsilon} g(z)dz = \mathrm{PV}\int_{-\infty}^{\infty} g(x)dx + \int_{\Gamma_\varepsilon} g(z)dz. \tag{D.122}$$

According to Theorem D.6, the value of the integral over the indented contour is determined by half the residue at the singularity, namely:

$$\oint_{C_\varepsilon} g(z)dz = \pi i\,\mathrm{Res}(g, 0). \tag{D.123}$$

To evaluate this expression, we compute the residue of the symmetric function $g(z)$ at the origin. Recalling the definition $g(z) = \frac{1}{2}\left[\hat{\mathscr{C}}_G(z)e^{-ikz} + \hat{\mathscr{C}}_G(-z)e^{ikz}\right]$, and utilising the residues of the base auxiliary function $h(z)$ from Lemma D.3, we obtain:

$$\mathrm{Res}(g, 0) = \frac{1}{2}\left[\mathrm{Res}\Big(\hat{\mathscr{C}}_G(z)e^{-ikz}, 0\Big) + \mathrm{Res}\Big(\hat{\mathscr{C}}_G(-z)e^{ikz}, 0\Big)\right]. \tag{D.124}$$

Using the identity $\hat{\mathscr{C}}_G(z)e^{-ikz} = 2\pi h(z)$ together with Lemma D.3, the residue of the first term at the origin is given by:

$$\mathrm{Res}\Big(\hat{\mathscr{C}}_G(z)e^{-ikz}, 0\Big) = -if_t(-i). \tag{D.125}$$

Applying the change of variable $z \mapsto -z$ to the second term yields:

$$\mathrm{Res}\Big(\hat{\mathscr{C}}_G(-z)e^{ikz}, 0\Big) = if_t(-i). \tag{D.126}$$

Consequently,

$$\mathrm{Res}(g, 0) = \frac{1}{2}\Big[-if_t(-i) + if_t(-i)\Big] = 0. \tag{D.127}$$

Since the residue of $g(z)$ at the origin vanishes, it follows from the residue theorem that the entire contour integral is null. Furthermore, the contribution of the indentation Γ_ε also vanishes as $\varepsilon \to 0$, since it is proportional to $\mathrm{Res}(g, 0)$. Consequently, the Cauchy principal value coincides with the standard integral, and the balance of the contour segments in

equation (D.121) reduces to:

$$0 = \int_{\Gamma_0} g(z)dz + \int_{\Gamma_{-\varepsilon}} g(z)dz. \tag{D.128}$$

Given that it has already been demonstrated in Case 3 of Corollary D.3 that the integrals $\int_{\Gamma_R}$ and $\int_{\Gamma_{-R}}$ tend to zero as R approaches $+\infty$, we can promptly rewrite equation (D.121) as follows, also incorporating the result from equation (D.122):

$$0 = \int_{\Gamma_0} g(z)dz + \int_{\Gamma_{-\varepsilon}} g(z)dz. \tag{D.129}$$

To calculate the remaining line integrals, we first need to parametrise the curves and perform the integration along each curve separately.

Starting with the integral along Γ_0, let's define its parametrisation by $\gamma_0(t) = -t + 0i$, where $t \in [-R, R]$, and represent the function as $g(\gamma_0(t))$. Applying this parametrisation to the line integral definition, and performing the change of variable $z = -t$, we reach:

$$\int_{\Gamma_0} g(z)dz = \int_{-R}^{R} g\left(\gamma_0(t)\right)\gamma_0'(t)dt = \int_{-R}^{R} g\left(-t\right)(-1)\,dt = -\int_{-R}^{R} g\left(z\right)dz. \tag{D.130}$$

Similarly, with regard to the second integral along $\Gamma_{-\varepsilon}$, let's define its parametrisation by $\gamma_{-\varepsilon}(t) = t - \varepsilon i$, also with $t \in [-R, R]$, and denote the corresponding function as $g(\gamma_{-\varepsilon}(t))$. Using this parametrisation and performing the change of variable $z = t - \varepsilon i$, the line integral can be expressed as:

$$\int_{\Gamma_{-\varepsilon}} g(z)dz = \int_{-R}^{R} g\left(\gamma_{-\varepsilon}(t)\right)\gamma_{-\varepsilon}'(t)dt = \int_{-R}^{R} g\left(t-\varepsilon i\right)(1)\,dt = \int_{-R-\varepsilon i}^{R-\varepsilon i} g\left(z\right)dz. \tag{D.131}$$

Substituting the previous results into equation (D.129) and rearranging the terms, we obtain:

$$\int_{-R}^{R} g\left(z\right)dz = \int_{-R-\varepsilon i}^{R-\varepsilon i} g\left(z\right)dz. \tag{D.132}$$

Now, let's take the limit as $R \to +\infty$ on both sides of the equation (D.132), and multiply each side by $\frac{1}{2\pi}$:

$$\frac{1}{2\pi}\lim_{R\to+\infty}\int_{-R}^{R} g\left(z\right)dz = \frac{1}{2\pi}\lim_{R\to+\infty}\int_{-R-\varepsilon i}^{R-\varepsilon i} g\left(z\right)dz. \tag{D.133}$$

Replacing $g(z)$ in the right-hand side of equation (D.133), and then performing the change of variable $-z = u$ to the second integral, yields:

$$\begin{aligned}\frac{1}{2\pi}\lim_{R\to+\infty}\int_{-R}^{R} g\left(z\right)dz &= \frac{1}{2\pi}\lim_{R\to+\infty}\int_{-R-\varepsilon i}^{R-\varepsilon i}\frac{1}{2}\left(\hat{\mathscr{C}_G}(z)e^{-ikz} + \hat{\mathscr{C}_G}(-z)e^{ikz}\right)dz \\ &= \frac{1}{2}\lim_{R\to+\infty}\left[\int_{-R-\varepsilon i}^{R-\varepsilon i}\frac{\hat{\mathscr{C}_G}(z)e^{-ikz}}{2\pi}dz + \int_{-R+\varepsilon i}^{R+\varepsilon i}\frac{\hat{\mathscr{C}_G}(u)e^{-iku}}{2\pi}du\right].\end{aligned} \tag{D.134}$$

Changing, once more, the variable of the second integral, such that $u = z$, as R tends to $+\infty$, results in:

$$\frac{1}{2\pi}\int_{-\infty}^{+\infty} g\left(z\right) dz = \frac{1}{2}\left[\int_{-\infty-\varepsilon i}^{+\infty-\varepsilon i} \frac{\hat{\mathscr{C}}_G(z)e^{-ikz}}{2\pi}dz + \int_{-\infty+\varepsilon i}^{+\infty+\varepsilon i} \frac{\hat{\mathscr{C}}_G(z)e^{-ikz}}{2\pi}dz\right], \tag{D.135}$$

with $0 < \varepsilon < 1$.

In relation to the right-hand side of equation (D.135), it is easy to note that the first integral corresponds to the case $\alpha > 0$, while the second integral, after the variable change, matches the case where $-1 < \alpha < 0$.

Substituting the integrals with the respective results derived from equations (D.96) and (D.120), and noting that $R_{-\varepsilon,G} = f_t(-i)$ for $-1 < -\varepsilon < 0$, equation (D.135) can be written as

$$\frac{1}{2\pi}\int_{-\infty}^{+\infty} g(z)\, dz = \frac{1}{2}\big(C_G(k) + C_G(k) - f_t(-i)\big) = C_G(k) - \frac{f_t(-i)}{2}. \tag{D.136}$$

Rearranging the terms and substituting, again, the function $g(z)$, now on the left-hand side of equation (D.136), as $R \to +\infty$, yields:

$$C_G(k) = \frac{f_t(-i)}{2} + \frac{1}{2\pi}\int_{-\infty}^{+\infty} \frac{1}{2}\left(\hat{\mathscr{C}}_G(z)e^{-ikz} + \hat{\mathscr{C}}_G(-z)e^{ikz}\right) dz. \tag{D.137}$$

For simplicity, let's now focus solely on the two integrals. That said, let's split them into two parts and adjust the integration domain for each of the resulting four integrals. As a result, we reach:

$$\int_{-\infty}^{0} \frac{\hat{\mathscr{C}}_G(z)e^{-ikz}}{2}dz + \int_{-\infty}^{0} \frac{\hat{\mathscr{C}}_G(-z)e^{ikz}}{2}dz + \int_{0}^{+\infty} \frac{\hat{\mathscr{C}}_G(z)e^{-ikz}}{2}dz + \int_{0}^{+\infty} \frac{\hat{\mathscr{C}}_G(-z)e^{ikz}}{2}dz.$$

Performing two changes of variables to the first two integrals, starting with $z = -u$ and then $u = z$, we arrive at:

$$\int_{0}^{+\infty} \frac{\hat{\mathscr{C}}_G(-z)e^{ikz}}{2}dz + \int_{0}^{+\infty} \frac{\hat{\mathscr{C}}_G(z)e^{-ikz}}{2}dz + \int_{0}^{+\infty} \frac{\hat{\mathscr{C}}_G(z)e^{-ikz}}{2}dz + \int_{0}^{+\infty} \frac{\hat{\mathscr{C}}_G(-z)e^{ikz}}{2}dz.$$

At last, aggregating the similar terms and plugging in the previous result into equation (D.137), leads to:

$$C_G(k) = \frac{f_t(-i)}{2} + \frac{1}{2\pi}\int_{0}^{+\infty} \left(\hat{\mathscr{C}}_G(-z)e^{ikz} + \hat{\mathscr{C}}_G(z)e^{-ikz}\right) dz. \tag{D.138}$$

Next, we apply the results of *Proposition* (D.4) to the first integral, as described in equation (D.30), which states that $\overline{\hat{c}_{\alpha,G}(u)} = \hat{c}_{\alpha,G}(-u)$, leading to:

$$C_G(k) = \frac{f_t(-i)}{2} + \frac{1}{2\pi}\int_{0}^{+\infty} \left(\overline{\hat{\mathscr{C}}_G(z)e^{-ikz}} + \hat{\mathscr{C}}_G(z)e^{-ikz}\right) dz. \tag{D.139}$$

Knowing that $z + \overline{z} = 2\mathrm{Re}(z)$, we can rewrite equation (D.139) as:

$$C_G(k) = \frac{f_t(-i)}{2} + \frac{1}{2\pi}\int_{0}^{+\infty} 2.\mathrm{Re}\left[e^{-ikz}\hat{\mathscr{C}}_G(z)\right] dz. \tag{D.140}$$

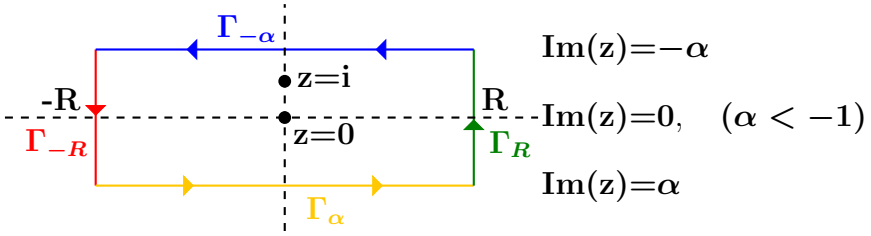
Thus, we finally reach the formula for the *unmodified option price* in the case $\alpha = 0$:

$$C_G(k) = \frac{f_t(-i)}{2} + \frac{1}{\pi}\int_0^{+\infty} \text{Re}\left[e^{-ikz}\hat{\mathscr{C}}_G(z)\right] dz. \tag{D.141}$$

D.3.2.6 Case 4: pricing formula for α <-1

Let's delve into the case $\alpha < -1$, maintaining the same conditions for C and $h(z)$ as before: C remains a simple closed contour and $h(z)$ is an analytic function within C, except for a finite set of isolated singularities. In the current scenario, both singularities $z = 0$ and $z = i$ are inside the contour.

The next rectangle exhibits the closed contour C:



where:

$\Gamma_\alpha = \{z \in \mathbb{C} : Im(z) = \alpha,\ \alpha < -1 \wedge Re(z) \in [-R, R]\}$

$\Gamma_R = \{z \in \mathbb{C} : Re(z) = R \wedge Im(z) \in [-\alpha, \alpha]\}$

$\Gamma_{-\alpha} = \{z \in \mathbb{C} : Im(z) = -\alpha,\ -\alpha > 1 \wedge Re(z) \in [-R, R]\}$

$\Gamma_{-R} = \{z \in \mathbb{C} : Re(z) = -R \wedge Im(z) \in [-\alpha, \alpha]\}$

$C = \Gamma_\alpha \cup \Gamma_R \cup \Gamma_{-\alpha} \cup \Gamma_{-R}$

This figure illustrates the integration contour for Case 4. Note that the condition $\alpha < -1$ implies that the upper segment $\Gamma_{-\alpha}$ lies above the line $\Im(z) = 1$, thereby enclosing the pole at $z = i$. The real axis $Im(z) = 0$ is shown solely for reference.

That said, the line integral of $h(z)$ along the closed contour C can be calculated by summing the integrals corresponding to the four sides of the rectangle:

$$\oint_C h(z)\, dz = \int_{\Gamma_{-\alpha}} h(z)dz + \int_{\Gamma_R} h(z)dz + \int_{\Gamma_\alpha} h(z)dz + \int_{\Gamma_{-R}} h(z)dz. \tag{D.142}$$

Using the *Cauchy's residue theorem*, we can obtain the contour integral by summing the residues associated with the poles inside C. Since, in this case, both $z = 0$ and $z = i$ are enclosed by the contour, we need to add the residues given by Lemma D.3 and Lemma D.4. As a result:

$$\oint_C h(z)\, dz = 2\pi i \sum_{k=1}^{n} \text{Res}(h, z_k) = 2\pi i \left(\frac{-i f_t(-i)}{2\pi} + \frac{i f_t(0) e^k}{2\pi}\right) = f_t(-i) - e^k f_t(0). \tag{D.143}$$

Since it has already been proven in Case 4 of Corollary D.3 that the integrals $\int_{\Gamma_R}$ and $\int_{\Gamma_{-R}}$ tend to zero as $R \to +\infty$, we can promptly rewrite equation (D.142) discarding these integrals, and incorporating the result from equation (D.143), as follows:

$$f_t(-i) - e^k f_t(0) = \int_{\Gamma_{-\alpha}} h(z)dz + \int_{\Gamma_\alpha} h(z)dz. \tag{D.144}$$

To compute the remaining line integrals, again, we will need to parametrise the curves and then perform the integration along each curve separately.
Let's then start by evaluating the first integral along the curve $\Gamma_{-\alpha}$, defining its parametrization by $\gamma_1(t) = -t - \alpha i$, where $t, \in, [-R, R]$, and denoting the function as $h(\gamma_1(t))$. Applying this parametrisation to the line integral definition, and performing the change of variable $u = -t$, we reach:

$$\int_{\Gamma_{-\alpha}} h(z)dz = \int_{-R}^{R} h\left(\gamma_1(t)\right)\gamma_1'(t)dt = \int_{-R}^{R} h\left(-t-\alpha i\right)(-1)\,dt = -\int_{-R}^{R} h\left(u-\alpha i\right)du. \tag{D.145}$$

Moving on to the second integral along Γ_α, let's define its parametrisation by $\gamma_2(t) = t+\alpha i$, also with $t \in [-R, R]$, and denote the corresponding function as $g(\gamma_2(t))$. Using this parametrisation and performing the change of variable $u = t$, the line integral can be expressed as:

$$\int_{\Gamma_{\alpha}} h(z)dz = \int_{-R}^{R} h\left(\gamma_2(t)\right)\gamma_2'(t)dt = \int_{-R}^{R} h\left(t+\alpha i\right)(1)\,dt = \int_{-R}^{R} h\left(u+\alpha i\right)du. \tag{D.146}$$

Plugging in the previous results into equation (D.144) and rearranging the terms, we obtain:

$$\int_{-R}^{R} h\left(u+\alpha i\right)du = f_t(-i) - e^k f_t(0) + \int_{-R}^{R} h\left(u-\alpha i\right)du. \tag{D.147}$$

Taking the limit as $R \to +\infty$ on both sides of the equation (D.147), and performing the change of variable $z = u + \alpha i$ on the left-hand side integral, we have:

$$\lim_{R\to+\infty}\int_{-R+\alpha i}^{R+\alpha i} h\left(z\right)dz = f_t(-i) - e^k f_t(0) + \lim_{R\to+\infty}\int_{-R}^{R} h\left(u-\alpha i\right)du. \tag{D.148}$$

Replacing $h(z)$ in equation (D.148), and substituting R with $+\infty$, results in:

$$\int_{-\infty+\alpha i}^{+\infty+\alpha i} \frac{1}{2\pi}\hat{\mathscr{C}_G}(z)e^{-ikz}dz = f_t(-i) - e^k f_t(0) + \int_{-\infty}^{+\infty} \frac{\hat{\mathscr{C}_G}\left(u-\alpha i\right)e^{-ik(u-\alpha i)}}{2\pi}du. \tag{D.149}$$

Knowing that the left-hand side corresponds to the call price given by equation (D.54), we are able to rewrite the previous expression in the following manner:

$$C_G(k) = f_t(-i) - e^k f_t(0) + \int_{-\infty}^{+\infty} \frac{\hat{\mathscr{C}_G}\left(u-\alpha i\right)e^{-ik(u-\alpha i)}}{2\pi}du. \tag{D.150}$$

For simplicity, let's now focus solely on the integral, dividing it into two parts and performing two changes of variables to the first integral. Starting with $u = -z$ and then substituting z with u, we arrive at:

$$\int_{0}^{+\infty} \frac{\hat{\mathscr{C}_G}\left(-u-\alpha i\right)e^{-ik(-u-\alpha i)}}{2\pi}du + \int_{0}^{+\infty} \frac{\hat{\mathscr{C}_G}\left(u-\alpha i\right)e^{-ik(u-\alpha i)}}{2\pi}du. \tag{D.151}$$

Now, applying the results of *Corollary D.2* to the first integral, specified in equation (D.36), which states that $\overline{\hat{\mathscr{C}_G}(u-\alpha i)} = \hat{\mathscr{C}_G}(-u-\alpha i)$, we have:

$$\frac{1}{2\pi}\int_{0}^{+\infty} \left(\overline{\hat{\mathscr{C}_G}\left(u-\alpha i\right)e^{-ik(u-\alpha i)}} + \hat{\mathscr{C}_G}\left(u-\alpha i\right)e^{-ik(u-\alpha i)}\right)du. \tag{D.152}$$

Incorporating the previous results into equation (D.150), and recognising that $z + \overline{z} = 2\mathrm{Re}(z)$, leads to:

$$C_G(k) = f_t(-i) - e^k f_t(0) + \frac{1}{2\pi} \int_0^{+\infty} 2\mathrm{Re}\left[e^{-ik(u-\alpha i)} \hat{\mathscr{C}}_G(u - \alpha i)\right] du. \tag{D.153}$$

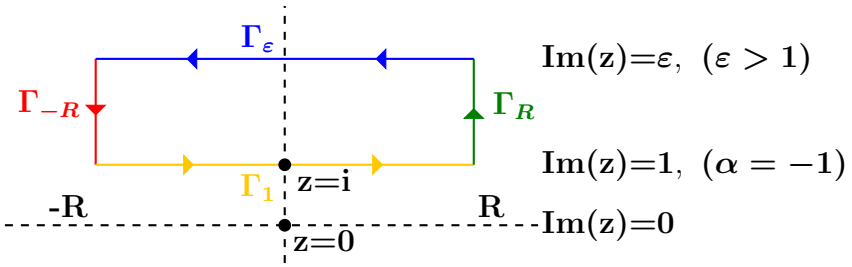
Finally, making one final variable change by setting $z = u - \alpha i$, we reach the final formula for the *unmodified option price* in the case where $\alpha < -1$:

$$C_G(k) = \frac{1}{\pi} \int_{0-\alpha i}^{+\infty-\alpha i} \mathrm{Re}\left[e^{-ikz} \hat{\mathscr{C}}_G(z)\right] dz + f_t(-i) - e^k f_t(0). \tag{D.154}$$

D.3.2.7 Case 5: pricing formula for α =-1

Let us now contemplate the case $\alpha = -1$. In this scenario, the symmetric auxiliary function $g(z)$ is integrated along the line $\Gamma_1 = \{z \in \mathbb{C} : \mathrm{Im}(z) = 1\}$. Since this integration path passes through the simple pole of $g(z)$ at $z = i$, and absolute convergence fails for $\alpha = -1$ due to the critical decay of $g(z)$ at infinity, the integral along Γ_1 is interpreted in the symmetric Cauchy principal value sense. More precisely, all integrals in this case are understood in the sense of a Cauchy principal value, defined via symmetric truncation in the real direction, $\mathrm{PV}\int_{\Gamma_1} g(z)\, dz := \lim_{R\to\infty} \int_{-R+i}^{R+i} g(z)\, dz$. Equivalently, we introduce a regularised contour C_ε obtained by locally deforming Γ_1 in a neighbourhood of $z = i$ by a small semicircular indentation of radius $\varepsilon > 0$.

We then consider a closed rectangular contour C bounded by Γ_1 and Γ_ε, with $\varepsilon > 1$, together with the vertical segments $\Gamma_{\pm R}$, such that the function $g(z)$ is holomorphic in the interior of C.



where:

$\Gamma_1 = \{z \in \mathbb{C} : Im(z) = 1 \wedge Re(z) \in [-R, R]\}$

$\Gamma_R = \{z \in \mathbb{C} : Re(z) = R \wedge Im(z) \in [1, \varepsilon], \varepsilon > 1\}$

$\Gamma_\varepsilon = \{z \in \mathbb{C} : Im(z) = \varepsilon, \varepsilon > 1 \wedge Re(z) \in [-R, R]\}$

$\Gamma_{-R} = \{z \in \mathbb{C} : Re(z) = -R \wedge Im(z) \in [1, \varepsilon], \varepsilon > 1\}$

$C = \Gamma_1 \cup \Gamma_R \cup \Gamma_\varepsilon \cup \Gamma_{-R}$

As before, we can obtain the line integral of $g(z)$ along the closed contour C by adding the integrals representing the four sides of the rectangle:

$$\oint_C g(z)\, dz = \int_{\Gamma_1} g(z)\, dz + \int_{\Gamma_R} g(z)\, dz + \int_{\Gamma_\varepsilon} g(z)\, dz + \int_{\Gamma_{-R}} g(z)\, dz. \tag{D.155}$$

According to the residue theorem for poles on the contour (see Theorem D.6), the contour integral over a regularised path may be written as:

$$\oint_{C_\varepsilon} g(z)\,dz = 2\pi i \sum_{z_k \in \mathrm{int}(C)} \mathrm{Res}(g, z_k) + \pi i \sum_{z_k \in C} \mathrm{Res}(g, z_k). \tag{D.156}$$

In the present case, the regularised contour encloses no poles in its interior. The only singularity of $g(z)$ relevant to the contour integral is the simple pole at $z = i$, which lies on the contour itself. Formally, equation (D.156) therefore reduces to:

$$\oint_{C_\varepsilon} g(z)\,dz = \pi i\ \mathrm{Res}(g, i). \tag{D.157}$$

As in Case 3, however, the integral is understood in the Cauchy principal value sense and evaluated via a symmetric regularisation of the contour. Although the function $g(z)$ possesses a simple pole on the integration path, the contribution arising from the semicircular indentation around $z = i$ is exactly cancelled by the symmetric displacement of the horizontal contour segments. Consequently, the pole does not contribute to the contour integral, and one obtains:

$$\oint_{C_\varepsilon} g(z)\,dz = 0. \tag{D.158}$$

Given that it has already been shown in Case 5 of Corollary D.3 that the integrals $\int_{\Gamma_R} g(z)\,dz$ and $\int_{\Gamma_{-R}} g(z)\,dz$ tend to zero as R approaches $+\infty$, we can immediately discard them from equation (D.155). Therefore, we can reformulate (D.155) as follows, also incorporating the results from equation (D.158):

$$0 = \int_{\Gamma_1} g(z)dz + \int_{\Gamma_\varepsilon} g(z)dz. \tag{D.159}$$

To calculate the remaining line integrals, we first need to parametrise the curves and perform the integration along each curve separately.

Beginning with the integral along Γ_1, let's define its parametrisation by $\gamma_1(t) = t+i$, where $t \in [-R, R]$, and represent the respective function as $g(\gamma_1(t))$. Applying this parametrisation to the line integral definition and performing the change of variable $z = t + i$, we reach:

$$\int_{\Gamma_1} g(z)dz = \int_{-R}^{R} g\left(\gamma_1(t)\right)\gamma_1'(t)dt = \int_{-R}^{R} g\left(t + \varepsilon i\right)(1)\,dt = \int_{-R+i}^{R+i} g\left(z\right)dz. \tag{D.160}$$

Similarly, with regard to the second integral along Γ_ε, let's define its parametrisation by $\gamma_\varepsilon(t) = -t + \varepsilon i$, where $t \in [-R, R]$ and $\varepsilon > 0$, and denote the corresponding function as $g(\gamma_\varepsilon(t))$. Using this parametrisation and performing a change of variable, setting $z = -t + \varepsilon i$, we arrive at:

$$\int_{\Gamma_\varepsilon} g(z)dz = \int_{-R}^{R} g\left(\gamma_\varepsilon(t)\right)\gamma_\varepsilon'(t)dt = \int_{-R}^{R} g\left(-t + \varepsilon i\right)(-1)dt = -\int_{-R+\varepsilon i}^{R+\varepsilon i} g\left(z\right)dz. \tag{D.161}$$

Substituting the previous results into equation (D.159) and rearranging the terms, we obtain:

$$\int_{-R+i}^{R+i} g\left(z\right) dz = \int_{-R+\varepsilon i}^{R+\varepsilon i} g\left(z\right) dz. \tag{D.162}$$

Now, let's take the limit as $R \to +\infty$ on both sides of the equation (D.162), and multiply each side by $\frac{1}{2\pi}$:

$$\frac{1}{2\pi} \lim_{R\to+\infty} \int_{-R+i}^{R+i} g\left(z\right) dz = \frac{1}{2\pi} \lim_{R\to+\infty} \int_{-R+\varepsilon i}^{R+\varepsilon i} g\left(z\right) dz. \tag{D.163}$$

Replacing $g(z)$ on the right-hand side of the previous equation (D.163), and then performing the change of variable $-z = u$ to the second integral, yields:

$$\begin{aligned} \frac{1}{2\pi} \lim_{R\to+\infty} \int_{-R+i}^{R+i} g\left(z\right) dz &= \frac{1}{2\pi} \lim_{R\to+\infty} \int_{-R+\varepsilon i}^{R+\varepsilon i} \frac{1}{2} \left(\hat{\mathscr{C}}_G(z) e^{-ikz} + \hat{\mathscr{C}}_G(-z) e^{ikz}\right) dz \\ &= \frac{1}{2} \lim_{R\to+\infty} \left[\int_{-R+\varepsilon i}^{R+\varepsilon i} \frac{\hat{\mathscr{C}}_G(z) e^{-ikz}}{2\pi} dz + \int_{-R-\varepsilon i}^{R-\varepsilon i} \frac{\hat{\mathscr{C}}_G(u) e^{-iku}}{2\pi} du \right]. \end{aligned} \tag{D.164}$$

Changing, once more, the variable of the second integral, such that $u = z$, as R tends to $+\infty$, results in:

$$\frac{1}{2\pi} \int_{-\infty+i}^{+\infty+i} g\left(z\right) dz = \frac{1}{2} \left[\int_{-\infty+\varepsilon i}^{+\infty+\varepsilon i} \frac{\hat{\mathscr{C}}_G(z) e^{-ikz}}{2\pi} dz + \int_{-\infty-\varepsilon i}^{+\infty-\varepsilon i} \frac{\hat{\mathscr{C}}_G(z) e^{-ikz}}{2\pi} dz \right], \tag{D.165}$$

where $\varepsilon > 1$ in both integrals.

Regarding the right-hand side of equation (D.165), as in *Case 3*, note that the first integral coincides with the representation obtained in *Case 4* ($\alpha < -1$) and therefore yields the same correction term $f_t(-i) - e^k f_t(0)$ by analytic continuation. The second integral matches *Case 1* ($\alpha > 0$) and does not generate any additional contribution.

Substituting the integrals with the respective results derived from equations (D.96) and (D.154), we can rewrite equation (D.165) as follows:

$$\frac{1}{2\pi} \int_{-\infty+i}^{+\infty+i} g\left(z\right) dz = \frac{1}{2} \left(\left(C_G(k) - R_{\varepsilon,G}\right) + C_G(k) \right), \tag{D.166}$$

where $C_G(k)$ represents the call option price, incorporating the correction term $R_{\varepsilon,G}$ inherited from the $\alpha < -1$ case.

As in the case $\alpha < -1$, the correction term $R_{\varepsilon,G}$ is given by $f_t(-i) - e^k f_t(0)$, yielding:

$$\frac{1}{2\pi} \int_{-\infty+i}^{+\infty+i} g\left(z\right) dz = \frac{1}{2} \big(C_G(k) + C_G(k) - f_t(-i) + e^k f_t(0)\big) = C_G(k) - \frac{f_t(-i) - e^k f_t(0)}{2}. \tag{D.167}$$

Rearranging the terms and substituting, again, the function $g(z)$, now on the left-hand side of equation (D.167), as $R \to +\infty$, we get:

$$C_G(k) = \frac{f_t(-i) - e^k f_t(0)}{2} + \frac{1}{2\pi} \int_{-\infty+i}^{+\infty+i} \frac{1}{2} \left(\hat{\mathscr{C}}_G(z) e^{-ikz} + \hat{\mathscr{C}}_G(-z) e^{ikz}\right) dz. \tag{D.168}$$

For simplicity, let's focus solely on the two integrals. That said, let's split them into two parts and adjust the integration domain for each of the resulting four integrals. As a result, we reach:

$$\int_{-\infty+i}^{0+i} \frac{\hat{\mathscr{C}}_G(z)e^{-ikz}}{2}dz + \int_{-\infty+i}^{0+i} \frac{\hat{\mathscr{C}}_G(-z)e^{ikz}}{2}dz + \int_{0+i}^{+\infty+i} \frac{\hat{\mathscr{C}}_G(z)e^{-ikz}}{2}dz + \int_{0+i}^{+\infty+i} \frac{\hat{\mathscr{C}}_G(-z)e^{ikz}}{2}dz.$$

Performing two changes of variables to the first two integrals, starting with $z = -u$ and then $u = z$, we arrive at:

$$\int_{0-i}^{+\infty-i} \frac{\hat{\mathscr{C}}_G(-z)e^{ikz}}{2}dz + \int_{0-i}^{+\infty-i} \frac{\hat{\mathscr{C}}_G(z)e^{-ikz}}{2}dz + \int_{0+i}^{+\infty+i} \frac{\hat{\mathscr{C}}_G(z)e^{-ikz}}{2}dz + \int_{0+i}^{+\infty+i} \frac{\hat{\mathscr{C}}_G(-z)e^{ikz}}{2}dz.$$

Next, applying the results of *Proposition* (D.4) to the first and fourth integrals, as described in equation (D.30), which states that $\overline{\hat{c}_{\alpha,G}(u)} = \hat{c}_{\alpha,G}(-u)$, leads to:

$$\int_{0-i}^{+\infty-i} \frac{\overline{\hat{\mathscr{C}}_G(z)e^{-ikz}}}{2}dz + \int_{0-i}^{+\infty-i} \frac{\hat{\mathscr{C}}_G(z)e^{-ikz}}{2}dz + \int_{0+i}^{+\infty+i} \frac{\hat{\mathscr{C}}_G(z)e^{-ikz}}{2}dz + \int_{0+i}^{+\infty+i} \frac{\overline{\hat{\mathscr{C}}_G(z)e^{-ikz}}}{2}dz.$$

Given that $z + \overline{z} = 2\mathrm{Re}(z)$, we can rewrite the previous expression as:

$$\int_{0-i}^{+\infty-i} \mathrm{Re}\left[e^{-ikz}\hat{\mathscr{C}}_G(z)\right]dz + \int_{0+i}^{+\infty+i} \mathrm{Re}\left[e^{-ikz}\hat{\mathscr{C}}_G(z)\right]dz. \tag{D.169}$$

Plugging in the previous result into equation (D.168), leads to:

$$C_G(k) = \frac{f_t(-i) - e^k f_t(0)}{2} + \frac{1}{2\pi}\left[\int_{0-i}^{+\infty-i} \mathrm{Re}\left[e^{-ikz}\hat{\mathscr{C}}_G(z)\right]dz + \int_{0+i}^{+\infty+i} \mathrm{Re}\left[e^{-ikz}\hat{\mathscr{C}}_G(z)\right]dz\right]. \tag{D.170}$$

To evaluate the first integral in equation (D.170), we shift the integration contour from $\mathrm{Im}(z) = -1$ to $\mathrm{Im}(z) = 1$. The pole at $z = i$ lies on the final line $\mathrm{Im}(z) = 1$ and is not crossed. Interpreted as an endpoint in the principal-value (indentation) sense, it contributes no additional term. By contrast, the shift crosses the pole at $z = 0$ (located at $\mathrm{Im}(z) = 0$), which lies between the two contours. To determine the contribution from this crossing, we first compute the residue of the integrand $e^{-ikz}\hat{\mathscr{C}}_G(z)$ at $z = 0$. Since $e^{-ikz}\hat{\mathscr{C}}_G(z) = 2\pi\, h(z)$ and using Lemma D.4, we obtain:

$$\mathrm{Res}\big(e^{-ikz}\hat{\mathscr{C}}_G, 0\big) = 2\pi\,\mathrm{Res}(h, 0) = 2\pi\frac{-i\, f_t(-i)}{2\pi} = -i\, f_t(-i). \tag{D.171}$$

By Corollary D.4, a transverse crossing contributes $i\pi$ times the residue at the crossing point. Therefore:

$$i\pi\,\mathrm{Res}\big(e^{-ikz}\hat{\mathscr{C}}_G, 0\big) = i\pi\big(-i\, f_t(-i)\big) = \pi\, f_t(-i). \tag{D.172}$$

As a result, the shift yields:

$$\int_{0-i}^{+\infty-i} \mathrm{Re}\Big[e^{-ikz}\hat{\mathscr{C}}_G(z)\Big]dz = \int_{0+i}^{+\infty+i} \mathrm{Re}\Big[e^{-ikz}\hat{\mathscr{C}}_G(z)\Big]dz + \pi\, f_t(-i). \tag{D.173}$$

Substituting equation (D.173) into equation (D.170), yields:

$$C_G(k) = \frac{f_t(-i) - e^k f_t(0)}{2} + \frac{1}{2\pi}\left[\int_{0+i}^{+\infty+i} \mathrm{Re}\Big[e^{-ikz}\hat{\mathscr{C}}_G(z)\Big]\, dz + \pi\, f_t(-i) + \int_{0+i}^{+\infty+i} \mathrm{Re}\Big[e^{-ikz}\hat{\mathscr{C}}_G(z)\Big]\, dz\right]. \tag{D.174}$$

Aggregating the similar terms, equation (D.174) becomes:

$$C_G(k) = \frac{1}{2\pi}\int_{0+i}^{+\infty+i} 2\,\mathrm{Re}\Big[e^{-ikz}\hat{\mathscr{C}}_G(z)\Big]\, dz + \frac{f_t(-i) - e^k f_t(0)}{2} + \frac{f_t(-i)}{2}. \tag{D.175}$$

Thus, simplifying equation (D.175), we finally reach:

$$C_G(k) = \frac{1}{\pi}\int_{0+i}^{+\infty+i} \mathrm{Re}\Big[e^{-ikz}\hat{\mathscr{C}}_G(z)\Big]\, dz + f_t(-i) - \frac{e^k f_t(0)}{2}. \tag{D.176}$$

APPENDIX E

Jump-diffusion models

E.1. Theorems, definitions and propositions

Definition E.1 (*Relationship between the Characteristic Function and the Moment Generating Function*). *Let Y be a random variable with distribution function $F_Y(y)$, characteristic function $\phi_Y(u)$, and moment generating function (MGF) $M_Y(t)$. The relationship between the characteristic function and the moment generating function is given by:*

$$\phi_Y(u) = \mathbb{E}[e^{iuY}], \tag{E.1}$$

and

$$M_Y(t) = \mathbb{E}[e^{tY}], \tag{E.2}$$

where $\mathbb{E}$ denotes the expected value. For real values of t and u, the characteristic function $\phi_Y(u)$ is related to the moment generating function $M_Y(t)$ by the following:

$$\phi_Y(u) = M_Y(iu). \tag{E.3}$$

This shows that the characteristic function $\phi_Y(u)$ can be obtained by evaluating the moment generating function $M_Y(t)$ at $t = iu$.

E.2. Additional results and proofs

Proposition E.1 (*Relationship between the Parameter μ_J and the Characteristic Function $\phi_Y(u)$*). *Let Y be a random variable with characteristic function $\phi_Y(u) = \mathbb{E}[e^{iuY}]$ and parameter μ_J defined as $\mu_J = \mathbb{E}[e^Y - 1]$. The relationship between μ_J and $\phi_Y(u)$ evaluated at $u = -i$ is given by:*

$$\mu_J = \phi_Y(-i) - 1, \tag{E.4}$$

where $\phi_Y(-i) = \mathbb{E}[e^Y]$.

Proof: The parameter μ_J can be rewritten as:

$$\mu_J = \mathbb{E}[e^Y] - 1. \tag{E.5}$$

The characteristic function $\phi_Y(u)$ is defined as:

$$\phi_Y(u) = \mathbb{E}[e^{iuY}]. \tag{E.6}$$

When evaluated at $u = -i$, it becomes:

$$\phi_Y(-i) = \mathbb{E}[e^{-i(-i)Y}] = \mathbb{E}[e^Y]. \tag{E.7}$$

Thus, we obtain:

$$\mu_J = \phi_Y(-i) - 1. \tag{E.8}$$

This concludes the relationship between the parameter μ_J and the characteristic function $\phi_Y(u)$ evaluated at $u = -i$. □

Proposition E.2 (*Relationship between jump transform and the characteristic function $\phi_Y(u)$*). *Let Y be a random variable representing the jump size with characteristic function $\phi_Y(u) = \mathbb{E}[e^{iuY}]$ and its associated jump transform represented by $\theta(c,t) = \int_{\mathbb{R}} e^{cy} d(\nu_t(y))$. Then:*

$$\theta(c,t) = \phi_Y(-ci). \tag{E.9}$$

Proof: By definition of characteristic function, we have:

$$\phi_Y(u) = \mathbb{E}[e^{iuY}] = \int_{\mathbb{R}} e^{iuy} f(dy). \tag{E.10}$$

If $u = -ci$ and representing the density f by $\eta_t(y)$ we obtain for every $c \in \mathbb{C}$

$$\begin{aligned} \phi_Y(-ci) &= \int_{\mathbb{R}} e^{i(-ci)y} \eta_t(dy) \\ &= \int_{\mathbb{R}} e^{cy} d(\eta_t(y)), \end{aligned} \tag{E.11}$$

which by definition is the jump transform defined in (3.4), proving (E.9). □

Proposition E.3 (*Relationship between the Parameter μ_J and the jump transform $\theta(c,t)$*). *Let Y be a random variable representing the jump size distribution and the mean percentage jump size μ_J defined as $\mu_J = \mathbb{E}[e^Y - 1]$. The relationship between μ_J and the jump transform $\theta(c,t) = \int_{\mathbb{R}} e^{cz} d(\nu_t(z))$ is given by:*

$$\mu_J = \theta(1,t) - 1. \tag{E.12}$$

Proof: Using the relation in Proposition E.2 with $c = 1$, we obtain $\theta(1,t) = \phi_Y(-i)$. Knowing the identity (E.4) we have $\mu_j = \phi_Y(-i) - 1 = \theta(1,t) - 1$, which proves (E.12). □

E.3. Chapter 5 jump-diffusion models proofs

E.3.1. Merton (1973) jump-diffusion model

Proposition E.4. *In Merton's model, the characteristic function of the jump size distribution Y takes the form:*

$$\phi_Y(u) = \exp\left(imu - \tfrac{1}{2}\delta^2 u^2\right). \tag{E.13}$$

Proof: Since the jump size distribution Y follows a Normal distribution with $Y \sim \mathcal{N}(m, \delta^2)$, we compute:

$$\phi_Y(u) = \mathbb{E}\left[e^{iuY}\right] = \frac{1}{\sqrt{2\pi\delta^2}} \int_{-\infty}^{+\infty} \exp\left(iuy - \frac{(y-m)^2}{2\delta^2}\right) dy. \tag{E.14}$$

We now complete the square in the exponent. Expanding and regrouping, we get:

$$\begin{aligned} iuy - \frac{(y-m)^2}{2\delta^2} &= iuy - \frac{y^2 - 2my + m^2}{2\delta^2} \\ &= -\frac{1}{2\delta^2}\left[y^2 - 2(m + iu\delta^2)y + m^2\right] \\ &= -\frac{1}{2\delta^2}\Big(y - (m + iu\delta^2)\Big)^2 + imu - \frac{1}{2}\delta^2 u^2. \end{aligned} \tag{E.15}$$

Substituting equation (E.15) into equation (E.14) factors the integrand:

$$\phi_Y(u) = e^{\,imu - \frac{1}{2}\delta^2 u^2}\ \frac{1}{\sqrt{2\pi\delta^2}} \int_{-\infty}^{+\infty} \exp\left(-\frac{(y - (m + iu\delta^2))^2}{2\delta^2}\right) dy. \tag{E.16}$$

Performing the change of variables $z = \frac{y-(m+iu\delta^2)}{\delta}$, (so that $dy = \delta\, dz$), the remaining integral is the standard Gaussian integral, $\frac{1}{\sqrt{2\pi}} \int_{\mathbb{R}} e^{-\frac{1}{2}z^2} dz$ which evaluates to one, yielding:

$$\phi_Y(u) = \exp\big(imu - \tfrac{1}{2}\delta^2 u^2\big)\,, \tag{E.17}$$

which proves (E.13). □

Corollary E.1 (*Mean percentage jump size μ_J in Merton (1976) model*). *Using the characteristic function derived in Proposition E.4 with Proposition E.1, and evaluating at $u = -i$, yields:*

$$\mu_J = \phi_Y(-i) - 1 = e^{\,m + \frac{1}{2}\delta^2} - 1. \tag{E.18}$$

Remark E.1. *Note that μ_J can also be obtained using the relation in Proposition E.3, from which $\mu_J = \theta(1,t) - 1 = e^{m+\frac{1}{2}\delta} - 1$ follows immediately.*

E.3.2. Kou's model

Proposition E.5. *The characteristic function of the jump size distribution Y in Kou (2002) model is given by:*

$$\phi_Y(u) = \frac{p_2\eta_2}{iu + \eta_2} - \frac{p_1\eta_1}{iu - \eta_1}. \tag{E.19}$$

Proof: Using previous relation the characteristic

$$\phi_Y(u) = \mathbb{E}_{\mathbb{Q}^T}\left[e^{iuY}\right] = \int_{-\infty}^{+\infty} e^{iuy}\Big(p_1\eta_1 e^{-\eta_1 y}\mathbb{1}_{\{y\geq 0\}} + p_2\eta_2 e^{\eta_2 y}\mathbb{1}_{\{y<0\}}\Big)\, dy. \tag{E.20}$$

Evaluating the integrals, we obtain:

$$\begin{aligned} \phi_Y(u) &= p_2\eta_2 \int_{-\infty}^{0} e^{(iu+\eta_2)y} dy + p_1\eta_1 \int_{0}^{+\infty} e^{(iu-\eta_1)y} dy \\ &= p_2\eta_2 \left[\frac{e^{(iu+\eta_2)y}}{iu + \eta_2}\right]_{-\infty}^{0} + p_1\eta_1 \left[\frac{e^{(iu-\eta_1)y}}{iu - \eta_1}\right]_{0}^{+\infty} \\ &= \frac{p_2\eta_2}{iu + \eta_2} - \frac{p_1\eta_1}{iu - \eta_1}. \end{aligned} \tag{E.21}$$

□

Corollary E.2 (*Mean percentage jump size* μ_J *in Kou (2002) model*). *Using the characteristic function derived in Proposition E.5 with Proposition E.1, and evaluating at* $u = -i$*, we get:*

$$\mu_J = \phi_Y(-i) - 1 = \frac{p_2\eta_2}{1+\eta_2} - \frac{p_1\eta_1}{1-\eta_1} - 1. \tag{E.22}$$

Remark E.2. *Note that* μ_J *can also be obtained using the relation in Proposition E.3, from which* $\mu_J = \theta(1,t) - 1 = \frac{p_2\eta_2}{1+\eta_2} - \frac{p_1\eta_1}{1-\eta_1} - 1$ *follows immediately.*

E.3.3. Bakshi, Cao and Chen (1997) model

E.3.3.1 Bakshi's as a particular case of Duffie's Model

In this affine structure, the vector X_t is a 3-dimensional vector defined as:

$$X_t = [ln(S_t), V_t, R_t], \tag{E.23}$$

where the natural logarithm of the asset price is the first element of the state vector, and $Y_t = [V_t, R_t]$ represents the vector of additional state variables for some admissible state space $D_y \subset \mathbb{R}^2$. With this setting, we can write Bakshi's model in matrix form, as follows:

$$\begin{bmatrix} dln(S_t) \\ dV_t \\ dR_t \end{bmatrix} = \begin{bmatrix} (R_t - q - \lambda\mu_J - \frac{1}{2}V_t)dt + \sqrt{V_t}dW_t^{S,\mathbb{Q}} + \int_{\mathbb{R}} xN_X(dt,dx) \\ (\theta_v - \kappa_v V_t)dt + \sigma_v\sqrt{V_t}dW_t^{v,\mathbb{Q}} \\ (\theta_r - \kappa_r R_t)dt + \sigma_r\sqrt{R_t}dW_t^{r,\mathbb{Q}} \end{bmatrix}, \tag{E.24}$$

and identify $\mu(t, X_t), \sigma(t, X_t)$ and dZ_t as in (3.3). Equivalently, we have:

$$\begin{bmatrix} dln(S_t) \\ dV_t \\ dR_t \end{bmatrix} = \begin{bmatrix} R_t - q - \lambda\mu_J - \frac{1}{2}V_t \\ \theta_v - \kappa_v V_t \\ \theta_r - \kappa_r R_t \end{bmatrix} dt + \begin{bmatrix} \sqrt{V_t}dW_t^{S,\mathbb{Q}} \\ \sigma_v\sqrt{V_t}dW_t^{v,\mathbb{Q}} \\ \sigma_r\sqrt{R_t}dW_t^{r,\mathbb{Q}} \end{bmatrix} + \begin{bmatrix} \int_{\mathbb{R}} xN_X(dt,dx) \\ 0 \\ 0 \end{bmatrix}. \tag{E.25}$$

Representing the correlated Brownian motions in terms of the standard uncorrelated Brownian motion as:

$$\begin{aligned} W_t^{S,\mathbb{Q}} &= \sqrt{1-\rho^2}\overline{W}_t^{S,\mathbb{Q}} + \rho\overline{W}_t^{v,\mathbb{Q}} \\ W_t^{v,\mathbb{Q}} &= \overline{W}_t^{v,\mathbb{Q}} \\ W_t^{r,\mathbb{Q}} &= \overline{W}_t^{r,\mathbb{Q}}, \end{aligned} \tag{E.26}$$

we obtain the system of SDE's also in terms of the uncorrelated Brownian motion:

$$\begin{bmatrix} dln(S_t) \\ dV_t \\ dR_t \end{bmatrix} = \begin{bmatrix} R_t - q - \lambda\mu_J - \frac{1}{2}V_t \\ \theta_v - \kappa_v V_t \\ \theta_r - \kappa_r R_t \end{bmatrix} dt + \begin{bmatrix} \sqrt{V_t}(\sqrt{1-\rho^2}\overline{W}_t^{S,\mathbb{Q}} + \rho\overline{W}_t^{v,\mathbb{Q}}) \\ \sigma_v\sqrt{V_t}d\overline{W}_t^{v,\mathbb{Q}} \\ \sigma_r\sqrt{R_t}d\overline{W}_t^{r,\mathbb{Q}} \end{bmatrix} + \begin{bmatrix} \int_{\mathbb{R}} xN_X(dt,dx). \\ 0 \\ 0 \end{bmatrix}. \tag{E.27}$$

Defining $dZ_1 = \int_{\mathbb{R}} xN_X(dt,dx)$, we can express terms in an equivalent form:

$$\begin{bmatrix} dln(S_t) \\ dV_t \\ dR_t \end{bmatrix} = \begin{bmatrix} R_t - q - \lambda\mu_J - \frac{1}{2}V_t \\ \theta_v - \kappa_v V_t \\ \theta_r - \kappa_r R_t \end{bmatrix} dt + \begin{bmatrix} \sqrt{V_t}\sqrt{1-\rho^2} & \rho\sqrt{V_t} & 0 \\ 0 & \sigma_v\sqrt{V_t} & 0 \\ 0 & 0 & \sigma_r\sqrt{R_t} \end{bmatrix} \begin{bmatrix} d\overline{W}_t^{S,\mathbb{Q}} \\ d\overline{W}_t^{v,\mathbb{Q}} \\ d\overline{W}_t^{r,\mathbb{Q}} \end{bmatrix} + \begin{bmatrix} dZ_1 \\ 0 \\ 0 \end{bmatrix}. \tag{E.28}$$

As a result, the drift $\mu(t, X_t)$ and the volatility term $\sigma(t, X_t)$ are given by:

$$\begin{aligned}\mu(t, X_t) &= \begin{bmatrix} R_t - q - \lambda\mu_J - \frac{1}{2}V_t \\ \theta_v - \kappa_v V_t \\ \theta_r - \kappa_r R_t \end{bmatrix} \\ \sigma(t, X_t) &= \begin{bmatrix} \sqrt{V_t}\sqrt{1-\rho^2} & \rho\sqrt{V_t} & 0 \\ 0 & \sigma_v\sqrt{V_t} & 0 \\ 0 & 0 & \sigma_r\sqrt{R_t} \end{bmatrix}.\end{aligned} \tag{E.29}$$

Recall that Duffie's model imposes an affine structure for both the drift $\mu(t, X_t) = K_0 + K_1 X_t$ and the definite positive matrix $\sigma(t, X_t)\sigma(t, X_t)^\top = H_0(t) + \sum_{k=1}^{n} H_x^k(t)(X_t)_k$ (see (3.5) and (3.6)). Then, we can write μ as:

$$\begin{aligned}\mu(t, X_t) &= \begin{bmatrix} -q - \lambda\mu_J \\ \theta_v \\ \theta_r \end{bmatrix} + \begin{bmatrix} R_t - \frac{1}{2}V_t \\ -\kappa_v V_t \\ -\kappa_r R_t \end{bmatrix} \\ &= \begin{bmatrix} -q - \lambda\mu_J \\ \theta_v \\ \theta_r \end{bmatrix} + \begin{bmatrix} 0 & -\frac{1}{2} & 1 \\ 0 & -\kappa_v & 0 \\ 0 & 0 & -\kappa_r \end{bmatrix} \begin{bmatrix} ln(S_t) \\ V_t \\ R_t \end{bmatrix},\end{aligned} \tag{E.30}$$

and conclude that

$$K_0(t) = \begin{bmatrix} -q - \lambda\mu_J \\ \theta_v \\ \theta_r \end{bmatrix}, \; K_x(t) = \begin{bmatrix} 0 & -\frac{1}{2} & 1 \\ 0 & -\kappa_v & 0 \\ 0 & 0 & -\kappa_r \end{bmatrix}. \tag{E.31}$$

Next, to identify the matrices involved in the affine structure of $\sigma(t, X_t)\sigma(t, X_t)^\top$, we consider

$$\begin{aligned}\sigma(t, X_t)\sigma(t, X_t)^\top &= \begin{bmatrix} \sqrt{V_t}\sqrt{1-\rho^2} & \rho\sqrt{V_t} & 0 \\ 0 & \sigma_v\sqrt{V_t} & 0 \\ 0 & 0 & \sigma_r\sqrt{R_t} \end{bmatrix} \begin{bmatrix} \sqrt{V_t}\sqrt{1-\rho^2} & 0 & 0 \\ \rho\sqrt{V_t} & \sigma_v\sqrt{V_t} & 0 \\ 0 & 0 & \sigma_r\sqrt{R_t} \end{bmatrix} \\ &= \begin{bmatrix} V_t(1-\rho^2) + \rho^2 V_t & \sigma_v\rho V_t & 0 \\ \sigma_v\rho V_t & \sigma_v^2 V_t & 0 \\ 0 & 0 & \sigma_r^2 R_t \end{bmatrix} \\ &= \begin{bmatrix} V_t & \sigma_v\rho V_t & 0 \\ \sigma_v\rho V_t & \sigma_v^2 V_t & 0 \\ 0 & 0 & \sigma_r^2 R_t \end{bmatrix},\end{aligned} \tag{E.32}$$

and conclude that

$$(H_0(t))_{i,j} = \left(H_x^{(1)}(t)\right)_{i,j} = 0, \text{for } i, j = 1, 2, 3\,, \tag{E.33}$$

$$H_x^{(2)} = \begin{bmatrix} 1 & \sigma_v\rho & 0 \\ \sigma_v\rho & \sigma_v^2 & 0 \\ 0 & 0 & 0 \end{bmatrix}, \tag{E.34}$$

$$\left(H_x^{(3)}(t)\right)_{i,j} = \sigma_r^2 \mathbb{1}\{i = j = 3\}, \tag{E.35}$$

and

$$R_t = \rho_0(t) + \rho_x(t)^\top X_t = 0 + \begin{bmatrix} 0 & 0 & 1 \end{bmatrix} \begin{bmatrix} ln(S_T) \\ V_t \\ R_t \end{bmatrix} = R_t, \tag{E.36}$$

$$\rho_0(t) = 0,\ \rho_x(t) = \begin{bmatrix} 0 & 0 & 1 \end{bmatrix}^\top. \tag{E.37}$$

Assume now the 3-dimensional pure jump process is $dZ_t^{\mathbb{Q}} = [\int_{\mathbb{R}} xN_X(dt, dx), 0, 0]'$. Then, the process $Z_{t,1}^{\mathbb{Q}} = \int_0^t \int_{\mathbb{R}} xN_X(dt, dx)$ exhibit jumps with an arrival intensity $\lambda(X_t, t) = \lambda \in [0, +\infty[$, so that

$$\lambda(X_t, t) = l_0(t) + l_x(t)^\top X_t = \lambda + \begin{bmatrix} 0 & 0 & 0 \end{bmatrix} \begin{bmatrix} ln(S_T) \\ V_t \\ R_t \end{bmatrix} = \lambda, \tag{E.38}$$

which implies $l_0(t) = \lambda$ and $l_x(t) = \begin{bmatrix} 0 & 0 & 0 \end{bmatrix}^\top$. The associated probability distribution ν_t, can be defined through the following jump transform θ:

$$\begin{aligned} \theta(c, t) &= \int_{\mathbb{R}^3} e^{c^{'}Z} d(\nu_t(z)) \\ &= \int_{\mathbb{R}} e^{c_1 z_1} d(\nu_t(z_1)) \\ &= \int_{\mathbb{R}} e^{c_1 z_1} \frac{1}{\sqrt{2\pi\sigma_J^2}} e^{-\frac{1}{2}\frac{(z_1 - ln(1+\mu_J) + \frac{1}{2}\sigma_J^2)^2}{\sigma_J^2}} dz_1 \\ &= e^{c_1(ln(1+\mu_J) - \frac{1}{2}\sigma_J^2) + \frac{1}{2}c_1^2\sigma_J^2}. \end{aligned} \tag{E.39}$$

Again, μ_J can be directly recovered from the jump transform θ, where $\mu_J = \theta(1, t) - 1$. The derivation of this relation can be found in Proposition E.1.

We next consider the system of ODEs that characterises the exponential–affine transform. In particular, recall that the ODE for β used in the transform (3.11) is given by equation (3.12), i.e.,

$$\beta'(t, T, u) = \rho_x(t) - K_x(t)^\top \beta(t, T, u) - \frac{1}{2}\left[\beta(t, T, u) H_x(t) \beta(t, T, u)\right] - \left[\theta(\beta(t, T, u), t) - 1\right] l_x(t). \tag{E.40}$$

Note that in this case, $\beta(t, T, u) H_x(t) \beta(t, T, u)$ is now a 3-dimensional vector, such that:

$$\beta(t, T, u) H_x(t) \beta(t, T, u) = \begin{bmatrix} \beta(t, T, u)^\top H_x^{(1)}(t) \beta(t, T, u) \\ \beta(t, T, u)^\top H_x^{(2)}(t) \beta(t, T, u) \\ \beta(t, T, u)^\top H_x^{(3)}(t) \beta(t, T, u) \end{bmatrix}.$$

Substituting the relevant terms from (5.52), (5.54), (5.56), (5.57), (5.58) and (5.59) into this ODE, the ODE (5.60) becomes:

$$\begin{aligned}\beta'(t,T,u) &= \begin{bmatrix}0 & 0 & 1\end{bmatrix}^\top - \begin{bmatrix}0 & -\frac{1}{2} & 1\\ 0 & -\kappa_v & 0\\ 0 & 0 & -\kappa_r\end{bmatrix}^\top \begin{bmatrix}\beta_1\\ \beta_2\\ \beta_3\end{bmatrix} - \frac{1}{2}\begin{bmatrix}\beta(t,T,u)^\top H_x^{(1)}(t)\beta(t,T,u)\\ \beta(t,T,u)^\top H_x^{(2)}(t)\beta(t,T,u)\\ \beta(t,T,u)^\top H_x^{(3)}(t)\beta(t,T,u)\end{bmatrix}\\ &\quad - \left[\theta(\beta(t,T,u),t)-1\right]\begin{bmatrix}0 & 0 & 0\end{bmatrix}^\top\\ &= \begin{bmatrix}0\\ 0\\ 1\end{bmatrix} - \begin{bmatrix}0\\ -\frac{1}{2}\beta_1 - \kappa_v\beta_2\\ \beta_1 - \kappa_r\beta_3\end{bmatrix} - \frac{1}{2}\begin{bmatrix}0\\ \beta_1^2 + 2\sigma_v\rho\beta_1\beta_2 + \sigma_v^2\beta_2^2\\ \sigma_r^2\beta_3^2\end{bmatrix}\\ &= \begin{bmatrix}0\\ \frac{1}{2}\beta_1 + \kappa_v\beta_2 - \frac{1}{2}\beta_1^2 - \sigma_v\rho\beta_1\beta_2 - \frac{1}{2}\sigma_v^2\beta_2^2\\ 1 - \beta_1 + \kappa_r\beta_3 - \frac{1}{2}\sigma_r^2\beta_3^2\end{bmatrix}.\end{aligned} \tag{E.41}$$

Applying the same substitutions to the ODE for α given in equation (3.13), we have:

$$\begin{aligned}\alpha'(t,T,u) &= \rho_0(t) - \beta(t,T,u)^\top K_0(t) - \frac{1}{2}\beta(t,T,u)^\top H_0(t)\beta(t,T,u) - \left[\theta(\beta(t,T,u),t)-1\right] l_0(t)\\ &= 0 - \begin{bmatrix}\beta_1 & \beta_2 & \beta_3\end{bmatrix}\begin{bmatrix}-q-\lambda\mu_J\\ \theta_v\\ \theta_r\end{bmatrix} - \frac{1}{2}\begin{bmatrix}\beta_1 & \beta_2 & \beta_3\end{bmatrix}\begin{bmatrix}0 & 0 & 0\\ 0 & 0 & 0\\ 0 & 0 & 0\end{bmatrix}\begin{bmatrix}\beta_1\\ \beta_2\\ \beta_3\end{bmatrix}\\ &\quad - \left[e^{\beta_1(ln(1+\mu_J)-\frac{1}{2}\sigma_J^2)+\frac{1}{2}\beta_1^2\sigma_J^2} - 1\right]\lambda\\ &= \left(q+\lambda\mu_J\right)\beta_1 - \beta_2\theta_v - \beta_3\theta_r - \lambda\left[e^{\beta_1(ln(1+\mu_J)-\frac{1}{2}\sigma_J^2)+\frac{1}{2}\beta_1^2\sigma_J^2} - 1\right].\end{aligned} \tag{E.42}$$

Based on the fact that $\beta_1'(t,T,u) = 0$, and using the terminal condition $\beta(T,T,u) = u$, we obtain the solution to the first ODE:

$$\beta_1(t,T,u) = u_1. \tag{E.43}$$

Turning to the second ODE, we begin by substituting β_1 into the second expression outlined in equation (E.41), yielding the following equation:

$$\frac{\partial\beta_2(t,T,u)}{\partial t} = \frac{1}{2}u_1 - \frac{1}{2}u_1^2 + (\kappa_v - u_1\rho\sigma_v)\beta_2 - \frac{1}{2}\sigma_v^2\beta_2^2. \tag{E.44}$$

It is easy to verify that ODE (E.44) is a Riccati equation. Solving this equation with respect to β_2, results in:

$$\beta_2 = \frac{k_2 - \exp\left(\frac{\sigma_v^2(k_1-k_2)}{2}(t+C)\right)k_1}{1 - \exp\left(\frac{\sigma_v^2(k_1-k_2)}{2}(t+C)\right)}, \tag{E.45}$$

where C is a constant of integration. Having determined the general solution for β_2, we now proceed to calculate the particular solution. Starting by imposing the boundary condition $\beta_2(T,T,u) = u_2$ to equation (E.45), we obtain the following expression associated

with the constant C:

$$\exp\left(\frac{\sigma_v^2(k_1-k_2)}{2}C\right) = \exp\left(-\frac{\sigma_v^2(k_1-k_2)}{2}T\right)\frac{u_2-k_2}{u_2-k_1}. \tag{E.46}$$

Substituting this result into equation (E.45), we arrive at the particular solution for ODE (E.44):

$$\beta_2(t,T,u) = \frac{2u_2\xi_v(u_1) + [u_2(u_1\rho\sigma_v - \kappa_v - \xi_v(u_1)) + u_1(u_1-1)]\left[1-e^{-\xi_v(u_1)\tau}\right]}{2\xi_v(u_1) - \gamma_v^+(u_1,u_2)[1-e^{-\xi_v(u_1)\tau}]}, \tag{E.47}$$

where $\tau = T-t$ and:

$$\begin{aligned}\gamma_v^+(u_1,u_2) &= u_2\sigma_v^2 - \kappa_v + u_1\rho\sigma_v + \xi_v(u_1),\\ \xi_v(u_1) &= \sqrt{(\kappa_v - u_1\rho\sigma_v)^2 - u_1(u_1-1)\sigma_v^2}\,.\end{aligned} \tag{E.48}$$

A complete derivation of β_2, covering both the general and particular solutions, is provided in Appendix E.3.3.2.

Proceeding to the third ODE, we begin by substituting the solution for β_1 calculated in equation (5.62) into the third expression outlined in equation (E.41), resulting, as in the previous case, in a Riccati equation:

$$\frac{\partial\beta_3(t,T,u)}{\partial t} = 1 - u_1 + \kappa_r\beta_3 - \frac{1}{2}\sigma_r^2\beta_3^2. \tag{E.49}$$

Solving this equation with respect to β_3, results in:

$$\beta_3 = \frac{k_2 - \exp\left(\frac{\sigma_r^2(k_1-k_2)}{2}(t+C)\right)k_1}{1-\exp\left(\frac{\sigma_r^2(k_1-k_2)}{2}(t+C)\right)}, \tag{E.50}$$

where C is a constant of integration.

Having determined the general solution for β_3, we now proceed to calculate the particular solution. Imposing the boundary condition $\beta_3(T,T,u) = u_3$ to equation (E.50), we obtain the expression associated with the constant C:

$$\exp\left(\frac{\sigma_r^2(k_1-k_2)}{2}C\right) = \exp\left(-\frac{\sigma_r^2(k_1-k_2)}{2}T\right)\frac{u_3-k_2}{u_3-k_1}. \tag{E.51}$$

Substituting in the general solution we arrive at the particular solution for ODE (E.49):

$$\beta_3 = \frac{2u_3\xi_r(u_1) + [2(u_1-1) - u_3(\xi_r(u_1)+k_r)][1-e^{-\xi_r(u_1)\tau}]}{2\xi_r(u_1) - \gamma_r^+(u_1,u_3)[1-e^{-\xi_r(u_1)\tau}]}. \tag{E.52}$$

where $\tau = T-t$, and:

$$\begin{aligned}\gamma_r^+(u_1,u_3) &= u_3\sigma_r^2 - \kappa_r + \xi_r(u_1),\\ \xi_r(u_1) &= \sqrt{\kappa_r^2 - 2\sigma_r^2(u_1-1)}.\end{aligned} \tag{E.53}$$

A detailed derivation of the solution for β_3 can be found in Appendix E.3.3.3.

Having derived the different values of $\beta(t,T,u)$, we now proceed to determine $\alpha(t,T,u)$ using ODE (5.61). Thus, substituting β_1 into this equation, we obtain:

$$\alpha'(t,T,u) = (q+\lambda\mu_J)\,\beta_1 - \beta_2\theta_v - \beta_3\theta_r - \lambda\left[e^{\beta_1(ln(1+\mu_J)-\frac{1}{2}\sigma_J^2)+\frac{1}{2}\beta_1^2\sigma_J^2} - 1\right]. \tag{E.54}$$

Next, integrating both sides of equation (E.54) from t to T, yields:

$$\begin{aligned}\alpha(T,T,u) - \alpha(t,T,u) = (q+\lambda\mu_J)\,\beta_1\tau - \theta_v\int_t^T \beta_2\,ds - \theta_r\int_t^T \beta_3\,ds \\ - \lambda\tau\left[(1+\mu_J)^{\beta_1} e^{\beta_1(\beta_1-1)\frac{\sigma_J^2}{2})} - 1\right],\end{aligned} \tag{E.55}$$

where $\tau = T - t$.

Regarding equation (E.55), it remains to compute the second and third terms of the right-hand side of the equation. To evaluate these terms, we use the partial fraction decomposition and the equating coefficients method, obtaining the solutions for β_2 and β_3. Substituting the solutions into ODE (E.55), imposing the boundary condition $\alpha(T,T,u) = 0$, and recalling that $\beta_1(t,T,u) = u_1$ (as derived in equation (5.62)) we obtain the following solution for α:

$$\begin{aligned}\alpha(t,T,u) &= -\theta_v\frac{u_2\left(\xi_v(u_1) - \kappa_v + u_1\rho\sigma_v\right) + u_1(u_1-1)}{\gamma_v^-(u_1,u_2)}\tau \\ &- \theta_v\left(\frac{2u_1(u_1-1) + 2u_2(u_2\sigma_v^2 - 2\kappa_v + 2u_1\rho\sigma_v)}{\gamma_v^-(u_1,u_2)\gamma_v^+(u_1,u_2)}\right)\times\ln\left(1 - \frac{\gamma_v^+(u_1,u_2)\left(1-e^{-\xi_v(u_1)\tau}\right)}{2\xi_v(u_1)}\right) \\ &- \theta_r\frac{u_3\left(\xi_r(u_1) - \kappa_r\right) + 2(u_1-1)}{\gamma_r^-(u_1,u_3)}\tau \\ &- \theta_r\left(\frac{4(u_1-1) + 2u_3(u_3\sigma_r^2 - 2k_r)}{\gamma_r^-(u_1,u_3)\gamma_r^+(u_1,u_3)}\right)\times\ln\left(1 - \frac{\gamma_r^+(u_1,u_3)(1-e^{-\xi_r(u_1)\tau})}{2\xi_r(u_1)}\right) \\ &+ \lambda\tau\left[(1+\mu_J)^{u_1}e^{u_1(u_1-1)\frac{\sigma_J^2}{2}} - 1\right] - \lambda u_1\mu_J\tau - qu_1\tau.\end{aligned} \tag{E.56}$$

where $\gamma_v^{\pm}(u_1,u_2)$, $\xi_v(u_1)$, $\gamma_r^{\pm}(u_1,u_3)$ and $\xi_r(u_1)$ are given by:

$$\begin{aligned}\gamma_v^{\pm}(u_1,u_2) &= u_2\sigma_v^2 - \kappa_v + u_1\rho\sigma_v \pm \xi_v(u_1), \\ \xi_v(u_1) &= \sqrt{\left(\kappa_v - u_1\rho\sigma_v\right)^2 - u_1(u_1-1)\sigma_v^2}, \\ \gamma_r^{\pm}(u_1,u_3) &= u_3\sigma_r^2 - \kappa_r \pm \xi_r(u_1), \\ \xi_r(u_1) &= \sqrt{\kappa_r^2 - 2\sigma_r^2(u_1-1)}.\end{aligned} \tag{E.57}$$

For completeness, a detailed derivation of $\alpha(t,T,u)$ is provided in Appendix E.3.3.4.

With all coefficients determined, the exponential-affine solution for the transform (3.9) takes the form:

$$\psi(u,t,T;X_t) = \exp\left[\alpha(t,T,u) + \beta_1(t,T,u)\ln(S_t) + \beta_2(t,T,u)V_t + \beta_3(t,T,u)R_t\right], \tag{E.58}$$

with $u \in \mathbb{C}^3$ and $t \le T$, where α, β_1, β_2 and β_3 are given by equations (5.67),(5.62),(5.63) and (5.65) respectively.

As done in previous models we need to compute the time-t price of a risk-free pure discount

bond which can also be expressed in terms of the same transform:

$$\begin{aligned} P(t,T) &= \mathbb{E}^{\mathbb{Q}}\left[\exp\left(-\int_t^T r(X_s,s)\,ds\right)\Big|\mathcal{F}_t\right] \\ &= \psi((0,\underline{0}),t,T,X_t) \\ &= \exp\left[\alpha(t,T,(0,\underline{0})) + \beta(t,T,(0,\underline{0}))' \cdot X_t\right]. \end{aligned} \tag{E.59}$$

where $\underline{0}$ is a null vector in $\mathbb{R}^2$ and X_t is the 3-dimensional vector defined in equation (5.50).

Note that setting $u_1 = 0$ and $u_2 = 0$ in equations (5.62) and (5.63), we conclude that both β_1 and β_2 are zero. Applying the same procedure to equation (5.65), we arrive at the following expression for β_3:

$$\beta_3(t,T,0) = \frac{2(e^{-\xi_r(0)\tau}-1)}{2\xi_r(0) + (\xi_r(0)-\kappa_r)(e^{-\xi_r(0)\tau}-1)}, \tag{E.60}$$

where $\xi_r(0) = \sqrt{\kappa_r^2 + 2\sigma_r^2}$, and $\tau = T - t$.

With this result, we can now proceed to determine α. Building on the fact that $\gamma_r^+(0,0) = \sqrt{\kappa_r^2+2\sigma_r^2} - \kappa_r$ and $\gamma_r^-(0,0) = -\sqrt{\kappa_r^2+2\sigma_r^2} - \kappa_r$, and setting $u_1 = u_2 = u_3 = 0$, we arrive at following expression for α:

$$\alpha(t,T,0) = -\theta_r\left[\frac{2\tau}{\sqrt{\kappa_r^2+2\sigma_r^2}+\kappa_r} + \frac{2}{\sigma_r^2}\ln\left(1 - \frac{(\sqrt{\kappa_r^2+2\sigma_r^2}-\kappa_r)(1-e^{-\tau\sqrt{\kappa_r^2+2\sigma_r^2}})}{2\sqrt{\kappa_r^2+2\sigma_r^2}}\right)\right], \tag{E.61}$$

where $\tau = T - t$.

Having determined the β_1, β_2, β_3 and α, the price of the risk-free pure discount bond defined in equation (5.70) can be expressed as:

$$P(t,T) = \exp\left[\alpha(t,T,0) + \beta_3(t,T,0)R_t\right], \tag{E.62}$$

where $\alpha(t,T,0)$ is defined as specified in equation (5.72), and $\beta_3(t,T,0)$ as in equation (5.71).

Finally, within Lee's framework, the call option price can be expressed in terms of the marginal characteristic function of the terminal log-price under the forward-T measure. As explained when presenting the general definition in equation (4.10), in this setting the function corresponds to f_2. Therefore, in Bakshi, Cao and Chen (1997) model the marginal characteristic function under $\mathbb{Q}^T$ takes the form:

$$f_2(T,\phi;S_t,Y_t) = \frac{\mathbb{E}^{\mathbb{Q}}\left[\exp\left(-\int_t^T r(X_s,s)\,ds\right)e^{i\phi\ln(S_T)}\Big|\mathcal{F}_t\right]}{P(t,T)}. \tag{E.63}$$

Since the numerator in equation (5.74) is a special case of the general exponential–affine transform in equation (3.9), we can write Bakshi's marginal characteristic function under the forward $T-$measure as follows:

$$f_2(T,\phi;S_t,Y_t) = \frac{\psi(i\phi,\underline{0},t,T;(\ln(S_t),Y_t))}{P(t,T)}. \tag{E.64}$$

with ψ being defined as

$$\begin{aligned}\psi(i\phi, \underline{0}, t, T; (\ln(S_t), Y_t)) = \exp[&\alpha(t, T, i\phi, \underline{0}) + \beta_1(t, T, i\phi, \underline{0}) \ln(S_t) \\ &+ \beta_2(t, T, i\phi, \underline{0}) V_t + \beta_3(t, T, i\phi, \underline{0}) R_t],\end{aligned} \tag{E.65}$$

where $\tau = T - t$, and

$$\begin{aligned}\alpha(t, T, i\phi, \underline{0}) = &-\theta_v \frac{i\phi(i\phi - 1)}{\gamma_v^-(i\phi, 0)} \tau \\ &- \theta_v \left(\frac{2i\phi(i\phi - 1)}{\gamma_v^-(i\phi, 0)\gamma_v^+(i\phi, 0)} \right) \times \ln \left(1 - \frac{\gamma_v^+(i\phi, 0) \left(1 - e^{-\xi_v(i\phi)\tau}\right)}{2\xi_v(i\phi)} \right) \\ &- \theta_r \frac{2(i\phi - 1)}{\gamma_r^-(i\phi, 0)} \tau \\ &- \theta_r \left(\frac{4(i\phi - 1)}{\gamma_r^-(i\phi, 0)\gamma_r^+(i\phi, 0)} \right) \times \ln \left(1 - \frac{\gamma_r^+(i\phi, 0)(1 - e^{-\xi_r(u_1)\tau})}{2\xi_r(i\phi)} \right) \\ &+ \lambda\tau \left[(1 + \mu_J)^{i\phi} e^{i\phi(i\phi - 1)\frac{\sigma_J^2}{2}} - 1 \right] - \lambda i\phi\mu_J\tau - qi\phi\tau \,,\end{aligned} \tag{E.66}$$

$$\beta_1(t, T, i\phi, \underline{0}) = i\phi,$$

$$\beta_2(t, T, i\phi, \underline{0}) = \frac{[i\phi(i\phi - 1)] \left[1 - e^{-\xi_v(i\phi)\tau}\right]}{2\xi_v(i\phi) - \gamma_v^+(i\phi, 0)[1 - e^{-\xi_v(i\phi)\tau}]}, \text{ and}$$

$$\beta_3(t, T, i\phi, \underline{0}) = \frac{[2(i\phi - 1)]}{2\xi_r(i\phi) - \gamma_r^+(i\phi, 0) \left[1 - e^{-\xi_r(i\phi)\tau}\right]}.$$

E.3.3.2 Derivation of the solution for β_2

To obtain the solution for the second ODE in the Bakshi, Cao and Chen (1997) model, which corresponds to β_2 (or, equivalently, β_r), we begin by substituting β_1 into the second expression outlined in equation (E.41), yielding the following equation:

$$\frac{\partial \beta_2(t, T, u)}{\partial t} = \frac{1}{2}u_1 - \frac{1}{2}u_1^2 + (\kappa_v - u_1\rho\sigma_v)\beta_2 - \frac{1}{2}\sigma_v^2\beta_2^2. \tag{E.67}$$

It is easy to verify that ODE (E.67) is a Riccati equation. To simplify the problem, we need to convert it into a second-order linear differential equation. Therefore, rearranging the terms, equation (E.44) can be rewritten as:

$$\frac{d\beta_2(t, T, u)}{\frac{1}{2}u_1 - \frac{1}{2}u_1^2 + (\kappa_v - u_1\rho\sigma_v)\beta_2 - \frac{1}{2}\sigma_v^2\beta_2^2} = dt. \tag{E.68}$$

Analysing the second-order equation in the denominator of the left-hand side fraction, we find two distinct roots, k_1 and k_2, given by:

$$k_1 = \frac{\kappa_v - u_1\rho\sigma_v + \xi_v(u_1)}{\sigma_v^2}, \quad k_2 = \frac{\kappa_v - u_1\rho\sigma_v - \xi_v(u_1)}{\sigma_v^2}, \tag{E.69}$$

where $\xi_v(u_1) = \sqrt{(\kappa_v - u_1\rho\sigma_v)^2 - u_1(u_1 - 1)\sigma_v^2}$.
Using the solutions to factor equation (E.68), we obtain the following ODE for β_2 evaluated

at (t, T, u):

$$\frac{d\beta_2}{-\frac{1}{2}\sigma_v^2\left[\beta_2 - k_1\right]\left[\beta_2 - k_2\right]} = dt. \tag{E.70}$$

From the partial fraction decomposition, we know that:

$$\frac{1}{-\frac{1}{2}\sigma_v^2\left[\beta_2 - k_1\right]\left[\beta_2 - k_2\right]} = \frac{a}{-\frac{1}{2}\sigma_v^2\beta_2 + \frac{1}{2}\sigma_v^2 k_1} + \frac{b}{\beta_2 - k_2}, \tag{E.71}$$

which implies, by the equating coefficients method, that:

$$\begin{aligned} a\left(\beta_2 - k_2\right) + b\left(-\frac{1}{2}\sigma_v^2\beta_2 + \frac{1}{2}\sigma_v^2 k_1\right) = 1 \Leftrightarrow \left(a - \frac{1}{2}\sigma_v^2 b\right)\beta_2 + \left(\frac{1}{2}\sigma_v^2 k_1 b - a k_2\right) = 1 \\ \Rightarrow \begin{cases} a - \frac{1}{2}\sigma_v^2 b = 0 \\ \frac{1}{2}\sigma_v^2 k_1 b - a k_2 = 1 \end{cases} \Rightarrow \begin{cases} a = \frac{1}{k_1 - k_2} \\ b = \frac{2}{\sigma_v^2(k_1 - k_2)} \end{cases}. \end{aligned} \tag{E.72}$$

As a result, equation (E.71) can be rewritten as follows:

$$\frac{\frac{1}{k_1 - k_2}d\beta_2}{-\frac{1}{2}\sigma_v^2\beta_2 + \frac{1}{2}\sigma_v^2 k_1} + \frac{\frac{2}{\sigma_v^2(k_1 - k_2)}d\beta_2}{\beta_2 - k_2} = dt. \tag{E.73}$$

Rearranging the terms and applying the integral to equation (E.73), we get:

$$\begin{aligned} \frac{-2}{\sigma_v^2(k_1 - k_2)}\int \frac{d\beta_2}{\beta_2 - k_1} + \frac{2}{\sigma_v^2(k_1 - k_2)}\int \frac{d\beta_2}{\beta_2 - k_2} = t + C, \\ \frac{-2}{\sigma_v^2(k_1 - k_2)} ln\left|\beta_2 - k_1\right| + \frac{2}{\sigma_v^2(k_1 - k_2)} ln\left|\beta_2 - k_2\right| = t + C, \end{aligned} \tag{E.74}$$

where C is a constant of integration. Simplifying equation (E.74), yields:

$$\frac{2}{\sigma_v^2(k_1 - k_2)} ln\left|\frac{\beta_2 - k_2}{\beta_2 - k_1}\right| = t + C. \tag{E.75}$$

Solving equation (E.75) with respect to β_2, results in:

$$\beta_2 = \frac{k_2 - \exp\left(\frac{\sigma_v^2(k_1 - k_2)}{2}\left(t + C\right)\right)k_1}{1 - \exp\left(\frac{\sigma_v^2(k_1 - k_2)}{2}\left(t + C\right)\right)}. \tag{E.76}$$

Having determined the general solution for β_2, we now proceed to calculate the particular solution. Starting by imposing the boundary condition $\beta_2(T, T, u) = u_2$ to equation (E.76), we obtain the following expression associated with the constant C:

$$\begin{aligned} u_2 = \frac{k_2 - \exp\left(\frac{\sigma_v^2(k_1 - k_2)}{2}\left(t + C\right)\right)k_1}{1 - \exp\left(\frac{\sigma_v^2(k_1 - k_2)}{2}\left(t + C\right)\right)} \Leftrightarrow \exp\left(\frac{\sigma_v^2(k_1 - k_2)}{2}(T + C)\right) = \frac{u_2 - k_2}{u_2 - k_1} \Leftrightarrow \\ \exp\left(\frac{\sigma_v^2(k_1 - k_2)}{2}C\right) = \exp\left(-\frac{\sigma_v^2(k_1 - k_2)}{2}T\right)\frac{u_2 - k_2}{u_2 - k_1}. \end{aligned} \tag{E.77}$$

Substituting this result into equation (E.76), leads to:

$$\begin{aligned}\beta_2 &= \frac{k_2 - \exp\left(\frac{\sigma_v^2(k_1-k_2)}{2}(t+C)\right)k_1}{1-\exp\left(\frac{\sigma_v^2(k_1-k_2)}{2}(t+C)\right)} = \frac{k_2 - \exp\left(\frac{\sigma_v^2(k_1-k_2)}{2}t\right)\exp\left(\frac{\sigma_v^2(k_1-k_2)}{2}C\right)k_1}{1-\exp\left(\frac{\sigma_v^2(k_1-k_2)}{2}t\right)\exp\left(\frac{\sigma_v^2(k_1-k_2)}{2}C\right)} \\ &= \frac{k_2 - \exp\left(\frac{\sigma_v^2(k_1-k_2)}{2}t\right)\exp\left(-\frac{\sigma_v^2(k_1-k_2)}{2}T\right)\frac{u_2-k_2}{u_2-k_1}k_1}{1-\exp\left(\frac{\sigma_v^2(k_1-k_2)}{2}t\right)\exp\left(-\frac{\sigma_v^2(k_1-k_2)}{2}T\right)\frac{u_2-k_2}{u_2-k_1}} = \frac{k_2 - \exp\left(-\frac{\sigma_v^2(k_1-k_2)}{2}\tau\right)\frac{u_2-k_2}{u_2-k_1}k_1}{1-\exp\left(-\frac{\sigma_v^2(k_1-k_2)}{2}\tau\right)\frac{u_2-k_2}{u_2-k_1}}.\end{aligned} \tag{E.78}$$

To solve equation (E.78), we begin by identifying and calculating its components to simplify the process. Substituting k_1 and k_2 derived in equation (E.69), defining $\gamma_v^{\pm}(u_1,u_2) = u_2\sigma_v^2 - \kappa_v + u_1\rho\sigma_v \pm \xi_v(u_1)$, and knowing that $\xi_v^2(u_1) = (\kappa_v - u_1\rho\sigma_v)^2 - u_1(u_1-1)\sigma_v^2$, we have:

$$k_1 - k_2 = \frac{\kappa_v - u_1\rho\sigma_v + \xi_v(u_1)}{\sigma_v^2} - \frac{\kappa_v - u_1\rho\sigma_v - \xi_v(u_1)}{\sigma_v^2} = \frac{2\xi_v(u_1)}{\sigma_v^2}, \tag{E.79}$$

and

$$\frac{u_2-k_2}{u_2-k_1} = \frac{u_2 - \frac{\kappa_v - u_1\rho\sigma_v - \xi_v(u_1)}{\sigma_v^2}}{u_2 - \frac{\kappa_v - u_1\rho\sigma_v + \xi_v(u_1)}{\sigma_v^2}} = \frac{u_2\sigma_v^2 - \kappa_v + \sigma_v\rho u_1 + \xi_v(u_1)}{u_2\sigma_v^2 - \kappa_v + \sigma_v\rho u_1 - \xi_v(u_1)} = \frac{\gamma_v^+(u_1,u_2)}{\gamma_v^-(u_1,u_2)}, \tag{E.80}$$

and

$$\begin{aligned}\frac{u_2-k_2}{u_2-k_1}k_1 &= \frac{u_2 - \frac{\kappa_v - u_1\rho\sigma_v - \xi_v(u_1)}{\sigma_v^2}}{u_2 - \frac{\kappa_v - u_1\rho\sigma_v + \xi_v(u_1)}{\sigma_v^2}}\frac{\kappa_v - u_1\rho\sigma_v + \xi_v(u_1)}{\sigma_v^2} \\ &= \frac{u_2\kappa_v\sigma_v^2 - u_2u_1\rho\sigma_v^3 + u_2\xi_v(u_1)\sigma_v^2 - \kappa_v^2 - u_1^2\rho^2\sigma_v^2 + \xi_v^2(u_1) + 2k_vu_1\rho\sigma_v}{\sigma_v^2(u_2\sigma_v^2 - k_v + u_1\rho\sigma_v - \xi_v(u_1))} \\ &= \frac{u_2\kappa_v\sigma_v^2 - u_2u_1\rho\sigma_v^3 + u_2\xi_v(u_1)\sigma_v^2 - u_1(u_1-1)\sigma_v^2}{\sigma_v^2\gamma_v^-(u_1,u_2)} \\ &= \frac{u_2\kappa_v - u_2u_1\rho\sigma_v + u_2\xi_v(u_1) - u_1(u_1-1)}{\gamma_v^-(u_1,u_2)}.\end{aligned} \tag{E.81}$$

Then, plugging in the terms given by equations (E.79), (E.80) and (E.81) into equation (E.78), leads to:

$$\begin{aligned}\beta_2 &= \frac{\frac{\kappa_v - u_1\rho\sigma_v - \xi_v(u_1)}{\sigma_v^2} - e^{-\xi_v(u_1)\tau}\frac{u_2\kappa_v - u_2u_1\rho\sigma_v + u_2\xi_v(u_1) - u_1(u_1-1)}{\gamma_v^-(u_1,u_2)}}{1 - e^{-\xi_v(u_1)\tau}\frac{\gamma_v^+(u_1,u_2)}{\gamma_v^-(u_1,u_2)}} \\ &= \frac{[\kappa_v - u_1\rho\sigma_v - \xi_v(u_1)]\gamma_v^-(u_1,u_2) + \sigma_v^2e^{-\xi_v(u_1)\tau}[u_2(u_1\rho\sigma_v - \kappa_v - \xi_v(u_1)) + u_1(u_1-1)]}{\sigma_v^2[\gamma_v^-(u_1,u_2) - e^{-\xi_v(u_1)\tau}\gamma_v^+(u_1,u_2)]},\end{aligned} \tag{E.82}$$

where $\tau = T - t$.

Substituting $\gamma_v^-(u_1,u_2)$ in the numerator, and noting that $\gamma_v^-(u_1,u_2) = \gamma_v^+(u_1,u_2) -$

$2\xi_v(u_1)$, we can rewrite equation (E.82) as follows:

$$\begin{aligned}\beta_2 = &\frac{u_2\kappa_v\sigma_v^2 - k_v^2 + 2k_v u_1\rho\sigma_v - u_2 u_1\rho\sigma_v^3 - u_1^2\rho^2\sigma_v^2 - u_2\xi_v(u_1)\sigma_v^2 + \xi_v^2(u_1)}{\sigma_v^2[-2\xi_v(u_1) + \gamma_v^+(u_1,u_2)[1-e^{-\xi_v(u_1)\tau}]]} \\ &+ \frac{\sigma_v^2 e^{-\xi_v(u_1)\tau}[u_2(u_1\rho\sigma_v - \kappa_v - \xi_v(u_1)) + u_1(u_1-1)]}{\sigma_v^2[-2\xi_v(u_1) + \gamma_v^+(u_1,u_2)[1-e^{-\xi_v(u_1)\tau}]]}.\end{aligned} \tag{E.83}$$

Again, replacing $\xi_v^2(u_1)$ in the numerator, equation (E.83) simplifies to:

$$\begin{aligned}\beta_2 = &\frac{u_2\kappa_v\sigma_v^2 - u_2 u_1\rho\sigma_v^3 - u_2\xi_v(u_1)\sigma_v^2 - u_1(u_1-1)\sigma_v^2}{\sigma_v^2[-2\xi_v(u_1) + \gamma_v^+(u_1,u_2)[1-e^{-\xi_v(u_1)\tau}]]} \\ &+ \frac{\sigma_v^2 e^{-\xi_v(u_1)\tau}[u_2(u_1\rho\sigma_v - \kappa_v - \xi_v(u_1)) + u_1(u_1-1)]}{\sigma_v^2[-2\xi_v(u_1) + \gamma_v^+(u_1,u_2)[1-e^{-\xi_v(u_1)\tau}]]}.\end{aligned} \tag{E.84}$$

Cancelling the term σ_r^2 from both the numerator and the denominator, results in the following expression:

$$\beta_2 = \frac{-u_2(u_1\rho\sigma_v - \kappa_v + \xi_v(u_1)) - u_1(u_1-1) + e^{-\xi_v(u_1)\tau}[u_2(u_1\rho\sigma_v - \kappa_v - \xi_v(u_1)) + u_1(u_1-1)]}{-2\xi_v(u_1) + \gamma_v^+(u_1,u_2)[1-e^{-\xi_v(u_1)\tau}]}. \tag{E.85}$$

Finally, summing and subtracting $u_2\xi_v(u_1)$ in the numerator, and multiplying both the numerator and denominator by -1, we arrive at the particular solution for ODE (E.67):

$$\beta_2(t,T,u) = \frac{2u_2\xi_v(u_1) + [u_2(u_1\rho\sigma_v - \kappa_v - \xi_v(u_1)) + u_1(u_1-1)]\,[1-e^{-\xi_v(u_1)\tau}]}{2\xi_v(u_1) - \gamma_v^+(u_1,u_2)[1-e^{-\xi_v(u_1)\tau}]}, \tag{E.86}$$

where $\tau = T - t$, and:

$$\begin{aligned}\gamma_v^+(u_1,u_2) &= u_2\sigma_v^2 - \kappa_v + u_1\rho\sigma_v + \xi_v(u_1), \\ \xi_v(u_1) &= \sqrt{(\kappa_v - u_1\rho\sigma_v)^2 - u_1(u_1-1)\sigma_v^2}.\end{aligned} \tag{E.87}$$

E.3.3.3 Derivation of the solution for β_3

To obtain the solution for the third ODE in the Bakshi, Cao and Chen (1997) model, which corresponds to β_3 (or, equivalently, β_v), we begin by substituting the solution for β_1 calculated in equation (E.43) into the third expression outlined in equation (E.41), resulting, as in the previous case, in a Riccati equation:

$$\frac{\partial\beta_3(t,T,u)}{\partial t} = 1 - u_1 + \kappa_r\beta_3 - \frac{1}{2}\sigma_r^2\beta_3^2. \tag{E.88}$$

Again, we begin by rearranging the terms, as shown below:

$$\frac{d\beta_3(t,T,u)}{-\frac{1}{2}\sigma_r^2\beta_3^2 + \kappa_r\beta_3 + 1 - u_1} = dt. \tag{E.89}$$

Analysing the second-order equation in the denominator of the left-hand side fraction, we find two distinct roots, k_1 and k_2, given by:

$$k_1 = \frac{\kappa_r + \xi_r(u_1)}{\sigma_r^2} \quad \text{and} \quad k_2 = \frac{\kappa_r - \xi_r(u_1)}{\sigma_r^2}, \tag{E.90}$$

where $\xi_r(u_1) = \sqrt{\kappa_r^2 - 2\sigma_r^2(u_1 - 1)}$.
Using the solutions to factor equation (E.89), we obtain the following ODE for β_3 evaluated at (t, T, u):

$$\frac{d\beta_3}{-\frac{1}{2}\sigma_r^2 \left[\beta_3 - k_1\right]\left[\beta_3 - k_2\right]} = dt. \tag{E.91}$$

From the partial fraction decomposition, we know that:

$$\frac{1}{-\frac{1}{2}\sigma_r^2 \left[\beta_3 - k_1\right]\left[\beta_3 - k_2\right]} = \frac{a}{-\frac{1}{2}\sigma_r^2\beta_3 + \frac{1}{2}\sigma_r^2 k_1} + \frac{b}{\beta_3 - k_2}, \tag{E.92}$$

which implies, by the equating coefficients method, that:

$$\begin{aligned} a\left(\beta_3 - k_2\right) + b\left(-\frac{1}{2}\sigma_r^2\beta_3 + \frac{1}{2}\sigma_r^2 k_1\right) = 1 \Leftrightarrow \left(a - \frac{1}{2}\sigma_r^2 b\right)\beta_3 + \left(\frac{1}{2}\sigma_r^2 k_1 b - a k_2\right) = 1 \\ \Rightarrow \begin{cases} a - \frac{1}{2}\sigma_r^2 b = 0 \\ \frac{1}{2}\sigma_r^2 k_1 b - a k_2 = 1 \end{cases} \Rightarrow \begin{cases} a = \frac{1}{k_1 - k_2} \\ b = \frac{2}{\sigma_r^2(k_1 - k_2)} \end{cases}. \end{aligned} \tag{E.93}$$

As a result, equation (E.91) can be rewritten as follows:

$$\frac{\frac{1}{k_1 - k_2}d\beta_3}{-\frac{1}{2}\sigma_r^2\beta_3 + \frac{1}{2}\sigma_r^2 k_1} + \frac{\frac{2}{\sigma_r^2(k_1 - k_2)}d\beta_3}{\beta_3 - k_2} = dt. \tag{E.94}$$

Rearranging the terms and applying the integral to equation (E.95), we get:

$$\begin{aligned} \frac{-2}{\sigma_r^2(k_1 - k_2)}\int \frac{d\beta_3}{\beta_3 - k_1} + \frac{2}{\sigma_r^2(k_1 - k_2)}\int \frac{d\beta_3}{\beta_3 - k_2} = t + C, \\ \frac{-2}{\sigma_r^2(k_1 - k_2)} ln\left|\beta_3 - k_1\right| + \frac{2}{\sigma_r^2(k_1 - k_2)} ln\left|\beta_3 - k_2\right| = t + C, \end{aligned} \tag{E.95}$$

where C is a constant of integration. Simplifying equation (E.95), yields:

$$\frac{2}{\sigma_r^2(k_1 - k_2)} ln\left|\frac{\beta_3 - k_2}{\beta_3 - k_1}\right| = t + C. \tag{E.96}$$

Solving equation (E.96) with respect to β_3, results in:

$$\beta_3 = \frac{k_2 - \exp\left(\frac{\sigma_r^2(k_1 - k_2)}{2}\left(t + C\right)\right)k_1}{1 - \exp\left(\frac{\sigma_r^2(k_1 - k_2)}{2}\left(t + C\right)\right)}. \tag{E.97}$$

Having determined the general solution for β_3, we now proceed to calculate the particular solution. Starting by imposing the boundary condition $\beta_3(T, T, u) = u_3$ to equation (E.97), we obtain the following expression associated with the constant C:

$$\begin{aligned} u_3 = \frac{k_2 - \exp\left(\frac{\sigma_r^2(k_1 - k_2)}{2}\left(t + C\right)\right)k_1}{1 - \exp\left(\frac{\sigma_r^2(k_1 - k_2)}{2}\left(t + C\right)\right)} \Leftrightarrow \exp\left(\frac{\sigma_r^2(k_1 - k_2)}{2}(T + C)\right) = \frac{u_3 - k_2}{u_3 - k_1} \Leftrightarrow \\ \exp\left(\frac{\sigma_r^2(k_1 - k_2)}{2}C\right) = \exp\left(-\frac{\sigma_r^2(k_1 - k_2)}{2}T\right)\frac{u_3 - k_2}{u_3 - k_1}. \end{aligned} \tag{E.98}$$

Substituting this result into equation (E.97), leads to:

$$\beta_3 = \frac{k_2 - \exp\left(\frac{\sigma_r^2(k_1-k_2)}{2}(t+C)\right)k_1}{1-\exp\left(\frac{\sigma_r^2(k_1-k_2)}{2}(t+C)\right)} = \frac{k_2 - \exp\left(\frac{\sigma_r^2(k_1-k_2)}{2}t\right)\exp\left(\frac{\sigma_r^2(k_1-k_2)}{2}C\right)k_1}{1-\exp\left(\frac{\sigma_r^2(k_1-k_2)}{2}t\right)\exp\left(\frac{\sigma_r^2(k_1-k_2)}{2}C\right)}$$
$$= \frac{k_2 - \exp\left(\frac{\sigma_r^2(k_1-k_2)}{2}t\right)\exp\left(-\frac{\sigma_r^2(k_1-k_2)}{2}T\right)\frac{u_3-k_2}{u_3-k_1}k_1}{1-\exp\left(\frac{\sigma_r^2(k_1-k_2)}{2}t\right)\exp\left(-\frac{\sigma_r^2(k_1-k_2)}{2}T\right)\frac{u_3-k_2}{u_3-k_1}} = \frac{k_2 - \exp\left(-\frac{\sigma_r^2(k_1-k_2)}{2}\tau\right)\frac{u_3-k_2}{u_3-k_1}k_1}{1-\exp\left(-\frac{\sigma_r^2(k_1-k_2)}{2}\tau\right)\frac{u_3-k_2}{u_3-k_1}}. \tag{E.99}$$

To solve equation (E.99), we begin by identifying and calculating its components to simplify the process. Substituting k_1 and k_2 derived in equation (E.90), defining $\gamma_r^{\pm}(u_1,u_3) = u_3\sigma_r^2 - \kappa_r \pm \xi_r(u_1)$, and knowing that $\xi_r^2(u_1) = K_r^2 - 2\sigma_r^2(u_1-1)$, we have:

$$k_1 - k_2 = \frac{\kappa_r + \xi_r(u_1)}{\sigma_r^2} - \frac{\kappa_r - \xi_r(u_1)}{\sigma_r^2} = \frac{2\xi_r(u_1)}{\sigma_r^2}, \tag{E.100}$$

and

$$\frac{u_3-k_2}{u_3-k_1} = \frac{u_3 - \frac{\kappa_r-\xi_r(u_1)}{\sigma_r^2}}{u_3 - \frac{\kappa_r+\xi_r(u_1)}{\sigma_r^2}} = \frac{u_3\sigma_r^2 - \kappa_r + \xi_r(u_1)}{u_3\sigma_r^2 - \kappa_r - \xi_r(u_1)} = \frac{\gamma_r^+(u_1,u_3)}{\gamma_r^-(u_1,u_3)}, \tag{E.101}$$

and

$$\frac{u_3-k_2}{u_3-k_1}k_1 = \frac{u_3 - \frac{\kappa_r-\xi_r(u_1)}{\sigma_r^2}}{u_3 - \frac{\kappa_r+\xi_r(u_1)}{\sigma_r^2}}\frac{\kappa_r+\xi_r(u_1)}{\sigma_r^2} = \frac{u_3\sigma_r^2k_r + u_3\sigma_r^2\xi_r(u_1) - k_r^2 + \xi_r^2(u_1)}{u_3\sigma_r^4 - \kappa_r\sigma_r^2 - \xi_r(u_1)\sigma_r^2}$$
$$= \frac{u_3\sigma_r^2k_r + u_3\sigma_r^2\xi_r(u_1) - 2\sigma_r^2(u_1-1)}{u_3\sigma_r^4 - \kappa_r\sigma_r^2 - \xi_r(u_1)\sigma_r^2} = \frac{u_3k_r + u_3\xi_r(u_1) - 2(u_1-1)}{u_3\sigma_r^2 - \kappa_r - \xi_r(u_1)},$$
$$= \frac{u_3k_r + u_3\xi_r(u_1) - 2(u_1-1)}{\gamma_r^-(u_1,u_3)}. \tag{E.102}$$

Then, plugging in the terms given by equations (E.100), (E.101) and (E.102) into equation (E.99), leads to:

$$\beta_3 = \frac{\frac{\kappa_r-\xi_r(u_1)}{\sigma_r^2} - e^{-\xi_r(u_1)\tau}\frac{u_3k_r+u_3\xi_r(u_1)-2(u_1-1)}{\gamma_r^-(u_1,u_3)}}{1-e^{-\xi_r(u_1)\tau}\frac{\gamma_r^+(u_1,u_3)}{\gamma_r^-(u_1,u_3)}}$$
$$= \frac{[(\kappa_r - \xi_r(u_1)]\gamma_r^-(u_1,u_3) - \sigma_r^2[u_3(\xi_r(u_1)+k_r) - 2(u_1-1)]e^{-\xi_r(u_1)\tau}}{\sigma_r^2[\gamma_r^-(u_1,u_3) - e^{-\xi_r(u_1)\tau}\gamma_r^+(u_1,u_3)]}, \tag{E.103}$$

where $\tau = T - t$.

Substituting $\gamma_r^-(u_1,u_3)$ in the numerator, and noting that $\gamma_r^-(u_1,u_3) = \gamma_r^+(u_1,u_3) - 2\xi_r(u_1)$, we can rewrite equation (E.103) as follows:

$$\beta_3 = \frac{\kappa_r u_3\sigma_r^2 - k_r^2 - u_3\xi_r(u_1)\sigma_r^2 + \xi_r^2 - \sigma_r^2[u_3(\xi_r(u_1)+k_r) - 2(u_1-1)]e^{-\xi_r(u_1)\tau}}{\sigma_r^2[\gamma_r^+(u_1,u_3) - 2\xi_r(u_1) - e^{-\xi_r(u_1)\tau}\gamma_r^+(u_1,u_3)]}. \tag{E.104}$$

Again, replacing $\xi_r^2(u_1)$ in the numerator, equation (E.104) simplifies to:

$$\beta_3 = \frac{\kappa_r u_3 \sigma_r^2 - u_3 \xi_r(u_1)\sigma_r^2 - 2\sigma_r^2(u_1 - 1) - \sigma_r^2[u_3(\xi_r(u_1) + k_r) - 2(u_1 - 1)]e^{-\xi_r(u_1)\tau}}{\sigma_r^2[-2\xi_r(u_1) + \gamma_r^+(u_1, u_3)[1 - e^{-\xi_r(u_1)\tau}]]}. \tag{E.105}$$

Cancelling the term σ_r^2 from both the numerator and the denominator, results in the following expression:

$$\beta_3 = \frac{\kappa_r u_3 - u_3 \xi_r(u_1) - 2(u_1 - 1) - [u_3(\xi_r(u_1) + k_r) - 2(u_1 - 1)]e^{-\xi_r(u_1)\tau}}{-2\xi_r(u_1) + \gamma_r^+(u_1, u_3)[1 - e^{-\xi_r(u_1)\tau}]}. \tag{E.106}$$

Finally, summing and subtracting $u_3\xi_r(u_1)$ in the numerator, and multiplying both the numerator and denominator by -1, we arrive at the particular solution for ODE (E.88):

$$\beta_3 = \frac{2u_3\xi_r(u_1) + [2(u_1 - 1) - u_3(\xi_r(u_1) + k_r)][1 - e^{-\xi_r(u_1)\tau}]}{2\xi_r(u_1) - \gamma_r^+(u_1, u_3)[1 - e^{-\xi_r(u_1)\tau}]}. \tag{E.107}$$

where $\tau = T - t$, and:

$$\begin{aligned} \gamma_r^+(u_1, u_3) &= u_3\sigma_r^2 - \kappa_r + \xi_r(u_1), \\ \xi_r(u_1) &= \sqrt{\kappa_r^2 - 2\sigma_r^2(u_1 - 1)}. \end{aligned} \tag{E.108}$$

E.3.3.4 Derivation of the solution for α

To determine $\alpha(t, T, u)$ using ODE (5.61), we first substitute β_1 into this equation, yielding:

$$\alpha'(t, T, u) = (q + \lambda\mu_J)\,\beta_1 - \beta_2\theta_v - \beta_3\theta_r - \lambda\left[e^{\beta_1(ln(1+\mu_J) - \frac{1}{2}\sigma_J^2) + \frac{1}{2}\beta_1^2\sigma_J^2} - 1\right]. \tag{E.109}$$

Next, integrating both sides of equation (E.109) from t to T, yields:

$$\begin{aligned} \alpha(T, T, u) - \alpha(t, T, u) = (q + \lambda\mu_J)\,\beta_1\tau - \theta_v \int_t^T \beta_2\, ds - \theta_r \int_t^T \beta_3\, ds \\ - \lambda\tau\left[(1 + \mu_J)^{\beta_1} e^{\beta_1(\beta_1 - 1)\frac{\sigma_J^2}{2})} - 1\right], \end{aligned} \tag{E.110}$$

where $\tau = T - t$.

Regarding equation (E.110), it remains to compute the second and third terms of the right-hand side of the equation. To evaluate these terms, we note that the two integrals take the form $\int_t^T \frac{A - Be^{-\omega(T-s)}}{C - De^{-\omega(T-s)}}\, ds$. Then, performing a change of variables where $y = e^{-\omega(T-s)}$, which implies $s = T + \frac{\ln(y)}{\omega}$ and $\frac{ds}{dy} = \frac{1}{\omega y}$. Furthermore, since $t \leq s \leq T$, it follows that $e^{-\omega\tau} \leq y \leq 1$. Therefore, integral form can be rewritten as follows:

$$\begin{aligned} \int_t^T \frac{A - Be^{-\omega(T-s)}}{C - De^{-\omega(T-s)}}\, ds &= \int_{e^{-\omega\tau}}^1 \frac{A - By}{C - Dy}\frac{1}{\omega y}\, dy \\ &= \frac{1}{\omega}\int_{e^{-\omega\tau}}^1 \frac{A - By}{(C - Dy)y}\, dy. \end{aligned} \tag{E.111}$$

Using partial fraction decomposition and the equating coefficients method, we get:

$$\frac{A - By}{(C - Dy)y} = \frac{E}{C - Dy} + \frac{F}{y} \Leftrightarrow Ey + F(C - Dy) = A - By \Leftrightarrow E = -B + \frac{A}{C}D \wedge F = \frac{A}{C}.$$

Applying this result to equation (E.111) and simplifying the terms, we arrive at:

$$\begin{aligned}
\int_t^T \frac{A - Be^{-\omega(T-s)}}{C - De^{-\omega(T-s)}}\, ds &= \frac{1}{w}\int_{e^{-\omega\tau}}^1 \left[\frac{-B + \frac{A}{C}D}{C - Dy} + \frac{\frac{A}{C}}{y}\right] dy \\
&= \frac{1}{w}\left[\int_{e^{-\omega\tau}}^1 \frac{AD - BC}{C(C - Dy)}\, dy + \int_{e^{-\omega\tau}}^1 \frac{A}{Cy}\, dy\right] \\
&= \frac{1}{w}\left[-\frac{AD - BC}{CD}\int_{e^{-\omega\tau}}^1 \frac{-D}{C - Dy}\, dy + \frac{A}{C}\int_{e^{-\omega\tau}}^1 \frac{1}{y}\, dy\right] \\
&= \frac{1}{w}\left[-\frac{AD - BC}{CD} ln(C - Dy) + \frac{A}{C} ln(y)\right]_{e^{-\omega\tau}}^1 \\
&= \frac{1}{w}\left[\frac{AD - BC}{CD}\left[ln(C - De^{-\omega\tau}) - ln(C - D)\right] + \frac{A}{C}\left[ln(1) - ln(e^{-\omega\tau})\right]\right] \\
&= \frac{1}{w}\left[\frac{AD - BC}{CD} ln\left(\frac{C - De^{-\omega\tau}}{C - D}\right) + \frac{A\omega\tau}{C}\right] \\
&= \frac{AD - BC}{CD\omega} ln\left(\frac{C - De^{-\omega\tau}}{C - D}\right) + \frac{A\tau}{C}.
\end{aligned} \tag{E.112}$$

With the solution for the general form established, we can now use it to determine the solution for the integral of β_2, as follows:

$$\int_t^T \beta_2\theta_v\, ds = \theta_v\left[\ln\left(\frac{C_v - D_v e^{-\xi_v(u_1)\tau}}{C_v - D_v}\right)\left(\frac{A_vD_v - B_vC_v}{C_vD_v\xi_v(u_1)}\right) + \frac{A_v\tau}{C_v}\right]. \tag{E.113}$$

Similarly, we can obtain the solution for the integral of β_3, as shown below:

$$\int_t^T \beta_3\theta_r\, ds = \theta_r\left[\ln\left(\frac{C_r - D_r e^{-\xi_r(u_1)\tau}}{C_r - D_r}\right)\left(\frac{A_rD_r - B_rC_r}{C_rD_r\xi_r(u_1)}\right) + \frac{A_r\tau}{C_r}\right]. \tag{E.114}$$

Finally, substituting the solutions for β_2 and β_3 into ODE (E.110), and imposing the boundary condition $\alpha(T, T, u) = 0$, we arrive at the α general form:

$$\begin{aligned}
\alpha(t, T, u) = &-(q + \lambda\mu_J)\, u_1\tau + \theta_v\left[\ln\left(\frac{C_v - D_v e^{-\xi_v(u_1)\tau}}{C_v - D_v}\right)\left(\frac{A_vD_v - B_vC_v}{C_vD_v\xi_v(u_1)}\right) + \frac{A_v\tau}{C_v}\right] \\
&+\theta_r\left[\ln\left(\frac{C_r - D_r e^{-\xi_r(u_1)\tau}}{C_r - D_r}\right)\left(\frac{A_rD_r - B_rC_r}{C_rD_r\xi_r(u_1)}\right) + \frac{A_r\tau}{C_r}\right] + \lambda\tau\left[(1 + \mu_J)^{\beta_1} e^{\beta_1(\beta_1 - 1)\frac{\sigma_J^2}{2})} - 1\right],
\end{aligned} \tag{E.115}$$

where $\tau = T - t$, and the constants A_v, B_v, C_v and D_v are defined in accordance with equation (E.86) as:

$$\begin{aligned}
A_v &= 2u_2\xi_v(u_1) + u_2(u_1\rho\sigma_v - \kappa_v - \xi_v(u_1)) + u_1(u_1 - 1),\\
B_v &= u_2(u_1\rho\sigma_v - \kappa_v - \xi_v(u_1)) + u_1(u_1 - 1),\\
C_v &= 2\xi_v(u_1) - \gamma_v^+(u_1, u_2),\\
D_v &= -\gamma_v^+(u_1, u_2),
\end{aligned}$$

while the constants A_r, B_r, C_r and D_r follow from equation (E.107) and are defined as:

$$\begin{aligned}
A_r &= 2u_3\xi_r(u_1) + 2(u_1 - 1) - u_3(\xi_r(u_1) + \kappa_r),\\
B_r &= 2(u_1 - 1) - u_3(\xi_r(u_1) + \kappa_r),\\
C_r &= 2\xi_r(u_1) - \gamma_r^+(u_1, u_3),\\
D_r &= -\gamma_r^+(u_1, u_3),
\end{aligned}$$

where, again, $\gamma_v^+(u_1, u_2)$, $\xi_v(u_1)$, $\gamma_r^+(u_1, u_3)$ and $\xi_r(u_1)$ are given by:

$$\begin{aligned}
\gamma_v^+(u_1, u_2) &= u_2\sigma_v^2 - \kappa_v + u_1\rho\sigma_v + \xi_v(u_1),\\
\xi_v(u_1) &= \sqrt{(\kappa_v - u_1\rho\sigma_v)^2 - u_1(u_1 - 1)\sigma_v^2},\\
\gamma_r^+(u_1, u_3) &= u_3\sigma_r^2 - \kappa_r + \xi_r(u_1),\\
\xi_r(u_1) &= \sqrt{\kappa_r^2 - 2\sigma_r^2(u_1 - 1)}.
\end{aligned} \tag{E.116}$$

Plugging in the constants into the α equation (E.115), leads to:

$$\begin{aligned}
\alpha(t, T, u) &= \theta_v \frac{-2u_2\xi_v(u_1)\gamma_v^+(u_1, u_2) - 2\xi_v(u_1)\left[u_2\left(u_1\rho\sigma_v - \kappa_v - \xi_v(u_1)\right) + u_1(u_1 - 1)\right]}{-\gamma_v^+(u_1, u_2)\left(2\xi_v(u_1) - \gamma_v^+(u_1, u_2)\right)\xi_v(u_1)}\\
&\times \ln\left(1 - \frac{\gamma_v^+(u_1, u_2)\left(1 - e^{-\xi_v(u_1)\tau}\right)}{2\xi_v(u_1)}\right) + \theta_v \frac{2u_2\xi_v(u_1) + u_2(u_1\rho\sigma_v - \kappa_v - \xi_v(u_1)) + u_1(u_1 - 1)}{2\xi_v(u_1) - \gamma_v^+(u_1, u_2)}\tau\\
&+ \theta_r\left(\frac{-2u_3\xi_r(u_1)\gamma_r^+(u_1, u_3) - 2\xi_r(u_1)\left[2(u_1 - 1) - u_3(\xi_r(u_1) + \kappa_r)\right]}{(2\xi_r(u_1) - \gamma_r^+(u_1, u_3))(-\gamma_r^+(u_1, u_3))\xi_r(u_1)}\right)\\
&\times \ln\left(1 - \frac{\gamma_r^+(u_1, u_3)(1 - e^{-\xi_r(u_1)\tau})}{2\xi_r(u_1)}\right) + \theta_r \frac{2u_3\xi_r(u_1) + 2(u_1 - 1) - u_3(\xi_r(u_1) + \kappa_r)}{2\xi_r(u_1) - \gamma_r^+(u_1, u_3)}\tau\\
&+ \lambda\tau\left[(1 + \mu_J)^{\beta_1} e^{\beta_1(\beta_1 - 1)\frac{\sigma_J^2}{2}} - 1\right] - (q + \lambda\mu_J)\, u_1\tau.
\end{aligned} \tag{E.117}$$

Substituting the terms $\gamma_v^+(u_1,u_2)$ and $\gamma_r^+(u_1,u_3)$ with the expressions outlined in equation (E.115), and recalling that $\beta_1(t,T,u)=u_1$ (as derived in equation (5.62)), yields:

$$\begin{aligned}
\alpha(t,T,u) &= \theta_v\left(\frac{-\xi_v(u_1)(-2u_1+2u_1^2+4u_1u_2\rho\sigma_v-4u_2\kappa_v+2u_2^2\sigma_v^2)}{\left(\gamma_v^+(u_1,u_2)-2\xi_v(u_1)\right)\gamma_v^+(u_1,u_2)\xi_v(u_1)}\right)\\
&\times\ln\left(1-\frac{\gamma_v^+(u_1,u_2)\left(1-e^{-\xi_v(u_1)\tau}\right)}{2\xi_v(u_1)}\right)-\theta_v\frac{u_2\xi_v(u_1)-u_2\kappa_v+u_2u_1\rho\sigma_v+u_1(u_1-1)}{\gamma_v^+(u_1,u_2)-2\xi_v(u_1)}\tau\\
&+\theta_r\left(\frac{-\xi_r(u_1)\left[2u_3^2\sigma_r^2-4u_3k_r+4u_1-4\right]}{(\gamma_r^+(u_1,u_3)-2\xi_r(u_1))\gamma_r^+(u_1,u_3)\xi_r(u_1)}\right)\times\ln\left(1-\frac{\gamma_r^+(u_1,u_3)(1-e^{-\xi_r(u_1)\tau})}{2\xi_r(u_1)}\right)\\
&-\theta_r\frac{u_3\xi_r(u_1)+2(u_1-1)-u_3\kappa_r)}{\gamma_r^+(u_1,u_3)-2\xi_r(u_1)}\tau+\lambda\tau\left[(1+\mu_J)^{u_1}e^{u_1(u_1-1)\frac{\sigma_J^2}{2}}-1\right]-\lambda u_1\mu_J\tau-qu_1\tau.
\end{aligned}\tag{E.118}$$

Finally, defining $\gamma_v^-(u_1,u_2)=u_2\sigma_v^2-\kappa_v+u_1\rho\sigma_v-\xi_v(u_1)$ and $\gamma_r^-(u_1,u_3)=u_3\sigma_r^2-\kappa_r-\xi_r(u_1)$, and noting that $\gamma_v^-(u_1,u_2)=\gamma_v^+(u_1,u_2)-2\xi_v(u_1)$ and $\gamma_r^-(u_1,u_3)=\gamma_r^+(u_1,u_3)-2\xi_r(u_1)$, we obtain the following solution for α:

$$\begin{aligned}
\alpha(t,T,u) &= -\theta_v\frac{u_2\left(\xi_v(u_1)-\kappa_v+u_1\rho\sigma_v\right)+u_1(u_1-1)}{\gamma_v^-(u_1,u_2)}\tau\\
&-\theta_v\left(\frac{2u_1(u_1-1)+2u_2(u_2\sigma_v^2-2\kappa_v+2u_1\rho\sigma_v)}{\gamma_v^-(u_1,u_2)\gamma_v^+(u_1,u_2)}\right)\times\ln\left(1-\frac{\gamma_v^+(u_1,u_2)\left(1-e^{-\xi_v(u_1)\tau}\right)}{2\xi_v(u_1)}\right)\\
&-\theta_r\frac{u_3\left(\xi_r(u_1)-\kappa_r\right)+2(u_1-1)}{\gamma_r^-(u_1,u_3)}\tau\\
&-\theta_r\left(\frac{4(u_1-1)+2u_3(u_3\sigma_r^2-2k_r)}{\gamma_r^-(u_1,u_3)\gamma_r^+(u_1,u_3)}\right)\times\ln\left(1-\frac{\gamma_r^+(u_1,u_3)(1-e^{-\xi_r(u_1)\tau})}{2\xi_r(u_1)}\right)\\
&+\lambda\tau\left[(1+\mu_J)^{u_1}e^{u_1(u_1-1)\frac{\sigma_J^2}{2}}-1\right]-\lambda u_1\mu_J\tau-qu_1\tau.
\end{aligned}\tag{E.119}$$

APPENDIX F

Results

F.1. Fourier inversion of the risk-neutral density

Fourier inversion methods provide an alternative to differentiation-based approaches by exploiting the relationship between option prices and the characteristic function of the logarithm of the underlying asset price under the risk-neutral measure. When the characteristic function of the log-price is available in closed or semi-closed form, this approach is particularly attractive, as it avoids numerical differentiation of option prices and allows the full risk-neutral density to be recovered directly through inversion. More precisely, the risk-neutral probability that the stock price at maturity exceeds a given threshold x, conditional on the information available at time t, can be expressed in terms of the characteristic function of the log-price via the Gil–Pelaez inversion formula (see the Fourier inversion theorem in Kendall and Stuart (1977), Melick and Thomas (1997), and Stuart and Ord (1991a, Theorem 3)), as follows:

$$\mathbb{Q}(S_T > x|\mathcal{F}_t) = \frac{1}{2} + \frac{1}{\pi}\int_0^{+\infty} \mathrm{Re}\left[e^{-\phi \ln(x) i}\frac{f(t,\phi,S_t,Y_t)}{i\phi}\right] d\phi, \tag{F.1}$$

where x denotes a real-valued threshold for the terminal asset price, and $f(t,\phi,S_t,Y_t)$ is the marginal characteristic function of $\ln(S_T)$ under the risk-neutral measure $\mathbb{Q}$, conditional on the current state variables (S_t, Y_t), defined as:

$$f(t,\phi,S_t,Y_t) = \mathbb{E}^{\mathbb{Q}}[e^{i\phi \ln(S_T)}|\mathcal{F}_t].$$

Here, ϕ is the argument of the characteristic function, and Y_t represents additional state variables, such as stochastic volatility or other risk factors. Equivalently, noting that the cumulative distribution function is the complement of the survival function, we obtain:

$$\begin{aligned}\mathbb{Q}(S_T \le x|\mathcal{F}_t) &= 1 - \mathbb{Q}(S_T > x|\mathcal{F}_t) \\ &= \frac{1}{2} - \frac{1}{\pi}\int_0^{+\infty} \mathrm{Re}\left[e^{-\phi \ln(x) i}\frac{f(t,\phi,S_t,Y_t)}{i\phi}\right] d\phi.\end{aligned} \tag{F.2}$$

Differentiating equation (F.2) with respect to x, and assuming sufficient regularity to justify the interchange of differentiation and integration via Leibniz's rule, yields the

following expression for the conditional risk-neutral density:

$$\begin{aligned}\frac{\partial \mathbb{Q}(S_T \leq x|\mathcal{F}_t)}{\partial x} &= -\frac{1}{\pi}\int_0^{+\infty} \mathrm{Re}\left[\frac{\partial}{\partial x} e^{-\phi \ln(x) i} \frac{f(t,\phi,S_t,Y_t)}{i\phi}\right] d\phi \\ &= -\frac{1}{\pi}\int_0^{+\infty} \mathrm{Re}\left[-\frac{\phi i}{x} e^{-\phi \ln(x) i} \frac{f(t,\phi,S_t,Y_t)}{i\phi}\right] d\phi \\ &= \frac{1}{\pi}\int_0^{+\infty} \mathrm{Re}\left[\frac{1}{x} e^{-\phi \ln(x) i} f(t,\phi,S_t,Y_t)\right] d\phi.\end{aligned} \tag{F.3}$$

The risk-neutral density associated with the terminal asset price S_T is therefore given by $q(t, S_t, Y_t, T, S_T, \theta)$:

$$q(t,S_t,Y_t,T,S_T,\theta) = \frac{1}{\pi}\int_0^{+\infty} \mathrm{Re}\left[\frac{e^{-\phi \ln(S_T) i} f(t,\phi,S_t,Y_t)}{S_T}\right] d\phi, \tag{F.4}$$

where θ is the vector of model parameters. Consequently, the price of a European-call option can be written as a function of the previous density:

$$C_0 = E_Q[e^{-rT}(S_T - X)^+] = e^{-rT}\int_X^{+\infty} (S_T - X) q(t,S_t,Y_t,T,S_T,\theta) dS_T. \tag{F.5}$$

Approximating the improper integral in equation (F.4) by replacing it with a finite weighted sum, whose nodes and weights are determined by a Gauss–Kronrod quadrature rule, yields:

$$\int_0^{+\infty} \mathrm{Re}\left[\frac{e^{-\phi \ln(S_T) i} f(t,\phi,S_t,Y_t)}{S_T}\right] d\phi \approx \sum_{j=1}^{N} w_j g(\phi_j).$$

As a result, the theoretical risk-neutral density given by equation (F.4) can be approximated numerically as follows:

$$\hat{q}(t,S_t,Y_t,T,S_T,\theta) = \frac{1}{\pi}\sum_{j=1}^{N} w_j g(\phi_j), \tag{F.6}$$

where the integrand $g(\phi)$ is given by:

$$g(\phi) = \mathrm{Re}\left[\frac{e^{-\phi \ln(S_T) i} f(t,\phi,S_t,Y_t)}{S_T}\right].$$

In this study, risk-neutral densities are recovered from the corresponding characteristic functions via Fourier inversion in the following form:

$$\hat{q}(S_T) = \frac{1}{\pi}\int_0^{+\infty} \mathrm{Re}\left[\frac{e^{-i\phi \ln S_T} f(\phi;\boldsymbol{\theta})}{S_T}\right] d\phi, \tag{F.7}$$

computed numerically with a Gauss–Kronrod integration scheme. Each density was normalised to integrate to one within a numerical tolerance of 5%, and checked for non-negativity.

F.2. Data and pre-processing information

F.2.1. Data filtering effect

Figure F.1 shows the effect of the both data filters (first 3/8 USD, then OTM filter) to the SPX option sample after the initial cleaning process.

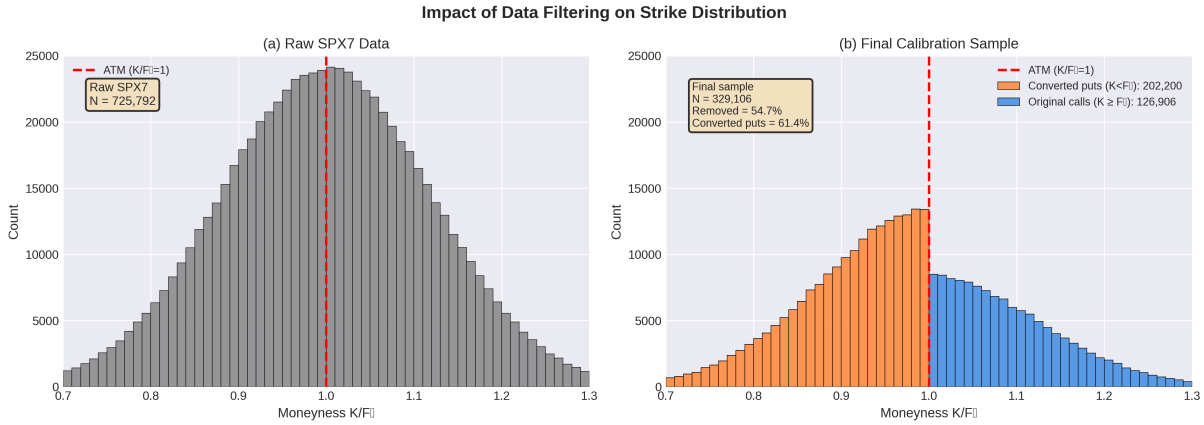


Figure F.1. Strike distribution before and after filtering. Panel (a): raw SPX sample ($N = 725{,}792$). Panel (b): final sample ($N = 329{,}106$); removed 54.7%; converted puts 61.4%. Dashed line: $K/F_0 = 1$

The initial dataset contained almost one million options. As shown in Figure F.1, we reached 725,792 contracts after the cleaning process, in which we removed observations with missing or inconsistent values. We retained SPX monthly contracts, and excluded maturities with $\tau < 7$ days. Quotes with mid prices below USD 3/8 were discarded following (Bakshi and Chen, 1997). We then kept out-of-the-money legs relative to the forward price F_0 (calls with $K \geq F_0$ and puts with $K < F_0$) and converted OTM puts into calls using put–call parity. After filtering, the final calibration sample included 329,106 observations, a reduction of 54.7% from the raw data. Converted puts accounted for 61.4% of the remaining observations (originally OTM puts with $K < F_0$), while original calls represented 38.6% (OTM calls with $K \geq F_0$). This asymmetric composition reflects the combined effect of the OTM filter (which retains calls with $K \geq F_0$ and puts with $K < F_0$) and the USD 3/8 price threshold. Since deep OTM puts typically trade at lower prices than the corresponding synthetic calls obtained via put-call parity, the price filter disproportionately removed options from the left tail of the strike distribution, truncating the natural negative skewness typically observed in equity index options. These filtering effects will be reflected in both the shape of the RND distribution and its corresponding moments.

Now, Figure F.2 lustrates the evolution of the proportion of converted puts in the final sample during the analysis period.

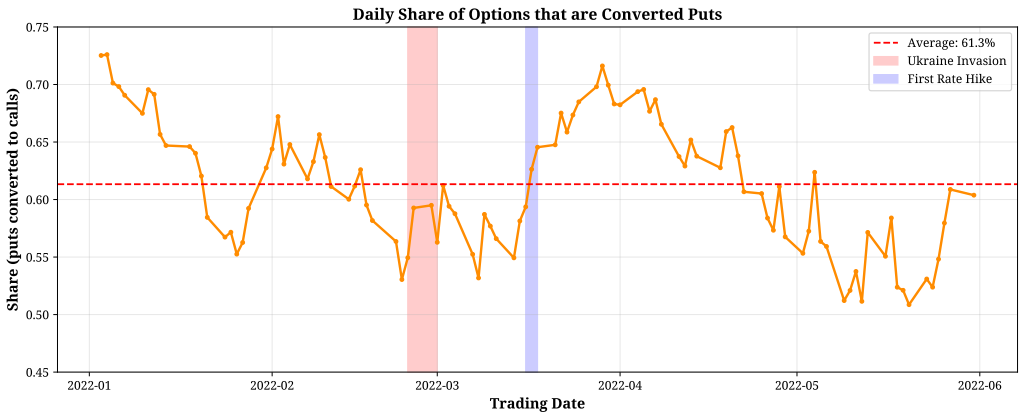


Figure F.2. Daily share of options that are converted puts. The dashed line indicates the sample average (61.3%). Shaded areas mark the Ukraine invasion (February 2022) and the first Fed rate hike (March 2022)

As shown in figure F.2, the proportion of converted puts varies considerably over time, ranging from 51% to 73%, with spikes during periods of market stress such as the Ukraine invasion and the first USA federal reserve rate hike in March 2022. The average of 61.3% confirms the high proportion of converted puts in the final sample, and justify the asymmetric impact of the price filter on deep OTM puts. This may have occurred due to the demand for puts by traders seeking downside protection during a period of elevated market uncertainty.

F.2.1.1 Data filtering sequence

Table F.1 compares the impact of two filtering approaches using a subset of the final data composition (12 trading days across 10 maturities), showing that applying the OTM filter first substantially alters the strike distribution by increasing the share of put options from 56.2% to 69.5%, while also reducing the overall sample size by 39%.

TABLE F.1. Impact of filtering order on a subset of the final dataset

Approach	**Final Sample**	**K < F (Puts)**	**K ≥ F (Calls)**
A: Price filter first (current)	49,304	27,726 (56.2%)	21,578 (43.8%)
B: OTM filter first	30,102 (-39%)	20,923 (69.5%)	9,179 (30.5%)

Notes: Approach A applies the USD 3/8 price filter before the OTM filter. Approach B applies the OTM filter before the price filter. The percentage change in final sample size for Approach B is relative to Approach A.

The order of data filtering operations can significantly impact the final sample composition and subsequent model calibration. Table F.1 compares the current approach (A), where the USD 3/8 price filter is applied before the out-of-the-money (OTM) filter, with an alternative (B), where the OTM filter is applied first. Reversing the order, results in a 39% smaller final sample and a more skewed composition. Specifically, applying the OTM filter first (Approach B) increases the proportion of puts (K < F) from 56.2% to 69.5%. This occurs because applying the price filter first symmetrically removes the cheapest deep-OTM puts and calls. In contrast, applying the OTM filter first creates a

sample that is then asymmetrically truncated by the price filter. This analysis confirms that the chosen filtering order is a critical methodological decision, as the resulting sample composition has a direct impact on model estimation, particularly for models like Bakshi that are highly sensitive to the empirical distribution of strikes.

F.2.2. Final sample statistics

Table F.2 presents a detailed overview of the final calibration sample characteristics, including the composition of converted puts and original calls, the maturity structure, and the distribution of observations across trading days and maturities.

Table F.2. Descriptive statistics of the final calibration sample

Sample Composition		**Maturity Structure**	
Total observations	329,106	Distinct maturities	23
Converted puts	202,200 (61.4%)	Min TTM (days)	7
Original calls	126,906 (38.6%)	Max TTM (days)	1,810
Raw sample	725,792	Mean TTM (days)	437
Removed	396,686 (54.7%)	Median TTM (days)	284
Trading Activity		**Calibration Blocks**	
Trading days	103	Total blocks	1,885
Avg. obs. per day	3,195	Avg. maturities per day	18.3
Avg. obs. per maturity	14,309	Avg. days per maturity	82.0

Notes: TTM = time-to-maturity. Converted puts refer to OTM puts transformed into calls via put–call parity. Calibration blocks represent unique trading day × maturity pairs used in model estimation.

F.3. Additional market data

Figure F.3 illustrates the market data and macroeconomic context for the sample period, showing the evolution of the S&P 500 index, the VIX volatility index, and the United States Federal Reserve policy rate.

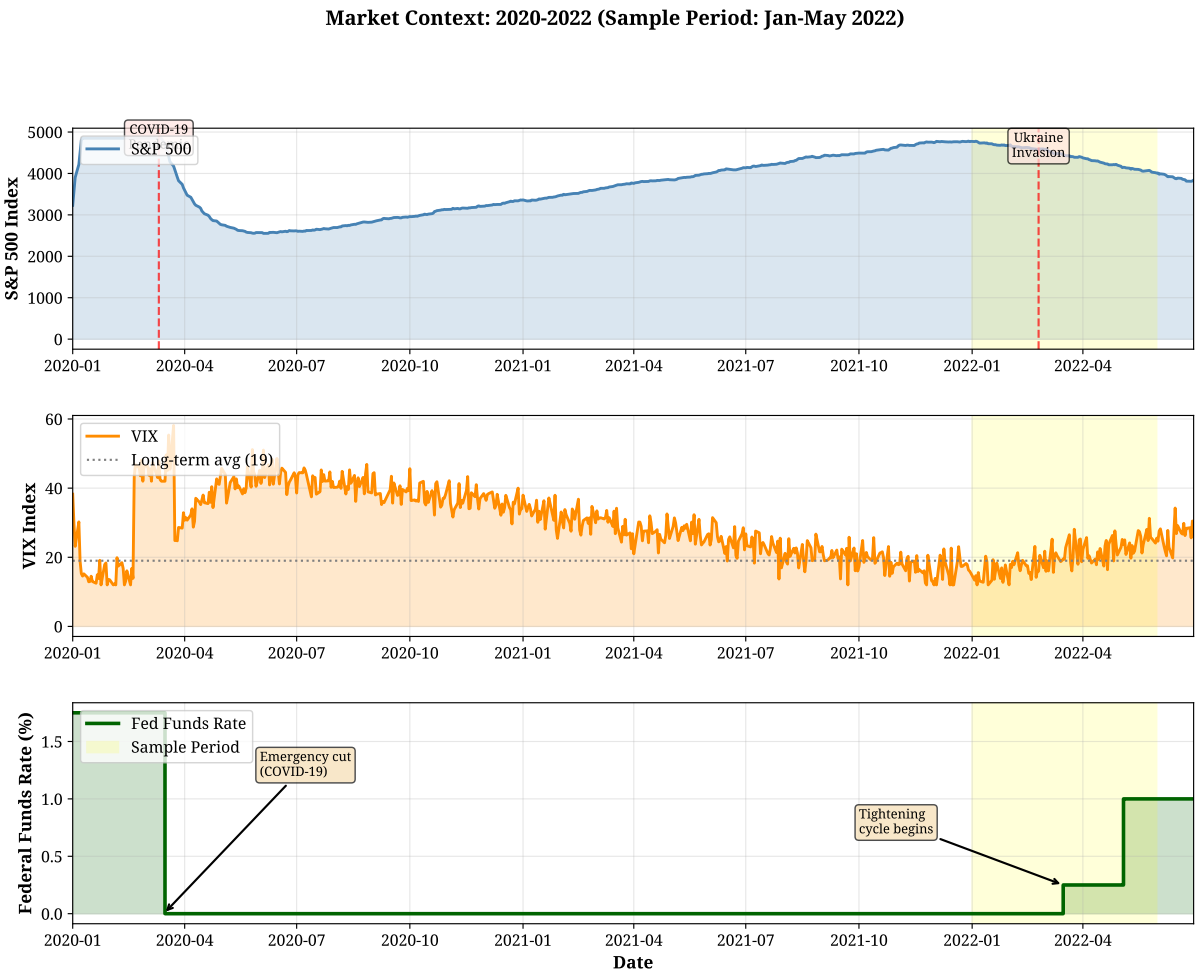


Figure F.3. Market context: 2020–2022 (sample period: January–May 2022). Top panel: S&P 500 index. Middle panel: VIX volatility index with long-term average (19). Bottom panel: Federal Reserve funds rate. Shaded areas highlight the COVID-19 crash (March 2020), the sample period (January–May 2022), and the Ukraine invasion (February 2022)

The sample period, from 1 January to end of May 2022, was marked by several shifts, both in terms of volatility and interest rate policy. After two years of near zero rates due to COVID-19 pandemic, the Federal Reserve began raising rates in March 2022, in fast pace, reaching 1.00% at the end of May. Combined with the Ukraine invasion in February, this led to a 13% drop in the S&P 500. The VIX averaged between 27 and 30 during this period, well above its long-term average of 19 points, reflecting high market uncertainty. This environment likely drove increased demand for put options as investors looked for downside protection.

F.4. Pricing Error Metrics

This section presents the pricing error and goodness-of-fit metrics used to evaluate the calibration performance of the option pricing model.

Let C_i^{mkt} denote the observed market price of option i, C_i^{model} the corresponding model-implied price, and N the number of options for a given trading day and maturity.

F.4.1. Sum of Squared Errors (SSE)

The calibration procedure minimizes the sum of squared pricing errors:

$$\mathrm{SSE} = \sum_{i=1}^{N} \left(C_i^{\mathrm{model}} - C_i^{\mathrm{mkt}}\right)^2. \tag{F.8}$$

F.4.2. Root Mean Squared Error (RMSE)

$$\mathrm{RMSE} = \sqrt{\frac{1}{N}\sum_{i=1}^{N} \left(C_i^{\mathrm{model}} - C_i^{\mathrm{mkt}}\right)^2}. \tag{F.9}$$

F.4.3. Mean Absolute Error (MAE)

$$\mathrm{MAE} = \frac{1}{N}\sum_{i=1}^{N} \left|C_i^{\mathrm{model}} - C_i^{\mathrm{mkt}}\right|. \tag{F.10}$$

F.4.4. Mean Absolute Percentage Error (MAPE)

$$\mathrm{MAPE} = \frac{100}{N}\sum_{i=1}^{N} \left|\frac{C_i^{\mathrm{model}} - C_i^{\mathrm{mkt}}}{C_i^{\mathrm{mkt}}}\right|. \tag{F.11}$$

F.4.5. Symmetric Mean Absolute Percentage Error (sMAPE)

The symmetric mean absolute percentage error is defined as:

$$\mathrm{sMAPE} = \frac{100}{N}\sum_{i=1}^{N} \frac{2\left|C_i^{\mathrm{model}} - C_i^{\mathrm{mkt}}\right|}{\left|C_i^{\mathrm{model}}\right| + \left|C_i^{\mathrm{mkt}}\right|}. \tag{F.12}$$

F.4.6. Coefficient of Determination (R^2)

$$R^2 = 1 - \frac{\sum_{i=1}^{N}\left(C_i^{\mathrm{mkt}} - C_i^{\mathrm{model}}\right)^2}{\sum_{i=1}^{N}\left(C_i^{\mathrm{mkt}} - \bar{C}^{\mathrm{mkt}}\right)^2}, \qquad \bar{C}^{\mathrm{mkt}} = \frac{1}{N}\sum_{i=1}^{N} C_i^{\mathrm{mkt}}. \tag{F.13}$$

F.4.7. Unexplained Variance (in basis points)

For interpretability, the fraction of price variance not explained by the model is reported in basis points as:

$$\text{Unexplained Variance}_{\mathrm{bps}} = 10{,}000 \times \left(1 - R^2\right). \tag{F.14}$$

F.5. Cubic Spline and Hermite Spline Smoothing

This section presents the theoretical definitions of the spline interpolation methods used to smooth the implied volatility smile in MATLAB.

F.5.1. Cubic Spline Interpolation

Let $\{(K_i, w_i)\}_{i=1}^{N}$ denote the observed strikes and total implied variances.

A cubic spline interpolant $S(K)$ is defined as a piecewise cubic polynomial such that, on each interval $[K_i, K_{i+1}]$,

$$S(K) = a_i + b_i(K - K_i) + c_i(K - K_i)^2 + d_i(K - K_i)^3, \tag{F.15}$$

subject to the conditions

$$S(K_i) = w_i, \tag{F.16}$$

$$S(K_{i+1}) = w_{i+1}, \tag{F.17}$$

$$S'(K_i^-) = S'(K_i^+), \tag{F.18}$$

$$S''(K_i^-) = S''(K_i^+), \tag{F.19}$$

for all interior knots K_i. These conditions ensure that the interpolant is twice continuously differentiable over the strike domain.

F.5.2. Hermite (Piecewise Cubic Hermite) Spline

The Hermite spline, also referred to as the piecewise cubic Hermite interpolating polynomial (PCHIP), is defined on each interval $[K_i, K_{i+1}]$ as:

$$H(K) = h_{00}(t)\, w_i + h_{10}(t)\, m_i(K_{i+1} - K_i) + h_{01}(t)\, w_{i+1} + h_{11}(t)\, m_{i+1}(K_{i+1} - K_i), \tag{F.20}$$

where:

$$t = \frac{K - K_i}{K_{i+1} - K_i}, \tag{F.21}$$

and the Hermite basis functions are given by:

$$h_{00}(t) = 2t^3 - 3t^2 + 1, \tag{F.22}$$

$$h_{10}(t) = t^3 - 2t^2 + t, \tag{F.23}$$

$$h_{01}(t) = -2t^3 + 3t^2, \tag{F.24}$$

$$h_{11}(t) = t^3 - t^2. \tag{F.25}$$

The slopes m_i are chosen so as to preserve the local shape of the data and avoid the introduction of spurious oscillations.

F.6. Calibration initial parameters and bounds

Table F.3 reports the initial values and parameter bounds used in the constrained optimisation. These choices follow parameter ranges reported in empirical studies on S&P 500 index option calibration (see, e.g., Bakshi, Cao and Chen (1997), Bates (2000), Pan (2002) and Eraker, Johannes, and Polson (2003)) and are refined to ensure numerical stability and convergence.

Table F.3. Initial values and bounds for model calibration parameters

Model	Parameter	Initial	Lower	Upper
Merton (1976)	σ (diffusion volatility)	0.180	0.050	1.000
	λ_j (jump intensity)	0.300	0.050	3.000
	m (jump mean)	−0.050	−0.300	0.300
	δ (jump variance)	0.020	0.000	0.200
Kou (2002)	σ (diffusion volatility)	0.200	0.050	0.600
	λ_j (jump intensity)	0.600	0.050	3.000
	p_1 (upward jump prob.)	0.350	0.050	0.950
	η_1 (upward jump rate)	20.000	1.200	60.000
	η_2 (downward jump rate)	10.000	2.000	60.000
Bakshi, Cao and Chen (1997)	θ_v (long-run variance)	0.040	0.005	0.080
	σ_v (vol of variance)	0.350	0.050	0.600
	κ_v (mean reversion speed)	2.000	0.200	4.000
	ρ (correlation)	−0.400	−0.950	0.600
	θ_r (long-run rate)	0.025	0.005	0.040
	σ_r (vol of rate)	0.030	0.005	0.080
	κ_r (rate mean reversion)	1.500	0.200	2.500
	λ_j (jump intensity)	0.800	0.100	1.500
	μ_J (jump mean)	−0.020	−0.150	0.100
	σ_J (jump std dev)	0.120	0.020	0.250

Notes: Parameters are estimated via constrained nonlinear optimization (fmincon with SQP algorithm). Initial values are updated adaptively across trading days when optimization converges successfully. The Bakshi, Cao and Chen (1997) model includes stochastic volatility, stochastic interest rates, and jumps.

F.7. Final parameters statistics for the three models calibrated

F.7.1. Calibrated parameter statistics for Merton (1976) JD model

Table F.4 reports the calibrated parameter statistics for the Merton (1976) model across all trading days and maturities.

Table F.4. Calibrated parameter statistics for Merton model

Component	Parameter	Mean	Median	Std Dev	Bounds	% at LB
Jumps	σ (diffusion volatility)	0.0969	0.0953	0.0285	0.050 1.000	5.8
	λ_J (jump intensity)	0.7982	0.4895	0.7427	0.050 3.000	0.0
	m (jump mean)	-0.2551	-0.3000	0.0668	−0.300 0.300	56.1
	δ (jump variance)	0.0613	0.0529	0.0442	0.000 0.200	2.3

Notes: Statistics computed across 1,885 observations (103 trading days × 18.3 average maturities per day). LB = lower bound. Bold values indicate parameters operating near bounds or exhibiting boundary behaviour.

F.7.2. Calibrated parameter statistics for Kou (2002) model

Table F.5 reports the calibrated parameter statistics for the Kou (2002) model across all trading days and maturities.

Table F.5. Calibrated parameter statistics for Kou model

Component	Parameter	Mean	Median	Std Dev	Bounds	% at LB
Jumps	σ (diffusion volatility)	0.0992	0.0910	0.0278	0.050 0.600	0.4
	λ_J (jump intensity)	1.2058	0.8735	0.9154	0.050 3.000	0.0
	p_1 (upward jump prob.)	0.0581	0.0500	0.0530	0.050 0.950	91.0
	η_1 (upward jump rate)	28.5522	13.5169	24.9871	1.200 60.000	0.0
	η_2 (downward jump rate)	5.5329	4.6579	2.9650	2.000 60.000	3.0

Notes: Statistics computed across 1,885 observations (103 trading days × 18.3 average maturities per day). LB = lower bound. Bold values indicate parameters operating near bounds or exhibiting boundary behaviour.

F.7.3. Calibrated parameter statistics for Bakshi and Chen (1997) model

Table F.6 reports the calibrated parameter statistics for the Bakshi and Chen (1997) model across all trading days and maturities.

Table F.6. Calibrated parameter statistics for Bakshi model

Component	Parameter	Mean	Median	Std Dev	Bounds	% at LB	Literature
Stochastic Volatility	θ_v (long-run variance)	**0.0051**	**0.0050**	0.0017	0.005–0.080	**97.9**	0.01–0.04
	σ_v (vol of variance)	0.0930	0.0890	0.0400	0.050–0.600	15.5	0.10–0.40
	κ_v (mean reversion)	**0.2298**	**0.2000**	0.1310	0.200–4.000	**74.5**	2.0–4.0
	ρ (correlation)	−0.2428	−0.2228	0.1400	−0.950 to 0.600	1.0	−0.6 to −0.8
Stochastic Rates	θ_r (long-run rate)	0.0119	0.0110	0.0057	0.005–0.040	9.6	0.01–0.03
	σ_r (vol of rate)	0.0135	0.0066	0.0140	0.005–0.080	40.7	0.01–0.05
	κ_r (rate mean reversion)	1.0764	1.0993	0.6026	0.200–2.500	10.3	0.5–2.0
Jumps	λ_j (jump intensity)	**0.1381**	**0.1001**	0.0925	0.100–1.500	**66.3**	0.5–1.5
	μ_J (jump mean)	−0.1022	−0.1233	0.0523	−0.150 to 0.100	40.5	−0.10 to −0.05
	σ_J (jump std dev)	0.0999	0.0854	0.0607	0.020–0.250	9.8	0.05–0.15

Notes: Statistics computed across 1,885 observations (103 trading days × 18.3 average maturities per day). LB = lower bound. Literature ranges from Bakshi, Cao and Chen (1997), Bates (2000), Eraker, Johannes, and Polson (2004), and Pan (2002), based on S&P 500 calibrations (1980–2000). Bold values indicate parameters operating near bounds or exhibiting values inconsistent with literature. λ_j shows 66.3% at lower bound, with 98.9% below 0.5, confirming diffusion-heavy calibration. θ_v (97.9% at LB) and κ_v (74.5% at LB) also exhibit boundary behavior. ρ exhibits weak leverage effect (−0.24 vs expected −0.6 to −0.8).

The calibrated parameters show a pattern of diffusion-heavy behaviour, with three key parameters operating near their lower bounds: long-run variance (θ_v, 97.9% at bound), mean reversion speed (κ_v, 74.5% at bound), and jump intensity (λ_j, 66.3% at bound). This indicates that the model assigns dominant weight to persistent stochastic volatility rather than discrete jumps. The slow mean reversion ($\kappa_v = 0.23$ means that volatility persist over time, reducing the need for the use of jumps in capturing sudden price movements. While this configuration achieves excellent pricing accuracy, it may underestimate tail risk, as 98.9% of λ_j observations fall below 0.5.

F.8. Detailed calibration performance metrics and robustness tests

This section of the appendix presents detailed calibration performance metrics for Merton, Kou and Bakshi models, as well as several robustness tests to ensure the best methodologies were chosen in the main results tests.

F.8.1. Robustness checks

F.8.1.1 Different maturity aggregation methods

As a robustness check, Table F.7 presents pricing errors using an alternative aggregation methodology. Global fit was obtained averaging by trading date, then simple average across trading dates. Buckets imposed equal weight across all 1,885 contracts.

Table F.7. Pricing errors by maturity (Method B)

Maturity	N_{obs}	Model	RMSE	MAE	MAPE (%)	SSE	R^2	$1-R^2$ (bps)
0–30d	85	Merton	1.613	1.135	22.70	3 461.21	0.999973	0.273
		Kou	2.444	1.761	34.12	4 632.16	0.999956	0.439
		Bakshi	0.006	0.004	0.21	0.09	0.999999	0.000
31–90d	204	Merton	2.305	1.810	12.32	1 944.10	0.999985	0.150
		Kou	2.082	1.721	26.02	1 660.82	0.999986	0.145
		Bakshi	0.012	0.009	0.14	0.06	0.999999	0.000
91–180d	304	Merton	3.828	2.969	3.85	3 756.81	0.999972	0.279
		Kou	2.347	1.755	3.85	1 422.94	0.999989	0.107
		Bakshi	0.031	0.026	0.19	0.28	0.999999	0.000
181–270d	301	Merton	5.321	4.350	5.52	4 021.65	0.999968	0.325
		Kou	3.215	2.569	5.61	1 491.46	0.999988	0.120
		Bakshi	0.066	0.056	0.54	0.65	0.999999	0.000
271–365d	318	Merton	5.722	4.542	4.54	4 509.04	0.999963	0.369
		Kou	3.325	2.607	5.50	1 534.37	0.999987	0.128
		Bakshi	0.106	0.090	0.70	1.69	0.999999	0.000
> 365d	673	Merton	10.839	8.213	6.86	12 041.91	0.999864	1.361
		Kou	5.375	3.734	3.60	4 218.70	0.999951	0.491
		Bakshi	1.307	0.851	0.95	464.81	0.999994	0.057
All maturities	1 885	Merton	5.986	4.622	7.48	5 904.78	0.999940	0.598
		Kou	3.481	2.589	9.12	2 489.94	0.999974	0.256
		Bakshi	0.414	0.278	0.54	132.68	0.999998	0.016

Note: Robustness check. Global fit: average by trading date, then simple average across trading dates. Buckets: equally weighted across contracts. N_{obs} = number of option contracts (observations) per bucket. RMSE = root mean squared error; MAE = mean absolute error; MAPE = mean absolute percentage error; SSE = sum of squared errors; R^2 = coefficient of determination; $1-R^2$ (bps) = $(1 - R^2) \times 10{,}000$.

The similarity of results illustrated by the Table F.7, confirms that the conclusions provided in the main section text are robust to the aggregation method choice.

F.8.1.2 Short-term split bucket aggregation method

Table F.8 presents pricing errors using an alternative bucketing aggregation, in this case the short-term split approach.

Table F.8. Pricing errors by maturity bucket – Short-term split

Maturity	N_{obs}	Model	RMSE	MAE	MAPE (%)	SSE	R^2	$1-R^2$ (bps)
0–30d	85	Merton	1.613	1.135	22.70	3 461.21	0.999973	0.273
		Kou	2.444	1.761	34.12	4 632.16	0.999956	0.439
		Bakshi	0.006	0.004	0.21	0.09	0.999999	0.000
31–60d	102	Merton	1.979	1.585	14.74	1 478.20	0.999987	0.125
		Kou	2.271	1.913	29.86	2 061.98	0.999981	0.188
		Bakshi	0.008	0.006	0.14	0.03	0.999999	0.000
61–120d	202	Merton	3.010	2.319	4.60	2 955.07	0.999979	0.208
		Kou	1.971	1.524	5.37	1 278.62	0.999991	0.093
		Bakshi	0.019	0.015	0.13	0.13	0.999999	0.000
121–180d	202	Merton	4.081	3.176	3.78	3 923.88	0.999970	0.302
		Kou	2.477	1.850	3.62	1 450.07	0.999989	0.113
		Bakshi	0.036	0.030	0.22	0.34	0.999999	0.000
181–365d	619	Merton	5.527	4.450	5.02	4 273.13	0.999965	0.347
		Kou	3.270	2.588	5.56	1 512.17	0.999988	0.124
		Bakshi	0.087	0.074	0.62	1.18	0.999999	0.000
> 365d	673	Merton	10.888	8.247	6.83	12 137.55	0.999862	1.377
		Kou	5.380	3.735	3.60	4 242.39	0.999950	0.495
		Bakshi	1.304	0.847	0.95	464.58	0.999994	0.057

Note: Pricing errors with more granular short-term maturity buckets. Aggregation: average by trading date, then across trading dates (2 pivots). N_{obs} = number of option contracts (observations) per bucket. RMSE = root mean squared error; MAE = mean absolute error; MAPE = mean absolute percentage error; SSE = sum of squared errors; R^2 = coefficient of determination; $1-R^2$ (bps) = $(1 - R^2) \times 10{,}000$.

F.8.1.3 Market liquidity bucket aggregation method

Table F.9 presents pricing errors using an alternative bucketing aggregation, in this case the market liquidity approach.

Table F.9. Pricing errors by liquidity bucket

Maturity	N_{obs}	Model	RMSE	MAE	MAPE (%)	SSE	R^2	$1-R^2$ (bps)
0–30d	85	Merton	1.613	1.135	22.70	3 461.21	0.999973	0.273
		Kou	2.444	1.761	34.12	4 632.16	0.999956	0.439
		Bakshi	0.006	0.004	0.21	0.09	0.999999	0.000
31–60d	102	Merton	1.965	1.576	18.53	1 458.97	0.999987	0.125
		Kou	2.281	1.920	43.10	2 062.79	0.999981	0.193
		Bakshi	0.008	0.006	0.14	0.03	0.999999	0.000
61–90d	102	Merton	2.687	2.075	5.31	2 491.16	0.999982	0.177
		Kou	1.858	1.496	6.76	1 207.53	0.999991	0.090
		Bakshi	0.016	0.012	0.13	0.10	0.999999	0.000
91–180d	304	Merton	3.828	2.969	3.85	3 756.81	0.999972	0.279
		Kou	2.347	1.755	3.85	1 422.94	0.999989	0.107
		Bakshi	0.031	0.026	0.19	0.28	0.999999	0.000
181–365d	619	Merton	5.526	4.448	5.02	4 270.81	0.999965	0.347
		Kou	3.272	2.588	5.55	1 513.40	0.999988	0.124
		Bakshi	0.087	0.074	0.62	1.19	0.999999	0.000
>365d	673	Merton	10.839	8.213	6.86	12 041.91	0.999864	1.361
		Kou	5.375	3.734	3.60	4 218.70	0.999951	0.491
		Bakshi	1.307	0.851	0.95	464.81	0.999994	0.057

Note: Pricing errors by liquidity buckets using Method A. Aggregation: average by trading date, then across trading dates (2 pivots). N_{obs} = number of option contracts (observations) per bucket. RMSE = root mean squared error; MAE = mean absolute error; MAPE = mean absolute percentage error; SSE = sum of squared errors; R^2 = coefficient of determination; $1-R^2$ (bps) = $(1 - R^2) \times 10{,}000$.

F.8.1.4 Five quantiles bucket aggregation method

Table F.10 presents pricing errors using an alternative bucketing aggregation, in this five quantiles approach.

Table F.10. Pricing errors by time-to-maturity quantile

Quantile	N_{obs}	Model	RMSE	MAE	MAPE (%)	SSE	R^2	$1-R^2$ (bps)
Q1	377	Merton	2.361	1.814	13.18	2 585.92	0.999980	0.195
		Kou	2.174	1.702	24.58	2 264.31	0.999980	0.202
		Bakshi	0.013	0.010	0.15	0.09	0.999999	0.000
Q2	377	Merton	4.505	3.592	4.66	3 850.29	0.999969	0.305
		Kou	2.734	2.104	4.21	1 434.32	0.999989	0.115
		Bakshi	0.045	0.038	0.32	0.41	0.999999	0.000
Q3	377	Merton	5.665	4.560	4.78	4 506.48	0.999965	0.351
		Kou	3.350	2.660	5.94	1 585.76	0.999987	0.125
		Bakshi	0.089	0.076	0.65	1.18	0.999999	0.000
Q4	377	Merton	6.040	4.751	5.04	4 818.57	0.999957	0.435
		Kou	3.287	2.549	3.53	1 434.50	0.999987	0.132
		Bakshi	0.154	0.125	0.55	3.96	0.999999	0.000
Q5	377	Merton	14.319	10.713	8.07	16 863.74	0.999798	2.016
		Kou	6.722	4.495	3.73	5 896.38	0.999929	0.715
		Bakshi	2.095	1.350	1.27	763.55	0.999991	0.094

Note: Pricing errors by time-to-maturity quantile. Contracts are divided into five equal-sized groups (quintiles) based on time-to-maturity. Q1 = shortest maturities (0–20$^{\text{th}}$ percentile), Q5 = longest maturities (80–100$^{\text{th}}$ percentile). Aggregation: average by trading date, then across trading dates (2 pivots). N_{obs} = number of option contracts (observations) per quantile. RMSE = root mean squared error; MAE = mean absolute error; MAPE = mean absolute percentage error; SSE = sum of squared errors; R^2 = coefficient of determination; $1-R^2$ (bps) = $(1 - R^2) \times 10{,}000$.

F.9. Statistical moments and quantiles of RND using mean instead of median

Additionally, as a robustness check, we recomputed key moments and quantile statistics using standard mean aggregation. Table F.11 presents the statistical moments (mean, standard deviation, skewness, and kurtosis) and selected quantiles (Q10, Q50, Q90) of the risk-neutral densities extracted from S&P 500 options across six maturity buckets, with values representing means across daily observations.

The comparison of median and mean for the Bakshi model's global RND moments shows a clear difference in how the model handles asymmetry versus tail thickness. For Kurtosis, the median is 2.8155 and the mean is 2.8285. The difference is minimal (+0.0130, or +0.5%), confirming that the model's output is stable and close to a Gaussian distribution (Kurtosis ≈ 3) across all days. In contrast, Skewness shows a high relative variation: the median is near-zero (+0.0031), but the mean is −0.0079. Although the absolute difference is small (−0.0110), it represents a significant −357% change. This large variation occurs because the negative skewness is concentrated in a small number of daily observations where the model captures stronger directional risk. The mean is pulled into

Table F.11. Statistical moments and quantiles of risk-neutral densities (Mean)

Maturity	Model	Mean	Std Dev	Skewness	Kurtosis	Q10	Q50	Q90
0–30d	Merton	−0.002	0.069	−0.7074	4.2285	−0.088	0.004	0.080
	Kou	−0.002	0.072	−1.3838	14.2147	−0.081	0.003	0.080
	Bakshi	−0.015	0.163	0.0038	3.2393	−0.223	−0.015	0.193
31–90d	Merton	−0.005	0.109	−1.3584	6.1774	−0.149	0.015	0.108
	Kou	−0.005	0.114	−1.7278	10.5097	−0.138	0.014	0.109
	Bakshi	−0.069	0.362	−0.0020	2.9713	−0.534	−0.069	0.395
91–180d	Merton	−0.012	0.167	−1.6714	7.1015	−0.244	0.027	0.146
	Kou	−0.013	0.173	−1.9419	9.4681	−0.228	0.028	0.146
	Bakshi	−0.158	0.556	0.0315	2.7904	−0.881	−0.159	0.563
181–270d	Merton	−0.021	0.221	−1.7591	7.1483	−0.336	0.037	0.180
	Kou	−0.021	0.227	−2.0029	8.7938	−0.310	0.039	0.180
	Bakshi	−0.237	0.685	0.0360	2.7986	−1.128	−0.239	0.649
271–365d	Merton	−0.029	0.260	−1.6681	6.5131	−0.403	0.045	0.206
	Kou	−0.028	0.265	−1.8849	7.7146	−0.377	0.046	0.207
	Bakshi	−0.290	0.757	0.0092	2.8041	−1.274	−0.288	0.688
> 365d	Merton	−0.062	0.380	−1.2442	4.7549	−0.613	0.052	0.294
	Kou	−0.068	0.407	−1.5896	6.0152	−0.632	0.048	0.305
	Bakshi	−0.448	0.951	−0.0573	2.7730	−1.703	−0.429	0.768
Allmaturities	Merton	−0.033	0.257	−1.4550	5.9424	−0.400	0.038	0.207
	Kou	−0.035	0.270	−1.7679	8.1586	−0.394	0.037	0.212
	Bakshi	−0.280	0.712	−0.0079	2.8285	−1.210	−0.273	0.635

Note: Statistical moments and quantiles of RNDs extracted from S&P 500 options for the period Jan–May 2022, across six maturity buckets and aggregated across all maturities. All metrics are computed in normalised return space ($Z = \ln(S_T/F)$). Mean and standard deviation measure central tendency and dispersion; skewness captures asymmetry; kurtosis measures tail thickness. Q10, Q50, Q90 represent the 10th percentile, median, and 90th percentile of the risk-neutral distribution. Values represent means across daily observations.

negative territory by these few high-impact days, while the median remains near zero, representing the model's typical, symmetric output. This finding suggests that the model's response to market stress is through asymmetry (skewness), rather than through extreme tail thickness (kurtosis).

Aggregated moments mean vs. median comparison by model and maturity

Table F.12. Aggregated moments comparison by maturity (mean vs. median)

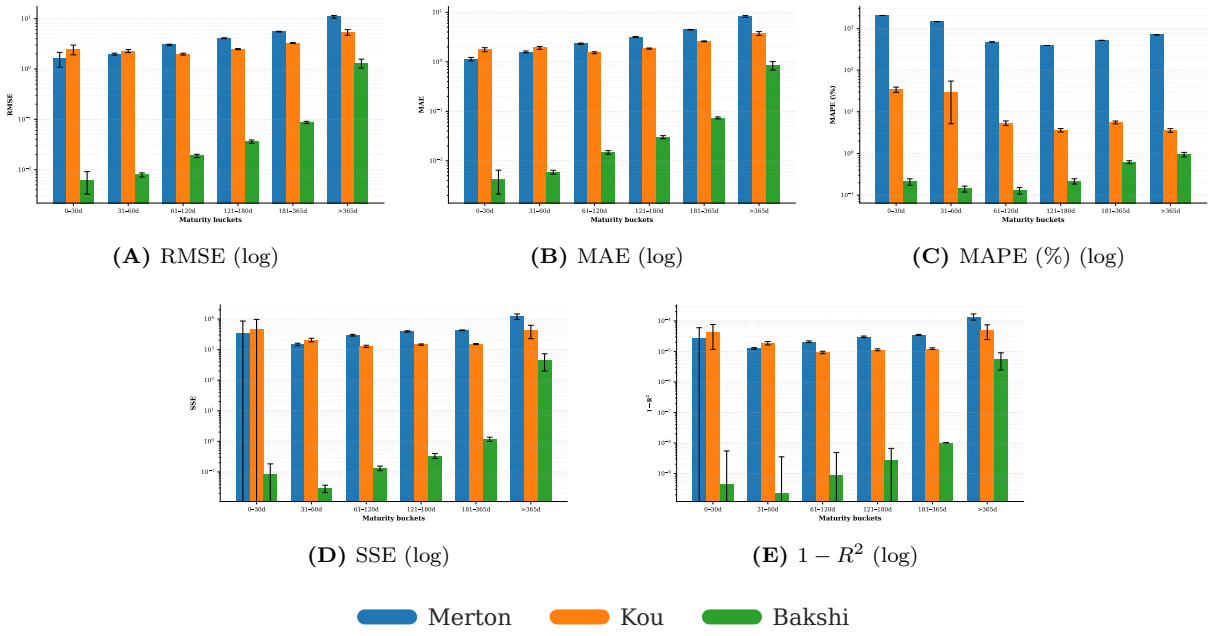
Bucket	Model	Aggregation	Mean	Std. Dev.	Skewness	Kurtosis
0-30d	Merton	Median	−0.001 631	0.070 371	−0.682 389	4.242 892
		Mean	−0.001 585	0.068 636	−0.707 403	4.228 529
	Kou	Median	−0.001 780	0.073 255	−1.305 378	11.580 191
		Mean	−0.001 775	0.072 357	−1.383 834	14.214 684
	Bakshi	Median	−0.013 962	0.167 636	0.000 596	3.014 136
		Mean	−0.014 918	0.162 513	0.003 806	3.239 314
31-90d	Merton	Median	−0.004 843	0.108 932	−1.387 394	6.123 211
		Mean	−0.005 058	0.109 331	−1.358 411	6.177 420
	Kou	Median	−0.005 183	0.113 830	−1.829 834	10.037 323
		Mean	−0.005 268	0.114 164	−1.727 791	10.509 653
	Bakshi	Median	−0.066 225	0.364 393	−0.003 731	2.994 818
		Mean	−0.068 999	0.361 775	−0.001 995	2.971 296
91-180d	Merton	Median	−0.012 032	0.167 851	−1.690 408	7.200 087
		Mean	−0.012 225	0.167 361	−1.671 380	7.101 515
	Kou	Median	−0.012 447	0.172 830	−1.972 111	9.459 667
		Mean	−0.012 568	0.172 639	−1.941 865	9.468 050
	Bakshi	Median	−0.155 762	0.553 939	0.032 608	2.773 107
		Mean	−0.158 049	0.556 346	0.031 538	2.790 404
181-270d	Merton	Median	−0.021 069	0.222 509	−1.763 014	7.118 194
		Mean	−0.020 952	0.221 403	−1.759 078	7.148 332
	Kou	Median	−0.021 081	0.226 893	−2.001 574	8.731 247
		Mean	−0.021 119	0.226 608	−2.002 901	8.793 799
	Bakshi	Median	−0.224 288	0.670 523	0.026 477	2.831 571
		Mean	−0.237 481	0.685 259	0.035 968	2.798 589
271-365d	Merton	Median	−0.028 304	0.259 726	−1.681 416	6.523 501
		Mean	−0.028 510	0.260 263	−1.668 080	6.513 142
	Kou	Median	−0.027 953	0.264 637	−1.903 665	7.737 873
		Mean	−0.028 167	0.265 255	−1.884 907	7.714 621
	Bakshi	Median	−0.307 973	0.781 466	−0.006 630	2.816 927
		Mean	−0.289 857	0.757 124	0.009 177	2.804 128
> 365d	Merton	Median	−0.051 374	0.357 725	−1.290 700	4.843 720
		Mean	−0.061 716	0.379 831	−1.244 185	4.754 870
	Kou	Median	−0.046 573	0.357 941	−1.564 396	5.857 239
		Mean	−0.068 013	0.406 928	−1.589 599	6.015 196
	Bakshi	Median	−0.458 922	0.968 342	−0.032 699	2.787 459
		Mean	−0.447 685	0.950 757	−0.057 331	2.773 042
All Maturities	Merton	Median	−0.025 916	0.248 206	−1.544 143	6.142 428
		Mean	−0.032 780	0.256 789	−1.454 967	5.942 352
	Kou	Median	−0.025 787	0.253 299	−1.800 594	7.734 523
		Mean	−0.035 083	0.269 679	−1.767 903	8.158 576
	Bakshi	Median	−0.272 244	0.738 981	0.003 074	2.815 484
		Mean	−0.279 566	0.711 505	−0.007 905	2.828 524

Note: Comparison of the four central moments of the RNDs across all maturity buckets and aggregated globally. Two aggregation methods are used: the median and the mean of the daily moment observations. All values are computed in the normalised log-return space ($Z = \ln(S_T/F)$). The results confirm the robustness of the main findings across the term structure.

We verified that computing statistics from pooled densities across time, yields qualitatively consistent results, as shown in table F.12, confirming the stability of our findings.

F.10. Other relevant error metrics and 3D RND figures

Figure F.4 presents five error metrics (RMSE, MAE, MAPE, SSE, and $1 - R^2$) across maturity buckets in logarithmic scale, demonstrating the consistent superiority of the Bakshi model across the entire term structure.

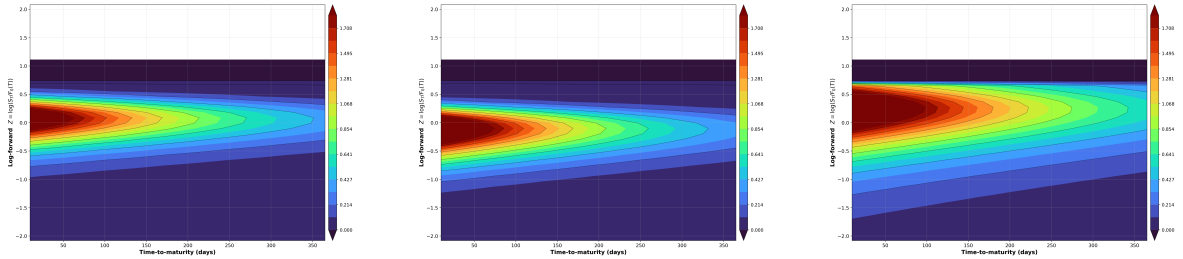


(A) RMSE (log) **(B)** MAE (log) **(C)** MAPE (%) (log)

(D) SSE (log) **(E)** $1 - R^2$ (log)

Figure F.4. Global error metrics across maturity buckets (log scale): RMSE, MAE, MAPE, SSE, and $1 - R^2$. Buckets are ordered along the horizontal axis to visualize the term-structure trend; lines are drawn for readability only. Colors: Merton—blue; Kou—orange; Bakshi—green.

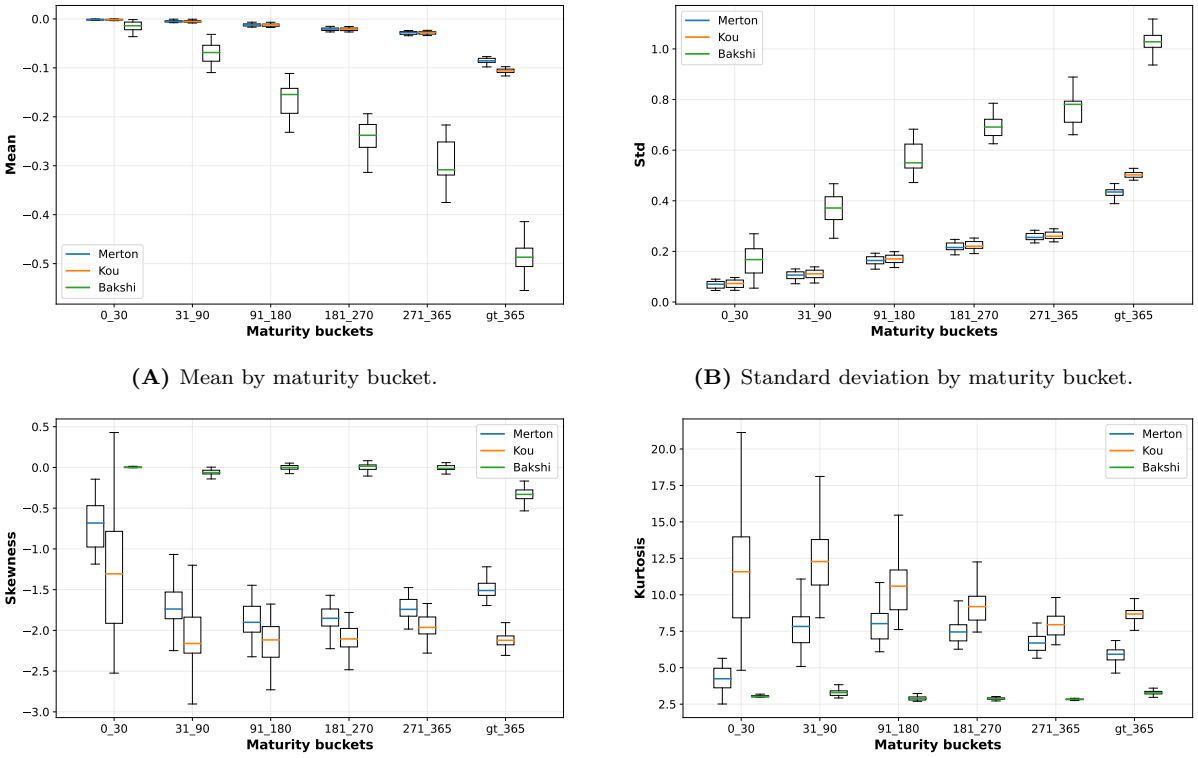
Figure F.5 presents risk-neutral density (RND) contour maps as a function of S_T and time-to-maturity τ for the three models, using the same colour scale to enable direct comparison. The maps reveal distinct distributional patterns: Merton and Kou exhibit concentrated probability mass around the forward price with visible tail asymmetry, while Bakshi displays a more diffuse, symmetric distribution, consistent with its near-zero skewness and diffusion-dominated calibration.



(A) Merton **(B)** Kou **(C)** Bakshi

Figure F.5. Risk-neutral density (RND) contour maps as a function of S_T and time-to-maturity τ for the three models. All panels use the **same color scale** to enable like-for-like comparison.

Figure F.6 presents boxplots of risk-neutral distribution moments in price space (Z_T) by maturity bucket, aggregated over trading days, illustrating location parameters (mean, standard deviation) and shape diagnostics (skewness, excess kurtosis) for each model. The results reveal a contrast. While Merton and Kou exhibit negatively skewed distributions with elevated kurtosis (consistent with typical equity index behaviour), Bakshi produces near-zero skewness and low kurtosis, reflecting its diffusion-dominated calibration.



(A) Mean by maturity bucket. **(B)** Standard deviation by maturity bucket.

(C) Skewness by maturity bucket. **(D)** Excess kurtosis by maturity bucket.

Figure F.6. Boxplots of risk-neutral distribution moments in price space (Z_T), by maturity bucket and aggregated over trading days. Top row: location and scale (mean, standard deviation). Bottom row: shape diagnostics (skewness, excess kurtosis).

F.11. Additional risk measures: statistical distances, Value-at-Risk and Expected Shortfall measure tables

F.11.1. Statistical Distances by Maturity

While Table 6.4 in the main body presents overall distances, Table F.13 provides a detailed breakdown by maturity bucket.

Table F.13. Statistical Distances Between Models by Maturity Bucket

Maturity	Merton vs Kou			Bakshi vs Kou			Bakshi vs Merton		
	JS	Hell	W1	JS	Hell	W1	JS	Hell	W1
0–30d	0.006351	0.080780	0.004534	0.211362	0.492857	0.087534	0.212451	0.499027	0.087972
31–90d	0.002049	0.046061	0.004525	0.265245	0.558042	0.234691	0.267739	0.561064	0.235139
91–180d	0.001989	0.044850	0.005740	0.268778	0.559710	0.368640	0.270043	0.562330	0.369588
181–270d	0.002421	0.049555	0.008117	0.256210	0.546982	0.448462	0.255830	0.545966	0.448692
271–365d	0.002176	0.046831	0.009293	0.239669	0.528941	0.525613	0.238408	0.525620	0.525482
> 365d	0.004148	0.064821	0.018015	0.204359	0.483510	0.600806	0.202363	0.483785	0.616453

Note: Statistical distances between risk-neutral densities of three jump-diffusion models (Merton 1976, Kou 2002, Bakshi 1997) by maturity bucket. JS = Jensen-Shannon divergence (range: $[0, \ln(2) \approx 0.693]$); Hell = Hellinger distance (range: $[0, 1]$); W1 = Wasserstein-1 (Earth Mover's Distance) in $Z = \ln(S_T/F)$ space. Lower values indicate more similar distributions. Values represent medians of daily distances across the sample period (January–May 2022). Merton and Kou show consistently small distances across all maturities, indicating similar risk-neutral densities. Bakshi shows large distances from both Merton and Kou, with distances generally increasing with maturity, reflecting the growing importance of stochastic volatility at longer horizons.

Table F.14. Value-at-Risk and Expected Shortfall of risk-neutral densities by maturity

Maturity	Model	Left Tail (Loss)						Right Tail (Gain)					
		VaR	ES	VaR	ES	VaR	ES	VaR	ES	VaR	ES	VaR	ES
		95%		97.5%		99%		95%		97.5%		99%	
0–30d	Merton	−0.125	−0.182	−0.167	−0.217	−0.212	−0.257	0.100	0.121	0.116	0.136	0.133	0.151
	Kou	−0.115	−0.196	−0.159	−0.255	−0.240	−0.332	0.102	0.127	0.119	0.140	0.139	0.160
	Bakshi	−0.290	−0.361	−0.343	−0.406	−0.404	−0.461	0.262	0.332	0.315	0.378	0.376	0.433
31–90d	Merton	−0.223	−0.313	−0.286	−0.371	−0.363	−0.449	0.130	0.158	0.149	0.176	0.171	0.198
	Kou	−0.220	−0.345	−0.305	−0.428	−0.415	−0.539	0.132	0.161	0.152	0.179	0.174	0.203
	Bakshi	−0.666	−0.820	−0.782	−0.921	−0.916	−1.041	0.532	0.684	0.647	0.784	0.780	0.902
91–180d	Merton	−0.359	−0.504	−0.461	−0.603	−0.589	−0.730	0.175	0.215	0.202	0.242	0.234	0.275
	Kou	−0.355	−0.540	−0.484	−0.667	−0.652	−0.829	0.173	0.214	0.198	0.240	0.228	0.271
	Bakshi	−1.074	−1.263	−1.234	−1.378	−1.393	−1.485	0.768	0.983	0.939	1.119	1.128	1.265
181–270d	Merton	−0.490	−0.681	−0.623	−0.810	−0.797	−0.978	0.215	0.265	0.248	0.298	0.288	0.341
	Kou	−0.484	−0.722	−0.656	−0.884	−0.875	−1.079	0.213	0.257	0.242	0.285	0.277	0.326
	Bakshi	−1.336	−1.588	−1.541	−1.747	−1.762	−1.909	0.883	1.158	1.093	1.336	1.335	1.542
271–365d	Merton	−0.576	−0.792	−0.730	−0.939	−0.932	−1.121	0.246	0.307	0.284	0.350	0.335	0.408
	Kou	−0.579	−0.842	−0.776	−1.015	−1.017	−1.217	0.243	0.298	0.277	0.332	0.320	0.380
	Bakshi	−1.610	−1.919	−1.856	−2.117	−2.129	−2.327	0.977	1.281	1.215	1.476	1.483	1.688
> 365d	Merton	−0.793	−1.046	−0.991	−1.207	−1.220	−1.373	0.339	0.461	0.410	0.550	0.542	0.683
	Kou	−0.812	−1.092	−1.044	−1.262	−1.287	−1.424	0.342	0.429	0.396	0.490	0.466	0.591
	Bakshi	−2.092	−2.458	−2.393	−2.686	−2.710	−2.909	1.119	1.494	1.409	1.735	1.736	2.009
All maturities	Merton	−0.548	−0.756	−0.695	−0.899	−0.889	−1.078	0.238	0.294	0.274	0.333	0.322	0.385
	Kou	−0.549	−0.805	−0.737	−0.975	−0.972	−1.176	0.236	0.284	0.268	0.316	0.308	0.361
	Bakshi	−1.499	−1.740	−1.707	−1.883	−1.905	−2.009	0.958	1.251	1.188	1.441	1.446	1.653

Note: Value-at-Risk (VaR) and Expected Shortfall (ES) of risk-neutral densities extracted from S&P 500 options using three jump-diffusion models (Merton 1976, Kou 2002, Bakshi 1997) across six maturity buckets and aggregated across all maturities. All metrics computed in normalized return space ($Z = \ln(S_T/F)$). VaR represents the threshold at the specified confidence level; ES (also known as CVaR or conditional VaR) represents the expected value beyond the VaR threshold. Left tail measures capture downside risk (losses), while right tail measures capture upside potential (gains). Values represent medians across daily observations (January–May 2022). For interpretation: $\text{VaR}_{95\%} = -0.125$ means there is a 5% probability of losses exceeding 11.8%.

F.12. Bakshi smoothing error metrics by maturity

Table F.15. Pricing errors by maturity bucket

Maturity	N_{obs}	Method	RMSE	MAE	MAPE (%)	sMAPE (%)	MAE	Conv (%)	CV (%)
0–30d	26	Original	0.010 6	0.008 2	0.23	0.24	0.008 2	96.15	91.53
0–30d	26	Cubic	0.003 6	0.002 7	0.16*	7.71	0.002 7	100.00	34.39
0–30d	26	Hermite	0.003 6	0.002 7	0.16	0.14	0.002 7	100.00	34.18
30–60d	34	Original	0.007 6	0.005 0	0.15	0.14	0.005 0	100.00	29.16
30–60d	34	Cubic	0.007 5	0.004 8	0.11	3.46	0.004 8	100.00	29.07
30–60d	34	Hermite	0.007 5	0.004 8	0.11	0.13	0.004 8	100.00	29.59
60–90d	28	Original	0.011 6	0.007 5	0.09	0.10	0.007 5	100.00	25.98
60–90d	28	Cubic	0.011 4	0.007 3	0.09	2.68	0.007 3	100.00	40.19
60–90d	28	Hermite	0.011 4	0.007 3	0.09	0.13	0.007 3	100.00	40.87
90–180d	90	Original	0.023 7	0.018 9	0.12	0.13	0.018 9	100.00	23.21
90–180d	90	Cubic	0.022 9	0.018 1	0.12	3.40	0.018 1	100.00	34.85
90–180d	90	Hermite	0.022 9	0.018 1	0.12	0.15	0.018 1	100.00	34.15
180–270d	85	Original	0.056 3	0.048 0	0.49	0.51	0.048 0	100.00	15.64
180–270d	85	Cubic	0.054 3	0.045 9	0.48	18.70	0.045 9	100.00	22.69
180–270d	85	Hermite	0.054 3	0.045 9	0.51	0.57	0.045 9	100.00	23.19
270–365d	37	Original	0.082 2	0.070 5	0.71	0.76	0.070 5	100.00	12.14
270–365d	37	Cubic	0.078 9	0.067 3	0.70	28.06	0.067 3	100.00	15.34
270–365d	37	Hermite	0.078 9	0.067 3	0.75	0.84	0.067 3	100.00	15.97
All maturities	300	Original	0.036 2	0.030 1	0.31	0.33	0.030 1	99.67	51.81
All maturities	300	Cubic	0.034 4	0.028 4	0.30	11.20	0.028 4	100.00	41.39
All maturities	300	Hermite	0.034 4	0.028 4	0.31	0.36	0.028 4	100.00	41.39

Note: RMSE = Root Mean Squared Error; MAE = Mean Absolute Error; MAPE = Mean Absolute Percentage Error; sMAPE = Symmetric Mean Absolute Percentage Error; Conv (%) = percentage of calibrations that converged; CV (%) = Coefficient of Variation. For *Cubic* in bucket **0–30d** on 05-Jan-2022 there was an extreme outlier: MAPE $\approx 4.95 \times 10^{11}\%$. Entries marked with * (0–30d, Cubic) indicate this outlier is excluded from the reported statistics.